ELECTROMAGNETICALLY INDUCED TRANSPARENCY AND QUANTUM EFFECTS IN OPTOMECHANICAL SYSTEMS

By

SUMEI HUANG

Bachelor of Science in Physics Education
Fujian Normal University
Fuzhou, Fujian, China
2001

Master of Science in Theoretical Physics
Fujian Normal University
Fuzhou, Fujian, China
2004

Submitted to the Faculty of the
Graduate College of
Oklahoma State University
in partial fulfillment of
the requirements for
the Degree of
DOCTOR OF PHILOSOPHY
December, 2011

ELECTROMAGNETICALLY INDUCED TRANSPARENCY AND QUANTUM EFFECTS IN OPTOMECHANICAL SYSTEMS

Dissertation Approved:

Dr. Girish S. Agarwal

Dissertation advisor

Dr. Xincheng Xie

Dr. Albert T. Rosenberger

Dr. Yin Guo

Dr. Daniel Grischkowsky

Dr. Jacques H. H. Perk

Dr. Sheryl A. Tucker

Dean of the Graduate College

TABLE OF CONTENTS

LIST OF TABLES

Table Page

LIST OF FIGURES

CHAPTER 1

INTRODUCTION

1.1 Optomechanical System

1.1.1 Overview

Radiation pressure force, due to the momentum carried by light, has received considerable attention since Kepler proposed that the tail of a comet was caused by the force exerted by the sunlight in the 16th century. It was deduced theoretically by J. C. Maxwell in 1871, and first observed experimentally [1, 2] in the early 1900s. With the invention of lasers in the 1970s, it has been shown that radiation pressure force can be used to manipulate atoms [3, 4, 5] i.e., to slow them, cool them, or trap them, owing to the relatively large power of the laser fields. In 2004, it was first demonstrated experimentally that radiation pressure force exerted by the light stored inside an optical cavity can be use to cool the motion of a mechanical oscillator made of roughly 10^{15} atoms in a cavity optomechanical system which parametrically couples an optical cavity and a mechanical resonator through radiation pressure [6].

Due to rapid advances in micro- and nanofabrication techniques, various geometries of the optomechanical system have been developed, such as a Fabry-Perot cavity with mirrored microcantilevels [7], or with one movable end mirror [8, 9], or with a movable semitransparent membrane in the middle of the cavity [10, 11, 12, 13], or with a Bose-Einstein condensate [14], or with a trapped macroscopic ensemble of ultracold atoms [15], radially vibrating microspheres [16], radially vibrating microtoroids [17, 18], GaAs nano-optomechanical disk resonator [19], and optomechanical

crystals [20]. Meanwhile, the optomechanical coupling idea has been extended to nanoelectromechanical systems, formed by a nanomechanical resonator capacitively coupled to a superconducting microwave cavity [21, 22, 23, 24]. The major challenge in all of these setups is to achieve simultaneously a high optical finesse (currently in the range from 10^3 to 10^5) and a high mechanical quality factor (currently in the range from 10^3 to 10^5).

It has been shown theoretically and experimentally that such optomechanical systems at macroscopic scale can exhibit a very rich quantum effects, which usually exist in the microscopic system. For example, squeezing of the light field [25, 26], superposition state [27, 28], quantum non-demolition measurements of photon numbers [29, 30], the preparation of a mechanical oscillator in a squeezed state of motion [31, 32, 33], the creation of entangled photon pairs [34], the entanglement between the light and mechanical mode [35, 36], entangling two mechanical oscillators [37, 38, 39], and Fock state detection [10]. Moreover, the optomechanical coupling in such systems induces nonlinear behaviors, including an optical spring effect [40, 41], bistability [41, 42], multistability [43], self-induced oscillations [44, 45, 46], optomechanical normal mode splitting [22, 47, 48, 49, 50], and optomechanically induced transparency [51, 52, 53, 54, 55].

Due to unavoidable coupling of the mechanical oscillator to its surrounding thermal environment, the random, thermal motion associated with mechanical dissipation mask the quantum behaviors. To see quantum effects in large objects, they must be cooled down to its quantum ground state. The ground state cooling requires that the mechanical oscillator's temperature T must be reduced so that $T \ll \frac{\hbar\omega_m}{k_B}$, where $\hbar$ is Planck's constant h divided by 2π, k_B is Boltzmann's constant, ω_m is the resonance frequency of the mechanical oscillator, typically between a few kilohertz and a few hundred megahertz. For a mechanical oscillator with a resonance frequency of 1kHz (100MHz), the ground state cooling requires $\hbar\omega_m/k_B$=50 nK (5 mK), which

are below those achievable with standard cryogenic cooling. So far, significant effort has been devoted to developing alternative cooling techniques. In the past few years, extraordinary progress has been made in cooling a mechanical resonator down to its quantum ground state [6, 7, 8, 9, 10, 56]. In 2009, the minimum achievable phonon number of the mechanical oscillator is 63 in a toroidal microresonator [57], 37 in a microsphere resonator [58], and 35 in a Fabry-Perot cavity [59]. In 2010, the preparation of mechanical resonator with the final phonon number below 10 was reported in Refs. [23, 60]. Recent work has shown experimentally that laser cooling can reduce the average occupancy of the mechanical oscillator below unity [61, 62, 63]. However, the ground state cooling has so far not been reached experimentally.

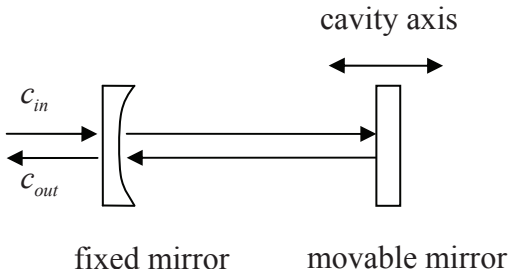

Figure 1.1: A Fabry-Perot cavity with one fixed partially transmitting mirror and one movable totally reflecting mirror.

1.1.2 The Dispersive Optomechanical System

The canonical optomechanical system is a Fabry-Perot cavity with one heavy, fixed partially transmitting mirror and one light, movable totally reflecting mirror of effective mass m (typically in the micro or nanogram range), as shown in Fig. 1.1. The system is driven by an external laser at frequency ω_l, then the circulating photons in the cavity will exert a radiation pressure force on the movable mirror due to momentum transfer from the intracavity photons to the movable mirror. Here, the movable mirror is modeled as a single mode quantum harmonic oscillator. Moreover, when the

mechanical frequency ω_m is much smaller than the cavity free spectral range $(c/2L)$, where L is the initial cavity length, the input laser drives only one cavity mode ω_c and scattering of photons from the driven mode into other cavity modes is negligible [64].

During the cavity round-trip time $t = 2L/c$, there are n photons hitting on the surfaces of the movable mirrors, the momentum transferred to the movable mirror will be $P = 2n\hbar\omega_c/c$, hence the radiation pressure force acting on the movable mirror would be $F = P/t = n\hbar\frac{\omega_c}{L}$. The force is proportional to the instantaneous photon number in the cavity. Moreover, the movable mirror is in thermal equilibrium with its environment at temperature T. Thus the mirror can move under the influence of the radiation pressure and in the same time undergoes Brownian motion as a result of its interaction with the environment. In turn, the movable mirror's small oscillation changes the length of the cavity and shifts the cavity resonance frequency so that the phase and amplitude of the cavity field are changed. This in turn changes the radiation pressure force experienced by the mirror such that the optical and mechanical dynamics are coupled. Thus the cavity resonance frequency depends on the displacement q of the movable mirror, represented by $\omega_c(q) = \frac{n\pi c}{L+q}$, where n is the mode number in the cavity, c is the light speed in vacuum, L is the initial cavity length. For small displacements of the mirror, $q << L$, the frequency $\omega_c(q)$ can be approximated to the first order of q

$$\omega_c(q) \approx \omega_c + gq, \tag{1.1}$$

where $\omega_c = \frac{n\pi c}{L}$, $g = -\omega_c/L$ is the linear coupling constant between the cavity field and the movable mirror, the minus sign in g implies that the cavity resonance frequency decreases when increasing the displacement q of the mirror elongates the cavity.

What we discussed previously is the linear optomechanical coupling case, i.e., the frequency shift of the cavity field depends linearly on the displacement of the

mechanical oscillator. However, in a Fabry Perot cavity with a vibrating membrane in the middle of the optical cavity [10, 11, 12, 13], if the membrane is positioned at an antinode of the intracavity standing wave, the optomechanical coupling is quadratic i.e., the frequency shift of the cavity field depends quadratically on the displacement of the mechanical oscillator. If we expand the cavity frequency $\omega_c(q)$ about the antinode point q_0, then

$$\begin{aligned} \omega_c(q) &= \omega_c(q_0) + \frac{\partial \omega_c(q)}{\partial q}\Big|_{q=q_0} q + \frac{1}{2}\frac{\partial^2 \omega_c(q)}{\partial q^2}\Big|_{q=q_0} q^2 + \cdots \\ &\approx \omega_c(q_0) + \frac{1}{2}\frac{\partial^2 \omega_c(q)}{\partial q^2}\Big|_{q=q_0} q^2, \end{aligned} \tag{1.2}$$

since at the antinode $\frac{\partial \omega_c(q)}{\partial q}\Big|_{q_0} = 0$. Compared to the linear optomechanical coupling system, the quadratic optomechanical system has the advantage in the quantum nondemolition measurement of mechanical energy quantization [10, 11, 12].

Note that the cavity decay rate only depends on the transmission of the fixed mirror, and is unrelated to the mechanical motion. Therefore, the optomechanical coupling via radiation pressure is dispersive.

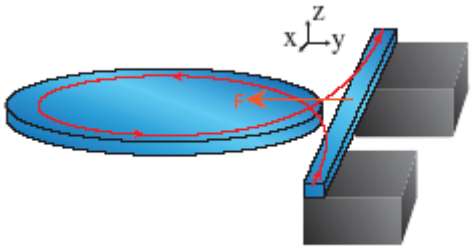

Figure 1.2: The optomechaical system that consists of a microdisk resonator coupled to a waveguide (from Ref.[67]).

1.1.3 The Reactive Optomechanical System

In other optomechanical devices, the optomechanical coupling is induced by optical gradient force such as in silicon waveguide evanescently coupled to a microdisk

resonator [67], suspended silicon photonic waveguides [68, 69], SiN nanowire evanescently coupled to a microtoroidal resonator [70], and in "zipper" cavities formed by two adjacent photonic crystal wires [71]. In this thesis, we focus on the optomechanical design proposed by [67], as shown in Fig. 1.2. The freestanding silicon waveguide with 10 μm length, 300 nm height, and 300 nm width is supported by two single-sided photonic crystal waveguide structures. The microdisk resonator with a radius of 40 μm is placed in close to the waveguide with a gap of 250 nm. A laser is injected into the waveguide, then light is coupled into and out of the microdisk through the evanescent fields from the waveguide and microdisk in the air gap, which decay exponentially with the distance from their geometric boundaries. And the dipoles in the waveguide induced by the evanescent field from the microdisk in turn interacts with the evanescent field from the microdisk and generate a gradient optical force. Under the action of this force, the waveguide is attracted toward the microdisk. Further the displacement of the waveguide modifies the resonance frequency of the microdisk resonator and the extrinsic photon decay rate of the microdisk resonator. Thus the coupling between the waveguide and the microdisk resonator is dispersive and reactive.

1.2 Sideband Cooling of the Nano Mechanical Mirror

Recent experiments have demonstrated that the mechanical mirror can be cooled by the dynamical back-action of radiation pressure [7, 8, 9]. And it is possible to cool the mechanical mirror to the quantum ground state by resolved sideband cooling as first shown theoretically in Refs. [47, 66]. Sideband cooling was demonstrated experimentally by Kippenberg [57] and by Wang [58]. Both these experiments started the system at about 1.5K and showed cooling down to about 200 mK. The amount of cooling depends on the system parameters and the laser power. Harris et. al. has shown that the lowest temperature achieved is 6.82 mK in an optical cavity with a

vibrating membrane [10].

Before we give details of the theoretical discussion of sideband cooling, we discuss the physics which shows why sideband cooling results in cooling. When the pump field with frequency ω_l interacts with the mechanical mirror with frequency ω_m, absorption and emission of phonons create the Stokes field $(\omega_l + \omega_m)$ and the anti-Stokes field $(\omega_l - \omega_m)$. During the Stokes process, the pump field extracts a quantum of energy $\hbar\omega_m$ from the movable mirror, leading to the cooling of the movable mirror. While during the anti-Stokes process, the pump field emits a quantum of energy $\hbar\omega_m$ to the movable mirror, leading to the heating of the movable mirror. If the pump frequency is detuned below the cavity resonance frequency by an amount ω_m, the amplitude of the Stokes field is resonantly enhanced, since the frequency of the Stokes field is close to the cavity resonance frequency ω_c; however, the anti-Stokes field is suppressed since its frequency is far away from the cavity resonance frequency, thus the optomechanical coupling causes the cooling of the mirror. Further in the resolved sideband limit, the cavity amplitude decay rate κ is much less than the mechanical oscillation frequency ω_m. In this case, the linewidth κ of the cavity field is much smaller than the frequency spacing $2\omega_m$ between the Stokes field and the anti-Stokes field, thus the amplitude of the anti-Stokes field is close to zero, ground state cooling becomes possible.

We now develop the theoretical treatment of sideband cooling. The studied system is a Fabry-Perot cavity with one fixed partially transmitting mirror and one movable totally reflecting mirror of effective mass m and damping rate γ_m, as shown in Fig. 1.1. The Hamiltonian of the system in a rotating frame with respect to the laser frequency ω_l is given by

$$H = \hbar(\omega_c - \omega_l)c^\dagger c - \hbar\omega_m \chi c^\dagger c Q + \frac{\hbar\omega_m}{4}(Q^2 + P^2) + i\hbar\varepsilon(c^\dagger - c). \qquad (1.3)$$

In Eq. (1.3), the first term is the energy of the cavity field, c and $c^\dagger$ are the annihilation and creation operators for the cavity field satisfying the commutation relation $[c, c^\dagger] = 1$. The second term describes the interaction of the movable mirror with

the cavity field, the dimensionless parameter $\chi = \frac{1}{\omega_m}\frac{\omega_c}{L}\sqrt{\frac{\hbar}{2m\omega_m}}$ is the optomechanical coupling constant between the cavity and the movable mirror. The third term gives the energy of the movable mirror, described by the dimensionless position and momentum operators Q and P, defined by $Q = \sqrt{\frac{2m\omega_m}{\hbar}}q$ and $P = \sqrt{\frac{2}{m\hbar\omega_m}}p$ with commutation relation $[Q, P] = 2i$. The fourth term describes the cavity driven by a laser with power $\wp$, and $\varepsilon = \sqrt{\frac{2\kappa\wp}{\hbar\omega_l}}$.

The time evolution of the system operators can be derived by using the Heisenberg equations of motion and adding the corresponding damping and noise terms. We find a set of nonlinear quantum Langevin equations as follows,

$$\begin{aligned}
\dot{Q} &= \omega_m P, \\
\dot{P} &= 2\omega_m \chi c^\dagger c - \omega_m Q - \gamma_m P + \xi, \\
\dot{c} &= -i(\omega_c - \omega_l - \omega_m \chi Q)c + \varepsilon - \kappa c + \sqrt{2\kappa}c_{in}, \\
\dot{c}^\dagger &= i(\omega_c - \omega_l - \omega_m \chi Q)c^\dagger + \varepsilon - \kappa c^\dagger + \sqrt{2\kappa}c_{in}^\dagger.
\end{aligned} \tag{1.4}$$

Here c_{in} is the input vacuum noise operator with zero mean value and nonzero correlation function in the time domain

$$\langle \delta c_{in}(t)\delta c_{in}^\dagger(t')\rangle = \delta(t - t'). \tag{1.5}$$

The force ξ is the Brownian noise operator associated with the mechanical damping, whose mean value is zero, and its correlation function reads

$$\langle \xi(t)\xi(t')\rangle = \frac{1}{\pi}\frac{\gamma_m}{\omega_m}\int \omega e^{-i\omega(t-t')}\left[1 + \coth(\frac{\hbar\omega}{2k_B T})\right]d\omega, \tag{1.6}$$

where k_B is the Boltzmann constant and T is the thermal bath temperature. The steady-state solution to Eq. (1.4) can be obtained by setting all the time derivatives in Eq. (1.4) to zero. They are

$$P_s = 0,\ Q_s = 2\chi|c_s|^2,\ c_s = \frac{\varepsilon}{\kappa + i\Delta}, \tag{1.7}$$

where

$$\Delta = \omega_c - \omega_l - \omega_m \chi Q_s \tag{1.8}$$

is the effective cavity detuning, in which the term $-\omega_m \chi Q_s$ is the cavity resonance frequency shift due to radiation pressure. The Q_s denotes the steady-state position of the movable mirror. And c_s represents the steady-state amplitude of the cavity field.

In order to investigate cooling of the movable mirror, we need to calculate the fluctuations of the system. We linearize the nonlinear equation (1.4) by writing each operator of the system as the sum of its steady-state mean value and a small fluctuation with zero mean value,

$$Q = Q_s + \delta Q, \quad P = P_s + \delta P, \quad c = c_s + \delta c. \tag{1.9}$$

Inserting Eq. (1.9) into Eq. (1.4), then assuming $|c_s| \gg 1$, the linearized quantum Langevin equations for the fluctuation operators take the form

$$\begin{aligned}
\delta\dot{Q} &= \omega_m \delta P, \\
\delta\dot{P} &= 2\omega_m \chi (c_s^* \delta c + c_s \delta c^\dagger) - \omega_m \delta Q - \gamma_m \delta P + \xi, \\
\delta\dot{c} &= -(\kappa + i\Delta)\delta c + i\omega_m \chi c_s \delta Q + \sqrt{2\kappa}\delta c_{in}, \\
\delta\dot{c}^\dagger &= -(\kappa - i\Delta)\delta c^\dagger - i\omega_m \chi c_s^* \delta Q + \sqrt{2\kappa}\delta c_{in}^\dagger.
\end{aligned} \tag{1.10}$$

We transform Eq. (1.10) to the frequency domain by using $f(t) = \frac{1}{2\pi}\int_{-\infty}^{+\infty} f(\omega) e^{-i\omega t} d\omega$ and $f^\dagger(t) = \frac{1}{2\pi}\int_{-\infty}^{+\infty} f^\dagger(-\omega) e^{-i\omega t} d\omega$, where $f^\dagger(-\omega) = [f(-\omega)]^\dagger$, and solve it, we obtain the position fluctuations of the movable mirror

$$\begin{aligned}
\delta Q(\omega) = -\tfrac{\omega_m}{d(\omega)}[2\sqrt{2\kappa}\omega_m \chi \{[\kappa - i(\Delta + \omega)] c_s^* \delta c_{in}(\omega) + [\kappa + i(\Delta - \omega)] c_s \delta c_{in}^\dagger(-\omega)\} \\
+ [(\kappa - i\omega)^2 + \Delta^2]\xi(\omega)],
\end{aligned} \tag{1.11}$$

where

$$d(\omega) = 4\omega_m^3 \chi^2 \Delta |c_s|^2 + (\omega^2 - \omega_m^2 + i\gamma_m \omega)[(\kappa - i\omega)^2 + \Delta^2]. \tag{1.12}$$

In Eq. (1.11), the first term proportional to χ is the contribution of radiation pressure, while the second term involving $\xi(\omega)$ is the contribution of the thermal noise. In the absence of the cavity field, the movable mirror will make Brownian motion, $\delta Q(\omega) = \omega_m \xi(\omega)/(\omega_m^2 - \omega^2 - i\gamma_m\omega)$, whose susceptibility has a Lorentzian shape centered at frequency ω_m with full width at half maximum γ_m.

The two-time correlation function of the fluctuations in position of the movable mirror is given by

$$\frac{1}{2}(\langle \delta Q(t)\delta Q(t+\tau)\rangle + \langle \delta Q(t+\tau)\delta Q(t)\rangle) = \frac{1}{2\pi}\int_{-\infty}^{+\infty} \mathrm{d}\omega S_Q(\omega)\mathrm{e}^{\mathrm{i}\omega\tau}, \tag{1.13}$$

in which $S_Q(\omega)$ is the spectrum of fluctuations in position of the movable mirror, defined by

$$\frac{1}{2}(\langle \delta Q(\omega)\delta Q(\Omega)\rangle + \langle \delta Q(\Omega)\delta Q(\omega)\rangle) = 2\pi S_Q(\omega)\delta(\omega+\Omega). \tag{1.14}$$

By aid of the correlation functions of the noise sources in the frequency domain,

$$\begin{aligned} &\langle \delta c_{in}(\omega)\delta c_{in}^{\dagger}(-\Omega)\rangle = 2\pi\delta(\omega+\Omega), \\ &\langle \xi(\omega)\xi(\Omega)\rangle = 4\pi\tfrac{\gamma_m}{\omega_m}\omega\left[1+\coth(\tfrac{\hbar\omega}{2k_BT})\right]\delta(\omega+\Omega). \end{aligned} \tag{1.15}$$

we obtain the spectrum of fluctuations in position of the movable mirror

$$\begin{aligned} S_Q(\omega) &= \frac{\omega_m^2}{|d(\omega)|^2}\{8\omega_m^2\chi^2\kappa(\kappa^2+\omega^2+\Delta^2)|c_s|^2 + 2\frac{\gamma_m}{\omega_m}\omega[(\Delta^2+\kappa^2-\omega^2)^2 \\ &\quad +4\kappa^2\omega^2]\coth(\frac{\hbar\omega}{2k_BT})\}. \end{aligned} \tag{1.16}$$

In Eq. (1.16), the first term involving χ arises from radiation pressure, while the second term originates from the thermal noise. So the spectrum $S_Q(\omega)$ of the movable mirror depends on radiation pressure and the thermal noise. Then Fourier transforming $\delta\dot{Q} = \omega_m\delta P$ in Eq. (1.10), we obtain $\delta P(\omega) = -\frac{\mathrm{i}\omega}{\omega_m}\delta Q(\omega)$, which leads to the spectrum of fluctuations in momentum of the movable mirror

$$S_P(\omega) = \frac{\omega^2}{\omega_m^2}S_Q(\omega). \tag{1.17}$$

The phonon number n in the movable mirror can be calculated from the total energy of the movable mirror

$$\frac{\hbar\omega_m}{4}(\langle\delta Q^2\rangle + \langle\delta P^2\rangle) = \hbar\omega_m\left(n+\frac{1}{2}\right),\ n = [\exp(\hbar\omega_m/(k_BT)) - 1]^{-1}, \tag{1.18}$$

where the variances of position and momentum are $\langle\delta Q^2\rangle = \frac{1}{2\pi}\int_{-\infty}^{+\infty} S_Q(\omega)\mathrm{d}\omega$ and $\langle\delta P^2\rangle = \frac{1}{2\pi}\int_{-\infty}^{+\infty} S_P(\omega)\mathrm{d}\omega$. Then the effective temperature T_{eff} of the movable mirror can be determined from the phonon number $n$in the movable mirror, which is

$$T_{eff} = \frac{\hbar\omega_m}{k_B\ln(1+\frac{1}{n})}. \tag{1.19}$$

The parameters used are from an experimental paper on optomechanical normal mode splitting [50]: the wavelength of the laser $\lambda = 2\pi c/\omega_l = 1064$ nm, $L = 25$ mm, $m = 145$ ng, $\omega_m = 2\pi\times 947\times 10^3$ Hz, the mechanical quality factor $Q^{'} = \omega_m/\gamma_m = 6700$, $\kappa = 2\pi\times 215\times 10^3$ Hz, $\kappa/\omega_m \approx 0.23$, thus the system is operating in resolved sideband regime. And in the high temperature limit $k_BT \gg \hbar\omega_m$, the approximation $\coth(\hbar\omega/2k_BT) \approx 2k_BT/\hbar\omega$ can be made. The laser is detuned below the cavity resonance frequency by an amount $\Delta = \omega_m$. We work in the stable regime.

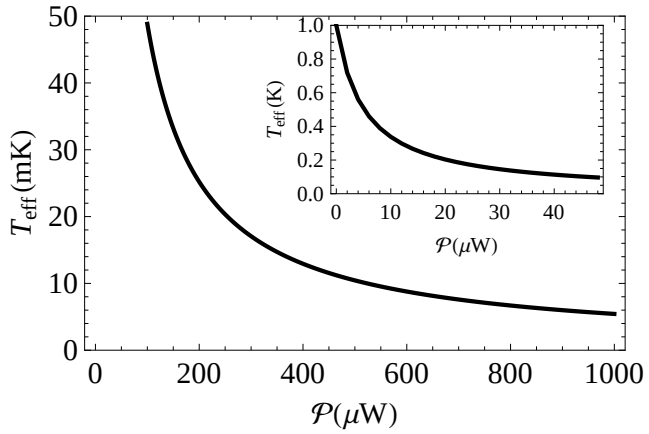

Figure 1.3: The effective temperature T_{eff} (mK) of the movable mirror as a function of the laser power $\wp$ (μW). The initial temperature is taken to be 1 K.

Figure 1.3 shows the variation of the effective temperature T_{eff} of the movable mirror with the laser power $\wp$. It is clear to see that the effective temperature T_{eff} of

the movable mirror decreases with increases the laser power $\wp$. When $\wp = 100$ μW, the movable mirror can be cooled to about 50 mK, a factor of 20 below the starting temperature of 1 K [57, 58]. If the laser power is further increased to 1 mW, the movable mirror can be cooled to about 6 mK. Therefore the movable mirror can be effectively cooled in the resolved sideband limit.

1.3 Degenerate Parametric Amplification

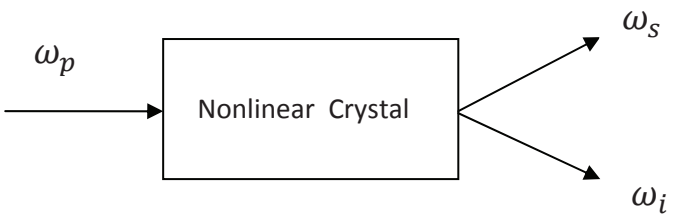

Figure 1.4: Parametric amplifier.

In a parametric amplifier [72], a pump beam at higher frequency ω_p interacts with a nonlinear crystal, a signal and idler modes at lower frequencies ω_s and ω_i would be generated, as shown in Fig. 1.4. During the nonlinear optical process, the energy is conserved $\omega_p = \omega_s + \omega_i$. If the signal and the idler modes have identical frequencies, such a parametric amplifier is called a degenerate parametric amplifier. In the following, we will show that the degenerate parametric amplifier can be used as a generator of a single-mode squeezed state.

The Hamiltonian for degenerate parametric amplification, in the interaction picture, is

$$H_{int} = \hbar\mu(a^{\dagger 2}b + a^2 b^\dagger), \tag{1.20}$$

where b and a are the annihilation operators for the pump and signal modes, respectively, and μ is a coupling strength between the pump field and the nonlinear crystal, and it is related to the second-order nonlinear susceptibility. Assuming that

the pump field is a strong coherent classical field and pump depletion is neglected, thus the operators b and $b^\dagger$ can be represented by $\beta e^{-i\phi}$ and $\beta e^{i\phi}$, where β and ϕ are the real amplitude and phase of the coherent pump field. Hence the Hamiltonian (1.20) becomes

$$H_{int} = \hbar\mu\beta(a^{\dagger 2}e^{-i\phi} + a^2 e^{i\phi}), \tag{1.21}$$

The time evolution of the signal mode can be derived by the Heisenberg equation of motion, which yields

$$\begin{aligned} \dot{a} &= -i\Omega a^\dagger e^{-i\phi}, \\ \dot{a}^\dagger &= i\Omega a e^{i\phi}. \end{aligned} \tag{1.22}$$

Here $\Omega = 2\mu\beta$ is the effective Rabi frequency. The solution to Eq. (1.22) is

$$\begin{aligned} a(t) &= a_0 \cosh(\Omega t) - i a_0^\dagger \sinh(\Omega t) e^{-i\phi}, \\ a^\dagger(t) &= a_0^\dagger \cosh(\Omega t) + i a_0 \sinh(\Omega t) e^{i\phi}, \end{aligned} \tag{1.23}$$

where $a_0 = a(0)$. For $\phi = \pi/2$, when the signal initially is in a vacuum state, the variances in the two quadratures $X_1 = (a + a^\dagger)/2$ and $X_2 = (a - a^\dagger)/2i$ are given by

$$\begin{aligned} (\Delta X_1)_t^2 &= \frac{1}{4}e^{-2u}, \\ (\Delta X_2)_t^2 &= \frac{1}{4}e^{2u}, \end{aligned} \tag{1.24}$$

where $u = \Omega t$ is the effective squeezing parameter. Eq. (1.24) shows the output from the degenerate parametric amplifier can be squeezed state, and the squeezing exists in the X_1 quadrature.

1.4 Standard Quantum Limit

For a one-dimensional harmonic oscillator with mass m and frequency ω_m, its Hamiltonian is $H_0 = \frac{p^2}{2m} + \frac{1}{2}m\omega_m^2 q^2$, where p is the momentum operator and q is the position operator, satisfying the commutation relation $[q, p] = i\hbar$. In the ground state, the

fluctuations in the position and the momentum are not equal to zero due to the zero-point energy. They are

$$\delta q = \sqrt{\frac{\hbar}{2m\omega_m}}, \delta p = \sqrt{\frac{m\hbar\omega_m}{2}}, \tag{1.25}$$

respectively, which are called the standard quantum limit. These fluctuations have no classical analog. If we write the position operator q and the momentum operator p in terms of the dimensionless position operator Q and momentum operator P, $q = \sqrt{\frac{\hbar}{2m\omega_m}}Q$ and $p = \sqrt{\frac{m\hbar\omega_m}{2}}P$, then the standard quantum limit would be

$$\delta Q = \delta P = 1, \tag{1.26}$$

thus the fluctuations in the two dimensionless quadratures are identical, each of them is equal to unity. For very high-precision interferometers, the standard quantum limit limits their sensitivity. To improve their sensitivity, this limit need to be beaten, which means that the fluctuations need to be reduced below the standard quantum limit. According to the Heisenberg uncertainty principle $\Delta A \Delta B \geq \frac{1}{2}|\langle [A, B]\rangle|$, where $\Delta A = (\langle A^2\rangle - \langle A\rangle^2)^{1/2}$ and similarly for ΔB, the fluctuations in position and momentum should satisfy the inequality

$$\delta Q \delta P \geq 1, \tag{1.27}$$

thus the fluctuations in the position and momentum could not be reduced below unity simultaneously. If the fluctuations in position is less than unity, the fluctuations in momentum should be larger than unity, or vice versa. Moreover, the harmonic oscillator is said to be squeezed if either $\delta Q < 1$ or $\delta P < 1$. Therefore, as the standard quantum limit is beaten, the harmonic oscillator is quadrature squeezed.

1.5 Homodyne Detection

Homodyne detection is usually used to measure the amplitude and the phase quadrature components of the light field. In this section, we describe balanced homodyne detection [73].

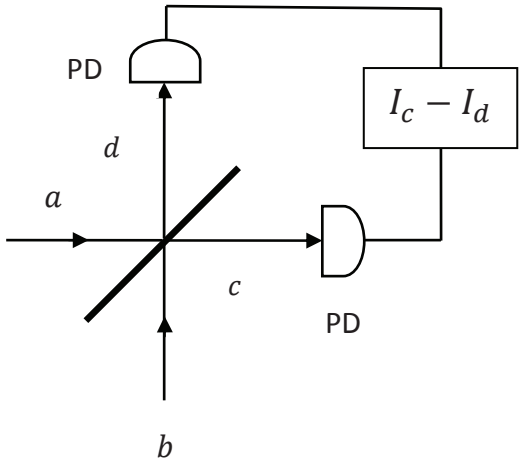

Figure 1.5: Balanced homodyne detection. PD:photodetector.

Figure 1.5 schematically shows a balanced homodyne detection setup. The signal light and a strong local laser light, described by the annihilation operators a and b, respectively, are mixed on a 50/50 beam splitter. The two output fields c and d can be obtained through the relation

$$\begin{aligned} c &= \frac{1}{\sqrt{2}}(a+ib), \\ d &= \frac{1}{\sqrt{2}}(b+ia). \end{aligned} \tag{1.28}$$

The two output fields c and d are detected individually by two photodetectors. Then the two intensities $I_c = \langle c^\dagger c\rangle$ and $I_d = \langle d^\dagger d\rangle$ measured by the two photodetectors are subtracted each other, the result is

$$\begin{aligned} I_c - I_d &= \langle n_{cd}\rangle = \langle c^\dagger c - d^\dagger d\rangle, \\ &= i\langle a^\dagger b - a b^\dagger\rangle. \end{aligned} \tag{1.29}$$

Assuming the b mode to be in the coherent state $|\beta e^{-i\omega t}\rangle$, and $\beta = |\beta|e^{-i\psi}$, the operator b can be replaced by $|\beta|e^{-i(\omega t+\psi)}$, we obtain

$$\langle n_{cd}\rangle = |\beta|[a e^{i\omega t}e^{-i\theta} + a^\dagger e^{-i\omega t}e^{i\theta}], \tag{1.30}$$

where $\theta = \psi + \pi/2$. Assuming that the signal mode a has the same frequency as that of the local oscillator b, thus $a = a_0 e^{-i\omega t}$, Eq. (1.30) reduces to

$$\langle n_{cd} \rangle = 2|\beta|\langle X(\theta) \rangle, \tag{1.31}$$

where $\langle X(\theta) \rangle = \frac{1}{2}(a_0 e^{-i\theta} + a_0 e^{i\theta})$ is the field quadrature operator at the angle θ. By changing θ, which can be done by changing the phase ψ of the local oscillator, an arbitrary quadrature component of the signal field can be measured.

Moreover, the balanced homodyne detection can be used to detect the squeezed state. The variance of the output signal can be found to be

$$\langle (\Delta n_{cd})^2 \rangle = 4|\beta|^2 \langle (\Delta X(\theta))^2 \rangle, \tag{1.32}$$

The squeezing condition for the signal is $\langle (\Delta X(\theta))^2 \rangle < \frac{1}{4}$, we have $\langle (\Delta n_{cd})^2 \rangle < |\beta|^2$.

1.6 Electromagnetically Induced Transparency

Generally, if a laser light passes through a two-level atomic system whose atoms are all in the ground state, the light will be strongly absorbed if the laser field is near resonant with the atomic transition. However, for a three-level atomic system whose atoms are all in the lowest-energy state, the atomic system becomes transparent for a weak probe field tuned to an atomic transition resonance when a strong coupling field is applied to the other atomic transition. This phenomenon is called as electromagnetically induced transparency (EIT). The effect of EIT allows a weak signal field to propagate without being absorbed by the atomic medium. It was theoretically proposed in 1989 [74] and first experimentally demonstrated in 1991 [75]. Meanwhile, the phenomenon of EIT [76] is accompanied by a sharp dispersion change in the transmitted probe field on resonance, which leads to the generation of ultrafast light [77, 78] and ultraslow light [79, 80, 81]. Accordingly considerable interest has been dedicated to EIT due to its potential applications in an optical switch [82], optical storage [83, 84, 85, 86].

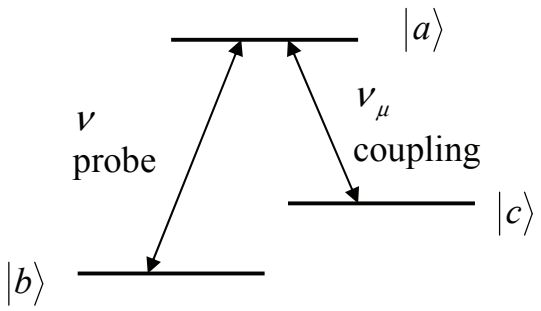

Figure 1.6: A three-level Λ-type atomic system, where the probe field at frequency ν couples levels $|b\rangle$ and $|a\rangle$, while the coupling field at frequency ν_μ couples levels $|c\rangle$ and $|a\rangle$.

We consider a three-level Λ-type atomic system [72], as shown in Fig. 1.6. The atoms have one upper level $|a\rangle$ and two lower levels $|b\rangle$ and $|c\rangle$ with energies $\hbar\omega_a$, $\hbar\omega_b$, and $\hbar\omega_c$, where the transitions $|b\rangle \rightarrow |a\rangle$ and $|c\rangle \rightarrow |a\rangle$ are dipole allowed, but the transition $|b\rangle \rightarrow |c\rangle$ is dipole forbidden since $|c\rangle$ is a metastable state. The levels $|a\rangle$ and $|b\rangle$ are coupled by a weak probe field of amplitude ε at frequency ν, while the levels $|a\rangle$ and $|c\rangle$ are coupled by a strong coupling field at frequency ν_μ. The coupling strength of the probe field to the atomic transition $|b\rangle \rightarrow |a\rangle$ is described by the Rabi frequency $\wp_{ab}\varepsilon/\hbar$, where $\wp_{ab}$ is the electric-dipole transition matrix element, and it is assumed to be real. The interaction strength between the coupling field and the $|c\rangle \rightarrow |a\rangle$ transition is characterized by the complex Rabi frequency $\Omega_\mu \exp(-i\phi_\mu)$, and Ω_μ is assumed to be real.

The state of the atom can be written as a linear combination of states $|a\rangle$, $|b\rangle$, and $|c\rangle$, i.e., $|\Psi\rangle = C_a(t)|a\rangle + C_b(t)|b\rangle + C_c(t)|c\rangle$. Here, $C_a(t)$, $C_b(t)$, and $C_c(t)$ are the probability amplitudes corresponding to the three atomic levels $|a\rangle$, $|b\rangle$, and $|c\rangle$, respectively. The density matrix operator of the atom takes form

$$\begin{aligned}\rho &= |\Psi\rangle\langle\Psi| \\ &= [C_a(t)|a\rangle + C_b(t)|b\rangle + C_c(t)|c\rangle][C_a^*(t)\langle a| + C_b^*(t)\langle b| + C_c^*(t)\langle c|]\end{aligned}$$

$$
\begin{aligned}
= \; & |C_a(t)|^2|a\rangle\langle a| + C_a(t)C_b^*(t)|a\rangle\langle b| + C_a(t)C_c^*(t)|a\rangle\langle c| \\
& + C_b(t)C_a^*(t)|b\rangle\langle a| + |C_b(t)|^2|b\rangle\langle b| + C_b(t)C_c^*(t)|b\rangle\langle c| \\
& + C_c(t)C_a^*(t)|c\rangle\langle a| + C_c(t)C_b^*(t)|c\rangle\langle b| + |C_c(t)|^2|c\rangle\langle c|. \qquad (1.33)
\end{aligned}
$$

Taking the matrix elements, we get

$$
\begin{aligned}
\rho_{aa} &= \langle a|\rho|a\rangle = |C_a(t)|^2, \\
\rho_{ab} &= \langle a|\rho|b\rangle = C_a(t)C_b^*(t), \\
\rho_{ac} &= \langle a|\rho|c\rangle = C_a(t)C_c^*(t), \\
\rho_{ba} &= \langle b|\rho|a\rangle = C_b(t)C_a^*(t), \\
\rho_{bb} &= \langle b|\rho|b\rangle = |C_b(t)|^2, \\
\rho_{bc} &= \langle b|\rho|c\rangle = C_b(t)C_c^*(t), \\
\rho_{ca} &= \langle c|\rho|a\rangle = C_c(t)C_a^*(t), \\
\rho_{cb} &= \langle c|\rho|b\rangle = C_c(t)C_b^*(t), \\
\rho_{cc} &= \langle c|\rho|c\rangle = |C_c(t)|^2. \qquad (1.34)
\end{aligned}
$$

Hence, the three-level atom can be described by the 3×3 density matrix ρ,

$$
\rho = \begin{pmatrix} \rho_{aa} & \rho_{ab} & \rho_{ac} \\ \rho_{ba} & \rho_{bb} & \rho_{bc} \\ \rho_{ca} & \rho_{cb} & \rho_{cc} \end{pmatrix}, \qquad (1.35)
$$

where the diagonal elements $\rho_{ii} = \langle i|\rho|i\rangle$ $(i = a, b, c)$ describe the populations in the three levels, respectively, and the off-diagonal elements $\rho_{ij} = \langle i|\rho|j\rangle$ $(i, j = a, b, c$ and $i \neq j)$ represent the atomic coherence between levels. The density matrix is a Hermitian operator satisfying $\rho = \rho^\dagger$.The off-diagonal decay rates for ρ_{ab}, ρ_{ac}, and ρ_{cb} are denoted by γ_1, γ_2, and γ_3, respectively. Since the level $|c\rangle$ is assumed to be a metastable state, $\gamma_3 << \gamma_1$.

In the rotating-wave approximation, the Hamiltonian of the system is given by

$$
H = \hbar\omega_a|a\rangle\langle a| + \hbar\omega_b|b\rangle\langle b| + \hbar\omega_c|c\rangle\langle c|
$$

$$+[-\frac{\hbar}{2}(\frac{\wp_{ab}\mathcal{E}}{\hbar}e^{-i\nu t}|a\rangle\langle b|+\Omega_\mu e^{-i\phi_\mu}e^{-i\nu_\mu t}|a\rangle\langle c|)+H.C.], \tag{1.36}$$

where the first three terms are the free energies of the atomic three levels, and the last four terms gives the interactions of the three-level atoms with the probe field and the coupling field.

The time evolution for the density matrix elements ρ_{ab}, ρ_{cb}, and ρ_{ac} can be derived by using the Liouville equation $\dot{\rho}_{ij}=-\frac{i}{\hbar}[H,\rho_{ij}]$ and considering the corresponding damping term, which yields

$$\begin{aligned}
\dot{\rho}_{ab} &= -(i\omega_{ab}+\gamma_1)\rho_{ab}-\frac{i}{2}\frac{\wp_{ab}\mathcal{E}}{\hbar}e^{-i\nu t}(\rho_{aa}-\rho_{bb})+\frac{i}{2}\Omega_\mu e^{-i\phi_\mu}e^{-i\nu_\mu t}\rho_{cb},\\
\dot{\rho}_{cb} &= -(i\omega_{cb}+\gamma_3)\rho_{cb}-\frac{i}{2}\frac{\wp_{ab}\mathcal{E}}{\hbar}e^{-i\nu t}\rho_{ca}+\frac{i}{2}\Omega_\mu e^{i\phi_\mu}e^{i\nu_\mu t}\rho_{ab},\\
\dot{\rho}_{ac} &= -(i\omega_{ac}+\gamma_2)\rho_{ac}-\frac{i}{2}\Omega_\mu e^{-i\phi_\mu}e^{-i\nu_\mu t}(\rho_{aa}-\rho_{cc})+\frac{i}{2}\frac{\wp_{ab}\mathcal{E}}{\hbar}e^{-i\nu t}\rho_{bc},
\end{aligned} \tag{1.37}$$

where ω_{ab}, ω_{cb}, and ω_{ac} are the Bohr frequencies, $\omega_{ab}=\omega_a-\omega_b$, $\omega_{cb}=\omega_c-\omega_b$, and $\omega_{ac}=\omega_a-\omega_c$. We assume all atoms are initially in the lowest-energy state $|b\rangle$,

$$\rho_{bb}(0)=1,\ \rho_{aa}(0)=\rho_{cc}(0)=\rho_{ac}(0)=0. \tag{1.38}$$

Since the probe field is very weak, most of the atoms keep staying in the lowest-energy state $|b\rangle$ at any time so that the atomic population in level $|b\rangle$ is close to unity. Thus we can adopt the approximation condition

$$\rho_{bb}(t)\approx 1,\ \rho_{aa}(t)\approx\rho_{cc}(t)\approx\rho_{ac}(t)\approx 0. \tag{1.39}$$

Thus Eq. (1.37) reduces to

$$\begin{aligned}
\dot{\rho}_{ab} &= -(i\omega_{ab}+\gamma_1)\rho_{ab}+\frac{i}{2}\frac{\wp_{ab}\mathcal{E}}{\hbar}e^{-i\nu t}+\frac{i}{2}\Omega_\mu e^{-i\phi_\mu}e^{-i\nu_\mu t}\rho_{cb},\\
\dot{\rho}_{cb} &= -(i\omega_{cb}+\gamma_3)\rho_{cb}+\frac{i}{2}\Omega_\mu e^{i\phi_\mu}e^{i\nu_\mu t}\rho_{ab}.
\end{aligned} \tag{1.40}$$

Then we convert the usual density-matrix elements ρ_{ij} to slowly varying variables $\tilde{\rho}_{ij}$ in order to remove the fast optical oscillation by using the following transformations

$$\begin{aligned}
\rho_{ab} &= \tilde{\rho}_{ab}e^{-i\nu t},\\
\rho_{cb} &= \tilde{\rho}_{cb}e^{-i(\nu+\omega_{ca})t},
\end{aligned} \tag{1.41}$$

thus the time evolution of the slowly varying density-matrix elements $\tilde{\rho}_{ab}$ and $\tilde{\rho}_{cb}$ is given by

$$\begin{aligned}\dot{\tilde{\rho}}_{ab} &= -(\gamma_1 - i\Delta)\tilde{\rho}_{ab} + \frac{i}{2}\frac{\wp_{ab}\mathcal{E}}{\hbar} + \frac{i}{2}\Omega_\mu e^{-i\phi_\mu}\tilde{\rho}_{cb}, \\ \dot{\tilde{\rho}}_{cb} &= -(\gamma_3 - i\Delta)\tilde{\rho}_{cb} + \frac{i}{2}\Omega_\mu e^{i\phi_\mu}\tilde{\rho}_{ab}, \end{aligned} \tag{1.42}$$

where $\Delta = \nu - \omega_{ab}$ is the detuning of the probe frequency ν from the frequency ω_{ab} of the $|b\rangle \rightarrow |a\rangle$ transition, and we assume that the coupling field is resonant with the $|c\rangle \rightarrow |a\rangle$ transition, i.e., $\nu_\mu = \omega_{ac}$.

We write Eq. (1.42) in the matrix form as

$$\dot{R} = -MR + A, \tag{1.43}$$

where

$$R = \begin{pmatrix} \tilde{\rho}_{ab} \\ \tilde{\rho}_{cb} \end{pmatrix}, \; M = \begin{pmatrix} \gamma_1 - i\Delta & -\frac{i}{2}\Omega_\mu e^{-i\phi_\mu} \\ -\frac{i}{2}\Omega_\mu e^{i\phi_\mu} & \gamma_3 - i\Delta \end{pmatrix}, \; A = \begin{pmatrix} \frac{i\wp_{ab}\mathcal{E}}{2\hbar} \\ 0 \end{pmatrix}, \tag{1.44}$$

then integrating

$$\begin{aligned} R(t) &= \int_{-\infty}^{t} e^{-M(t-t')} A dt' \\ &= M^{-1}A, \end{aligned} \tag{1.45}$$

we obtain

$$\rho_{ab}(t) = \frac{i\wp_{ab}\mathcal{E}e^{-i\nu t}(\gamma_3 - i\Delta)}{2\hbar\Big[(\gamma_1 - i\Delta)(\gamma_3 - i\Delta) + \frac{\Omega_\mu^2}{4}\Big]}. \tag{1.46}$$

The dielectric response of the atomic system to the probe field is determined by the electric polarization P. The polarization of an ensemble of identical atoms will be $P = 2\wp_{ab}\rho_{ab}(t)e^{i\nu t}N_a$, where N_a is the atom number density for the three-level atoms. In addition, the linear polarization is related to the amplitude $\mathcal{E}$ of the probe field through $P = \epsilon_0\chi\mathcal{E}$, where ε_0 is the electric permittivity of free space and χ is the

electric susceptibility of the atomic system. Hence, the susceptibility of the Λ system is given by

$$\begin{aligned} \chi &= \frac{N_a \wp_{ab}^2}{\epsilon_0 \hbar} \frac{i(\gamma_3 - i\Delta)}{(\gamma_1 - i\Delta)(\gamma_3 - i\Delta) + \frac{\Omega_\mu^2}{4}}, \\ &= \chi' + i\chi'', \end{aligned} \tag{1.47}$$

where χ' and χ'' are the real and imaginary parts of the complex susceptibility χ of the atomic system. The χ' and χ'' determine the dispersion and absorption of the probe field, respectively. It is seen that from Eq. (1.47), on resonance, if there is a coupling field, i.e., $\Omega_\mu \neq 0$, $\chi' = 0$ and $\chi'' = \frac{N_a \wp_{ab}^2}{\epsilon_0 \hbar} \frac{\gamma_3}{\gamma_1 \gamma_3 + \frac{\Omega_\mu^2}{4}}$, which is proportional to γ_3. If the decay rate γ_3 is very small (or approaching zero), the imaginary part of the electric susceptibility would be negligibly small. We plot the real and imaginary parts of the susceptibility in units of $\frac{N_a \wp_{ab}^2}{\gamma_1 \epsilon_0 \hbar}$ as a function of the normalized detuning Δ/γ_1 without and with the coupling field, as shown in Figs. 1.7 and 1.8. In the

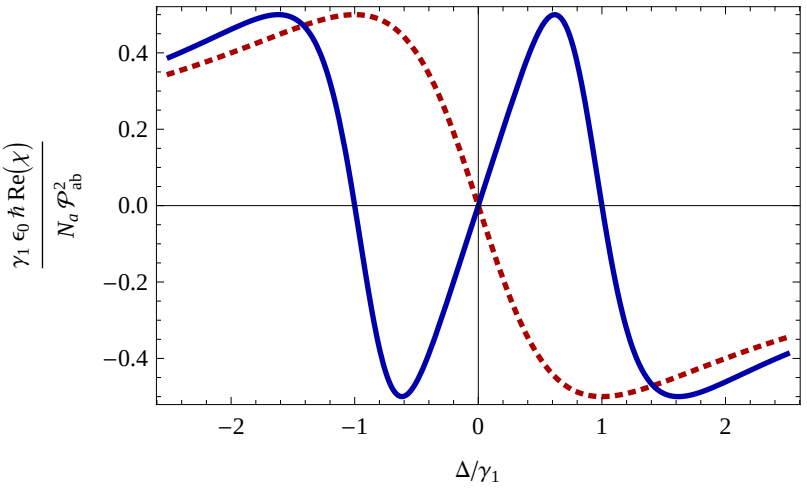

Figure 1.7: The real part of the susceptibility in units of $\frac{N_a \wp_{ab}^2}{\gamma_1 \epsilon_0 \hbar}$ as a function of the normalized detuning Δ/γ_1 in the absence (dotted) and in the presence (solid) of the coupling field.

absence of the coupling field, $\Omega_\mu = 0$, the curve χ'' has a Lorentzian lineshape, and the curve χ' exhibits the anomalous dispersion since the slope of χ' at the line center

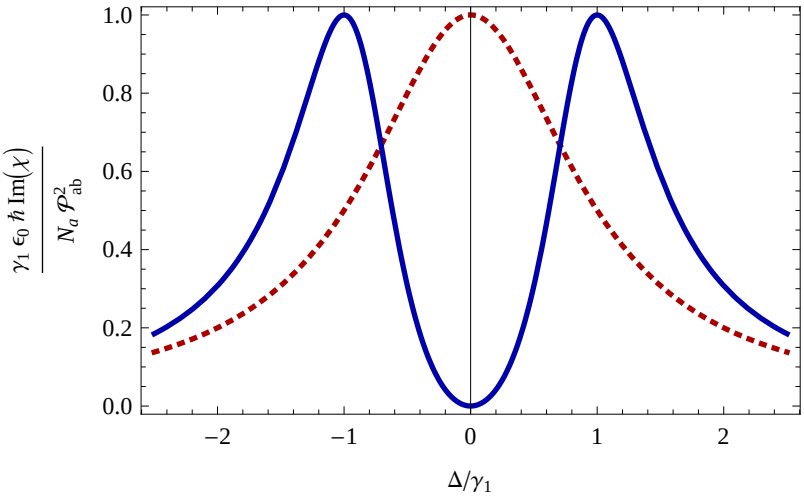

Figure 1.8: The imaginary part of the susceptibility in units of $\frac{N_a \wp_{ab}^2}{\gamma_1 \epsilon_0 \hbar}$ as a function of the normalized detuning Δ/γ_1 in the absence (dotted) and in the presence (solid) of the coupling field.

is less than zero. In the presence of the coupling field, $\Omega_\mu = 2\gamma_1$, and $\gamma_1 >> \gamma_3 (\gamma_3 = 10^{-4}\gamma_1)$, when $\Delta = 0$, $\omega_{ab} = \nu$, the probe field is in resonance with the $|b\rangle \rightarrow |a\rangle$ atomic transition, we can see $\chi'' \approx 0$, the medium becomes completely transparent for the probe field, thus the probe field can propagate through the atoms without any absorption even with most of the atoms in the lowest-energy state $|b\rangle$. It has been calculated that the width of the transparency window depends on the Rabi frequency Ω_μ, which is related to the power of the coupling field. And increasing the power of the coupling field, the EIT dip becomes wider due to power broadening. We also note $\chi' = 0$ as $\Delta = 0$, hence the refractive index of the medium is equal to unity since the refractive index is related to the susceptibility by $n(\nu) = [1 + \chi'(\nu) + i\chi''(\nu)]^{0.5}$. Thus the phase velocity of the probe field propagating through the medium is equal to that in vacuum. Moreover, the slope of the curve χ' at the line center is larger than zero, thus the curve χ' exhibits the normal dispersion. And the steepness of the curve χ' where the absorption vanishes depends on the power of the coupling field, i.e., the curve χ' becomes steeper at the line center by decreasing the power of the coupling

field, implying that the group velocity can be dramatically reduced, and even can be reduced to zero such that the probe field can be completely stopped and stored within the atomic medium.

In summary, when the coupling field resonant with the $|c\rangle \rightarrow |a\rangle$ atomic transition is applied, the interaction of a three-level Λ-type atomic system with a weak probe field depends on the frequency of the probe field. If the frequency of the probe field matches the frequency of the $|b\rangle \rightarrow |a\rangle$ transition, the EIT phenomenon occurs, the effect of the atomic system on the probe field can be eliminated.

1.7 Organization

Chapter 2 shows that an optical parametric amplifier inside a cavity can considerably improve the cooling of the micromechanical mirror by radiation pressure. The micromechanical mirror can be cooled from room temperature 300 K to sub-Kelvin temperatures, which is much lower than what is achievable in the absence of the parametric amplifier. This is further illustrated in case of a precooled mirror, where one can reach millikelvin temperatures starting with about 1 K. Our work demonstrates the fundamental dependence of radiation pressure effects on photon statistics.

Chapter 3 discusses how an optical parametric amplifier inside the cavity can affect the normal-mode splitting behavior of the coupled movable mirror and the cavity field. We work in the resolved sideband regime. The spectra exhibit a double-peak structure as the parametric gain is increased. Moreover, for a fixed parametric gain, the double-peak structure of the spectrum is more pronounced with increasing the input laser power. We give results for mode splitting. The widths of the split lines are sensitive to parametric gain.

Chapter 4 presents that squeezing of a nanomechanical mirror can be generated by injecting broad band squeezed vacuum light and laser light into the cavity. We work in the resolved sideband regime. We find that in order to obtain the maximum

momentum squeezing of the movable mirror, the squeezing parameter of the input light should be about 1. We can obtain more than 70% squeezing. Besides, for a fixed squeezing parameter, decreasing the temperature of the environment or increasing the laser power increases the momentum squeezing. We find very large squeezing with respect to thermal fluctuations, for instance at 1 mK, the momentum fluctuations go down by a factor more than one hundred.

Chapter 5 presents a scheme for entangling two separated nanomechanical oscillators by injecting broad band squeezed vacuum light and laser light into the ring cavity. We work in the resolved sideband regime. We find that in order to obtain the maximum entanglement of the two oscillators, the squeezing parameter of the input light should be about 1. We report significant entanglement over a very wide range of power levels of the pump and temperatures of the environment.

Chapter 6 discusses Stokes and anti-Stokes processes in cavity optomechanics in the regime of strong coupling. The Stokes and anti-Stokes signals exhibit prominently the normal-mode splitting. We report gain for the Stokes signal. We also report lifetime splitting when the pump power is less than the critical power for normal-mode splitting. The nonlinear Stokes processes provide a useful method for studying the strong-coupling regime of cavity optomechanics. We also investigate the correlations between the Stokes and the anti-Stokes photons produced spontaneously by the optomechanical system. At zero temperature, our nanomechanical system leads to the correlations between the spontaneously generated photons exhibiting photon antibunching and those violating the Cauchy-Schwartz inequality.

Chapter 7 discusses the dynamical behavior of a nanomechanical mirror in a high-quality cavity under the action of a coupling laser and a probe laser. We demonstrate the existence of the analog of electromagnetically induced transparency (EIT) in the output field at the probe frequency. Our calculations show explicitly the origin of EIT-like dips as well as the characteristic changes in dispersion from anomalous to

normal in the range where EIT dips occur. Remarkably the pump-probe response for the optomechanical system shares all the features of the Λ system as discovered by Harris and collaborators.

Chapter 8 studies the optomechanical design introduced by M. Li et. al. [Phys. Rev. Lett. 103, 223901 (2009)], which is very effective for investigation of the effects of reactive coupling. We show the normal mode splitting that is due solely to reactive coupling rather than due to dispersive coupling. We suggest feeding the waveguide with a pump field along with a probe field and scanning the output probe for evidence of reactive-coupling-induced normal mode splitting.

Chapter 9 shows that dissipatively coupled nanosystems can be prepared in states which beat the standard quantum limit of the mechanical motion. We show that the reactive coupling between the waveguide and the microdisk resonator can generate the squeezing of the waveguide by injecting a quantum field and laser into the resonator through the waveguide. The waveguide can show about 70-75% of maximal squeezing for temperature about 1-10 mK. The maximum squeezing can be achieved with an incident pump power of only 12 μW for a temperature of about 1 mK. Even for temperatures of 20 mK, achievable by dilution refrigerators, the maximum squeezing is about 60%.

Chapter 10 describes how electromagnetically induced transparency can arise in quadratically coupled optomechanical systems. Due to quadratic coupling, the underlying optical process involves a two-phonon process in an optomechanical system, and this two-phonon process makes the mean displacement, which plays the role of atomic coherence in traditional electromagnetically induced transparency (EIT), zero. We show how the fluctuation in displacement can play a role similar to atomic coherence and can lead to EIT-like effects in quadratically coupled optomechanical systems. We show how such effects can be studied using the existing optomechanical systems.

Chapter 11 discusses electromagnetically induced transparency (EIT) using quan-

tized fields in optomechanical systems. The weak probe field is a narrowband squeezed field. We present a homodyne detection of EIT in the output quantum field. We find that the EIT dip exists even though the photon number in the squeezed vacuum is at the single-photon level. The EIT with quantized fields can be seen even at temperatures on the order of 100 mK, thus paving the way for using optomechanical systems as memory elements.

Chapter 12 demonstrate theoretically the possibility of using nano mechanical systems as single photon routers. We show how EIT in cavity optomechanical systems can be used to produce a switch for a probe field in a single photon Fock state using very low pumping powers of few microwatt. We present estimates of vacuum and thermal noise and show the optimal performance of the single photon switch is deteriorated by only few percent even at temperatures of the order of 20 mK.

Chapter 13 gives the summary of what we have done in this thesis and the direction of the future work.

CHAPTER 2

ENHANCEMENT OF CAVITY COOLING OF A MICROMECHANICAL MIRROR USING PARAMETRIC INTERACTIONS

2.1 Overview

Recently there is considerable interest in micromechanical mirrors. These are macroscopic quantum mechanical systems and the important question is how to reach their quantum characteristics [8, 87, 88, 89]. The thermal noise limits many highly sensitive optical measurements [90, 91]. We also note that there has been considerable interest in using micromirrors for producing superpositions of macroscopic quantum states if such micromirrors can be cooled to their quantum ground states [27, 28]. Thus cooling of micromechanical resonators becomes a necessary prerequisite for all such studies. So far two different ways to cool a mechanical resonator mode have been proposed. One is the active feedback scheme [7, 92, 93, 116], where a viscous force is fed back to the movable mirror to decrease its Brownian motion. The other is the passive feedback scheme [6, 8, 9, 56, 95, 159], in which the Brownian motion of the movable mirror is damped by the radiation pressure force exerted by photons in an appropriately detuned optical cavity.

Clearly we need to think of methods which can cool the micromirror toward its ground state. Since radiation pressure depends on the number of photons, one would think that the cooling of the micromirror can be manipulated by using effects of the photon statistics. In this chapter, we propose and analyze a method to achieve cooling of a movable mirror to sub-Kelvin temperatures by using a type I optical

parametric amplifier inside a cavity. We remind the reader of the great success of cavities with parametric amplifiers in the production of nonclassical light [97, 98, 99]. The movable mirror can reach a minimum temperature of about a few hundred mK, a factor of 500 below room temperature 300 K. The lowering of the temperature is achieved by changes in photon statistics due to parametric interactions [100, 101, 102, 103, 104, 105]. Note that if the mirror is already precooled to say about 1 K, then we show that by using an optical parametric amplifier we can cool to about millikelvin temperatures or less.

The chapter is organized as follows. In Sec. II we describe the model and derive the quantum Langevin equations. In Sec. III we obtain the stability conditions, calculate the spectrum of fluctuations in position and momentum of the movable mirror, and define the effective temperature of the movable mirror. In Sec. IV we show how the movable mirror can be effectively cooled by using the parametric amplifier inside the cavity.

2.2 Model

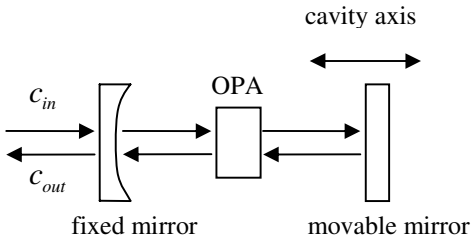

Figure 2.1: Sketch of the cavity used to cool a micromechanical mirror. The cavity contains a nonlinear crystal which is pumped by a laser (not shown) to produce parametric amplification and to change photon statistics in the cavity.

We consider a degenerate optical parametric amplifier (OPA) inside a Fabry-Perot cavity with one fixed partially transmitting mirror and one movable totally reflecting mirror in contact with a thermal bath in equilibrium at temperature T, as shown

in Fig. 2.1. The movable mirror is free to move along the cavity axis and is treated as a quantum mechanical harmonic oscillator with effective mass m, frequency ω_m, and energy decay rate γ_m. The effect of the thermal bath can be modeled by a Langevin force. The cavity field is driven by an input laser field with frequency ω_L and positive amplitude related to the input laser power P by $\tilde{\varepsilon} = \sqrt{P/(\hbar\omega_L)}$. When photons in the cavity reflect off the surface of the movable mirror, the movable mirror will receive the action of the radiation pressure force, which is proportional to the instantaneous photon number inside the cavity. So the mirror can oscillate under the effects of the thermal Langevin force and the radiation pressure force. Meanwhile, the movable mirrors motion changes the length of the cavity; hence the movable mirror displacement from its equilibrium position will induce a phase shift on the cavity field.

Here we assume the system is in the adiabatic limit, which means $\omega_L \ll \pi c/L$; c is the speed of light in vacuum and L is the cavity length in the absence of the cavity field. We assume that the motion of the mirror is so slow that the scattering of photons to other cavity modes can be ignored, thus we can consider one cavity mode only [64, 106], say, ω_c. Moreover, in the adiabatic limit, the number of photons generated by the Casimir effect [107], retardation, and Doppler effects is negligible [26, 92, 108]. Under these conditions, the total Hamiltonian for the system in a frame rotating at the laser frequency ω_L can be written as

$$\begin{aligned} H &= \hbar(\omega_c - \omega_L)n_c - \hbar\chi n_c q + \frac{1}{2}(\frac{p^2}{m} + m\omega_m^2 q^2) \\ &\quad + i\hbar\varepsilon(c^\dagger - c) + i\hbar G(e^{i\theta}c^{\dagger 2} - e^{-i\theta}c^2). \end{aligned} \tag{2.1}$$

Here c and $c^\dagger$ are the annihilation and creation operators for the field inside the cavity, respectively; $n_c = c^\dagger c$ is the number of the photons inside the cavity; and q and p are the position and momentum operators for the movable mirror. The parameter $\chi = \omega_c/L$ is the coupling constant between the cavity and the movable mirror; and

$\varepsilon = \sqrt{2\kappa}\tilde{\varepsilon}$. Note that κ is the photon decay rate due to the photon leakage through the fixed partially transmitting mirror. Further $\kappa = \pi c/(2FL)$, where F is the cavity finesse. In Eq. (2.1), G is the nonlinear gain of the OPA, and θ is the phase of the field driving the OPA. The parameter G is proportional to the pump driving the OPA.

In Eq. (2.1), the first term corresponds to the energy of the cavity field, the second term arises from the coupling of the movable mirror to the cavity field via radiation pressure, the third term gives the energy of the movable mirror, the fourth term describes the coupling between the input laser field and the cavity field, and the last term is the coupling between the OPA and the cavity field.

The motion of the system can be described by the Heisenberg equations of motion and adding the corresponding damping and noise terms, which leads to the following quantum Langevin equations:

$$\begin{aligned}
\dot{q} &= \tfrac{p}{m}, \\
\dot{p} &= -m\omega_m^2 q + \hbar\chi n_c - \gamma_m p + \xi, \\
\dot{c} &= i(\omega_L - \omega_c + \chi q)c + \varepsilon + 2Ge^{i\theta}c^\dagger - \kappa c + \sqrt{2\kappa}c_{in}, \\
\dot{c}^\dagger &= -i(\omega_L - \omega_c + \chi q)c^\dagger + \varepsilon + 2Ge^{-i\theta}c - \kappa c^\dagger + \sqrt{2\kappa}c_{in}^\dagger.
\end{aligned} \tag{2.2}$$

Here c_{in} is the input vacuum noise operator with zero mean value; its correlation function is [141]

$$\begin{aligned}
\langle \delta c_{in}(t)\delta c_{in}^\dagger(t')\rangle &= \delta(t-t'), \\
\langle \delta c_{in}(t)\delta c_{in}(t')\rangle &= \langle \delta c_{in}^\dagger(t)\delta c_{in}(t')\rangle = 0.
\end{aligned} \tag{2.3}$$

The force ξ is the Brownian noise operator resulting from the coupling of the movable mirror to the thermal bath, whose mean value is zero, and it has the following correlation function at temperature T [108]:

$$\langle \xi(t)\xi(t')\rangle = \frac{\hbar\gamma_m}{2\pi} m \int \omega e^{-i\omega(t-t')} \left[\coth(\frac{\hbar\omega}{2k_BT}) + 1\right] d\omega, \tag{2.4}$$

where k_B is the Boltzmann constant and T is the thermal bath temperature. In order to analyze Eq. (2.2), we use standard methods from quantum optics [110]. A detailed calculation of the temperature for $G = 0$ is given by Paternostro et al. [35]. By setting all the time derivatives in Eq. (2.2) to zero, we obtain the steady-state mean values

$$p_s = 0,\ q_s = \frac{\hbar\chi|c_s|^2}{m\omega_m^2},\ c_s = \frac{\kappa - i\Delta + 2Ge^{i\theta}}{\kappa^2 + \Delta^2 - 4G^2}\varepsilon, \tag{2.5}$$

where

$$\Delta = \omega_c - \omega_L - \chi q_s = \Delta_0 - \chi q_s = \Delta_0 - \frac{\hbar\chi^2|c_s|^2}{m\omega_m^2} \tag{2.6}$$

is the effective cavity detuning, including the radiation pressure effects. The modification of the detuning by the χq_s term depends on the range of parameters. The q_s denotes the new equilibrium position of the movable mirror relative to that without the driving field. Further c_s represents the steady-state amplitude of the cavity field. Note that q_s and c_s can display optical multistable behavior, which is a nonlinear effect induced by the radiation-pressure coupling of the movable mirror to the cavity field. Mathematically this is contained in the dependence of the detuning parameter Δ on the mirrors amplitude q_s. It is evident from Eqs. (2.5) and (2.6) that Δ satisfies a fifth-order equation and in principle can have five real solutions implying multistability. Generally, in this case, at most three solutions would be stable. The bistable behavior is reported in Refs. [41, 42].

2.3 Radiation Pressure and Quantum Fluctuations

In order to determine the cooling of the mirror, we need to find out the fluctuations in the mirrors amplitude. Since the problem is nonlinear, we assume that the nonlinearity is weak. We are thus interested in the dynamics of small fluctuations around the steady state of the system. Such a linearized analysis is quite common in quantum optics [110, 111]. So we write each operator of the system as the sum of its steady

state mean value and a small fluctuation with zero mean value,

$$q = q_s + \delta q, \quad p = p_s + \delta p, \quad c = c_s + \delta c. \tag{2.7}$$

Inserting Eq. (2.7) into Eq. (2.2), then assuming $|c_s| \gg 1$, we get the linearized quantum Langevin equations for the fluctuation operators

$$\begin{aligned}
\delta\dot{q} &= \tfrac{\delta p}{m}, \\
\delta\dot{p} &= -m\omega_m^2\delta q + \hbar\chi(c_s\delta c^\dagger + c_s^*\delta c) - \gamma_m\delta p + \xi, \\
\delta\dot{c} &= -i\Delta\delta c + i\chi c_s\delta q + 2Ge^{i\theta}\delta c^\dagger - \kappa\delta c + \sqrt{2\kappa}\delta c_{in}, \\
\delta\dot{c^\dagger} &= i\Delta\delta c^\dagger - i\chi c_s^*\delta q + 2Ge^{-i\theta}\delta c - \kappa\delta c^\dagger + \sqrt{2\kappa}\delta c_{in}^\dagger.
\end{aligned} \tag{2.8}$$

Introducing the cavity field quadratures $\delta x = \delta c^\dagger + \delta c$ and $\delta y = i(\delta c^\dagger - \delta c)$, and the input noise quadratures $\delta x_{in} = \delta c_{in}^\dagger + \delta c_{in}$ and $\delta y_{in} = i(\delta c_{in}^\dagger - \delta c_{in})$, Eq. (2.8) can be written in the matrix form

$$\dot{f} = Af(t) + \eta(t), \tag{2.9}$$

where $f(t)$ is the column vector of the fluctuations, and $\eta(t)$ is the column vector of the noise sources. For the sake of simplicity, their transposes are

$$\begin{aligned}
f(t)^T &= (\delta q, \delta p, \delta x, \delta y), \\
\eta(t)^T &= (0, \xi, \sqrt{2\kappa}\delta x_{in}, \sqrt{2\kappa}\delta y_{in});
\end{aligned} \tag{2.10}$$

and the matrix A is given by

$$A = \begin{pmatrix}
0 & \frac{1}{m} & 0 & 0 \\
-m\omega_m^2 & -\gamma_m & \hbar\chi\frac{c_s + c_s^*}{2} & \hbar\chi\frac{c_s - c_s^*}{2i} \\
i\chi(c_s - c_s^*) & 0 & 2G\cos\theta - \kappa & \Delta + 2G\sin\theta \\
\chi(c_s + c_s^*) & 0 & 2G\sin\theta - \Delta & -(\kappa + 2G\cos\theta)
\end{pmatrix}. \tag{2.11}$$

The solutions to Eq. (2.9) are stable only if all the eigenvalues of the matrix A have negative real parts. Applying the Routh-Hurwitz criterion [112, 113], we get the

stability conditions

$$
\begin{aligned}
&2\kappa(\kappa^2-4G^2+\Delta^2+2\kappa\gamma_m)+\gamma_m(2\kappa\gamma_m+\omega_m^2)>0,\\
&(2\kappa+\gamma_m)^2[\frac{2\hbar\chi^2|c_s|^2}{m}\Delta+\frac{2\hbar\chi^2(c_s^2+c_s^{*2})G\sin\theta}{m}\\
&\quad+\frac{2i\hbar\chi^2(c_s^2-c_s^{*2})G\cos\theta}{m}]+2\kappa\gamma_m\{(\kappa^2-4G^2+\Delta^2)^2\\
&\quad+(2\kappa\gamma_m+\gamma_m^2)(\kappa^2-4G^2+\Delta^2)\\
&\quad+\omega_m^2[2(\kappa^2+4G^2-\Delta^2)+\omega_m^2+2\kappa\gamma_m]\}>0,\\
&\omega_m^2(\kappa^2-4G^2+\Delta^2)-\frac{2\hbar\chi^2|c_s|^2}{m}\Delta\\
&\quad-\frac{2\hbar\chi^2(c_s^2+c_s^{*2})G\sin\theta}{m}-\frac{2i\hbar\chi^2(c_s^2-c_s^{*2})G\cos\theta}{m}>0.
\end{aligned}
\tag{2.12}
$$

Note that in the absence of coupling χ, the conditions (2.12) become equivalent to

$$\kappa^2-4G^2+\Delta^2>0 \tag{2.13}$$

The condition for the threshold for parametric oscillations is $\kappa^2-4G^2+\Delta^2=0$. We always would work under the condition that (2.13) is satisfied. Further for $\chi\neq 0$ we would do numerical simulations using parameters so that conditions (2.12) are satisfied.

On Fourier transforming all operators and noise sources in Eq. (2.8) and solving it in the frequency domain, the position fluctuations of the movable mirror are given by

$$
\begin{aligned}
\delta q(\omega)=&-\tfrac{1}{d(\omega)}([\Delta^2+(\kappa-i\omega)^2-4G^2]\xi(\omega)\\
&-i\hbar\sqrt{2\kappa}\chi\{[(\omega+i\kappa-\Delta)c_s+2iGe^{i\theta}c_s^*]\delta c_{in}^\dagger(\omega)\\
&+[(\omega+i\kappa+\Delta)c_s^*+2iGe^{-i\theta}c_s]\delta c_{in}(\omega)\}),
\end{aligned}
\tag{2.14}
$$

where $d(\omega)=2\hbar\chi^2(\Delta|c_s|^2+iGe^{-i\theta}c_s^2-iGe^{i\theta}c_s^{*2})+m(\omega^2-\omega_m^2+i\omega\gamma_m)[\Delta^2+(\kappa-i\omega)^2-4G^2]$. In Eq. (2.14), the first term proportional to $\xi(\omega)$ originates from the thermal noise, while the second term proportional to χ arises from radiation pressure. So the position fluctuations of the movable mirror are now determined by the thermal noise

and radiation pressure. Notice that if there is no radiation pressure, the movable mirror will make Brownian motion, $\delta q(\omega) = -\xi(\omega)/[m(\omega^2 - \omega_m^2 + i\omega\gamma_m)]$, whose susceptibility has a Lorentzian shape centered at frequency ω_m with width γ_m.

The spectrum of fluctuations in position of the movable mirror is defined by

$$S_q(\omega) = \frac{1}{4\pi}\int d\Omega e^{-i(\omega+\Omega)t}\langle\delta q(\omega)\delta q(\Omega) + \delta q(\Omega)\delta q(\omega)\rangle. \tag{2.15}$$

To calculate the spectrum, we need the correlation functions of the noise sources in the frequency domain,

$$\begin{aligned}
&\langle\delta c_{in}(\omega)\delta c_{in}^{\dagger}(\Omega)\rangle = 2\pi\delta(\omega+\Omega),\\
&\langle\xi(\omega)\xi(\Omega)\rangle = 2\pi\hbar\gamma_m m\omega\left[1+\coth(\tfrac{\hbar\omega}{2k_BT})\right]\delta(\omega+\Omega).
\end{aligned} \tag{2.16}$$

Substituting Eq. (2.14) and Eq. (2.16) into Eq. (2.15), we obtain the spectrum of fluctuations in position of the movable mirror

$$\begin{aligned}
S_q(\omega) = \tfrac{\hbar}{|d(\omega)|^2}\{&2\kappa\hbar\chi^2[(\kappa^2+\omega^2+\Delta^2+4G^2)|c_s|^2\\
&+2Ge^{i\theta}c_s^{*2}(\kappa-i\Delta)+2Ge^{-i\theta}c_s^2(\kappa+i\Delta)]\\
&+m\gamma_m\omega[(\Delta^2+\kappa^2-\omega^2-4G^2)^2+4\kappa^2\omega^2]\\
&\times\coth(\tfrac{\hbar\omega}{2k_BT})\}.
\end{aligned} \tag{2.17}$$

In Eq. (2.17), the first term is the radiation pressure contribution, whereas the second term corresponds to the thermal noise contribution. Then Fourier transforming $\dot{q} = \delta p/m$ in Eq. (2.8), we obtain $\delta p(\omega) = -im\omega\delta q(\omega)$, which leads to the spectrum of fluctuations in momentum of the movable mirror

$$S_p(\omega) = m^2\omega^2 S_q(\omega). \tag{2.18}$$

For a system in thermal equilibrium, we can use the equipartition theorem to define temperature $\frac{1}{2}m\omega_m^2\langle q^2\rangle = \frac{\langle p^2\rangle}{2m} = \frac{1}{2}k_BT_{eff}$, where $\langle q^2\rangle = \frac{1}{2\pi}\int_{-\infty}^{+\infty}S_q(\omega)d\omega$, and $\langle p^2\rangle = \frac{1}{2\pi}\int_{-\infty}^{+\infty}S_p(\omega)d\omega$. However, here we are dealing with a driven system and $\frac{1}{2}m\omega_m^2\langle q^2\rangle \neq$

$\frac{\langle p^2\rangle}{2m}$, hence the question is how to define temperature. We use an effective temperature defined by the total energy of the movable mirror $k_B T_{eff} = \frac{1}{2}m\omega_m^2\langle q^2\rangle + \frac{\langle p^2\rangle}{2m}$. We also introduce the parameter $r = m^2\omega_m^2\langle q^2\rangle/\langle p^2\rangle$.This parameter gives us the relative importance of fluctuations in position and momentum of the mirror. We mention that one can calculate the quantum state of the oscillator and we find that the Wigner function is Gaussian.

Equation (2.17) is our key result which tells how the temperature of the micromirror would depend on the parameters of the cavity: κ, gain of the OPA, external laser power, etc. We specifically investigate the dependence of the temperature on the gain G and the phase θ associated with the parametric amplification process. In the limit of $G \to 0$, the result (2.17) reduces to the one derived by Paternostro et al.[35].

2.4 Cooling Mirror to About Sub-Kelvin Temperatures

In this section, we present the possibility of cooling the micromirror to temperatures of about sub-Kelvin by using parametric amplifiers inside cavities. In all the numerical calculations we choose the values of the parameters which are similar to those used in recent experiments: $\lambda_L = 2\pi c/\omega_L = 1064$ nm, $L = 25$ mm, $P = 4$ mW, $m = 15$ ng, $\omega_m/(2\pi) = 275$ kHz, and the mechanical quality factor $Q = \omega_m/\gamma_m = 2.1 \times 10^4$. Further in the high-temperature limit $k_B T \gg \hbar\omega$, we have $\coth(\hbar\omega/2k_B T) \approx 2k_B T/\hbar\omega$.

2.4.1 From Room Temperature (T=300 K) to About Sub-Kelvin Temperatures

If we choose $\kappa = 10^8$ s^{-1}, $F = 188.4$, $G = 0$ to satisfy the stability conditions (2.12), the detuning must satisfy $\Delta_0 \geq 4 \times 10^6 \text{s}^{-1}$. Figure 2.2 gives the variations of the χq_s, the effective temperature T_{eff}, and the parameter r with the detuning Δ_0. It should be borne in mind that for the range of the detuning shown in Fig. 2.2,

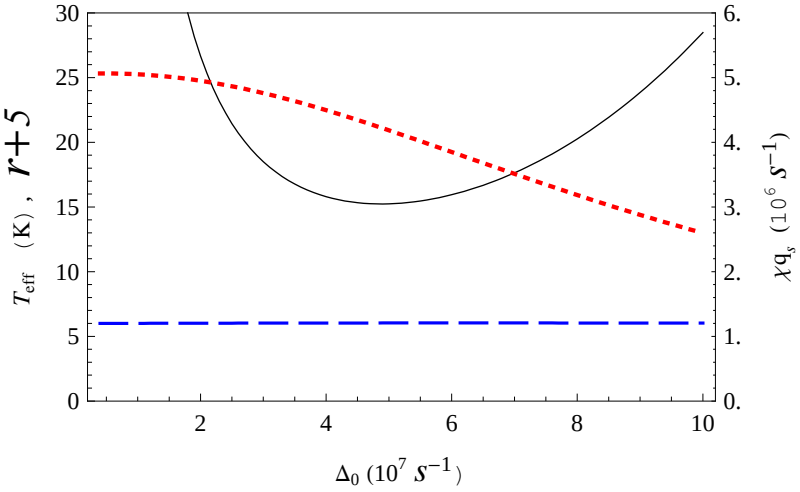

Figure 2.2: The dotted curve indicates the χq_s (10^6 s^{-1}) as a function of the detuning Δ_0 (10^7 s^{-1}) (rightmost vertical scale). The solid curve shows the effective temperature T_{eff}(K) as a function of the detuning Δ_0 (10^7 s^{-1}) (leftmost vertical scale). The dashed curve represents the parameter r as a function of the detuning Δ_0 (10^7 s^{-1}) (leftmost vertical scale). Parameters: cavity decay rate $\kappa = 10^8$ s^{-1}, cavity finesse $F = 188.4$, parametric gain G=0.

$\Delta = \Delta_0 - \chi q_s \approx \Delta_0$. We find the χq_s is single valued, so the movable mirror is monostable. Note that the parameter r is very close to unity, $\frac{1}{2}m\omega_m^2\langle q^2\rangle \approx \frac{\langle p^2\rangle}{2m}$; the mirror is thus in nearly thermal equilibrium. Figure 2.2 shows the possibility of cooling the mirror to a temperature of 15.23 K for $\Delta_0 = 4.9 \times 10^7$ s^{-1}, which is in agreement with the previous calculation [35].

Now we keep the values of κ and F the same as in Fig. 2.2, and we choose parametric gain $G = 3.5 \times 10^7$ s^{-1} and parametric phase $\theta = 0$; the detuning must satisfy $\Delta_0 \geq 5.7 \times 10^7$ s^{-1}. If $\Delta_0 < 5.7 \times 10^7$ s^{-1} and for fixed κ and G, the system will be unstable. The threshold for unstable behavior occurs when any of the three conditions (2.12) is not satisfied. It may be noted that the threshold for parametric oscillation has been of great importance in connection with the production

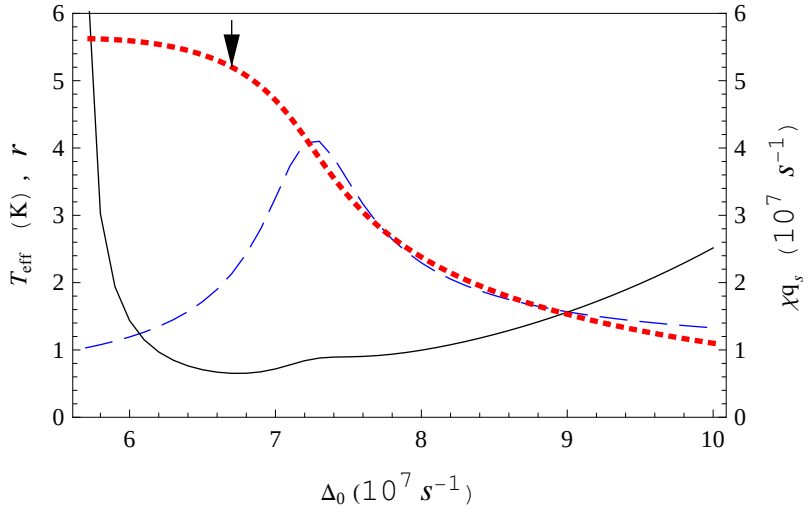

Figure 2.3: The dotted curve indicates the χq_s (10^7 s^{-1}) as a function of the detuning Δ_0 (10^7 s^{-1}) (rightmost vertical scale). The position that corresponds to the minimum effective temperature reached is indicated by the arrow. The solid curve shows the effective temperature T_{eff}(K) as a function of the detuning Δ_0 (10^7 s^{-1}) (leftmost vertical scale). The dashed curve represents the parameter r as a function of the detuning Δ_0 (10^7 s^{-1}) (leftmost vertical scale). Parameters: cavity decay rate $\kappa = 10^8$ s^{-1}, cavity finesse $F = 188.4$, parametric gain $G = 3.5 \times 10^7$s^{-1}, parametric phase $\theta = 0$.

of nonclassical-squeezed light. Near the parametric thresholds but under (2.13), large degrees of squeezing were produced [97, 98]. Thus it would be advantageous to work near the threshold of instability but below the instability point. Figure 2.3 shows the variations of the χq_s, the effective temperature T_{eff}, and the parameter r with the detuning Δ_0. We find the χq_s is still single valued, so the movable mirror is still monostable. The minimum temperature reached is 0.65 K for $\Delta_0 = 6.7 \times 10^7$ s^{-1}. Thus, with the parametric amplifier the minimum temperature is about a factor of 20 lower than the one without parametric interaction. Note that the parameter r is always larger than 1, implying that momentum fluctuations are suppressed over

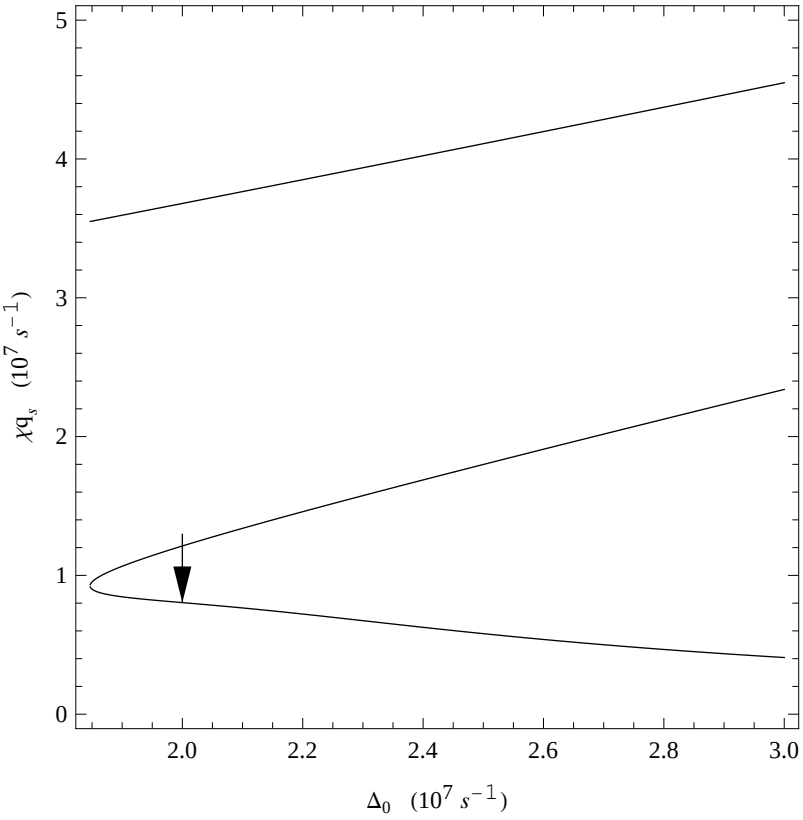

Figure 2.4: The behavior of χq_s (10^7 s^{-1}) shown as a function of the detuning Δ_0 (10^7 s^{-1}). The position that corresponds to the minimum effective temperature reached is indicated by the arrow. Parameters: cavity decay rate $\kappa = 10^7$ s^{-1}, cavity finesse $F = 1884$, parametric gain $G = 5 \times 10^6$s^{-1}, parametric phase $\theta = 3\pi/4$.

position fluctuations. Note that as one moves away from the threshold for parametric instability, the minimum temperature does not rise sharply which is in contrast to the behavior in Fig. 2.2, and is advantageous in giving one flexibility about the choice of the detuning parameter.

We next examine the case when the behavior of the system is multistable. For this purpose, we choose the cavity to have the higher quality factor. We choose $\kappa = 10^7$ s^{-1}, $F = 1884$, $G = 5 \times 10^6$ s^{-1} and $\theta = 3\pi/4$; then to satisfy the stability conditions (2.12), the detuning must satisfy $\Delta_0 \geq 1.847 \times 10^7$ s^{-1}. Figure 2.4 gives the behavior of χq_s as a function of the detuning Δ_0. We find the χq_s is multivalued, so the movable

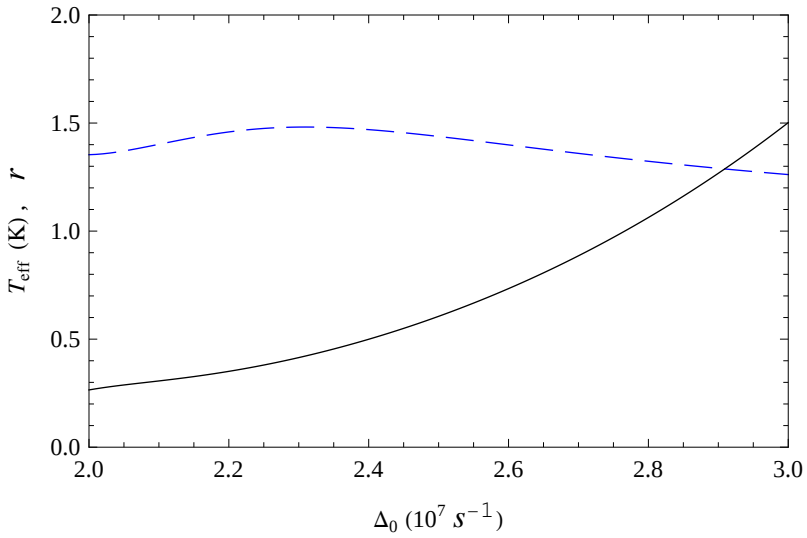

Figure 2.5: The solid curve shows the effective temperature T_{eff}(K) as a function of the detuning Δ_0 (10^7 s^{-1}). The dashed curve represents the parameter r as a function of the detuning Δ_0 (10^7 s^{-1}). Parameters: cavity decay rate $\kappa = 10^7$ s^{-1}, cavity finesse $F = 1884$, parametric gain $G = 5 \times 10^6$s^{-1}, parametric phase $\theta = 3\pi/4$.

mirror is multistable. By use of the lowest curve of the χq_s, we obtain the variations of the effective temperature T_{eff} and the parameter r with the detuning Δ_0, as shown in Fig. 2.5. We choose that the range of the detuning is 2.0×10^7 s^{-1} $- 3.0 \times 10^7$ s^{-1}. The minimum temperature achieved is 0.265 K for $\Delta_0 = 2.0 \times 10^7$ s^{-1}. Note that r is close to unity but larger than unity. The general trend is clear. By playing around with various parameters such as laser power, cavity finesse, and parametric gain, one can achieve a variety of different temperatures. As another example, if we choose $\kappa = 5 \times 10^6$ s^{-1}, $F = 3768$, $G = 10^7$ s^{-1} and $\theta = 0.2467 + \pi/2$, then we find that the minimum temperature is 0.092 K for $\Delta_0 = 2.13 \times 10^7 s^{-1}$.

2.4.2 From 1 K to Millikelvin Temperatures

If the thermal bath is cryogenically cooled down to a temperature of 1 K and the mirror is initially thermalized, then we can use radiation pressure effects and photon

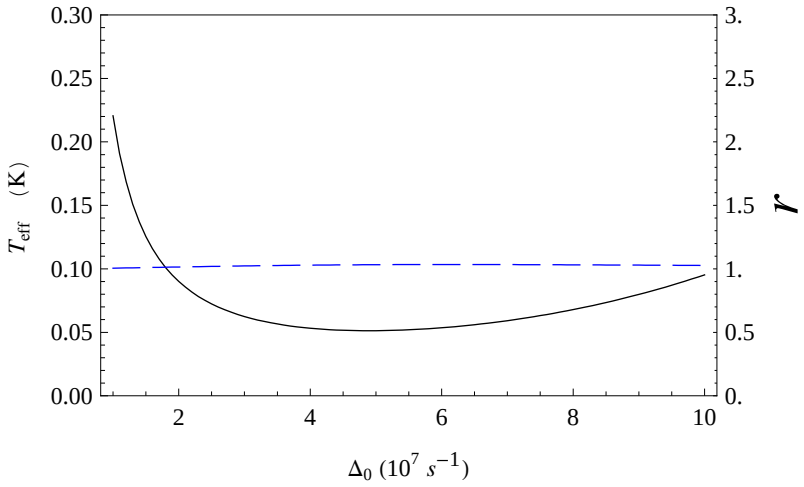

Figure 2.6: The solid curve shows the effective temperature T_{eff}(K) as a function of the detuning Δ_0 (10^7 s^{-1})(leftmost vertical scale). The dashed curve represents the parameter r as a function of the detuning Δ_0 (10^7 s^{-1})(rightmost vertical scale). Parameters: cavity decay rate $\kappa = 10^8$ s^{-1}, cavity finesse $F = 188.4$, parametric gain $G = 0$.

statistics to reach millikelvin or even lower temperatures.

If we choose $\kappa = 10^8$ s^{-1}, $F = 188.4$, $G = 0$, the effective temperature T_{eff} with the detuning Δ_0 is shown in Fig. 2.6. The minimum temperature reached is 0.051 K for $\Delta_0 = 4.9 \times 10^7$ s^{-1}. Next we examine how the effective temperature changes by the parametric interactions inside the cavity. We keep all other parameters as in Fig. 6 and choose parametric gain $G = 3.5 \times 10^7$ s^{-1} and phase $\theta = 0$. Then the effective temperature T_{eff} with the detuning Δ_0 exhibits behavior as shown in Fig. 2.7. The minimum temperature achieved is 0.0044 K for $\Delta_0 = 7.9 \times 10^7$ s^{-1}, a factor of 12 lower than the one without parametric interaction.

Finally it should be borne in mind that the radiation pressure depends on the number operator and then it is sensitive to the photon statistics of the field in the cavity. The photon statistics can be calculated from the quantum Langevin equations (2.8). It can be proved that the Wigner function W of the field in the cavity is

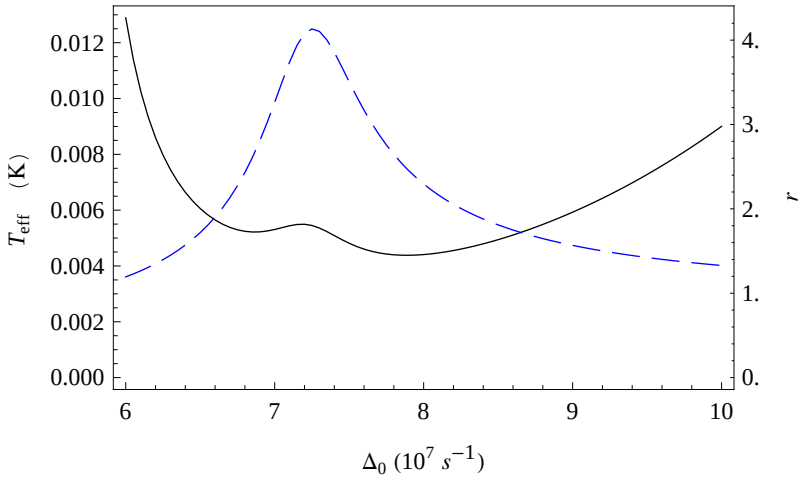

Figure 2.7: The solid curve shows the effective temperature T_{eff}(K) as a function of the detuning Δ_0 (10^7 s^{-1})(leftmost vertical scale). The dashed curve represents the parameter r as a function of the detuning Δ_0 (10^7 s^{-1})(rightmost vertical scale). Parameters: cavity decay rate $\kappa = 10^8$ s^{-1}, cavity finesse $F = 188.4$, parametric gain $G = 3.5 \times 10^7$ s^{-1}, parametric phase $\theta = 0$.

Gaussian of the form $\exp[\mu(\alpha - c_s)^2 + \nu(\alpha^* - c_s^*)^2 + \lambda(\alpha - c_s)(\alpha^* - c_s^*)]$ with μ, ν, λ determined by κ, Δ, G, θ, etc. The photon number distribution [103] associated with such a Gaussian Wigner function depends in an important way on the parameter μ and the inequality of μ and ν. The latter depend on $G \neq 0$ or on the presence of OPA in the cavity.

2.5 Conclusions

In conclusion, we have demonstrated how the addition of a parametric amplifier in a cavity can lead to cooling of the micromirror to a temperature; which is much lower than what is achieved in an identical experiment without the use of a parametric amplifier. The parametric processes inside the cavity change the quantum statistics of the field in the cavity. This change leads to lower cooling since the radiation pressure

effects are dependent on the photon number. Thus photon statistics becomes central to achieve lower cooling temperatures. The use of parametric processes could provide us with a way to cool the mirror to its quantum ground state or even squeeze it.

The content of this chapter has been published in *Phys. Rev. A* **79**, 013821 (2009).

CHAPTER 3

NORMAL MODE SPLITTING IN A COUPLED SYSTEM OF A NANOMECHANICAL OSCILLATOR AND A PARAMETRIC AMPLIFIER CAVITY

3.1 Overview

Recently there has been a major effort in applying many of the well tested ideas from quantum optics such as squeezing, quantum entanglement to optomechanical systems which are macroscopic systems. Thus observation of entanglement [28, 35, 36, 38, 114, 115], squeezing [25, 26] etc in optomechanical systems would enable one to study quantum behavior at macroscopic scale. This of course requires cooling such systems to their ground state and significant advances have been made in cooling the mechanical mirror to far below the temperature of the environment [7, 8, 9, 116, 117, 118, 119]. Further it has been pointed out that using optical back action one can possibly achieve the ground state cooling in the resolved sideband regime where the frequency of the mechanical mirror is much larger than the cavity decay rate, that is $\omega_m \gg \kappa$ [47, 66, 120].

Another key idea from quantum optics is the vacuum Rabi splitting [121, 122] which is due to strong interaction between the atoms and the cavity mode. The experimentalists have worked hard over the years to produce stronger and stronger couplings to produce larger and larger splittings [123, 124, 213]. Application of these ideas to macroscopic systems is challenging as well. In a recent paper Kippenberg *et al.* [48] proposed the possibility of normal mode splitting in the resolved sideband regime using optomechanical oscillators. In this chapter, we propose placing a type

I optical parametric amplifier inside the cavity to increase the coupling between the movable mirror and the cavity field, and this should make the observation of the normal mode splitting of the movable mirror and the output field more accessible.

The chapter is structured as follows. In Sec. II we present the model, derive the quantum Langevin equations, and give the steady-state mean values. In Sec. III we present solution to the linearized Langevin equations and give the spectrum of the movable mirror. In Sec. IV we analyse and estimate the amount of the normal mode splitting of the spectra. In Sec. V we calculate the spectra of the output field. In Sec. VI we discuss the mode splitting of the spectra of the movable mirror and the output field.

3.2 Model

The system under consideration, sketched in Fig. 3.1, is an optical parametric amplifier (OPA) placed within a Fabry-Perot cavity formed by one fixed partially transmitting mirror and one movable perfectly reflecting mirror in equilibrium with its environment at a low temperature. The movable mirror is treated as a quantum mechanical harmonic oscillator with effective mass m, frequency ω_m, and energy decay rate γ_m. An external laser enters the cavity through the fixed mirror, then the photons in the cavity will exert a radiation pressure force on the movable mirror due to momentum transfer. This force is proportional to the instantaneous photon number in the cavity.

In the adiabatic limit, the frequency ω_m of the movable mirror is much smaller than the free spectral range of the cavity $\frac{c}{2L}$ (c is the speed of light in vacuum and L is the cavity length), the scattering of photons to other cavity modes can be ignored, thus only one cavity mode ω_c is considered [64, 106]. The Hamiltonian for the system in a frame rotating at the laser frequency ω_L can be written as

$$H = \hbar(\omega_c - \omega_L)n_c - \hbar\omega_m\chi n_c Q + \frac{\hbar\omega_m}{4}(Q^2 + P^2)$$

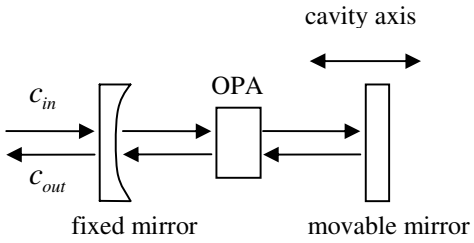

Figure 3.1: Sketch of the studied system. The cavity contains a nonlinear crystal which is pumped by a laser (not shown) to produce parametric amplification and to change photon statistics in the cavity.

$$+i\hbar\varepsilon(c^\dagger - c) + i\hbar G(e^{i\theta}c^{\dagger 2} - e^{-i\theta}c^2). \tag{3.1}$$

Here Q and P are the dimensionless position and momentum operators for the movable mirror, defined by $Q = \sqrt{\frac{2m\omega_m}{\hbar}}q$ and $P = \sqrt{\frac{2}{m\hbar\omega_m}}p$ with $[Q, P] = 2i$. In Eq. (3.1), the first term is the energy of the cavity field, $n_c = c^\dagger c$ is the number of the photons inside the cavity, c and $c^\dagger$ are the annihilation and creation operators for the cavity field satisfying the commutation relation $[c, c^\dagger] = 1$. The second term comes from the coupling of the movable mirror to the cavity field via radiation pressure, the dimensionless parameter $\chi = \frac{1}{\omega_m}\frac{\omega_c}{L}\sqrt{\frac{\hbar}{2m\omega_m}}$ is the optomechanical coupling constant between the cavity and the movable mirror. The third term corresponds the energy of the movable mirror. The fourth term describes the coupling between the input laser field and the cavity field, ε is related to the input laser power $\wp$ by $\varepsilon = \sqrt{\frac{2\kappa\wp}{\hbar\omega_L}}$, where κ is the cavity decay rate. The last term is the coupling between the OPA and the cavity field, G is the nonlinear gain of the OPA, and θ is the phase of the field driving the OPA. The parameter G is proportional to the pump driving the OPA.

Using the Heisenberg equations of motion and adding the corresponding damping

and noise terms, we obtain the quantum Langevin equations as follows,

$$\begin{aligned}
\dot{Q} &= \omega_m P, \\
\dot{P} &= 2\omega_m \chi n_c - \omega_m Q - \gamma_m P + \xi, \\
\dot{c} &= -i(\omega_c - \omega_L - \omega_m \chi Q)c + \varepsilon + 2Ge^{i\theta}c^\dagger - \kappa c + \sqrt{2\kappa}c_{in}, \\
\dot{c}^\dagger &= i(\omega_c - \omega_L - \omega_m \chi Q)c^\dagger + \varepsilon + 2Ge^{-i\theta}c - \kappa c^\dagger + \sqrt{2\kappa}c_{in}^\dagger.
\end{aligned} \tag{3.2}$$

Here we have introduced the input vacuum noise operator c_{in} with zero mean value, which obeys the correlation function in the time domain [141]

$$\begin{aligned}
\langle \delta c_{in}(t) \delta c_{in}^\dagger(t') \rangle &= \delta(t - t'), \\
\langle \delta c_{in}(t) \delta c_{in}(t') \rangle &= \langle \delta c_{in}^\dagger(t) \delta c_{in}(t') \rangle = 0.
\end{aligned} \tag{3.3}$$

The force ξ is the Brownian noise operator resulting from the coupling of the movable mirror to the thermal bath, whose mean value is zero, and it has the following correlation function at temperature T [108]:

$$\langle \xi(t)\xi(t') \rangle = \frac{1}{\pi}\frac{\gamma_m}{\omega_m} \int \omega e^{-i\omega(t-t')} \left[1 + \coth(\frac{\hbar\omega}{2k_B T}) \right] d\omega, \tag{3.4}$$

where k_B is the Boltzmann constant and T is the thermal bath temperature. Following standard methods from quantum optics [110], we derive the steady-state solution to Eq. (3.2) by setting all the time derivatives in Eq. (3.2) to zero. They are

$$P_s = 0,\ Q_s = 2\chi|c_s|^2,\ c_s = \frac{\kappa - i\Delta + 2Ge^{i\theta}}{\kappa^2 + \Delta^2 - 4G^2}\varepsilon, \tag{3.5}$$

where

$$\Delta = \omega_c - \omega_L - \omega_m \chi Q_s \tag{3.6}$$

is the effective cavity detuning, depending on Q_s. The Q_s denotes the new equilibrium position of the movable mirror relative to that without the driving field. Further c_s represents the steady-state amplitude of the cavity field. From Eq. (3.5) and Eq. (3.6), we can see Q_s satisfies a fifth order equation, it can at most have five real

solutions. Therefore, the movable mirror displays an optical multistable behavior [41, 42, 43], which is a nonlinear effect induced by the radiation-pressure coupling of the movable mirror to the cavity field.

3.3 Radiation Pressure and Quantum Fluctuations

In order to investigate the normal mode splitting of the movable mirror and the output field, we need to calculate the fluctuations of the system. Since the problem is nonlinear, we assume that the nonlinearity is weak. Thus we can focus on the dynamics of small fluctuations around the steady state of the system. Each operator of the system can be written as the sum of its steady-state mean value and a small fluctuation with zero mean value,

$$Q = Q_s + \delta Q, \quad P = P_s + \delta P, \quad c = c_s + \delta c. \tag{3.7}$$

Inserting Eq. (3.7) into Eq. (3.2), then assuming $|c_s| \gg 1$, the linearized quantum Langevin equations for the fluctuation operators take the form

$$\begin{aligned}
\delta\dot{Q} &= \omega_m \delta P, \\
\delta\dot{P} &= 2\omega_m \chi (c_s^* \delta c + c_s \delta c^\dagger) - \omega_m \delta Q - \gamma_m \delta P + \xi, \\
\delta\dot{c} &= -(\kappa + i\Delta)\delta c + i\omega_m \chi c_s \delta Q + 2Ge^{i\theta}\delta c^\dagger + \sqrt{2\kappa}\delta c_{in}, \\
\delta\dot{c}^\dagger &= -(\kappa - i\Delta)\delta c^\dagger - i\omega_m \chi c_s^* \delta Q + 2Ge^{-i\theta}\delta c + \sqrt{2\kappa}\delta c_{in}^\dagger.
\end{aligned} \tag{3.8}$$

Introducing the cavity field quadratures $\delta x = \delta c + \delta c^\dagger$ and $\delta y = i(\delta c^\dagger - \delta c)$, and the input noise quadratures $\delta x_{in} = \delta c_{in} + \delta c_{in}^\dagger$ and $\delta y_{in} = i(\delta c_{in}^\dagger - \delta c_{in})$, Eq. (3.8) can be rewritten in the matrix form

$$\dot{f}(t) = Af(t) + \eta(t), \tag{3.9}$$

in which $f(t)$ is the column vector of the fluctuations, $\eta(t)$ is the column vector of the noise sources. Their transposes are

$$\begin{aligned} f(t)^T &= (\delta Q, \delta P, \delta x, \delta y), \\ \eta(t)^T &= (0, \xi, \sqrt{2\kappa}\delta x_{in}, \sqrt{2\kappa}\delta y_{in}); \end{aligned} \tag{3.10}$$

and the matrix A is given by

$$A = \begin{pmatrix} 0 & \omega_m & 0 & 0 \\ -\omega_m & -\gamma_m & \omega_m\chi(c_s + c_s^*) & -i\omega_m\chi(c_s - c_s^*) \\ i\omega_m\chi(c_s - c_s^*) & 0 & 2G\cos\theta - \kappa & 2G\sin\theta + \Delta \\ \omega_m\chi(c_s + c_s^*) & 0 & 2G\sin\theta - \Delta & -(2G\cos\theta + \kappa) \end{pmatrix}. \tag{3.11}$$

The system is stable only if all the eigenvalues of the matrix A have negative real parts. The stability conditions for the system can be derived by applying the Routh-Hurwitz criterion [112, 113]. This gives

$$\begin{aligned} &2\kappa(\kappa^2 - 4G^2 + \Delta^2 + 2\kappa\gamma_m) + \gamma_m(2\kappa\gamma_m + \omega_m^2) > 0, \\ &2\omega_m^3\chi^2(2\kappa + \gamma_m)^2[|c_s|^2\Delta + iG(c_s^2e^{-i\theta} - c_s^{*2}e^{i\theta})] \\ &\quad +\kappa\gamma_m\{(\kappa^2 - 4G^2 + \Delta^2)^2 + (2\kappa\gamma_m + \gamma_m^2) \\ &\quad \times(\kappa^2 - 4G^2 + \Delta^2) + \omega_m^2[2(\kappa^2 + 4G^2 - \Delta^2) \\ &\quad +\omega_m^2 + 2\kappa\gamma_m]\} > 0, \\ &\kappa^2 - 4G^2 + \Delta^2 - 4\omega_m\chi^2[|c_s|^2\Delta + iG(c_s^2e^{-i\theta} - c_s^{*2}e^{i\theta})] > 0. \end{aligned} \tag{3.12}$$

All the external parameters must be chosen to satisfy the stability conditions (3.12).

Taking Fourier transform of Eq. (3.8) by using $f(t) = \frac{1}{2\pi}\int_{-\infty}^{+\infty} f(\omega)e^{-i\omega t}d\omega$ and $f^\dagger(t) = \frac{1}{2\pi}\int_{-\infty}^{+\infty} f^\dagger(-\omega)e^{-i\omega t}d\omega$, where $f^\dagger(-\omega) = [f(-\omega)]^\dagger$, then solving it, we obtain

the position fluctuations of the movable mirror

$$\begin{aligned}\delta Q(\omega) = &-\tfrac{\omega_m}{d(\omega)}[2\sqrt{2\kappa}\omega_m\chi\{[(\kappa - i(\Delta+\omega))c_s^* + 2Ge^{-i\theta}c_s]\delta c_{in}(\omega) \\ &+[(\kappa + i(\Delta-\omega))c_s + 2Ge^{i\theta}c_s^*]\delta c_{in}^\dagger(-\omega)\} \\ &+[(\kappa - i\omega)^2 + \Delta^2 - 4G^2]\xi(\omega)],\end{aligned} \tag{3.13}$$

where

$$\begin{aligned}d(\omega) = &\,4\omega_m^3\chi^2[\Delta|c_s|^2 + iG(c_s^2e^{-i\theta} - c_s^{*2}e^{i\theta})] \\ &+(\omega^2 - \omega_m^2 + i\gamma_m\omega)[(\kappa - i\omega)^2 + \Delta^2 - 4G^2].\end{aligned} \tag{3.14}$$

In Eq. (3.13), the first term proportional to χ originates from radiation pressure, while the second term involving $\xi(\omega)$ is from the thermal noise. So the position fluctuations of the movable mirror are now determined by radiation pressure and the thermal noise. In the case of no coupling with the cavity field, the movable mirror will make Brownian motion, $\delta Q(\omega) = \omega_m\xi(\omega)/(\omega_m^2 - \omega^2 - i\gamma_m\omega)$, whose susceptibility has a Lorentzian shape centered at frequency ω_m with width γ_m.

The spectrum of fluctuations in position of the movable mirror is defined by

$$\frac{1}{2}(\langle\delta Q(\omega)\delta Q(\Omega)\rangle + \langle\delta Q(\Omega)\delta Q(\omega)\rangle) = 2\pi S_Q(\omega)\delta(\omega+\Omega). \tag{3.15}$$

To calculate the spectrum, we require the correlation functions of the noise sources in the frequency domain,

$$\begin{aligned}&\langle\delta c_{in}(\omega)\delta c_{in}^\dagger(-\Omega)\rangle = 2\pi\delta(\omega+\Omega), \\ &\langle\xi(\omega)\xi(\Omega)\rangle = 4\pi\tfrac{\gamma_m}{\omega_m}\omega\left[1 + \coth(\tfrac{\hbar\omega}{2k_BT})\right]\delta(\omega+\Omega).\end{aligned} \tag{3.16}$$

Substituting Eq. (3.13) and Eq. (3.16) into Eq. (3.15), we obtain the spectrum of fluctuations in position of the movable mirror [126]

$$\begin{aligned}S_Q(\omega) = &\tfrac{\omega_m^2}{|d(\omega)|^2}\{8\omega_m^2\chi^2\kappa[(\kappa^2 + \omega^2 + \Delta^2 + 4G^2)|c_s|^2 \\ &+2Ge^{i\theta}c_s^{*2}(\kappa - i\Delta) + 2Ge^{-i\theta}c_s^2(\kappa + i\Delta)] \\ &+2\tfrac{\gamma_m}{\omega_m}\omega[(\Delta^2 + \kappa^2 - \omega^2 - 4G^2)^2 + 4\kappa^2\omega^2] \\ &\times\coth(\tfrac{\hbar\omega}{2k_BT})\}.\end{aligned} \tag{3.17}$$

In Eq. (3.17), the first term involving χ arises from radiation pressure, while the second term originates from the thermal noise. So the spectrum $S_Q(\omega)$ of the movable mirror depends on radiation pressure and the thermal noise.

3.4 Normal Mode Splitting and the Eigenvalues of the Matrix A

The structure of all the spectra is determined by the eigenvalues of iA (Eq. (3.11)) or the complex zeroes of the function $d(\omega)$ defined by Eq. (3.14). Clearly we need the eigenvalues of iA as the solution of (Eq. (3.9)) in Fourier domain is $f(\omega) = i(\omega - iA)^{-1}\eta(\omega)$. Let us analyse the eigenvalues of Eq. (3.11). Note that in the absence of the coupling χ=0, the eigenvalues of iA are

$$\pm\sqrt{\omega_m^2 - \frac{\gamma_m^2}{4}} - \frac{i\gamma_m}{2}; \pm\sqrt{\Delta^2 - 4G^2} - i\kappa. \tag{3.18}$$

Thus the positive frequencies of the normal modes are given by $\sqrt{\Delta^2 - 4G^2}$, $\sqrt{\omega_m^2 - \frac{\gamma_m^2}{4}}$ ($\Delta > 2G, \omega_m > \frac{\gamma_m}{2}$). The case that we consider in this chapter corresponds to

$$\omega_m \gg \tfrac{\gamma_m}{2}; \Delta > 2G; \kappa \gg \gamma_m; \omega_m > \kappa. \tag{3.19}$$

The coupling between the normal modes would be most efficient in the degenerate case i.e. when $\omega_m = \sqrt{\Delta^2 - 4G^2}$. It is known from cavity QED that the normal mode splitting leads to symmetric (asymmetric) spectra in the degenerate (nondegenerate) case, provided that the dampings of the individual modes are much smaller than the coupling constant. Thus the mechanical oscillator is like the atomic oscillator, the cavity mode in the rotating frame acquires the effective frequency $\sqrt{\Delta^2 - 4G^2}$ which is dependent on the parametric coupling. All this applies provided that damping terms do not mix the modes significantly. An estimate of the splitting can be made by using the approximations given by Eq. (3.19) and the zeroes of $d(\omega)$. We find that the frequency splitting is given by [127]

$$\omega_\pm^2 \cong \tfrac{\omega_m^2 + \Delta^2 - 4G^2}{2} \pm \sqrt{(\tfrac{\omega_m^2 - \Delta^2 + 4G^2}{2})^2 + 4\omega_m^2 g^2}, \tag{3.20}$$

where we have defined

$$g^2 = \omega_m \chi^2 |c_s|^2 [\Delta + 2G\sin(\theta - 2\varphi)],\ e^{2i\varphi} = c_s^2/|c_s|^2. \tag{3.21}$$

It should be borne in mind that c_s is dependent on the parametric coupling G. The splitting is determined by the pump power, the couplings χ and G.

The parameters used are the same as those in the recent successful experiment on optomechanical normal mode splitting [50]: the wavelength of the laser $\lambda = 2\pi c/\omega_L = 1064$ nm, $L = 25$ mm, $m = 145$ ng, $\kappa = 2\pi \times 215 \times 10^3$ Hz, $\omega_m = 2\pi \times 947 \times 10^3$ Hz, $T = 300$ mK, the mechanical quality factor $Q^{'} = \omega_m/\gamma_m = 6700$, parametric phase $\theta = \pi/4$. And in the high temperature limit $k_B T \gg \hbar\omega_m$, we have $\coth(\hbar\omega/2k_B T) \approx 2k_B T/\hbar\omega$.

Figure 3.2 shows the roots of $d(\omega)$ in the domain $\mathrm{Re}(\omega) > 0$ for different values of G. Figure 3.3 shows imaginary parts of the roots of $d(\omega)$ for different values of G. The parametric coupling affects the width of the lines and this for certain range of parameters aids in producing well split lines. One root broadens and the other root narrows. The root that broadens is the one that moves further away from the position for $G = 0$.

3.5 The Spectra of the Output Field

In this section, we would like to calculate the spectra of the output field. The fluctuations $\delta c(\omega)$ of the cavity field can be obtained from Eq. (3.8). Further using the input-output relation [128] $c_{out}(\omega) = \sqrt{2\kappa}c(\omega) - c_{in}(\omega)$, the fluctuations of the output field are given by

$$\delta c_{out}(\omega) = V(\omega)\xi(\omega) + E(\omega)\delta c_{in}(\omega) + F(\omega)\delta c_{in}^{\dagger}(-\omega), \tag{3.22}$$

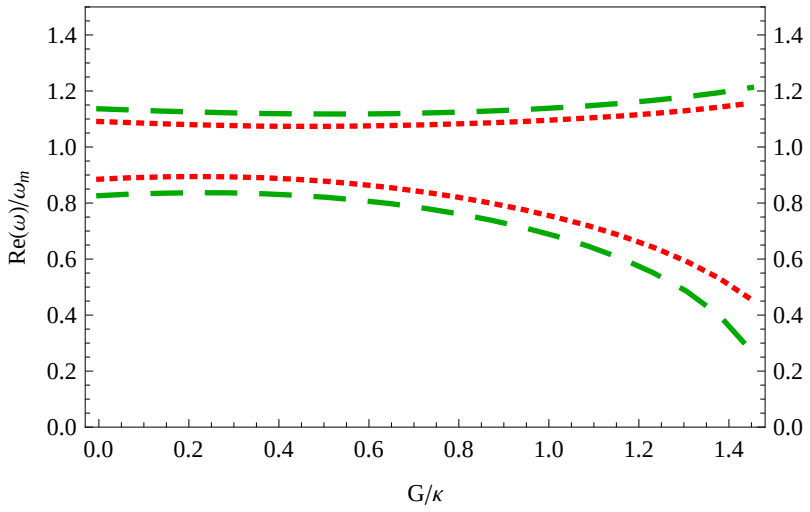

Figure 3.2: The roots of $d(\omega)$ in the domain $\mathrm{Re}(\omega) > 0$ as a function of parametric gain. $\wp = 6.9$ mW (dotted line), $\wp = 10.7$ mW (dashed line). Parameters: the cavity detuning $\Delta = \omega_m$.

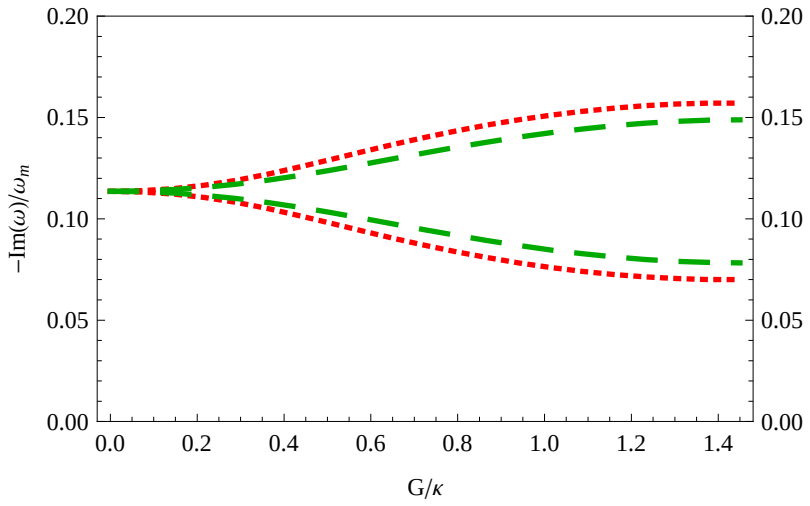

Figure 3.3: The imaginary parts of the roots of $d(\omega)$ as a function of parametric gain. $\wp = 6.9$ mW (dotted line), $\wp = 10.7$ mW (dashed line). Parameters: the cavity detuning $\Delta = \omega_m$.

where

$$
\begin{aligned}
V(\omega) &= -\tfrac{\sqrt{2\kappa}\omega_m^2\chi}{d(\omega)} i\{[\kappa - i(\omega+\Delta)]c_s - 2Ge^{i\theta}c_s^*\}, \\
E(\omega) &= \tfrac{2\kappa}{(\kappa-i\omega)^2+\Delta^2-4G^2}[-\tfrac{2\omega_m^3\chi^2}{d(\omega)} i\{[\kappa - i(\omega+\Delta)]c_s \\
&\quad -2Ge^{i\theta}c_s^*\}\{[\kappa - i(\omega+\Delta)]c_s^* + 2Ge^{-i\theta}c_s\} \\
&\quad +\kappa - i(\omega+\Delta)] - 1, \\
F(\omega) &= \tfrac{2\kappa}{(\kappa-i\omega)^2+\Delta^2-4G^2}[-\tfrac{2\omega_m^3\chi^2}{d(\omega)} i\{[\kappa - i(\omega+\Delta)]c_s \\
&\quad -2Ge^{i\theta}c_s^*\}\{[\kappa - i(\omega-\Delta)]c_s + 2Ge^{i\theta}c_s^*\} \\
&\quad +2Ge^{i\theta}].
\end{aligned}
\tag{3.23}
$$

In Eq. (3.22), the first term associated with $\xi(\omega)$ stems from the thermal noise of the mechanical oscillator, while the other two terms are from the input vacuum noise. So the fluctuations of the output field are influenced by the thermal noise and the input vacuum noise.

The spectra of the output field are defined as

$$
\begin{aligned}
\langle \delta c_{out}^\dagger(-\Omega)\delta c_{out}(\omega)\rangle &= 2\pi S_{cout}(\omega)\delta(\omega+\Omega), \\
\langle \delta x_{out}(\Omega)\delta x_{out}(\omega)\rangle &= 2\pi S_{xout}(\omega)\delta(\omega+\Omega), \\
\langle \delta y_{out}(\Omega)\delta y_{out}(\omega)\rangle &= 2\pi S_{yout}(\omega)\delta(\omega+\Omega).
\end{aligned}
\tag{3.24}
$$

where $\delta x_{out}(\omega)$ and $\delta y_{out}(\omega)$ are the Fourier transform of the fluctuations $\delta x_{out}(t)$ and $\delta y_{out}(t)$ of the output field , which are defined by $\delta x_{out}(t) = \delta c_{out}(t) + \delta c_{out}^\dagger(t)$ and $\delta y_{out}(t) = i[\delta c_{out}^\dagger(t) - \delta c_{out}(t)]$ [110]. Here $S_{cout}(\omega)$ denotes the spectral density of the output field, $S_{xout}(\omega)$ means the spectrum of fluctuations in the x quadrature of the output field, and $S_{yout}(\omega)$ is the spectrum of fluctuations in the y quadrature of the output field.

Combining Eq. (3.16), Eq. (3.22), and Eq. (3.24), we obtain the spectra of the

output field

$$
\begin{aligned}
S_{cout}(\omega) &= V^*(\omega)V(\omega) \times 2\tfrac{\gamma_m}{\omega_m}\omega[-1+\coth(\tfrac{\hbar\omega}{2k_BT})] + F^*(\omega)F(\omega),\\
S_{xout}(\omega) &= [V(-\omega)+V^*(\omega)][V(\omega)+V^*(-\omega)] \times 2\tfrac{\gamma_m}{\omega_m}\omega[-1+\coth(\tfrac{\hbar\omega}{2k_BT})]\\
&\quad +[E(-\omega)+F^*(\omega)][F(\omega)+E^*(-\omega)],\\
S_{yout}(\omega) &= -[V^*(\omega)-V(-\omega)][V^*(-\omega)-V(\omega)] \times 2\tfrac{\gamma_m}{\omega_m}\omega[-1+\coth(\tfrac{\hbar\omega}{2k_BT})]\\
&\quad -[F^*(\omega)-E(-\omega)][E^*(-\omega)-F(\omega)].
\end{aligned}
\tag{3.25}
$$

From Eq. (3.25), it is seen that any spectrum of the output field includes two terms, the first term is from the contribution of the thermal noise of the mechanical oscillator, the second term is from the contribution of the input vacuum noise.

We note that the spectra $S_Q(\omega)$, $S_{cout}(\omega)$, $S_{xout}(\omega)$, and $S_{yout}(\omega)$ are determined by the detuning Δ, parametric gain G, parametric phase θ, input laser power $\wp$, and cavity length L. In the following we will concentrate on discussing the dependence of the spectra on parametric gain and input laser power.

3.6 Numerical Results

In this section, we numerically evaluate the spectra $S_Q(\omega)$, $S_{cout}(\omega)$, $S_{xout}(\omega)$, and $S_{yout}(\omega)$ given by Eq. (3.17) and Eq. (3.25) to show the effect of an OPA in the cavity on the normal mode splitting of the movable mirror and the output field.

We typically imagine a setup like in the original squeezing experiment [97] where the experiment is done, for different levels of the pumping of OPA i.e., we start with $G = 0$ and then increase it to a value consistent with the stability requirements. We consider the degenerate case $\Delta = \omega_m$ for $G = 0$, and choose $\wp = 6.9$ mW. In order to satisfy the stability conditions (3.12), parametric gain must satisfy $G \leq 1.62\kappa$. The figures 3.4 – 3.7 show the spectra $S_Q(\omega)$, $S_{cout}(\omega)$, $S_{xout}(\omega)$, and $S_{yout}(\omega)$ as a function of the normalized frequency ω/ω_m for various values of parametric gain. When the OPA is absent ($G = 0$), the spectra barely show the normal mode splitting. As

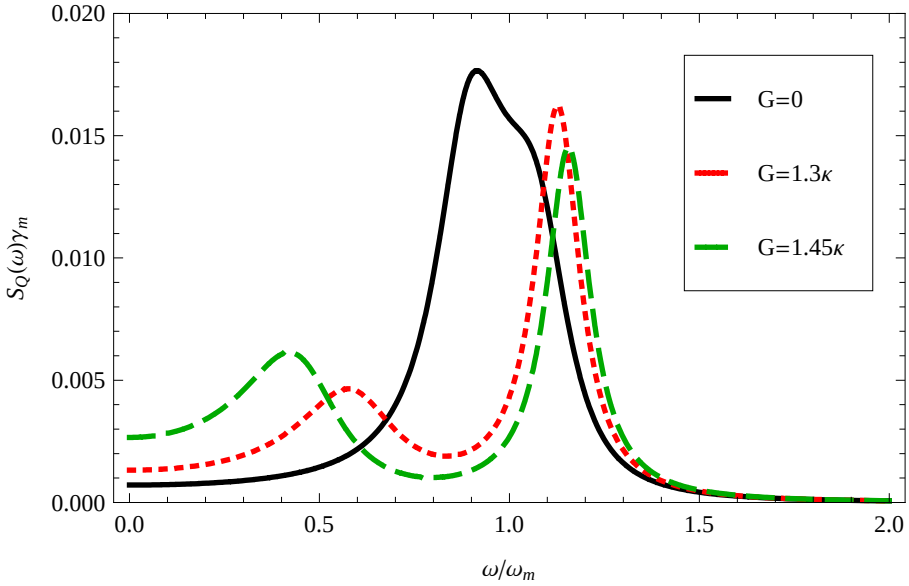

Figure 3.4: The scaled spectrum $S_Q(\omega) \times \gamma_m$ versus the normalized frequency ω/ω_m for different parametric gain. G= 0 (solid curve), 1.3κ (dotted curve), 1.45κ (dashed curve). Parameters: the cavity detuning $\Delta = \omega_m$, the laser power $\wp = 6.9$ mW.

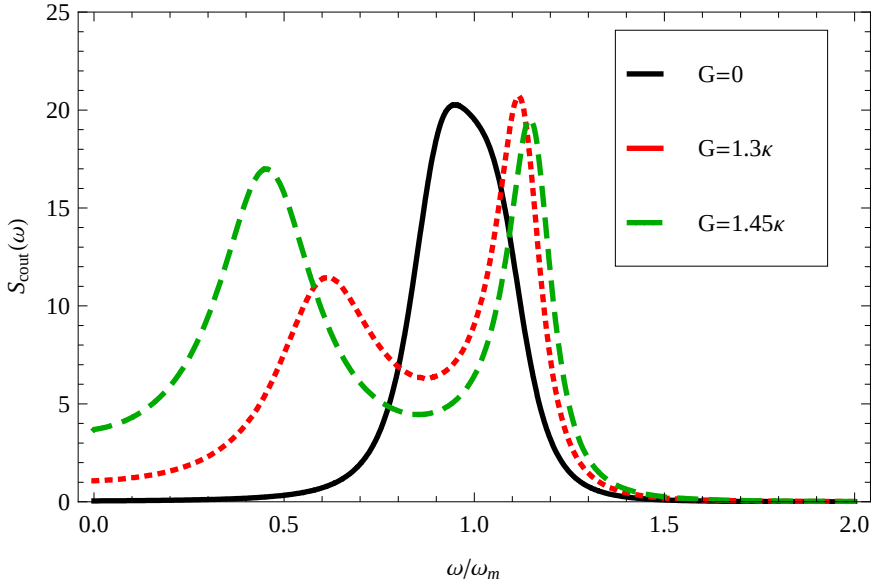

Figure 3.5: The spectrum $S_{cout}(\omega)$ versus the normalized frequency ω/ω_m for different parametric gain. G= 0 (solid curve), 1.3κ (dotted curve), 1.45κ (dashed curve). Parameters: the cavity detuning $\Delta = \omega_m$, the laser power $\wp = 6.9$ mW.

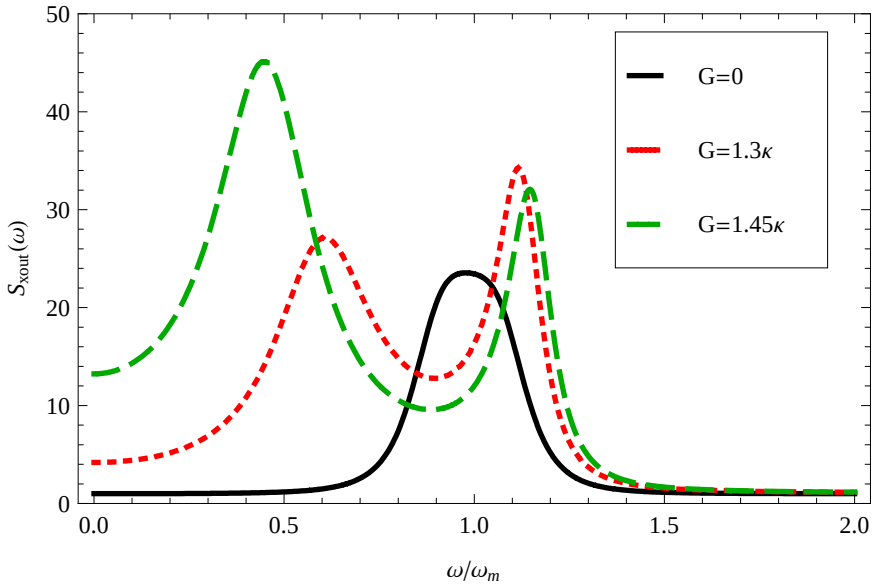

Figure 3.6: The spectrum $S_{xout}(\omega)$ versus the normalized frequency ω/ω_m for different parametric gain. G= 0 (solid curve), 1.3κ (dotted curve), 1.45κ (dashed curve). Parameters: the cavity detuning $\Delta = \omega_m$, the laser power $\wp = 6.9$ mW.

parametric gain is increased, the normal mode splitting becomes observable. This is due to significant changes in the line widths and position. When $G = 1.3\kappa$, two peaks can be found in the spectra. According to the numerical calculations of Figs. 3.2 and 3.3, these roots in units of ω_m are at (A) $G = 0$: $0.885 - 0.113i$, $1.091 - 0.113i$ for 6.9 mW pump power and $0.826 - 0.113i$, $1.136 - 0.113i$ for 10.7 mW pump power. (B) $G = 1.3\kappa$: $0.596 - 0.156i$, $1.129 - 0.070i$ for 6.9 mW pump power and $0.490 - 0.148i$, $1.178 - 0.079i$ for 10.7 mW pump power. We see that the line width of the two peaks is approximately same for $G = 0$ but for two different power levels. The line widths change significantly for $G \neq 0$. Note that the separation between two peaks becomes larger as parametric gain increases. The reason is that increasing the parametric gain causes a stronger coupling between the movable mirror and the cavity field due to an increase in the photon number in the cavity. The values of intracavity photon number $|c_s|^2$ are 2.68×10^9, 4.30×10^9, 5.65×10^9 for $G = 0$, 1.3κ, and 1.45κ respectively.

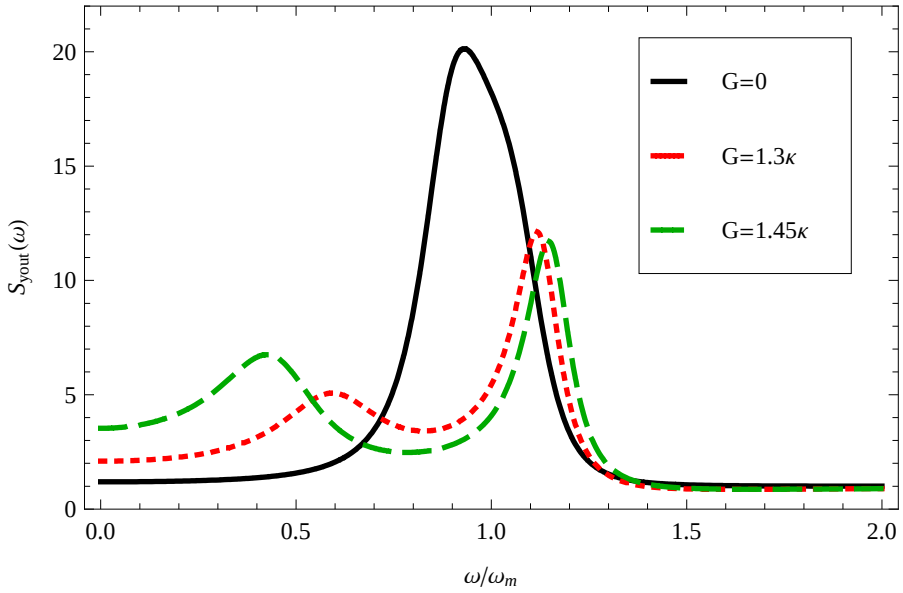

Figure 3.7: The spectrum $S_{yout}(\omega)$ versus the normalized frequency ω/ω_m for different parametric gain. G= 0 (solid curve), 1.3κ (dotted curve), 1.45κ (dashed curve). Parameters: the cavity detuning $\Delta = \omega_m$, the laser power $\wp = 6.9$ mW.

We have examined the contributions of various terms in Eq. (3.25) to the output spectrum. The dominant contribution comes from the mechanical oscillator. Note further the similarity [50] of the spectrum of the output quadrature y (Fig. 3.7) to the spectrum of the mechanical oscillator (Fig. 3.4). It should be borne in mind that the strong asymmetries in the spectra for $G \neq 0$ arise from the fact that by fixing Δ at ω_m, the frequencies of the cavity mode and the mechanical oscillator do not coincide if $G \neq 0$; $\chi = 0$. Besides the damping term κ, being not negligible compared to Δ, also contributes to asymmetries.

Now we fix parametric gain $G = 1.3\kappa$, and choose $\Delta = \sqrt{\omega_m^2 + 4G^2}$, the input laser power must satisfy $\wp \leq 55$ mW. The spectrum $S_Q(\omega)$ as a function of the normalized frequency ω/ω_m for increasing the input laser power is shown in Fig. 3.8. As we increase the laser power from 0.6 mW to 10.7 mW, the spectrum exhibits a doublet and the peak separation is proportional to the laser power, because the

coupling between the movable mirror and the cavity field for a given parametric gain G is increased with increasing the input laser power due to an increase in photon number.

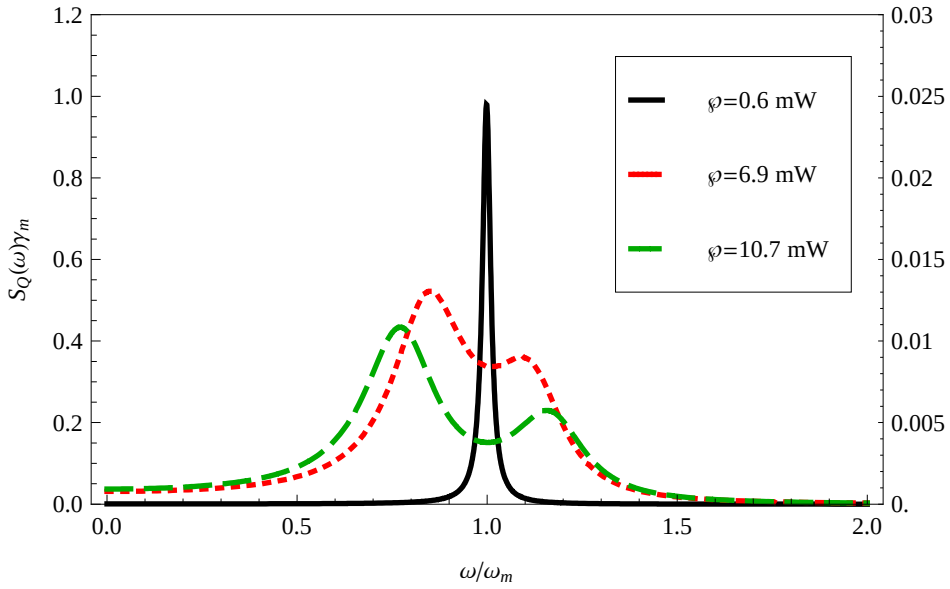

Figure 3.8: The scaled spectrum $S_Q(\omega) \times \gamma_m$ versus the normalized frequency ω/ω_m, each curve corresponds to a different input laser power. ℘= 0.6 mW (solid curve, leftmost vertical scale), 6.9 mW (dotted curve, rightmost vertical scale), 10.7 mW (dashed curve, rightmost vertical scale). Parameters: the cavity detuning $\Delta = \sqrt{\omega_m^2 + 4G^2}$, parametric gain $G = 1.3\kappa$.

For comparison, we also consider the case of the cavity without OPA ($G = 0$), the spectrum $S_Q(\omega)$ as a function of the normalized frequency ω/ω_m for increasing the input laser power at $\Delta = \omega_m$ is plotted in Fig. 3.9. We can see if the laser power is increased from 0.6 mW to 10.7 mW, the spectrum also displays normal mode splitting. However the normal mode with OPA (Fig. 3.8) are more pronounced than that in the absence of OPA (Fig. 3.9).

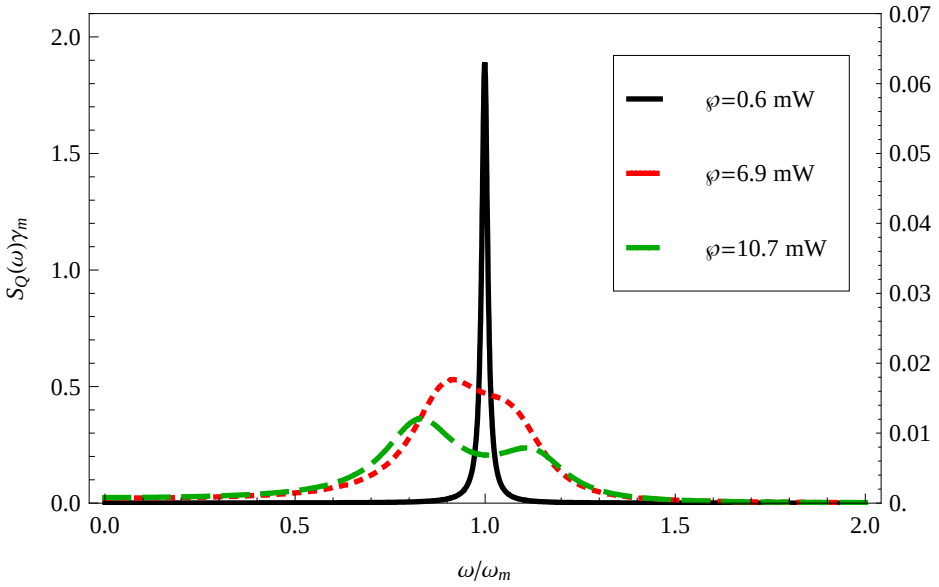

Figure 3.9: The scaled spectrum $S_Q(\omega) \times \gamma_m$ versus the normalized frequency ω/ω_m, each curve corresponds to a different input laser power. $\wp$= 0.6 mW (solid curve, leftmost vertical scale), 6.9 mW (dotted curve, rightmost vertical scale), 10.7 mW (dashed curve, rightmost vertical scale). Parameters: the cavity detuning $\Delta = \omega_m$, parametric gain $G = 0$.

3.7 Conclusions

In conclusion, we have shown how the normal mode splitting behavior of the movable mirror and the output field is affected by the OPA in the cavity. We work in the resolved sideband regime and operate under the stability conditions (3.12). We find that increasing parametric gain can make the spectra $S_Q(\omega)$, $S_{cout}(\omega)$, $S_{xout}(\omega)$, and $S_{yout}(\omega)$ evolve from a single peak to two peaks. Furthermore, for a given parametric gain, increasing input laser power can increase the amount of normal mode splitting of the movable mirror due to the stronger coupling between the movable mirror and the cavity field.

The content of this chapter has been published in *Phys. Rev. A* **80**, 033807 (2009).

CHAPTER 4

SQUEEZING OF A NANOMECHANICAL OSCILLATOR

4.1 Overview

The optomechanical system has attracted much attention because of its potential applications in high precision measurements and quantum information processing [28, 35, 36, 37, 88, 90, 129, 130, 131]. Meanwhile, it provides a means of probing quantum behavior of a macroscopic object if a nanomechanical oscillator can be cooled down to near its quantum ground state [38, 115]. Many of these applications are becoming possible due to advances in cooling the mirror [6, 7, 8, 9, 10, 56, 118]. Further as pointed out in Refs [47, 66, 120], the ground state cooling can be achieved in the resolved sideband regime where the frequency of the mechanical mirror is much larger than the cavity decay rate.

Squeezing of a nanomechanical oscillator plays a vital role in high-sensitive detection of position and force due to its less noise in one quadrature than the coherent state. A number of different methods have been developed to generate and enhance squeezing of a nanomechanical oscillator, such as coupling a nanomechanical oscillator to an atomic gas [132], a Cooper pair box [133], a SQUID device [215], using three-wave mixing [135] or Circuit QED [136], or by means of quantum measurement and feedback schemes [137, 138, 139, 140]. A recent paper [32] reports squeezed state of a mechanical mirror can be created by transfer of squeezing from a squeezed vacuum to a membrane within an optical cavity under the conditions of ground state cooling. We previously considered the possibility of using an OPA inside the cavity for changing the nature of the statistical fluctuations [126].

In this chapter, we propose a scheme that is capable of generating squeezing of the movable mirror by feeding broad band squeezed vacuum light along with the laser light. The achieved squeezing of the mirror depends on the temperature of the mirror, the laser power, and degree of squeezing of the input light. One can obtain squeezing which could be more than 70%.

The chapter is structured as follows. In Sec. II we describe the model, give the quantum Langevin equations, and obtain the steady-state mean values. In Sec. III we derive the stability conditions, calculate the mean square fluctuations in position and momentum of the movable mirror. In Sec. IV we analyze how the momentum squeezing of the movable mirror is affected by the squeezing parameter, the temperature of the environment, and the laser power. We also compare the momentum fluctuations of the movable mirror in the presence of the coupling to the cavity field with that in the absence of the coupling to cavity field. We find very large squeezing with respect to thermal fluctuations, for instance at 1 mK, the momentum fluctuations go down by a factor more than one hundred. Our predictions of squeezing are based on the parameters used in a recent experiment on normal mode splitting in a nanomechanical oscillator [50].

4.2 Model

The system to be considered, sketched in Fig. 4.1, is a Fabry-Perot cavity with one fixed partially transmitting mirror and one movable perfectly reflecting mirror in thermal equilibrium with its environment at a low temperature. The cavity with length L is driven by a laser with frequency ω_L, then the photons in the cavity will exert a radiation pressure force on the movable mirror due to momentum transfer. This force is proportional to the instantaneous photon number in the cavity. The mirror also undergoes thermal fluctuations due to environment. Under the effects of the two forces, the movable mirror makes oscillation around its equilibrium position.

Here we treat the movable mirror as a quantum mechanical harmonic oscillator with effective mass m, frequency ω_m and momentum decay rate γ_m. We further assume that the cavity is fed with squeezed light at frequency ω_S.

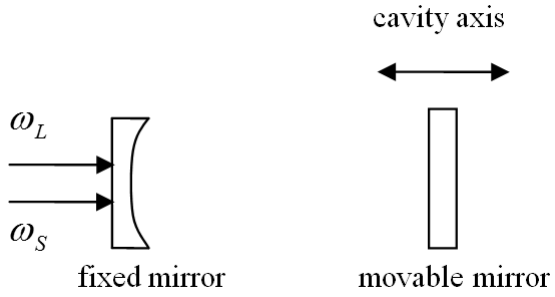

Figure 4.1: Sketch of the studied system. A laser with frequency ω_L and squeezed vacuum light with frequency ω_S enter the cavity through the partially transmitting mirror.

In the adiabatic limit, $\omega_m \ll \frac{c}{2L}$ (c is the speed of light in vacuum), we ignore the scattering of photons to other cavity modes, thus only one cavity mode ω_c is considered [64, 106]. In a frame rotating at the laser frequency, the Hamiltonian for the system can be written as

$$H = \hbar(\omega_c - \omega_L)n_c - \hbar g n_c Q + \frac{\hbar\omega_m}{4}(Q^2 + P^2) + i\hbar\varepsilon(c^\dagger - c), \tag{4.1}$$

we have used the normalized coordinates for the oscillator defined by $Q = \sqrt{\frac{2m\omega_m}{\hbar}}q$ and $P = \sqrt{\frac{2}{m\hbar\omega_m}}p$ with $[Q, P] = 2i$. This normalization implies that in the ground state of the nanomechanical mirror $\langle Q^2\rangle = \langle P^2\rangle = 1$. Further in Eq. (4.1) the first term is the energy of the cavity field, $n_c = c^\dagger c$ is the number of the photons inside the cavity, c and $c^\dagger$ are the annihilation and creation operators for the cavity field with $[c, c^\dagger] = 1$. The second term comes from the coupling of the movable mirror to the cavity field via radiation pressure, the parameter $g = \frac{\omega_c}{L}\sqrt{\frac{\hbar}{2m\omega_m}}$ is the optomechanical coupling constant between the cavity and the movable mirror. The third term corresponds the energy of the movable mirror. The fourth term describes

the coupling between the input laser field and the cavity field, ε is related to the input laser power $\wp$ by $\varepsilon = \sqrt{\frac{2\kappa\wp}{\hbar\omega_L}}$, where κ is the cavity decay rate associated with the transmission loss of the fixed mirror.

The equations of motion of the system can be derived by the Heisenberg equations of motion and adding the corresponding noise terms, this gives the quantum Langevin equations

$$\begin{aligned}
\dot{Q} &= \omega_m P, \\
\dot{P} &= 2gn_c - \omega_m Q - \gamma_m P + \xi, \\
\dot{c} &= i(\omega_L - \omega_c + gQ)c + \varepsilon - \kappa c + \sqrt{2\kappa}c_{in}, \\
\dot{c}^\dagger &= -i(\omega_L - \omega_c + gQ)c^\dagger + \varepsilon - \kappa c^\dagger + \sqrt{2\kappa}c_{in}^\dagger.
\end{aligned} \tag{4.2}$$

Here we have introduced the input squeezed vacuum noise operator c_{in} with frequency $\omega_S = \omega_L + \omega_m$. It has zero mean value, and nonzero time-domain correlation functions [141]

$$\begin{aligned}
\langle \delta c_{in}^\dagger(t)\delta c_{in}(t')\rangle &= N\delta(t-t'), \\
\langle \delta c_{in}(t)\delta c_{in}^\dagger(t')\rangle &= (N+1)\delta(t-t'), \\
\langle \delta c_{in}(t)\delta c_{in}(t')\rangle &= Me^{-i\omega_m(t+t')}\delta(t-t'), \\
\langle \delta c_{in}^\dagger(t)\delta c_{in}^\dagger(t')\rangle &= M^* e^{i\omega_m(t+t')}\delta(t-t').
\end{aligned} \tag{4.3}$$

where $N = \sinh^2(r)$, $M = \sinh(r)\cosh(r)e^{i\varphi}$, r is the squeezing parameter of the squeezed vacuum light, and φ is the phase of the squeezed vacuum light. For simplicity, we choose $\varphi = 0$. The force ξ is the thermal Langevin force resulting from the coupling of the movable mirror to the environment, whose mean value is zero, and it has the following correlation function at temperature T [108]:

$$\langle \xi(t)\xi(t')\rangle = \frac{\gamma_m}{\pi\omega_m}\int \omega e^{-i\omega(t-t')}\left[1 + \coth(\frac{\hbar\omega}{2k_BT})\right]d\omega, \tag{4.4}$$

where k_B is the Boltzmann constant and T is the temperature of the environment. By using standard methods [110], setting all the time derivatives in Eq. (4.2) to

zero, and solving it, we obtain the steady-state mean values

$$P_s = 0,\ Q_s = \frac{2g|c_s|^2}{\omega_m},\ c_s = \frac{\varepsilon}{\kappa + i\Delta}, \tag{4.5}$$

where

$$\Delta = \omega_c - \omega_L - gQ_s = \Delta_0 - gQ_s = \Delta_0 - \frac{2g^2|c_s|^2}{\omega_m} \tag{4.6}$$

is the effective cavity detuning, depending on Q_s. The Q_s denotes the new equilibrium position of the movable mirror relative to that without the driving field. Further c_s represents the steady-state amplitude of the cavity field. From Eq. (4.5) and Eq. (4.6), we can see Q_s satisfies a third order equation. For a given detuning Δ_0, Q_s will at most have three real values. Therefore, Q_s and c_s display an optical multistable behavior [41, 42, 43], which is a nonlinear effect induced by the radiation-pressure coupling of the movable mirror to the cavity field.

4.3 Radiation Pressure and Quantum Fluctuations

To study squeezing of the movable mirror, we need to calculate the fluctuations in the mirror's amplitude. Assuming that the nonlinear coupling between the cavity field and the movable mirror is weak, the fluctuation of each operator is much smaller than the corresponding steady-state mean value, thus we can linearize the system around the steady state. Writing each operator of the system as the sum of its steady-state mean value and a small fluctuation with zero mean value,

$$Q = Q_s + \delta Q,\quad P = P_s + \delta P,\quad c = c_s + \delta c. \tag{4.7}$$

Inserting Eq. (4.7) into Eq. (4.2), then assuming $|c_s| \gg 1$, the linearized quantum Langevin equations for the fluctuation operators can be expressed as follows,

$$\begin{aligned}
\delta\dot{Q} &= \omega_m \delta P, \\
\delta\dot{P} &= 2g(c_s^* \delta c + c_s \delta c^\dagger) - \omega_m \delta Q - \gamma_m \delta P + \xi, \\
\delta\dot{c} &= -(\kappa + i\Delta)\delta c + igc_s \delta Q + \sqrt{2\kappa}\delta c_{in}, \\
\delta\dot{c}^\dagger &= -(\kappa - i\Delta)\delta c^\dagger - igc_s^* \delta Q + \sqrt{2\kappa}\delta c_{in}^\dagger.
\end{aligned} \tag{4.8}$$

Introducing the cavity field quadratures $\delta x = \delta c + \delta c^\dagger$ and $\delta y = i(\delta c^\dagger - \delta c)$, and the input noise quadratures $\delta x_{in} = \delta c_{in} + \delta c_{in}^\dagger$ and $\delta y_{in} = i(\delta c_{in}^\dagger - \delta c_{in})$, Eq. (4.8) can be rewritten in the matrix form

$$\dot{f}(t) = Af(t) + \eta(t), \tag{4.9}$$

in which $f(t)$ is the column vector of the fluctuations, $\eta(t)$ is the column vector of the noise sources. Their transposes are

$$\begin{aligned}
f(t)^T &= (\delta Q, \delta P, \delta x, \delta y), \\
\eta(t)^T &= (0, \xi, \sqrt{2\kappa}\delta x_{in}, \sqrt{2\kappa}\delta y_{in});
\end{aligned} \tag{4.10}$$

and the matrix A is given by

$$A = \begin{pmatrix}
0 & \omega_m & 0 & 0 \\
-\omega_m & -\gamma_m & g(c_s + c_s^*) & -ig(c_s - c_s^*) \\
ig(c_s - c_s^*) & 0 & -\kappa & \Delta \\
g(c_s + c_s^*) & 0 & -\Delta & -\kappa
\end{pmatrix}. \tag{4.11}$$

The system is stable only if the real parts of all the eigenvalues of the matrix A are negative. The stability conditions for the system can be derived by applying the

Routh-Hurwitz criterion [112, 113], we get

$$\begin{aligned}
&\kappa\gamma_m[(\kappa^2+\Delta^2)^2+(2\kappa\gamma_m+\gamma_m^2-2\omega_m^2)(\kappa^2+\Delta^2)\\
&+\omega_m^2(4\kappa^2+\omega_m^2+2\kappa\gamma_m)]+2\omega_m\Delta g^2|c_s|^2\\
&\times(2\kappa+\gamma_m)^2>0,\\
&\omega_m(\kappa^2+\Delta^2)-4\Delta g^2|c_s|^2>0.
\end{aligned} \tag{4.12}$$

All the external parameters chosen in this paper satisfy the stability conditions (4.12) to ensure the system to be stable.

Fourier transforming each operator in Eq. (4.8) and solving it in the frequency domain, the position fluctuations of the movable mirror are given by

$$\begin{aligned}
\delta Q(\omega)=&\tfrac{1}{d(\omega)}(2\sqrt{2\kappa}\omega_m g\{[\kappa-i(\Delta+\omega)]c_s^*\delta c_{in}(\omega)\\
&+[\kappa+i(\Delta-\omega)]c_s\delta c_{in}^\dagger(-\omega)\}\\
&+\omega_m[(\kappa-i\omega)^2+\Delta^2]\xi(\omega)),
\end{aligned} \tag{4.13}$$

where $d(\omega)=-4\omega_m\Delta g^2|c_s|^2+(\omega_m^2-\omega^2-i\gamma_m\omega)[(\kappa-i\omega)^2+\Delta^2]$. In Eq. (4.13), the first term proportional to g originates from radiation pressure, while the second term involving ξ is from the thermal noise. So the position fluctuations of the movable mirror are now determined by radiation pressure and the thermal noise. In the case of no coupling with the cavity field, the movable mirror will make Brownian motion, $\delta Q(\omega)=\omega_m\xi(\omega)/(\omega_m^2-\omega^2-i\gamma_m\omega)$, whose susceptibility has a Lorentzian shape centered at frequency ω_m with width γ_m.

Taking Fourier transform of $\delta\dot{Q}=\omega_m\delta P$ in Eq. (4.8), we further obtain the momentum fluctuations of the movable mirror, $\delta P(\omega)=-i\frac{\omega}{\omega_m}\delta Q(\omega)$.

The mean square fluctuations in position and momentum of the movable mirror are determined by

$$\begin{aligned}
\langle\delta Q(t)^2\rangle&=\tfrac{1}{4\pi^2}\int\int_{-\infty}^{+\infty}d\omega d\Omega e^{-i(\omega+\Omega)t}\langle\delta Q(\omega)\delta Q(\Omega)\rangle,\\
\langle\delta P(t)^2\rangle&=\tfrac{1}{4\pi^2}\int\int_{-\infty}^{+\infty}d\omega d\Omega e^{-i(\omega+\Omega)t}\langle\delta P(\omega)\delta P(\Omega)\rangle.
\end{aligned} \tag{4.14}$$

To calculate the mean square fluctuations, we require the correlation functions of the noise sources in the frequency domain,

$$\begin{aligned}
\langle \delta c_{in}^{\dagger}(\omega)\delta c_{in}(\Omega)\rangle &= 2\pi N\delta(\omega+\Omega),\\
\langle \delta c_{in}(\omega)\delta c_{in}^{\dagger}(\Omega)\rangle &= 2\pi (N+1)\delta(\omega+\Omega),\\
\langle \delta c_{in}(\omega)\delta c_{in}(\Omega)\rangle &= 2\pi M\delta(\omega+\Omega-2\omega_m),\\
\langle \delta c_{in}^{\dagger}(\omega)\delta c_{in}^{\dagger}(\Omega)\rangle &= 2\pi M^{*}\delta(\omega+\Omega+2\omega_m),\\
\langle \xi(\omega)\xi(\Omega)\rangle &= 4\pi\gamma_m\tfrac{\omega}{\omega_m}\left[1+\coth(\tfrac{\hbar\omega}{2k_BT})\right]\delta(\omega+\Omega).
\end{aligned} \tag{4.15}$$

Combining Eqs. (4.13) – (4.15), after some calculations, the mean square fluctuations of Eq. (4.14) are written as

$$\begin{aligned}
\langle \delta Q(t)^2\rangle &= \tfrac{1}{2\pi}\textstyle\int_{-\infty}^{+\infty}\omega_m^2(A+Be^{-2i\omega_m t}+Ce^{2i\omega_m t})d\omega,\\
\langle \delta P(t)^2\rangle &= \tfrac{1}{2\pi}\textstyle\int_{-\infty}^{+\infty}[\omega^2 A+\omega(\omega-2\omega_m)Be^{-2i\omega_m t}\\
&\qquad +\omega(\omega+2\omega_m)Ce^{2i\omega_m t}]d\omega.
\end{aligned} \tag{4.16}$$

where

$$\begin{aligned}
A &= \tfrac{1}{d(\omega)d(-\omega)}(8\kappa g^2|c_s|^2\{(N+1)[\kappa^2+(\Delta+\omega)^2]\\
&\quad +N[\kappa^2+(\Delta-\omega)^2]\}+2\gamma_m\tfrac{\omega}{\omega_m}[(\Delta^2+\kappa^2-\omega^2)^2\\
&\quad +4\kappa^2\omega^2][1+\coth(\tfrac{\hbar\omega}{2k_BT})]),\\
B &= \tfrac{8\kappa g^2 c_s^{*2}M}{d(\omega)d(2\omega_m-\omega)}[\kappa-i(\Delta+\omega)][\kappa-i(\Delta+2\omega_m-\omega)],\\
C &= \tfrac{8\kappa g^2 c_s^{2}M^{*}}{d(\omega)d(-2\omega_m-\omega)}[\kappa+i(\Delta-\omega)][\kappa+i(\Delta+2\omega_m+\omega)].
\end{aligned} \tag{4.17}$$

In Eqs. (4.16) and (4.17), the term independent of g is from the thermal noise contribution; while those terms involving g arise from the radiation pressure contribution, including the influence of the squeezed vacuum light. Moreover, either $\langle \delta Q(t)^2\rangle$ or $\langle \delta P(t)^2\rangle$ contains three terms, the first term is independent of time, but the second and third terms are time-dependent, which causes $\langle \delta Q(t)^2\rangle$ and $\langle \delta P(t)^2\rangle$ vary with time. The complex exponential in Eq. (4.16) can be removed by working in the

interaction picture. Let's define b ($b^\dagger$) and $\tilde{b}$ ($\tilde{b}^\dagger$) be the annihilation (creation) operators for the oscillator in the Schrödinger and interaction picture with $[b, b^\dagger] = 1$ and $[\tilde{b}, \tilde{b}^\dagger] = 1$. The relations between them are $b = \tilde{b}e^{-i\omega_m t}$ and $b^\dagger = \tilde{b}^\dagger e^{i\omega_m t}$. Then using $Q = b + b^\dagger$, $P = i(b^\dagger - b)$, $\tilde{Q} = \tilde{b} + \tilde{b}^\dagger$, and $\tilde{P} = i(\tilde{b}^\dagger - \tilde{b})$, we get

$$\begin{aligned} \langle \delta\tilde{Q}^2 \rangle &= \tfrac{1}{2\pi} \int_{-\infty}^{+\infty} \omega_m^2 (A + B + C) d\omega, \\ \langle \delta\tilde{P}^2 \rangle &= \tfrac{1}{2\pi} \int_{-\infty}^{+\infty} [\omega^2 A + \omega(\omega - 2\omega_m)B + \omega(\omega + 2\omega_m)C] d\omega. \end{aligned} \tag{4.18}$$

According to the Heisenberg uncertainty principle,

$$\langle \delta\tilde{Q}^2 \rangle \langle \delta\tilde{P}^2 \rangle \geq |\frac{1}{2}[\tilde{Q}, \tilde{P}]|^2. \tag{4.19}$$

If either $\langle \delta\tilde{Q}^2 \rangle < 1$ or $\langle \delta\tilde{P}^2 \rangle < 1$, the movable mirror is said to be squeezed.

From Eqs. (4.17) and (4.18), we find $\langle \delta\tilde{Q}^2 \rangle$ or $\langle \delta\tilde{P}^2 \rangle$ is determined by the detuning Δ_0, the squeezing parameter r, the laser power $\wp$, the cavity length L, the temperature of the environment T, and so on. Here we focus on the dependence of $\langle \delta\tilde{Q}^2 \rangle$ and $\langle \delta\tilde{P}^2 \rangle$ on the squeezing parameter, the temperature of the environment, and the laser power.

4.4 Squeezing of the Movable Mirror

In this section, we numerically evaluate the mean square fluctuations in position and momentum of the movable mirror given by Eq. (4.18) to show squeezing of the movable mirror produced by feeding the squeezed vacuum light at the input mirror. We use the same parameters as those in the recent successful experiment on normal mode splitting in a nanomechanical oscillator [50]: the wave length of the laser $\lambda = \frac{2\pi c}{\omega_L} = 1064$ nm, $L = 25$ mm, $m = 145$ ng, $\kappa = 2\pi \times 215 \times 10^3$ Hz, $\omega_m = 2\pi \times 947 \times 10^3$ Hz, the mechanical quality factor $Q' = \frac{\omega_m}{\gamma_m} = 6700$. In the case of $k_B T \gg \hbar\omega_m$, we may approximate $\coth(\hbar\omega/(2k_B T)) \simeq 2k_B T/(\hbar\omega)$. In the case of $T = 0$ K, if $\omega < 0$, $\coth(\hbar\omega/(2k_B T)) \simeq -1$, if $\omega > 0$, $\coth(\hbar\omega/(2k_B T)) \simeq 1$. Through numerical calculations, it is found that squeezing of $\langle \delta\tilde{Q}^2 \rangle$ doesn't exist but squeezing of $\langle \delta\tilde{P}^2 \rangle$ exists. In the following we therefore concentrate on discussing $\langle \delta\tilde{P}^2 \rangle$.

Note that in the absence of the coupling to the cavity field, the movable mirror is in free space, and is coupled to the environment. Then the fluctuations are given by

$$\begin{aligned}\langle\delta\tilde{Q}^2\rangle = \langle\delta\tilde{P}^2\rangle &= 1+\frac{2}{e^{\hbar\omega_m/(k_BT)}-1} \\ &= \begin{cases} 1 & \text{for } T=0 \text{ K}, \\ 44 & \text{for } T=1 \text{ mK}, \\ 440 & \text{for } T=10 \text{ mK}. \end{cases}\end{aligned} \tag{4.20}$$

As well known no squeezing of the movable mirror occurs.

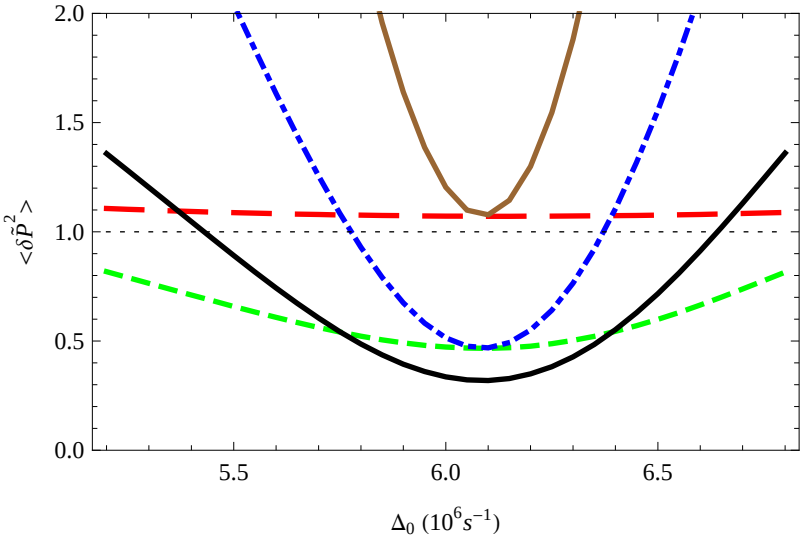

Figure 4.2: The mean square fluctuations $\langle\delta\tilde{P}^2\rangle$ versus the detuning Δ_0 (10^6 s^{-1}) for different values of the squeezing of the input field. $r=0$ (red, big dashed line), $r=0.5$ (green, small dashed line), $r=1$ (black, solid curve), $r=1.5$ (blue, dotdashed curve), $r=2$ (brown, solid curve). The minimum values of $\langle\delta\tilde{P}^2\rangle$ are 1.071 (r=0), 0.467 (r=0.5), 0.319 (r=1), 0.468 (r=1.5), 1.078 (r=2). The flat dotted line represents the variance of the coherent light ($\langle\delta\tilde{P}^2\rangle$=1). Parameters: the temperature of the environment $T=1$ mK, the laser power $\wp=6.9$ mW.

Now we consider fluctuations in the presence of the coupling to the cavity field. If we choose $T=1$ mK, and $\wp=6.9$ mW, the mean square fluctuations $\langle\delta\tilde{P}^2\rangle$ are

plotted as a function of the detuning Δ_0 in Fig. 4.2. Different graphs correspond to different values of the squeezing of the input light. In the case of no injection of the squeezed vacuum light ($r = 0$), which means that the squeezed vacuum light is replaced by an ordinary vacuum light, we find $\langle \delta \tilde{P}^2 \rangle$ is always larger than unity (the coherent level), the minimum value of $\langle \delta \tilde{P}^2 \rangle$ is 1.071, thus there is no momentum squeezing of the movable mirror. However, if we inject the squeezed vacuum light, it is seen that the momentum squeezing of the movable mirror occurs, and the maximum squeezing happens at about $r = 1$, the corresponding minimum value of $\langle \delta \tilde{P}^2 \rangle$ is 0.319, thus the maximum amount of squeezing is about 68%. So the injection of the squeezed vacuum light greatly reduces the fluctuations in momentum, because using the squeezed vacuum light increases the photon number in the cavity, which results in a stronger radiation pressure acting on the movable mirror. Note that the minimum value of $\langle \delta \tilde{P}^2 \rangle$ in the presence of the coupling to the cavity field is much less than that ($\langle \delta \tilde{P}^2 \rangle = 44$) in the absence of the coupling to the cavity field. So there is very large squeezing with respect to thermal fluctuations. The momentum fluctuations can be reduced by a factor more than one hundred.

Then we fix the squeezing parameter $r = 1$, the mean square fluctuations $\langle \delta \tilde{P}^2 \rangle$ as a function of the detuning Δ_0 for different temperature of the environment and laser power are shown in Figs. 4.3 – 4.5. For a given lase power, we find that the minimum value of $\langle \delta \tilde{P}^2 \rangle$ decreases with decrease of the temperature of the environment as expected. The lower is the temperature, the less is the thermal noise. At $T = 0$ K, the minimum value of $\langle \delta \tilde{P}^2 \rangle$ is the smallest due to no thermal noise, which corresponds to the maximum momentum squeezing of the movable mirror. For example, when $T = 0$ K and $\wp = 0.6$ mW, the minimum value of $\langle \delta \tilde{P}^2 \rangle$ is 0.252, the corresponding amount of squeezing is up to about 75%. Therefore, decreasing the temperature of the environment can enhance the amount of the momentum squeezing of the movable mirror. On the other hand, we note that when the temperature of the environment

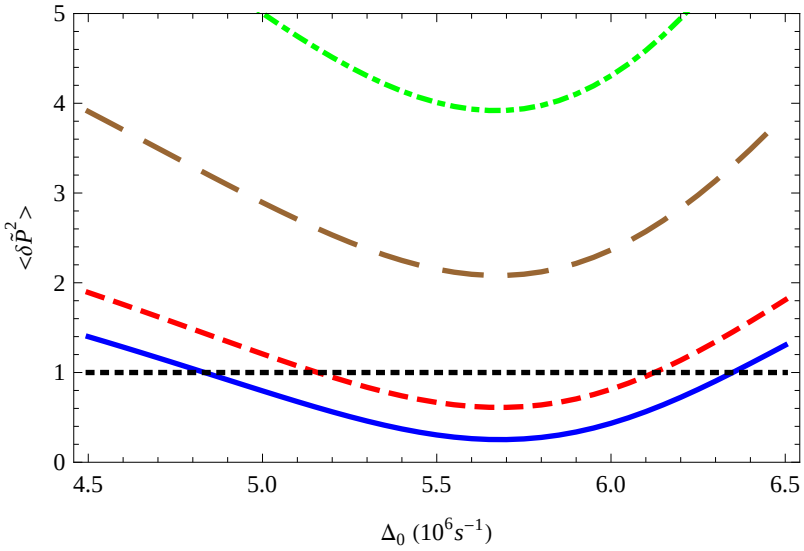

Figure 4.3: The mean square fluctuations $\langle\delta\tilde{P}^2\rangle$ versus the detuning Δ_0 (10^6 s^{-1}), each curve corresponds to a different temperature of the environment. T=0 K (blue, solid curve), 1 mK (red, small dashed curve), 5 mK (brown, big dashed curve), 10 mK (green, dotdashed curve). The minimum values of $\langle\delta\tilde{P}^2\rangle$ are 0.252 (T=0 K), 0.611 (T=1 mK), 2.082 (T=5 mK), 3.919 (T=10 mK). The flat dotted line represents the variance of the coherent light ($\langle\delta\tilde{P}^2\rangle$=1). Parameters: the squeezing parameter $r = 1$, the laser power $\wp = 0.6$ mW.

is high, for example, for $T = 10$ mK, and laser power 0.6 mW, the minimum value of $\langle\delta\tilde{P}^2\rangle$ is 3.919. In this case, there is no momentum squeezing, but if we increase the laser power to 6.9 mW, the minimum value of $\langle\delta\tilde{P}^2\rangle$ is 0.731, the movable mirror shows momentum squeezing, and the amount of squeezing will increase with increase of laser power. Therefore, when the temperature of the environment is high, the momentum squeezing of the movable mirror can be obtained by increasing the input laser power. The reason is that increasing the laser power can increase the photon number in the cavity. Moreover, for any specific temperature of the environment, the minimum value of $\langle\delta\tilde{P}^2\rangle$ in the presence of the radiation pressure coupling is always much less than that in the absence of the radiation pressure coupling.

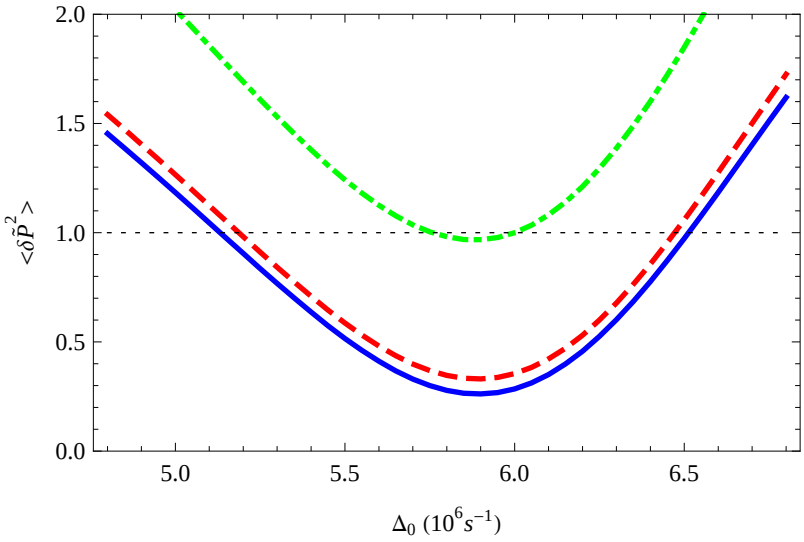

Figure 4.4: The mean square fluctuations $\langle\delta\tilde{P}^2\rangle$ versus the detuning Δ_0 (10^6 s^{-1}), each curve corresponds to a different temperature of the environment. T=0 K (solid curve), 1 mK (dashed curve), 10 mK (dotdashed curve). The minimum values of $\langle\delta\tilde{P}^2\rangle$ are 0.261 (T=0 K), 0.330 (T=1 mK), 0.968 (T=10 mK). The flat dotted line represents the variance of the coherent light ($\langle\delta\tilde{P}^2\rangle$=1). Parameters: the squeezing parameter $r = 1$, the laser power $\wp = 3.8$ mW.

4.5 Conclusions

In conclusion, we have found that squeezing of the movable mirror can be achieved by the injection of squeezed vacuum light and a laser. The result shows the maximum momentum squeezing of the movable mirror happens if squeezed vacuum light with r about 1 is injected into the cavity. For a given squeezing parameter and laser power, decreasing the temperature of the environment can enhance the maximum momentum squeezing of the movable mirror. In addition, the momentum squeezing of the movable mirror may be achieved by increasing the input laser power. Generation of squeezing of the movable mirror provides a new way to detect a weak force. Further the "feeding" of squeezed light can be used to squeeze collective degrees of freedom for several mirrors inside the cavity.

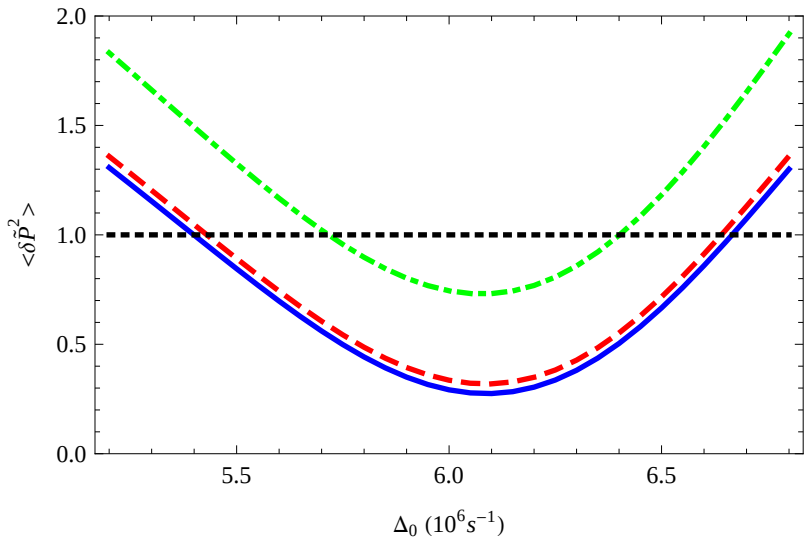

Figure 4.5: The mean square fluctuations $\langle\delta\tilde{P}^2\rangle$ versus the detuning Δ_0 (10^6 s^{-1}), each curve corresponds to a different temperature of the environment. T=0 K (solid curve), 1 mK (dashed curve), 10 mK (dotdashed curve). The minimum values of $\langle\delta\tilde{P}^2\rangle$ are 0.275 (T=0 K), 0.319 (T=1 mK), 0.731 (T=10 mK). The flat dotted line represents the variance of the coherent light ($\langle\delta\tilde{P}^2\rangle$=1). Parameters: the squeezing parameter $r = 1$, the laser power $\wp = 6.9$ mW.

CHAPTER 5

ENTANGLING NANOMECHANICAL OSCILLATORS IN A RING CAVITY BY FEEDING SQUEEZED LIGHT

5.1 Overview

It is well known that entanglement is a key resource for quantum information processing [142]. One now has fairly good understanding of how to produce entanglement among microscopic entities. In recent times there has been considerable interest in studying entanglement in mesoscopic and even microscopic systems [27, 143, 144, 145, 146]. Nanomechanical oscillators are beginning to be important candidates for the study of quantum mechanical features at mesoscopic scales. In fact the possibility of entangling two nanomechanical oscillators has been investigated from many different angles: such as entangling two mirrors in a ring cavity [147], entangling two mirrors of two independent optical cavities driven by a pair of entangled light beams [177], entangling two mirrors by using a double-cavity set up by driving with squeezed light [37], entangling two mirrors of a linear cavity driven by a classical laser field [149], entangling two mirrors in a ring cavity by using a phase-sensitive feedback loop [150], entangling two dielectric membranes suspended inside a cavity [38], and entangling two oscillators by entanglement swapping [151, 152]. Other proposals do not use cavity configurations but coupling to Cooper pair boxes [153]. Here we report a conceptually simple method to produce entanglement between two mirrors. Our proposal enables us to trace the physical origin of entanglement.

In this chapter, we propose a scheme for entangling two movable mirrors of a ring cavity by feeding broad band squeezed vacuum light along with the laser light.

The two movable mirrors are entangled based on their interaction with the cavity field. The achieved entanglement of the two movable mirrors depends on the degree of squeezing of the input light, the laser power, and the temperature of the movable mirrors. The feeding of the squeezed light has been considered to produce squeezing of a nanomechanical mirror [32, 33]. Further Pinard *et al.* [37] have considered entanglement of two mirrors in a double cavity configuration which is fed by squeezed light - one part of the cavity is fed by light squeezed in amplitude quadrature and the other is fed by light squeezed in phase quadrature. In contrast we consider a single mode ring cavity driven by a single component amplitude squeezed light. In our scheme the entanglement can be managed by an externally controllable field which is the squeezed light.

The chapter is organized as follows. In Sec. II we introduce the model, give the quantum Langevin equations, and obtain the steady-state mean values. In Sec. III we derive the stability conditions, calculate the mean square fluctuations in the relative momentum and the total displacement of the movable mirrors. In Sec. IV we analyze how the entanglement of the movable mirrors can be modified by the squeezing parameter, the laser power, and the temperature of the environment. The parameters chosen in the chapter are from a recent experiment on optomechanical normal mode splitting [50].

Before we present our calculations, we present a key idea behind our work. For a bipartite system, a sufficient criterion for entanglement is that the sum of continuous variables satisfies the inequality [154]

$$\langle(\Delta(q_1+q_2))^2\rangle+\langle(\Delta(p_1-p_2))^2\rangle<2, \tag{5.1}$$

where q_j and p_j $(j=1,2)$ are the position and momentum operators for two particles, respectively. They obey the commutation relation $[q_j,p_k]=i\delta_{jk}$ $(j,k=1,2)$.

Mancini *et al.* [26] have derived another sufficient condition for bipartite entan-

glement, which requires the product of continuous variables satisfies the inequality

$$\langle(\Delta(q_1+q_2))^2\rangle\langle(\Delta(p_1-p_2))^2\rangle < 1. \tag{5.2}$$

In this chapter, we will use equation (5.2) to show the entanglement between the two oscillating mirrors. Thus if we have a situation where the interaction occurs only via the relative coordinates q_1-q_2,p_1-p_2, then we can hold $\langle(\Delta(q_1+q_2))^2\rangle$ at its value, says $\simeq 1$, before interaction and if the interaction can make $\langle(\Delta(p_1-p_2))^2\rangle < 1$, then the inequality (5.2) would imply that the mirrors 1 and 2 are entangled. In the next section we discuss how this can be achieved by using a single mode ring cavity.

5.2 Model

The system under study, sketched in Fig. 5.1, is a ring cavity with one fixed partially transmitting mirror and two movable perfectly reflecting mirrors, driven by a laser with frequency ω_L. As the photons in the cavity with length $2L$ bounce off the movable mirrors, they will exert a radiation pressure force on the surfaces of the movable mirrors proportional to the instantaneous photon number in the cavity. The motion of the movable mirrors induced by the radiation pressure changes the cavity's length, and alters the intensity of the cavity field, which in turn modifies the radiation pressure force itself. Thus the interaction of the cavity field with the movable mirrors through the radiation pressure is a nonlinear effect. In addition, each mirror undergoes quantum Brownian motion due to its coupling to its own independent environment at the same low temperature T. The two movable mirrors are identical with the same effective mass m, mechanical frequency ω_m and momentum decay rate γ_m, and each mirror is modeled as a quantum mechanical harmonic oscillator. We further assume that the cavity is fed with squeezed light at frequency ω_S.

In the adiabatic limit, the cavity field is a single mode with frequency ω_c [64, 106], and we can neglect the retardation effect [155], neglect the photon creation in the

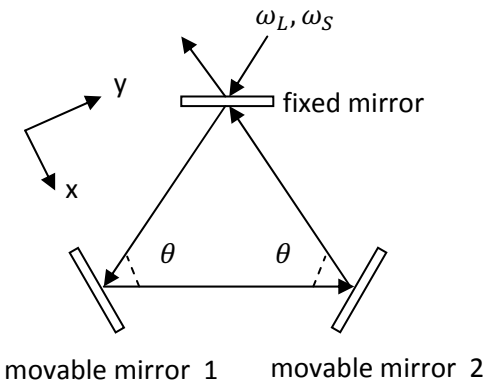

Figure 5.1: Sketch of the studied system. A laser with frequency ω_L and a squeezed vacuum light with frequency ω_S enter the ring cavity through the partially transmitting mirror.

cavity with moving boundaries due to the Casimir effect [156], and neglect the Doppler effect [157], thus the radiation pressure force does not depend on the velocity of the movable mirrors. Assuming the collisions of the photons on the surfaces of the movable mirrors are elastic, the momentum transferred to the mirrors per photon is $\hbar k_y - (-\hbar k_y) = 2\hbar k_y$ (see Fig. 5.1 for the direction of y), where $k_y = k\cos(\theta/2)$, k is the wave vector of the cavity field with $k = \omega_c/c$, and θ is the angle between the incident light and the reflected light at the surfaces of the movable mirrors. During the cavity round-trip time $t = 2L/c$, there are n_c photons hitting on the surfaces of the movable mirrors, so the radiation pressure force is $F = 2n_c\hbar k_y/t = n_c\hbar\frac{\omega_c}{L}\cos(\theta/2)$. In a reference frame rotating at the laser frequency, the Hamiltonian that describes the system can be written as

$$\begin{aligned} H &= \hbar(\omega_c - \omega_L)n_c + \hbar g n_c \cos(\theta/2)(Q_1 - Q_2) + \frac{\hbar\omega_m}{2}(Q_1^2 + P_1^2) \\ &\quad + \frac{\hbar\omega_m}{2}(Q_2^2 + P_2^2) + i\hbar\varepsilon(c^\dagger - c), \end{aligned} \tag{5.3}$$

we have defined dimensionless position and momentum operators for the oscillators

$Q_j = \sqrt{\frac{m\omega_m}{\hbar}} q_j$ and $P_j = \sqrt{\frac{1}{m\hbar\omega_m}} p_j$ (j=1,2) with $[Q_j, P_k] = i\delta_{jk}$ ($j,k = 1,2$). Further in equation (5.3), $n_c = c^\dagger c$ is the number of the photons inside the cavity, c and $c^\dagger$ are the annihilation and creation operators for the cavity field with $[c, c^\dagger] = 1$. The parameter $g = \frac{\omega_c}{L}\sqrt{\frac{\hbar}{m\omega_m}}$ is the optomechanical coupling constant between the cavity field and the movable mirrors in units of s^{-1}. The different signs in front of Q_1 and Q_2 are because the radiation pressure forces exerted on the two mirrors are opposite. The parameter ε is the coupling strength of the laser to the cavity field, which is related to the input laser power $\wp$ by $\varepsilon = \sqrt{\frac{2\kappa\wp}{\hbar\omega_L}}$, where κ is the photon decay rate by leaking out of the cavity.

In the system, the cavity field is damped by photon losses via the cavity output mirror at the rate κ, and the movable mirrors are damped due to momentum losses at the same rate γ_m. Meanwhile, there are two kinds of noises affecting on the system. One is the input squeezed vacuum noise operator c_{in} with frequency $\omega_S = \omega_L + \omega_m$. It has zero mean value, and nonzero time-domain correlation functions [141]

$$\begin{aligned}
\langle \delta c_{in}^\dagger(t)\delta c_{in}(t')\rangle &= N\delta(t-t'),\\
\langle \delta c_{in}(t)\delta c_{in}^\dagger(t')\rangle &= (N+1)\delta(t-t'),\\
\langle \delta c_{in}(t)\delta c_{in}(t')\rangle &= Me^{-i\omega_m(t+t')}\delta(t-t'),\\
\langle \delta c_{in}^\dagger(t)\delta c_{in}^\dagger(t')\rangle &= M^* e^{i\omega_m(t+t')}\delta(t-t').
\end{aligned} \tag{5.4}$$

where $N = \sinh^2(r)$, $M = \sinh(r)\cosh(r)e^{i\varphi}$, r and φ are respectively the squeezing parameter and phase of the squeezed vacuum light. For simplicity, we choose $\varphi = 0$. The other is quantum Brownian noises ξ_1 and ξ_2, which are from the coupling of the movable mirrors to their own environment. They are mutually independent with zero mean values and have the following correlation functions at temperature T [108]:

$$\langle \xi_j(t)\xi_k(t')\rangle = \frac{\delta_{jk}}{2\pi}\frac{\gamma_m}{\omega_m}\int \omega e^{-i\omega(t-t')}\left[1+\coth(\frac{\hbar\omega}{2k_BT})\right]d\omega, \tag{5.5}$$

where k_B is the Boltzmann constant and T is the temperature of the mirrors' environment, $j,k = 1,2$.

The dynamics of the cavity field interacting with the movable mirrors can be derived by the Heisenberg equations of motion and taking into account the effect of damping and noises, which gives the quantum Langevin equations

$$\begin{aligned}
\dot{Q}_1 &= \omega_m P_1, \\
\dot{Q}_2 &= \omega_m P_2, \\
\dot{P}_1 &= -g n_c \cos(\theta/2) - \omega_m Q_1 - \gamma_m P_1 + \xi_1, \\
\dot{P}_2 &= g n_c \cos(\theta/2) - \omega_m Q_2 - \gamma_m P_2 + \xi_2, \\
\dot{c} &= -i[\omega_c - \omega_L + g\cos(\theta/2)(Q_1 - Q_2)]c + \varepsilon - \kappa c + \sqrt{2\kappa} c_{in}, \\
\dot{c}^\dagger &= i[\omega_c - \omega_L + g\cos(\theta/2)(Q_1 - Q_2)]c^\dagger + \varepsilon - \kappa c^\dagger + \sqrt{2\kappa} c_{in}^\dagger.
\end{aligned} \tag{5.6}$$

From the second term of equation (5.3), we can see only the relative motion of the two movable mirrors is coupled to the cavity field via radiation pressure. On introducing the relative distance and the relative momentum of the movable mirrors by $Q_- = Q_1 - Q_2$ and $P_- = P_1 - P_2$, we find that equation (5.6) reduces to

$$\begin{aligned}
\dot{Q}_- &= \omega_m P_-, \\
\dot{P}_- &= -2 g n_c \cos(\theta/2) - \omega_m Q_- - \gamma_m P_- + \xi_1 - \xi_2, \\
\dot{c} &= -i[\omega_c - \omega_L + g\cos(\theta/2) Q_-]c + \varepsilon - \kappa c + \sqrt{2\kappa} c_{in}, \\
\dot{c}^\dagger &= i[\omega_c - \omega_L + g\cos(\theta/2) Q_-]c^\dagger + \varepsilon - \kappa c^\dagger + \sqrt{2\kappa} c_{in}^\dagger.
\end{aligned} \tag{5.7}$$

We would use standard methods of quantum optics [110] which have been adopted for discussions of quantum noise of nanomechanical mirrors [35, 36, 95, 108, 149], setting all the time derivatives in equation (5.7) to zero, and solving it, we obtain the steady-state mean values

$$P_-^s = 0,\ Q_-^s = -\frac{2g|c^s|^2\cos(\theta/2)}{\omega_m},\ c^s = \frac{\varepsilon}{\kappa + i\Delta}, \tag{5.8}$$

where

$$\Delta = \omega_c - \omega_L + g Q_-^s \cos(\theta/2) \tag{5.9}$$

is the effective cavity detuning, depending on Q_-^s. The Q_-^s denotes the new equilibrium relative distance between the movable mirrors. Further c^s represents the complex amplitude of the cavity field in the steady state. For a given input laser power, Q_-^s and c^s can take three distinct values, respectively. Therefore, the system displays an optical multistability [41, 42, 43], which is a nonlinear effect induced by the radiation pressure.

5.3 Radiation Pressure and Quantum Fluctuations

To investigate entanglement of the two movable mirrors, we have to calculate the fluctuations in the relative momentum of the movable mirrors. This fluctuations can be calculated analytically by using the linearization approach of quantum optics [110], provided that the nonlinear effect between the cavity field and the movable mirrors is weak. We write each operator of the system as the sum of its steady-state mean value and a small fluctuation with zero mean value,

$$Q_- = Q_-^s + \delta Q_-, \quad P_- = P_-^s + \delta P_-, \quad c = c^s + \delta c. \tag{5.10}$$

Inserting equation (5.10) into equation (5.7), then assuming the cavity field has a very large amplitude c^s with $|c^s| \gg 1$, one can obtain a set of linear quantum Langevin equations for the fluctuation operators,

$$\begin{aligned}
\delta\dot{Q}_- &= \omega_m \delta P_-, \\
\delta\dot{P}_- &= -2g\cos(\theta/2)(c^{s*}\delta c + c^s \delta c^\dagger) - \omega_m \delta Q_- - \gamma_m \delta P_- + \xi_1 - \xi_2, \\
\delta\dot{c} &= -(\kappa + i\Delta)\delta c - ig\cos(\theta/2)c^s \delta Q_- + \sqrt{2\kappa}\delta c_{in}, \\
\delta\dot{c}^\dagger &= -(\kappa - i\Delta)\delta c^\dagger + ig\cos(\theta/2)c^{s*}\delta Q_- + \sqrt{2\kappa}\delta c_{in}^\dagger.
\end{aligned} \tag{5.11}$$

Introducing the cavity field quadratures $\delta x = \delta c + \delta c^\dagger$ and $\delta y = i(\delta c^\dagger - \delta c)$, and the input noise quadratures $\delta x_{in} = \delta c_{in} + \delta c_{in}^\dagger$ and $\delta y_{in} = i(\delta c_{in}^\dagger - \delta c_{in})$, equation (5.11)

can be rewritten in the matrix form

$$\dot{f}(t) = Af(t) + \eta(t), \tag{5.12}$$

in which $f(t)$ is the column vector of the fluctuations, $\eta(t)$ is the column vector of the noise sources. Their transposes are

$$\begin{aligned} f(t)^T &= (\delta Q_-, \delta P_-, \delta x, \delta y), \\ \eta(t)^T &= (0, \xi_1 - \xi_2, \sqrt{2\kappa}\delta x_{in}, \sqrt{2\kappa}\delta y_{in}); \end{aligned} \tag{5.13}$$

and the matrix A is given by

$$A = \begin{pmatrix} 0 & \omega_m & 0 & 0 \\ -\omega_m & -\gamma_m & -g\cos(\theta/2)(c^s + c^{s*}) & ig\cos(\theta/2)(c^s - c^{s*}) \\ -ig\cos(\theta/2)(c^s - c^{s*}) & 0 & -\kappa & \Delta \\ -g\cos(\theta/2)(c^s + c^{s*}) & 0 & -\Delta & -\kappa \end{pmatrix}. \tag{5.14}$$

The solution of equation (5.12) is $f(t) = M(t)f(0) + \int_0^t M(t')\eta(t-t')dt'$, where $M(t) = e^{At}$. The system is stable and reaches its steady state as $t \to \infty$ only if the real parts of all the eigenvalues of the matrix A are negative so that $M(\infty) = 0$. The stability conditions for the system can be found by employing the Routh-Hurwitz criterion [113], we get

$$\begin{aligned} &\kappa\gamma_m[(\kappa^2 + \Delta^2)^2 + (2\kappa\gamma_m + \gamma_m^2 - 2\omega_m^2)(\kappa^2 + \Delta^2) + \omega_m^2(4\kappa^2 + \omega_m^2 \\ &\quad + 2\kappa\gamma_m)] + 2\omega_m\Delta g^2\cos^2(\theta/2)|c^s|^2(2\kappa + \gamma_m)^2 > 0, \\ &\omega_m(\kappa^2 + \Delta^2) - 4\Delta g^2\cos^2(\theta/2)|c^s|^2 > 0. \end{aligned} \tag{5.15}$$

All the parameters chosen in this chapter have been verified to satisfy the stability conditions (5.15).

Fourier transforming each operator in equation (5.11) by $f(t) = \frac{1}{2\pi}\int_{-\infty}^{+\infty} f(\omega)e^{-i\omega t}d\omega$ and solving it in the frequency domain, the relative momentum fluctuations of the

movable mirrors are given by

$$\begin{aligned}\delta P_-(\omega) &= \frac{i\omega}{d(\omega)}(2\sqrt{2\kappa}g\cos(\theta/2)\{[\kappa - i(\Delta+\omega)]c^{s*}\delta c_{in}(\omega) + [\kappa + i(\Delta-\omega)] \\ &\quad \times c^s \delta c_{in}^\dagger(-\omega)\} - [(\kappa - i\omega)^2 + \Delta^2][\xi_1(\omega) - \xi_2(\omega)]), \end{aligned} \tag{5.16}$$

where $d(\omega) = -4\omega_m \Delta g^2 |c^s|^2 \cos^2(\theta/2) + (\omega_m^2 - \omega^2 - i\gamma_m\omega)[(\kappa - i\omega)^2 + \Delta^2]$. Equation (5.16) shows $\delta P_-(\omega)$ has two contributions. The first term proportional to g originates from their interaction with the cavity field, while the second term involving $\xi_1(\omega)$ and $\xi_2(\omega)$ is from their interaction with their own environment. So the relative momentum fluctuations of the movable mirrors are now determined by radiation pressure and the thermal noise. In the case of no coupling with the cavity field ($g = 0$), the movable mirrors will make Brownian motion only, $\delta P_-(\omega) = -i\omega[\xi_1(\omega) - \xi_2(\omega)]/(\omega_m^2 - \omega^2 - i\gamma_m\omega)$, whose mechanical susceptibility $\chi(\omega) = 1/(\omega_m^2 - \omega^2 - i\gamma_m\omega)$ has a Lorentzian shape centered at the frequency ω_m with γ_m as full width at half maximum (FWHM).

The mean square fluctuations in the relative momentum of the movable mirrors are determined by

$$\langle \delta P_-(t)^2 \rangle = \frac{1}{4\pi^2} \int \int_{-\infty}^{+\infty} d\omega d\Omega e^{-i(\omega+\Omega)t} \langle \delta P_-(\omega) \delta P_-(\Omega) \rangle. \tag{5.17}$$

To calculate the mean square fluctuations, we require the correlation functions of the noise sources in the frequency domain. Fourier transforming equations (5.4) and (5.5) gives the frequency domain correlation functions

$$\begin{aligned} &\langle \delta c_{in}^\dagger(-\omega) \delta c_{in}(\Omega) \rangle = 2\pi N \delta(\omega + \Omega), \\ &\langle \delta c_{in}(\omega) \delta c_{in}^\dagger(-\Omega) \rangle = 2\pi (N+1) \delta(\omega + \Omega), \\ &\langle \delta c_{in}(\omega) \delta c_{in}(\Omega) \rangle = 2\pi M \delta(\omega + \Omega - 2\omega_m), \\ &\langle \delta c_{in}^\dagger(-\omega) \delta c_{in}^\dagger(-\Omega) \rangle = 2\pi M^* \delta(\omega + \Omega + 2\omega_m), \\ &\langle \xi_j(\omega) \xi_k(\Omega) \rangle = 2\pi \delta_{jk} \frac{\gamma_m}{\omega_m} \omega \left[1 + \coth(\tfrac{\hbar\omega}{2k_B T})\right] \delta(\omega + \Omega). \end{aligned} \tag{5.18}$$

Upon substituting equation (5.16) into equation (5.17) and taking into account equation (5.18), the mean square fluctuations of equation (5.17) are written as

$$\langle \delta P_-(t)^2 \rangle = \frac{1}{2\pi} \int_{-\infty}^{+\infty} [\omega^2 A + \omega(\omega - 2\omega_m) B e^{-2i\omega_m t} + \omega(\omega + 2\omega_m) C e^{2i\omega_m t}] d\omega. \quad (5.19)$$

where

$$\begin{aligned} A = & \tfrac{1}{d(\omega)d(-\omega)} (8\kappa g^2 \cos^2(\theta/2) |c^s|^2 \{(N+1)[\kappa^2 + (\Delta+\omega)^2] \\ & + N[\kappa^2 + (\Delta-\omega)^2]\} + 2\gamma_m \tfrac{\omega}{\omega_m} [(\Delta^2 + \kappa^2 - \omega^2)^2 + 4\kappa^2\omega^2] \\ & \times [1 + \coth(\tfrac{\hbar\omega}{2k_B T})]), \qquad (5.20) \\ B = & \tfrac{8\kappa g^2 \cos^2(\theta/2) c^{s*2} M}{d(\omega) d(2\omega_m - \omega)} [\kappa - i(\Delta+\omega)][\kappa - i(\Delta + 2\omega_m - \omega)], \\ C = & \tfrac{8\kappa g^2 \cos^2(\theta/2) c^{s2} M^*}{d(\omega) d(-2\omega_m - \omega)} [\kappa + i(\Delta-\omega)][\kappa + i(\Delta + 2\omega_m + \omega)]. \end{aligned}$$

In equations (5.19) and (5.20), the term independent of g is the thermal noise contribution; while all other terms involving g are the radiation pressure contribution, including the influence of the squeezed vacuum light. Moreover, $\langle \delta P_-(t)^2 \rangle$ is time-dependent, the explicit time dependence in equation (5.19) can be eliminated by working in the interaction picture. If we look the relative motion of the movable mirrors as a harmonic oscillator and introduce the annihilation (creation) operators b ($b^\dagger$) and $\tilde{b}$ ($\tilde{b}^\dagger$) for the oscillator in the Schrödinger and interaction picture with $[b, b^\dagger] = 1$ and $[\tilde{b}, \tilde{b}^\dagger] = 1$. They are related by $b = \tilde{b} e^{-i\omega_m t}$ and $b^\dagger = \tilde{b}^\dagger e^{i\omega_m t}$. Then using $P_- = i(b^\dagger - b)$, and $\tilde{P}_- = i(\tilde{b}^\dagger - \tilde{b})$, we get

$$\langle \delta \tilde{P}_-^2 \rangle = \frac{1}{2\pi} \int_{-\infty}^{+\infty} [\omega^2 A + \omega(\omega - 2\omega_m) B + \omega(\omega + 2\omega_m) C] d\omega. \quad (5.21)$$

According to equation (5.2), the movable mirrors are said to be entangled if $\langle \delta Q_+^2 \rangle$ and $\langle \delta \tilde{P}_-^2 \rangle$ satisfy the inequality

$$\langle \delta Q_+^2 \rangle \langle \delta \tilde{P}_-^2 \rangle < 1. \quad (5.22)$$

where $Q_+ = Q_1 + Q_2$, the total displacement of the two movable mirrors, which is not related to the radiation pressure, only determined by the thermal noise. At the

temperature T, the fluctuations $\langle \delta Q_+^2 \rangle$ are

$$\langle \delta Q_+^2 \rangle = 0.5 + \frac{1}{e^{\hbar\omega_m/(k_B T)} - 1} \tag{5.23}$$

Since $[Q_+, P_-] = [Q_1 + Q_2, P_1 - P_2] = 0$, Q_+ and P_- can be simultaneously measured with infinite precision. Thus Q_+ and $\tilde{P}_-$ can also be simultaneously measured with infinite precision.

From equations (5.20) and (5.21), we find $\langle \delta \tilde{P}_-^2 \rangle$ is affected by the detuning Δ, the squeezing parameter r, the laser power $\wp$, the cavity length L, the temperature of the environment T, and so on. In the following, we confine ourselves to discussing the dependence of $\langle \delta \tilde{P}_-^2 \rangle$ on the squeezing parameter, the laser power, and the temperature of the environment.

5.4 Entanglement of the Two Movable Mirrors

In the section, we would like to numerically evaluate the mean square fluctuations in the total displacement and the relative momentum of the movable mirrors given by equations (5.23) and (5.21) to show the entanglement of the two movable mirrors produced by feeding the squeezed vacuum light at the input mirror. To have fairly good idea of entanglement, we use the parameters of a recent experiment [50] although we are aware that the cavity geometry is different: the wavelength of the laser $\lambda = \frac{2\pi c}{\omega_L} = 1064$ nm, $L = 25$ mm, $m = 145$ ng, $\kappa = 2\pi \times 215 \times 10^3$ Hz, $\omega_m = 2\pi \times 947 \times 10^3$ Hz, the mechanical quality factor $Q' = \frac{\omega_m}{\gamma_m} = 6700$, $\theta = \pi/3$.

First we illustrate the squeezed vacuum light's effect on the entanglement between the movable mirrors. We find as $T = 41.4$ μK, the mean square fluctuations $\langle \delta Q_+^2 \rangle \approx 1$, which implies that as long as the mean square fluctuations $\langle \delta \tilde{P}_-^2 \rangle < 1$, there is an entanglement between the movable mirrors. The behavior of $\langle \delta \tilde{P}_-^2 \rangle$ at $\wp = 3.8$ mW is plotted as a function of the detuning Δ in Fig. 5.2. Different graphs correspond to different values of the squeezing of the input light. In the case of no injection of

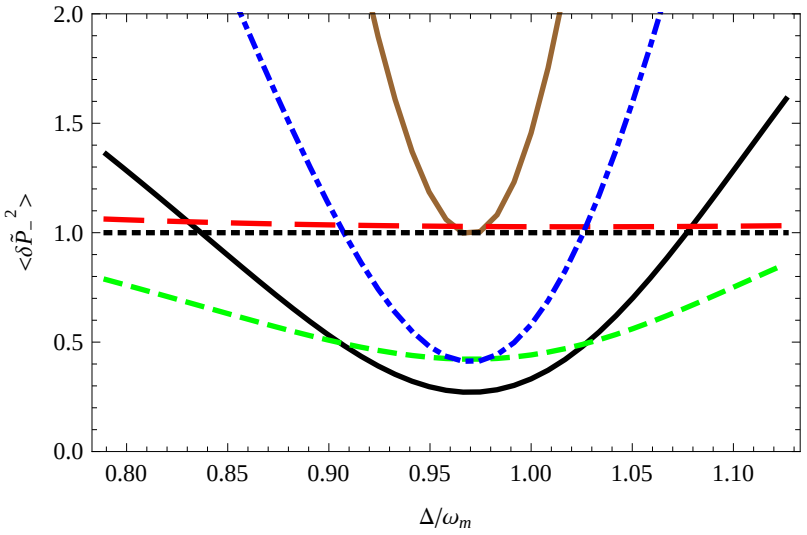

Figure 5.2: The mean square fluctuations $\langle\delta\tilde{P}_-^2\rangle$ versus the detuning Δ/ω_m for different values of the squeezing of the input field. $r = 0$ (red, big dashed line), $r = 0.5$ (green, small dashed line), $r = 1$ (black, solid curve), $r = 1.5$ (blue, dotdashed curve), $r = 2$ (brown, solid curve). The minimum values of $\langle\delta\tilde{P}_-^2\rangle$ are 1.027 (r=0), 0.422 (r=0.5), 0.271(r=1), 0.412 (r=1.5), 0.999 (r=2). The flat dotted line represents $\langle\delta\tilde{P}_-^2\rangle$=1. Parameters: the temperature of the environment $T = 41.4$ μK, the laser power $\wp = 3.8$ mW.

the squeezed vacuum light ($r = 0$), which means that the squeezed vacuum light is replaced by an ordinary vacuum light, we find $\langle\delta\tilde{P}_-^2\rangle$ is always larger than unity, the minimum value of $\langle\delta\tilde{P}_-^2\rangle$ is 1.027, obviously there is no entanglement between the movable mirrors. However, if we inject the squeezed vacuum light, it is seen that entanglement between the movable mirrors occurs, meaning that there is a quantum correlation between the movable mirrors, even through they are separated in space. We also find the movable mirrors are maximally entangled as the squeezing parameter is about $r = 1$, the corresponding minimum value of $\langle\delta\tilde{P}_-^2\rangle$ is 0.271. So the injection of the squeezed vacuum light leads to a significant reduction of the fluctuations in the relative momentum between the movable mirrors. This is due to the fact that

using the squeezed vacuum light increases the photon number in the cavity, which leads to a stronger radiation pressure acting on the movable mirrors and enhances the entanglement between the movable mirrors.

Next we consider the influence of the laser power on the maximum entanglement between the movable mirrors. We fix the squeezing parameter $r = 1$, and the temperature of the environment $T = 41.4$ μK. We have already known at this temperature, $\langle \delta Q_+^2 \rangle \approx 1$. Thus, if the mean square fluctuations $\langle \delta \tilde{P}_-^2 \rangle < 1$, the movable mirrors become entangled. The mean square fluctuations $\langle \delta \tilde{P}_-^2 \rangle$ as a function of the detuning Δ for different laser power are shown in Fig. 5.3. We find that significant entanglement occurs for a range of pumping powers.

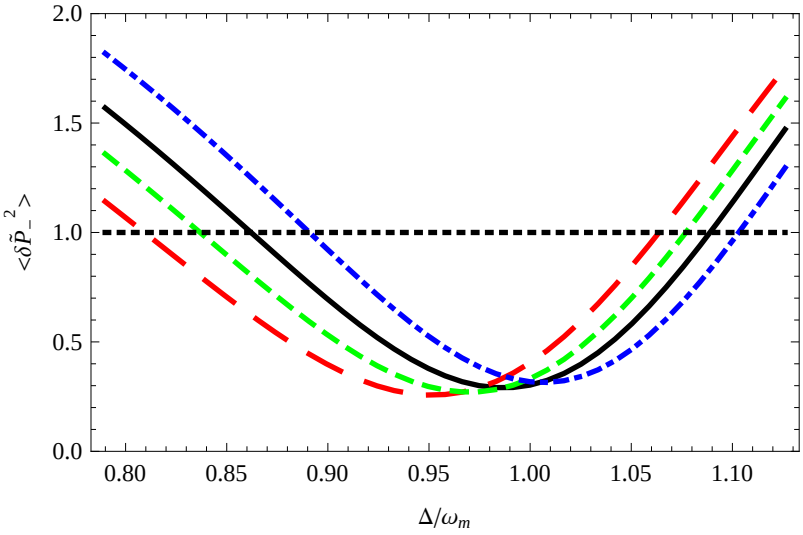

Figure 5.3: The mean square fluctuations $\langle \delta \tilde{P}_-^2 \rangle$ versus the detuning Δ/ω_m, each curve corresponds to a different laser power. $\wp$=0.6 mW (red, big dashed curve), 3.8 mW (green, small dashed curve), 6.9 mW (black, solid curve), 10.7 mW (blue, dotdashed curve). The minimum values of $\langle \delta \tilde{P}_-^2 \rangle$ are 0.257 ($\wp$=0.6 mW), 0.271 ($\wp$=3.8 mW), 0.291 ($\wp$=6.9 mW), 0.315 ($\wp$=10.7 mW). The flat dotted line represents $\langle \delta \tilde{P}_-^2 \rangle$=1. Parameters: the squeezing parameter $r = 1$, the temperature of the environment $T = 41.4$ μK.

We now show the effect of the temperature of the environment on the entanglement between the movable mirrors. We fix the squeezing parameter $r = 1$, the laser power $\wp = 3.8$ mW, and the detuning $\Delta = 0.965\omega_m$. The value of $\langle \delta Q_+^2 \rangle \langle \delta \tilde{P}_-^2 \rangle$ as a function of the temperature of the environment is presented in Fig. 5.4. As the temperature of

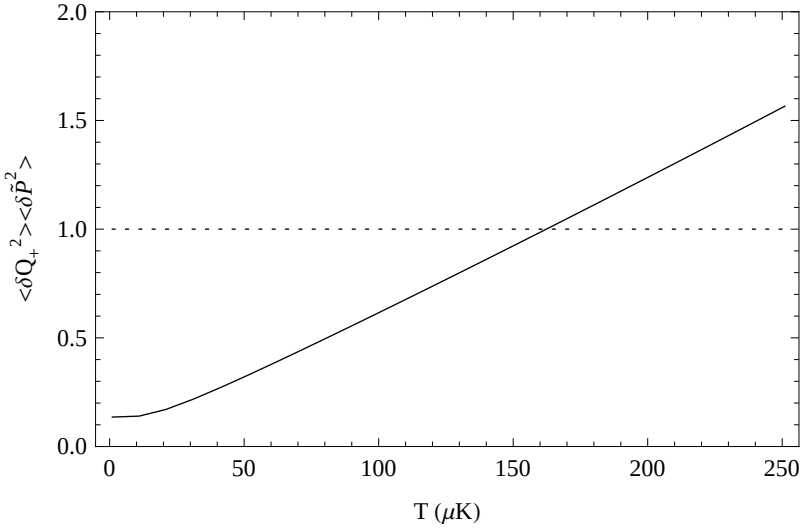

Figure 5.4: The value of $\langle \delta Q_+^2 \rangle \langle \delta \tilde{P}_-^2 \rangle$ versus the temperature of the environment T (μK). The minimum value of $\langle \delta Q_+^2 \rangle \langle \delta \tilde{P}_-^2 \rangle$ is 0.135 at $T = 0$ K. The flat dotted line represents $\langle \delta Q_+^2 \rangle \langle \delta \tilde{P}_-^2 \rangle$=1. Parameters: the squeezing parameter $r = 1$, the laser power $\wp = 3.8$ mW, the detuning $\Delta = 0.965\omega_m$.

the environment increases, the amount of entanglement monotonically decreases due to the thermal fluctuations. This is as expected. What is remarkable is that we find entanglement over a wide range of temperatures. As $T \geq 160$ μK, $\langle \delta Q_+^2 \rangle \langle \delta \tilde{P}_-^2 \rangle \geq 1$, the entanglement vanishes, the movable mirrors become completely separable. So decreasing the temperature of the environment can make the entanglement between the movable mirrors stronger. Note that substantial progress has been made in cooling the nanomechanical oscillators [6, 7, 8, 9, 10, 18, 56, 116, 120, 158, 159]. Further the ground state cooling using the resolved sideband regime might soon become feasible. Clearly the entanglement depends on both the quality factor of the cavity and the

temperature of the environment. The optical ring cavities are expected to yield much higher quality factor: $\kappa \approx 2\pi \times 10\text{kHz}$, see for example [160], though for fixed mirrors replaced by moving mirrors, the quality factor may be deteriorated. Metheods for detection of entanglement are discussed in [26, 37]. We note here that in our case we can deduce entanglement from the knowledge of $\langle \delta \tilde{P}_-^2 \rangle$. It can be shown from equation (5.11) that $\langle \delta \tilde{P}_-^2 \rangle$ can be obtained from the measurement of the fluctuations in the quadrature of the output field.

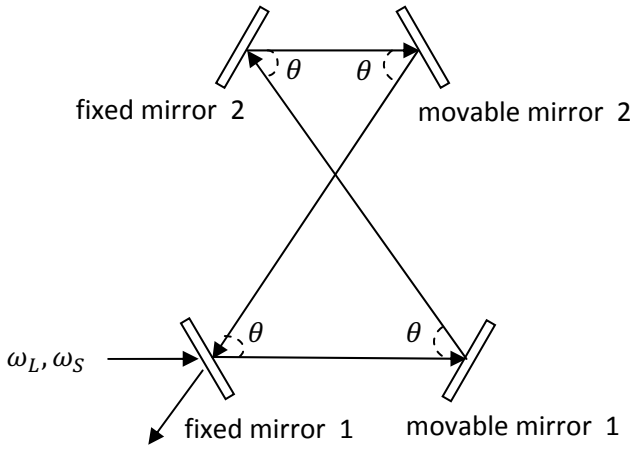

Figure 5.5: Sketch of 4-mirror ring cavity. A laser with frequency ω_L and squeezed vacuum light with frequency $\omega_S = \omega_L + \omega_m$ enter the ring cavity through the partially transmitting fixed mirror 1. The fixed mirror 2 and the two identical movable mirrors are perfectly reflecting.

If we use a different geometry of the ring cavity, as shown in Fig. 5.5, then we have the possibility of entangling other quadratures of the mirrors. In this case, the Hamiltonian of the system in the frame rotating at the laser frequency becomes

$$\begin{aligned} H = {} & \hbar(\omega_c - \omega_L) n_c - \hbar g n_c \cos(\theta/2)(Q_1 + Q_2) + \tfrac{\hbar\omega_m}{2}(Q_1^2 + P_1^2) \\ & + \tfrac{\hbar\omega_m}{2}(Q_2^2 + P_2^2) + i\hbar\varepsilon(c^\dagger - c), \end{aligned} \tag{5.24}$$

We note the interaction between the two movable mirrors and the cavity field depends only on the total displacement of the movable mirrors. The movable mirrors are said

to be entangled if δQ_-^2 and $\delta \tilde{P}_+^2$ satisfy the inequality [26, 154]

$$\langle \delta Q_-^2 \rangle \langle \delta \tilde{P}_+^2 \rangle < 1. \tag{5.25}$$

where $Q_- = Q_1 - Q_2$ and $P_+ = P_1 + P_2$. The Q_- is the relative displacement of the two movable mirrors, which is not related to the radiation pressure, only determined by the thermal noise. The P_+ is the total momentum of the two movable mirrors, and depends on the radiation pressure and the thermal noise. The relation between P_+ and $\tilde{P}_+$ is the same as the relation between P_- and $\tilde{P}_-$ we defined above. Since $[Q_-, P_+] = [Q_1 - Q_2, P_1 + P_2] = 0$, Q_- and P_+ can be simultaneously measured with infinite precision. Thus Q_- and $\tilde{P}_+$ can also be simultaneously measured with infinite precision. Through calculations, we find that $\langle \delta Q_-^2 \rangle$ and $\langle \delta \tilde{P}_+^2 \rangle$ in a 4-mirror ring cavity have the same form as $\langle \delta Q_+^2 \rangle$ (equation (5.23)) and$\langle \delta \tilde{P}_-^2 \rangle$ (equation (5.21)) in a 3-mirror ring cavity, respectively. If we choose the same parameters, the same numerical results will be obtained. Therefore, using a 4-mirror ring cavity, the entanglement between two oscillators can also be obtained.

5.5 Conclusions

In conclusion, we have found that the injection of squeezed vacuum light and a laser can entangle the two identical movable mirrors by the radiation pressure. The result shows the maximum entanglement of the movable mirrors happens if the squeezed vacuum light with r about 1 is injected into the cavity. We also find significant entanglement over a very wide range of input laser power and temperatures of the environment.

The content of this chapter has been published in *New J. Phys.* **11**, 103044 (2009).

CHAPTER 6

NORMAL-MODE SPLITTING AND ANTIBUNCHING IN STOKES AND ANTI-STOKES PROCESSES IN CAVITY OPTOMECHANICS: RADIATION-PRESSURE-INDUCED FOUR-WAVE-MIXING CAVITY OPTOMECHANICS

6.1 Overview

The nonlinearities in a system can be studied using a number of optical methods. Among these, Stokes and anti-Stokes processes, and more generally four-wave-mixing processes are quite common tools used to understand the nonlinear nature of the system [161]. With this in view we study the stimulated Stokes and anti-Stokes processes in cavity optomechanics. As is well known, the nonlinearity in cavity optomechanics arises from the radiation pressure [25, 41, 42, 130, 162, 163] on the moving mirror of the cavity. Thus, if the cavity is driven by a pump field of frequency ω_l and a Stokes field of frequency ω_s, then, due to radiation pressure, the output of the cavity would consist of fields at the applied frequencies ω_l and ω_s and a generated frequency $2\omega_l - \omega_s$. While some previous works [17, 164, 165] have explored the Stokes and anti-Stokes processes in the context of parametric oscillation instability, here we show how such processes can be conveniently used to study the phenomena of normal-mode splitting [48, 50, 121, 122, 123, 124, 213, 160, 166] arising from the strong coupling between the cavity and the mechanical mirror. Further, the system can act as an amplifier for the Stokes field. Needless to say, we work in a domain which is below the instability threshold.

Moreover, very interesting photon correlations between the Stokes and the anti-

Stokes photons have been reported in atomic vapors under conditions of electromagnetically induced transparency [212]. Here we also discuss the correlations between the photons created spontaneously by the optomechanical system. The correlations are found to be nonclassical.

The chapter is organized as follows. In Sec. II, we introduce the model, obtain the equation of motion for the oscillator and the cavity field, and solve it. In Sec. III, we calculate the output fields and thus obtain nonlinear susceptibilities for Stokes and anti-Stokes processes. In Sec. IV, we show that the Stokes field is amplified, and find very prominent normal-mode splittings in the output fields. Thus, stimulated Stokes and anti-Stokes processes provide us with a new tool for studying the strong coupling regime of optomechanics. We find that normal-mode splittings are especially pronounced in the two quadratures of the output fields. In Sec. V, we analyze the correlations between the spontaneously generated photons in the four-wave-mixing processes in the optomechanical system. We show that such correlations are intrinsically quantum.

6.2 Model: Stimulated Generation of Stokes and Anti-Stokes fields

We consider the system illustrated in Fig. 6.1, in which the cavity consists of two mirrors separated from each other by a distance L. The front mirror is fixed and partially transmitting; the end mirror is movable and perfectly reflecting. The cavity is driven by a pump field and a Stokes field obtained with lasers. Their frequencies are ω_l and ω_s, respectively. We would assume that the Stokes field is much weaker than the pump field. A radiation pressure produced by momentum transfer will act on the movable mirror, which is modeled as a harmonic oscillator with mass m, frequency ω_m, and momentum decay rate γ_m.

Considering a single-mode cavity ω_c, the Hamiltonian of the system in a frame

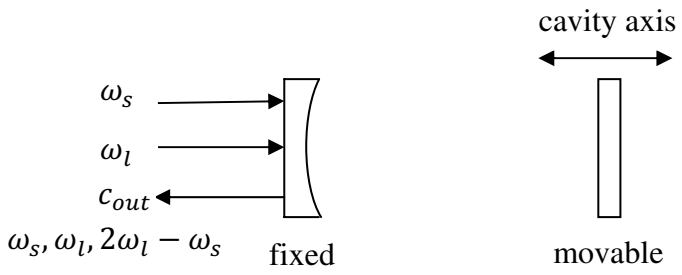

Figure 6.1: Sketch of the studied system. A pump field with frequency ω_l and a Stokes field with frequency ω_s enter the cavity through the partially transmitting mirror. The output fields c_{out} have three components $(\omega_l, \omega_s, 2\omega_l - \omega_s)$. No vacuum fields are shown here because we are examining only the mean response.

rotating at the pump frequency ω_l is written as

$$\begin{aligned} H = \hbar(\omega_c - \omega_l)n_c - \hbar\omega_m \chi n_c Q + \frac{\hbar\omega_m}{4}(Q^2 + P^2) \\ +i\hbar\varepsilon_l(c^\dagger - c) + i\hbar[\varepsilon_s e^{-i(\omega_s - \omega_l)t}c^\dagger - \varepsilon_s^* e^{i(\omega_s - \omega_l)t}c]. \end{aligned} \tag{6.1}$$

Here Q and P are the dimensionless operators representing the oscillator's position and momentum, defined by $Q = q\sqrt{2m\omega_m/\hbar}$ and $P = p\sqrt{2/(m\hbar\omega_m)}$ with $[Q, P] = 2i$. In Eq. (6.1), the first term is the energy of the cavity field, $n_c = c^\dagger c$ is the number of the photons inside the cavity and c and $c^\dagger$ are the annihilation and creation operators, respectively, for the cavity field satisfying the commutation relation $[c, c^\dagger] = 1$. The second term describes the nonlinear coupling of the movable mirror to the cavity field via radiation pressure, where the dimensionless parameter $\chi = (1/\omega_m)(\omega_c/L)\sqrt{\hbar/(2m\omega_m)}$ is the optomechanical coupling constant between the cavity field and the movable mirror. The third term corresponds to the energy of the movable mirror. The last two terms give the interactions of the cavity field with the pump field and the Stokes field, ε_l and ε_s are, respectively, the amplitudes of the pump field and the Stokes field inside the cavity. They are defined by $\varepsilon_l = \sqrt{2\kappa\wp/(\hbar\omega_l)}$ and $|\varepsilon_s| = \sqrt{2\kappa\wp_s/(\hbar\omega_s)}$, respectively, where $\wp$ is the pump power, $\wp_s$ is the power of the

Stokes field, and κ is the cavity decay rate due to the fixed mirror.

Let $\langle Q\rangle$, $\langle P\rangle$, $\langle c\rangle$, and $\langle c^\dagger\rangle$ be the expectation values of the operators Q, P, c, and $c^\dagger$, respectively. The time evolution of these expectation values can be derived by using the Heisenberg equations of motion and adding the damping terms:

$$\begin{aligned}
\langle\dot{Q}\rangle &= \omega_m\langle P\rangle,\\
\langle\dot{P}\rangle &= 2\omega_m\chi\langle n_c\rangle - \omega_m\langle Q\rangle - \gamma_m\langle P\rangle,\\
\langle\dot{c}\rangle &= -[\kappa + i(\omega_c - \omega_l - \omega_m\chi\langle Q\rangle)]\langle c\rangle + \varepsilon_l + \varepsilon_s e^{-i(\omega_s-\omega_l)t},\\
\langle\dot{c}^\dagger\rangle &= -[\kappa - i(\omega_c - \omega_l - \omega_m\chi\langle Q\rangle)]\langle c^\dagger\rangle + \varepsilon_l + \varepsilon_s^* e^{i(\omega_s-\omega_l)t}.
\end{aligned} \tag{6.2}$$

The derivation of Eq. (6.2) uses the well-known mean-field assumption $\langle Qc\rangle = \langle Q\rangle\langle c\rangle$. As the field ε_s at the Stokes frequency ω_s is much weaker than the pump field ε_l, we derive the steady-state solution of Eq. (6.2) to first order in ε_s, that is, we find $t \to \infty$ limit of the solutions:

$$\begin{pmatrix} \langle Q\rangle \\ \langle P\rangle \\ \langle c\rangle \\ \langle c^\dagger\rangle \end{pmatrix} = \begin{pmatrix} Q_0 \\ P_0 \\ c_0 \\ c_0^* \end{pmatrix} + \varepsilon_s e^{-i(\omega_s-\omega_l)t}\begin{pmatrix} Q_+ \\ P_+ \\ c_+ \\ c_-^* \end{pmatrix} + \varepsilon_s^* e^{i(\omega_s-\omega_l)t}\begin{pmatrix} Q_- \\ P_- \\ c_- \\ c_+^* \end{pmatrix}. \tag{6.3}$$

Thus Eq. (6.3) shows the cavity field $\langle c\rangle e^{-i\omega_l t}$ has three components, oscillating at the input frequencies ω_l and ω_s, and a new anti-Stokes frequency $2\omega_l - \omega_s$. By substituting Eq. (6.3) into Eq. (6.2), neglecting those terms containing ε_s^2, ε_s^{*2}, and $|\varepsilon_s|^2$ and equating coefficients of terms proportional to $e^{-i(\omega_s-\omega_l)t}$ and $e^{i(\omega_s-\omega_l)t}$, respectively, we find

$$
\begin{aligned}
Q_0 &= 2\chi|c_0|^2, \\
P_0 &= 0, \\
c_0 &= \frac{\varepsilon_l}{\kappa + i\Delta}, \\
c_+ &= \frac{1}{d(\omega_s - \omega_l)}\{[\kappa - i(\Delta + \omega_s - \omega_l)][(\omega_s - \omega_l)^2 - \omega_m^2 + i\gamma_m(\omega_s - \omega_l)] \\
&\quad -2i\omega_m^3\chi^2|c_0|^2\}, \\
c_- &= -\frac{2i\omega_m^3\chi^2 c_0^2}{d^*(\omega_s - \omega_l)}.
\end{aligned}
\tag{6.4}
$$

where

$$
\Delta = \omega_c - \omega_l - \omega_m\chi Q_0, \tag{6.5}
$$

is the effective detuning, and where

$$
\begin{aligned}
d(\omega_s - \omega_l) &= 4\omega_m^3\chi^2\Delta|c_0|^2 + [(\omega_s - \omega_l + \omega_m)(\omega_s - \omega_l - \omega_m) + i\gamma_m(\omega_s - \omega_l)] \\
&\quad \times[\kappa + i(\Delta - \omega_s + \omega_l)][\kappa - i(\Delta + \omega_s - \omega_l)].
\end{aligned}
\tag{6.6}
$$

For brevity we do not write explicit expressions for $Q\pm$, $P\pm$, etc. because we do not need these in the discussion that follows.

6.3 The Output Fields

To investigate normal-mode splitting of the output fields, we need to find the expectation value of the output fields. Using input-output relation [110] $\langle c_{out}\rangle + \varepsilon_l/\sqrt{2\kappa} + \varepsilon_s e^{-i(\omega_s-\omega_l)t}/\sqrt{2\kappa} = \sqrt{2\kappa}\langle c\rangle$, we can obtain the expectation value of the output fields

$$
\begin{aligned}
\langle c_{out}\rangle &= \sqrt{2\kappa}[c_0 + \varepsilon_s e^{-i(\omega_s-\omega_l)t}c_+ + \varepsilon_s^* e^{i(\omega_s-\omega_l)t}c_-] \\
&\quad -\varepsilon_l/\sqrt{2\kappa} - \varepsilon_s e^{-i(\omega_s-\omega_l)t}/\sqrt{2\kappa}.
\end{aligned}
\tag{6.7}
$$

If we write $\langle c_{out}\rangle$ as

$$
\langle c_{out}\rangle = c_l + \varepsilon_s e^{-i(\omega_s-\omega_l)t}c_s + \varepsilon_s^* e^{i(\omega_s-\omega_l)t}c_{as}, \tag{6.8}
$$

where c_l is the response at the pump frequency ω_l, c_s is the response at the Stokes frequency ω_s, and c_{as} is the response at the four-wave-mixing frequency $2\omega_l - \omega_s$ (anti-Stokes frequency). Then we have

$$\begin{aligned} c_l &= \frac{\sqrt{2\kappa}\varepsilon_l}{\kappa + i\Delta} - \frac{\varepsilon_l}{\sqrt{2\kappa}}, \\ c_s &= \frac{\sqrt{2\kappa}}{d(\omega_s - \omega_l)}\{[\kappa - i(\Delta + \omega_s - \omega_l)][(\omega_s - \omega_l)^2 - \omega_m^2 + i\gamma_m(\omega_s - \omega_l)] \\ &\quad -2i\omega_m^3\chi^2|c_0|^2\} - \frac{1}{\sqrt{2\kappa}}, \\ c_{as} &= -\sqrt{2\kappa}\frac{2i\omega_m^3\chi^2 c_0^2}{d^*(\omega_s - \omega_l)}. \end{aligned} \tag{6.9}$$

In the absence of the interaction between the cavity field and the movable mirror, one would expect the output fields to contain only two input components (ω_l and ω_s); no four-wave-mixing component appears. We can get this result from Eq. (6.9) by setting $\chi = 0$, which gives

$$\begin{aligned} c_l &= \frac{\sqrt{2\kappa}\varepsilon_l}{\kappa + i\Delta} - \frac{\varepsilon_l}{\sqrt{2\kappa}}, \\ c_s &= \frac{\sqrt{2\kappa}}{\kappa + i(\Delta - \omega_s + \omega_l)} - \frac{1}{\sqrt{2\kappa}}, \\ c_{as} &= 0, \end{aligned} \tag{6.10}$$

as expected. However, in the presence of the coupling with the oscillator ($\chi \neq 0$), [from Eq. (6.9), we have $c_l \neq 0, c_s \neq 0, c_{as} \neq 0$], the output fields contain three components. The generated signal would exhibit resonances whenever $\omega_s = \omega_l \pm \omega_m$. In addition, one would have the resonances produced by the cavity $\omega_s = \omega_l \pm \Delta$. These resonances are, of course, expected. The normal-mode splitting would arise as a result of strong coupling χ [48, 50, 166]. This is because the structure of the denominator in Eq. (6.9) depends on χ. We next present the roots of Eq. (6.6).

We use parameters which have been used in a recent experiment on the observation of the normal-mode splitting in the fluctuation spectra [50]: the wavelength of the

laser $\lambda = 2\pi c/\omega_l = 1064$ nm, $L = 25$ mm, $m = 145$ ng, $\kappa = 2\pi \times 215 \times 10^3$ Hz, $\omega_m = 2\pi \times 947 \times 10^3$ Hz, the mechanical quality factor $Q' = \omega_m/\gamma_m = 6700$, $\gamma_m = 2\pi \times 141$ Hz, $\Delta = \omega_m$. In this range of parameters, no parametric instabilities occur.

Figure 6.2 shows the dependence of the real parts of the roots of $d(\omega_s - \omega_l)$ in the domain $\mathrm{Re}(\omega_s - \omega_l) > 0$ on the pump power. Figure 6.3 shows the dependence of the imaginary parts of the roots of $d(\omega_s - \omega_l)$ on the pump power. For a small value of the pump power, the real parts of the roots of $d(\omega_s - \omega_l)$ have two equal values, so there is no splitting. However, there is lifetime splitting [168] as seen in Fig. 6.3. If we increase the pump power to a certain value, the real parts of $d(\omega_s - \omega_l)$ in the domain $\mathrm{Re}(\omega_s - \omega_l) > 0$ begin to have two different values, and the difference between two real parts of the roots of $d(\omega_s - \omega_l)$ in the domain $\mathrm{Re}(\omega_s - \omega_l) > 0$ is increased with increasing pump power.

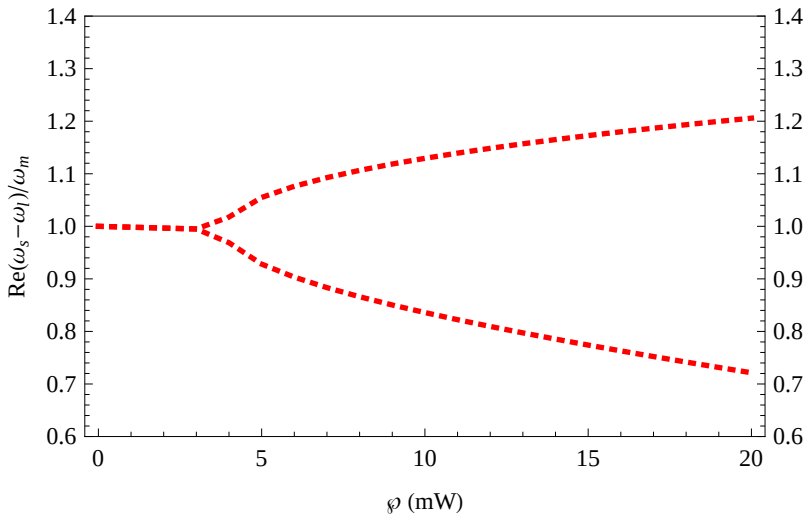

Figure 6.2: The roots of $d(\omega_s - \omega_l)$ in the domain $\mathrm{Re}(\omega_s - \omega_l) > 0$ as a function of the pump power $\wp$.

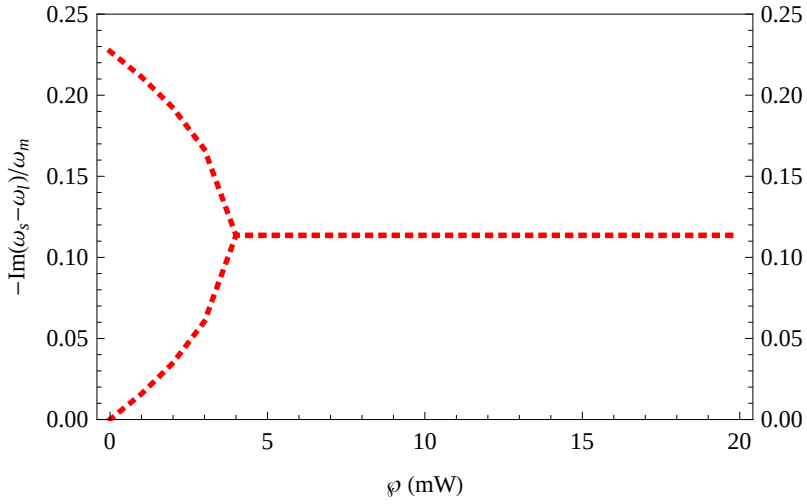

Figure 6.3: The imaginary parts of the roots of $d(\omega_s - \omega_l)$ as a function of the pump power $\wp$.

6.4 Normal-mode Splittings in the Output Fields

Before examining the normal-mode splitting in, say, the output anti-Stokes field, we examine Eq. (6.9) in the traditional limit of nonlinear optics; that is, we find the form of anti-Stokes field to lowest order in χ,

$$\begin{aligned} c_{as} &= -2\sqrt{2\kappa}i\omega_m^3\chi^2\varepsilon_l^2/\{(\kappa+i\Delta)^2[(\omega_s-\omega_l+\omega_m)(\omega_s-\omega_l-\omega_m) \\ &\quad -i\gamma_m(\omega_s-\omega_l)][\kappa-i(\Delta-\omega_s+\omega_l)][\kappa+i(\Delta+\omega_s-\omega_l)]\}, \end{aligned} \tag{6.11}$$

which has resonances as discussed after Eq. (6.10) and which is proportional to the pump power.

We next discuss the normal-mode splitting in the generated Stokes and anti-Stokes fields. It is useful to normalize all quantities to the input Stokes power $\wp_s$. For simplicity, we assume ε_s to be real. For our plots we would give the output power at the Stokes frequency ω_s in terms of the input Stokes power

$$G_s = \frac{\hbar\omega_s|\varepsilon_s c_s|^2}{\wp_s} = |\sqrt{2\kappa}c_s|^2, \tag{6.12}$$

and the two quadratures of the output fields at the Stokes frequency ω_s in terms of the square root of the input Stokes power. Let us denote these normalized quadratures by

v_s and $\tilde{v}_s$. These are defined as $v_s = \sqrt{2\kappa}\frac{c_s + c_s^*}{2}$ and $\tilde{v}_s = \sqrt{2\kappa}\frac{c_s - c_s^*}{2i}$. The quantity G_s is the gain of the cavity optomechanical four-wave mixer. In Figs. 6.4– 6.6, we have plotted v_s, $\tilde{v}_s$, and G_s, respectively, versus the normalized frequency $(\omega_s - \omega_l)/\omega_m$ for different pump powers. The quadrature v_s ($\tilde{v}_s$) exhibits absorptive (dispersive) behavior. As is known, there is a phase change on reflection and that is why the quadrature v_s shows absorptive behavior. The normal-mode splitting or the lifetime splittings are clearly seen depending on the input pump power in the quadratures v_s and $\tilde{v}_s$. The peak positions are in agreement with Fig. 6.2 for the case when the input pump power is such that normal-mode splitting occurs. The behavior of net gain as a function of ω_s is different due to the combination of absorptive and dispersive characteristics of the quadratures v_s and $\tilde{v}_s$. The gain shows normal-mode splitting for larger value of the pump power. Moreover, the maximum gain of the Stokes field is about 1.15. It should be borne in mind that the quadratures v_s and $\tilde{v}_s$ can be obtained by homodyne measurement.

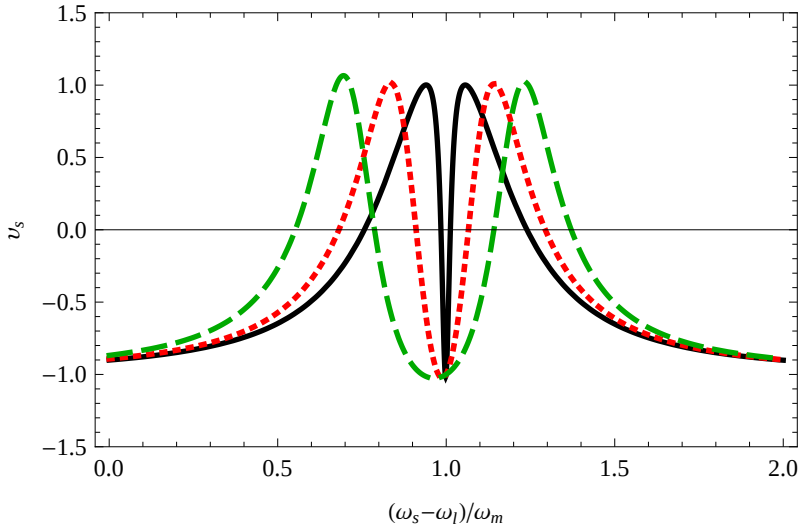

Figure 6.4: The normalized quadrature v_s plotted as a function of the normalized frequency $(\omega_s - \omega_l)/\omega_m$ for different pump power. $\wp = 1$ mW (solid curve), 6.9 mW (dotted curve), and 20 mW (dashed curve).

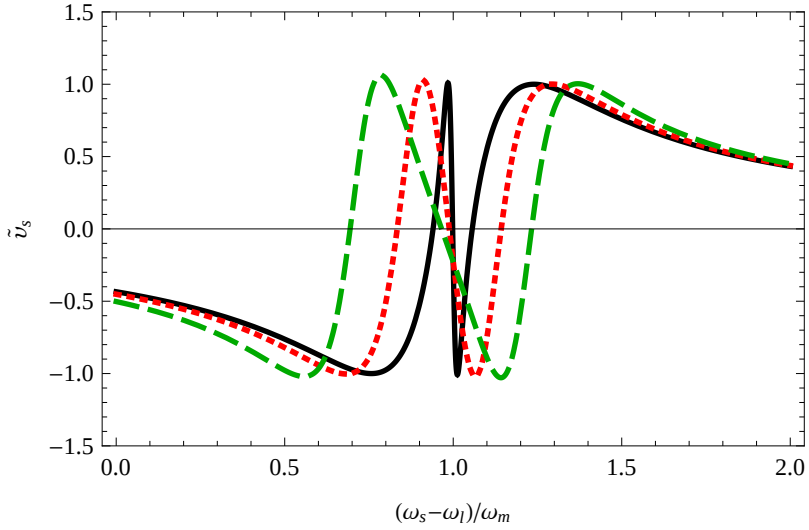

Figure 6.5: The normalized quadrature $\tilde{v}_s$ plotted as a function of the normalized frequency $(\omega_s - \omega_l)/\omega_m$ for different pump power. $\wp = 1$ mW (solid curve), 6.9 mW (dotted curve), and 20 mW (dashed curve).

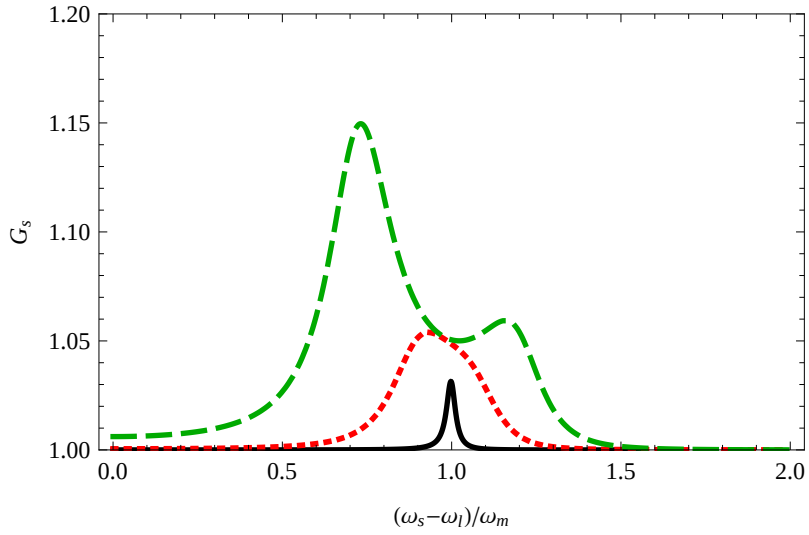

Figure 6.6: The normalized output power G_s plotted as a function of the normalized frequency $(\omega_s - \omega_l)/\omega_m$ for different pump power. $\wp = 1$ mW (solid curve), 6.9 mW (dotted curve), and 20 mW (dashed curve).

Likewise, the output power at the anti-Stokes frequency $2\omega_l - \omega_s$ in terms of the

input Stokes power is given by

$$G_{as} = \frac{\hbar(2\omega_l - \omega_s)|\varepsilon_s c_{as}|^2}{\wp_s} = |\sqrt{2\kappa}c_{as}|^2. \tag{6.13}$$

For brevity, we only show in Fig. 6.7 the function G_{as} against the normalized frequency $(\omega_s - \omega_l)/\omega_m$ for several values of the pump power. As can be seen in Fig. 6.7, increasing the pump power can make the signal of four-wave mixing evolve from one peak to double peaks. It is also seen that the maximum value of G_{as} is about 0.15 and the output power at the anti-Stokes frequency $(2\omega_l - \omega_s)$ is much less than the output power of the Stokes field. However, for larger pump powers, the maximum gain for Stokes and anti-Stokes fields are bigger. For example, for 40 mW pump power, the maximum of G_s and G_{as} are about 1.5 and 0.5, respectively.

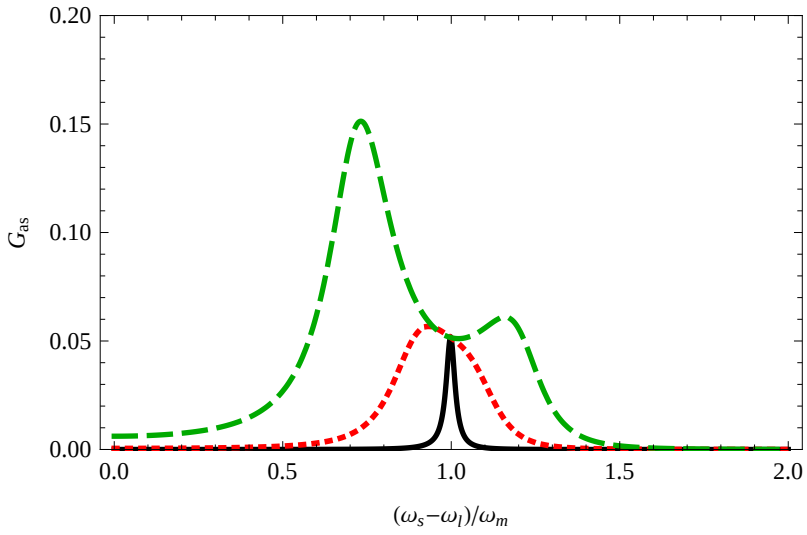

Figure 6.7: The normalized output power G_{as} plotted as a function of the normalized frequency $(\omega_s - \omega_l)/\omega_m$ for different pump power. $\wp = 1$ mW (solid curve), 6.9 mW (dotted curve), and 20 mW (dashed curve).

6.5 Spontaneous Generation of Stokes and Anti-stokes Photons: Quantum Correlations

So far we have considered stimulated processes. The Stokes and anti-Stokes fields are also generated spontaneously. In this case we have to include input vacuum fields. These vacuum fields would be broad band. Thus the field at frequency ω_s in Fig. 6.1 is to be replaced by a broad band quantum field c_{in} with zero mean value and with correlations $\langle \delta c_{in}(t)\delta c_{in}^{\dagger}(t')\rangle = \delta(t-t')$. The calculations of the output quantum fields are standard [26]. We have used these and introduced the Langevin force $\xi(t)$ which stems from the coupling of the movable mirror to the thermal environment having zero mean value with correlations [108]

$$\langle \xi(t)\xi(t')\rangle = \frac{1}{\pi}\frac{\gamma_m}{\omega_m}\int \omega e^{-i\omega(t-t')}\left[1+\coth\left(\frac{\hbar\omega}{2k_BT}\right)\right]d\omega, \tag{6.14}$$

where k_B is the Boltzmann constant and T is the temperature of the environment. The fluctuations of the output fields are obtained as

$$\delta c_{out}(\omega) = V(\omega)\xi(\omega) + E(\omega)\delta c_{in}(\omega) + F(\omega)\delta c_{in}^{\dagger}(-\omega), \tag{6.15}$$

where $\xi(\omega)$, $\delta c_{in}(\omega)$, and $\delta c_{in}^{\dagger}(-\omega)$ are the Fourier transform of the Langevin force $\xi(t)$ and the input vacuum fields $\delta c_{in}(t)$ and $\delta c_{in}^{\dagger}(t)$, respectively, and where

$$\begin{aligned} V(\omega) &= -\frac{\sqrt{2\kappa}\omega_m^2\chi}{d(\omega)}i[\kappa - i(\omega+\Delta)]c_0, \\ E(\omega) &= \frac{2\kappa}{d(\omega)}\{-2\omega_m^3\chi^2 i|c_0|^2 + (\omega^2-\omega_m^2+i\gamma_m\omega)[\kappa - i(\omega+\Delta)]\} - 1, \\ F(\omega) &= -\frac{4\kappa\omega_m^3\chi^2c_0^2}{d(\omega)}i. \end{aligned} \tag{6.16}$$

in which

$$d(\omega) = 4\omega_m^3\chi^2\Delta|c_0|^2 + (\omega^2-\omega_m^2+i\gamma_m\omega)\times[(\kappa-i\omega)^2+\Delta^2]. \tag{6.17}$$

In Eq. (6.15), the first term containing $\xi(\omega)$ is the contribution of the Langevin force acting on the movable mirror, while the other two terms come from the input vacuum

fields. So the fluctuations of the output fields depend on the Langevin force and the input vacuum fields. Further, we define time dependent $\delta c_{out}^{(s)}(t)$ and $\delta c_{out}^{(as)}(t)$, where $\delta c_{out}^{(s)}(t)$ represents the positive-frequency part of the fluctuations of the output fields, corresponding to Stokes component, and

$$\delta c_{out}^{(s)}(t) = \frac{1}{2\pi}\int_0^{\infty} \delta c_{out}(\omega) e^{-i\omega t} d\omega, \tag{6.18}$$

whereas $\delta c_{out}^{(as)}(t)$ represents the negative-frequency part of the fluctuations of the output fields, corresponding to anti-Stokes component, and

$$\delta c_{out}^{(as)}(t) = \frac{1}{2\pi}\int_{-\infty}^{0} \delta c_{out}(\omega) e^{-i\omega t} d\omega. \tag{6.19}$$

In the context of Stokes and anti-Stokes radiation generated by single atoms, several authors [169, 170, 212, 203] found important quantum correlations between the Stokes and anti-Stokes radiation. Such conclusions were drawn from the structure of photon-photon correlations. Motivated by these studies and the fact that we are dealing with a macroscopic system like a nanomechanical mirror; we examine photon-photon correlations in the generated radiation.

In the following, like in the work of Kolchin *et al.* [212], we do not differentiate between the Stokes and anti-Stokes photons. We calculate the coincidence probability defined by

$$g^{(2)}(\tau) = \frac{\langle 0|\delta c_{out}^{\dagger}(t)\delta c_{out}^{\dagger}(t+\tau)\delta c_{out}(t+\tau)\delta c_{out}(t)|0\rangle}{\langle 0|\delta c_{out}^{\dagger}(t)\delta c_{out}(t)|0\rangle\langle 0|\delta c_{out}^{\dagger}(t+\tau)\delta c_{out}(t+\tau)|0\rangle}, \tag{6.20}$$

in which τ is a time delay, and

$$\delta c_{out}(t) = \frac{1}{2\pi}\int_{-\infty}^{+\infty} \delta c_{out}(\omega) e^{-i\omega t} d\omega. \tag{6.21}$$

Now we would evaluate the photon-photon correlations of the output fields numerically. We choose the pump power $\wp$=1 and 4 mW and the temperature of the environment $T = 0$ K; the other parameters are the same as those mentioned in Sec. III. The correlation function $g^{(2)}(\tau)$ between the spontaneously generated photons versus

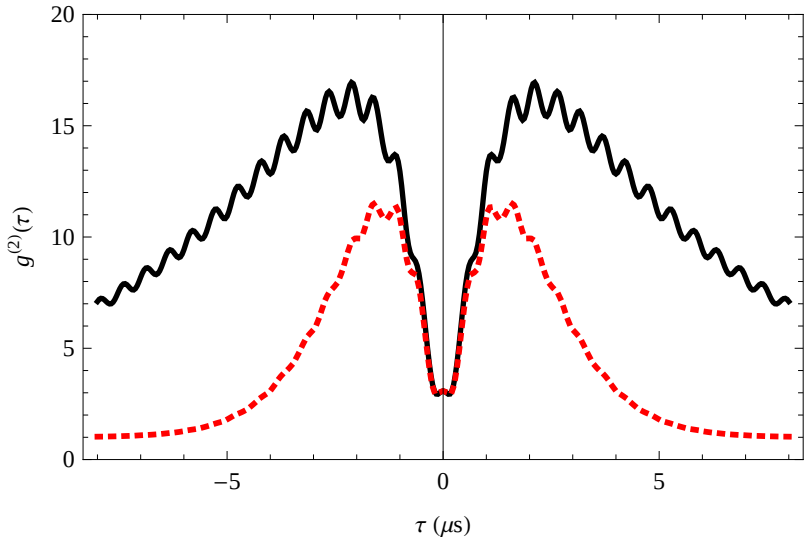

Figure 6.8: The normalized second-order correlation function $g^{(2)}(\tau)$ as a function of the time delay $\tau(\mu s)$ for different pump powers at $T = 0$K. $\wp$=1 mW (solid curve), and 4 mW(dotted curve).

the time delay τ for different pump powers at a temperature of $T = 0$K is displayed in Fig. 6.8. We find that $g^{(2)}(\tau)$ is symmetric. It is also seen that $g^{(2)}(\tau) > g^{(2)}(0)$ as $\tau \neq 0$. This demonstrates the presence of photon antibunching, which is definitely of quantum origin. Further, we note the Cauchy-Schwartz inequality $g^{(2)}(\tau) \leq g^{(2)}(0)$ is violated, and the degree of the violation of the Cauchy-Schwartz inequality becomes smaller with increasing pump power. For pump power $\wp = 1$ mW, the peak value of $g^{(2)}(\tau)$ is about 17, and $g^{(2)}(0) \approx 3$; thus, $g^{(2)}(\tau)/g^{(2)}(0) \approx$5.6. However, for $\wp = 4$ mW, the peak value of $g^{(2)}(\tau)$ is about 11.5, and $g^{(2)}(0) \approx 3$, so $g^{(2)}(\tau)/g^{(2)}(0) \approx$3.8. Therefore, the spontaneously generated photons from the optomechanical system at $T = 0$ K are correlated nonclassically, and the nonclassical correlation becomes weaker with increasing pump power. This is reminiscent of the parametric downconversion process which at low pumping powers produces significant quantum correlations.

6.6 Conclusions

We have shown that an optomechanical system driven by a pump field and a Stokes field can lead to generation of a four-wave-mixing signal. The Stokes field is amplified. We also find that normal-mode splitting occurs in both the generated fields, that is, in both Stokes and anti-Stokes fields. We also report lifetime splitting for pump power less than a critical power. Further, we have discussed the correlations of the photons generated from an optomechanical system by spontaneous processes. We find the correlations between these photons manifest the antibunching effect, and violate Cauchy-Schwartz inequality. Further, the violation of the Cauchy-Schwartz inequality becomes weaker with increasing pump power. Hence, the optomechanical system can be used to generate pairs of photons with quantum correlations. Thus the study of both stimulated and spontaneous Stokes and anti-Stokes signals provides us with a useful technique for studying the strong coupling regime of cavity optomechanics, as well as quantum fluctuations at macroscopic level.

The content of this chapter has been published in *Phys. Rev. A* **81**, 033830 (2010).

CHAPTER 7

THE ELECTROMAGNETICALLY INDUCED TRANSPARENCY IN MECHANICAL EFFECTS OF LIGHT

7.1 Overview

Since its original discovery in the context of atomic vapors, electromagnetically induced transparency (EIT) [76, 172, 173] has been at the center of many important developments in optical physics [174] and has led to many different applications, most notably in the context of slow light [79, 80, 212] and the production of giant nonlinear effects. EIT is helping the progress towards studying nonlinear optics at the single-photon level. EIT has been reported in many other systems [176]. More recently, EIT has been discovered in meta materials [177, 178, 179, 180] where resonant structures can be fabricated to correspond to dark and bright modes. Resonators provide certain advantages [181] because by design we can manipulate EIT to produce desired transmission properties of a structure. It would thus be especially interesting to study resonators coupled to other systems such as cavity optomechanical systems. Such nanomechanical systems have attracted considerable interest recently [38, 39, 48, 50, 117, 120, 182, 183]. In this chapter, we demonstrate the possibility of EIT in the context of cavity optomechanics.

Before discussing our model and results, we set the stage for EIT in cavity optomechanics. As in typical EIT experiments [76, 172, 173, 174], for example, in the context of atomic vapors, we need to examine the pump-probe response of a nanomechanical oscillator of frequency ω_m coupled to a high-quality cavity via radiation pressure effects [164, 165] as schematically shown in Fig. 7.1. Thus, the cavity os-

cillator of frequency ω_0 and the nano-oscillator interact nonlinearly with each other. The system is driven by a strong pump field of frequency ω_c. This is the coupling field. The probe field has frequency ω_p and is much weaker than the pump field. The mechanical oscillator's damping is much smaller than that of the cavity oscillator. This is very important for considerations of EIT. The decay rate of the mechanical oscillator plays the same role as the decay rate of the ground-state coherence in EIT experiments. The analog of the two-photon resonance condition where EIT occurs would be $\omega_c + \omega_m = \omega_p$. We show how the absorptive and dispersive responses of the probe change by the coupling field and how EIT emerges. We present a clear physical origin of EIT in such a system.

7.2 Model

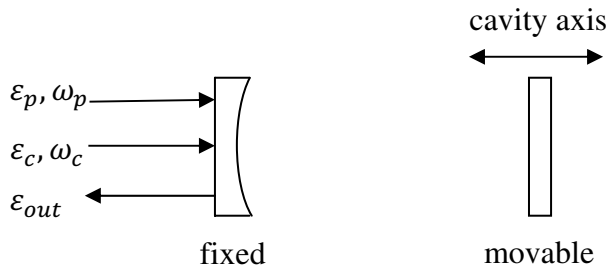

Figure 7.1: Sketch of the optomechanical system coupled to a high-quality cavity via radiation pressure effects.

Let us denote the cavity annihilation (creation) operator by c ($c^\dagger$) with the commutation relation $[c, c^\dagger] = 1$. The momentum and position operators of the nanomechanical oscillator with mass m are represented by p and q. We also introduce the amplitudes of the pump field and the probe field inside the cavity $\varepsilon_c = \sqrt{2\kappa\wp_c/(\hbar\omega_c)}$ and $\varepsilon_p = \sqrt{2\kappa\wp_p/(\hbar\omega_p)}$, where $\wp_c$ is the pump power, $\wp_p$ is the power of the probe

field, and κ is the cavity decay rate. Note that ε_c and ε_p have dimensions of frequency. The optomechanical coupling between the cavity field and the movable mirror can be described by the coupling constant $\chi_0 = \hbar\omega_0/L$, where L is the cavity length. The Hamiltonian describing the whole system reads

$$\begin{aligned} H = \hbar\omega_0 c^\dagger c + \left(\frac{p^2}{2m} + \frac{1}{2}m\omega_m^2 q^2\right) + i\hbar\varepsilon_c(c^\dagger e^{-i\omega_c t} - ce^{i\omega_c t}) \\ +i\hbar(c^\dagger\varepsilon_p e^{-i\omega_p t} - c\varepsilon_p^* e^{i\omega_p t}) - \chi_0 c^\dagger c q. \end{aligned} \tag{7.1}$$

This chapter deals with the mean response of the system to the probe field in the presence of the coupling field. Because we deal with the mean response of the system we do not include quantum fluctuations. This is similar to what has been done in the context of EIT work where one uses atomic mean value equations and all quantum fluctuations (due to either spontaneous emission or collisions) are ignored. Thus, we examine the mean value equations, which can be obtained from the Hamiltonian and by addition of the damping terms. We use the factorization assumption $\langle Qc\rangle = \langle Q\rangle\langle c\rangle$ and also transform the cavity field to a rotating frame at the frequency ω_c, $\langle c(t)\rangle = \langle\tilde{c}(t)\rangle e^{-i\omega_c t}$. The mean value equations are then given by

$$\begin{aligned} \langle\dot{q}\rangle &= \frac{\langle p\rangle}{m}, \\ \langle\dot{p}\rangle &= -m\omega_m^2\langle q\rangle + \chi_0\langle\tilde{c}^\dagger\rangle\langle\tilde{c}\rangle - \gamma_m\langle p\rangle, \\ \langle\dot{\tilde{c}}\rangle &= -\left[\kappa + i\left(\omega_0 - \omega_c - \frac{\chi_0}{\hbar}\langle q\rangle\right)\right]\langle\tilde{c}\rangle + \varepsilon_c + \varepsilon_p e^{-i(\omega_p-\omega_c)t}. \end{aligned} \tag{7.2}$$

The output field can be obtained by using the input-output relations [110]

$$\varepsilon_{out}(t) + \varepsilon_p e^{-i\omega_p t} + \varepsilon_c e^{-i\omega_c t} = 2\kappa\langle c\rangle. \tag{7.3}$$

We first note that in the absence of the coupling field, the output field is given by

$$\varepsilon_{out}(t) + \varepsilon_p e^{-i\omega_p t} = \varepsilon_T\varepsilon_p e^{-i\omega_p t} = \frac{2\kappa}{\kappa - i(\omega_p - \omega_0)}\varepsilon_p e^{-i\omega_p t}. \tag{7.4}$$

The quadratures of the field ε_T, defined by $\varepsilon_T = \upsilon_p + i\tilde{\upsilon}_p$, show the absorptive and dispersive behavior as a function of the detuning parameter $(\omega_p - \omega_0)$. The field quadratures, as is well known, can be measured by homodyne techniques [110].

Next, we examine the effect of the coupling field. Equations (7.2) are nonlinear, and therefore the steady-state response contains many Fourier components. We solve in the limit of arbitrary strength of the coupling field; however, we take the probe field to be weak. We specifically are interested in the response of the cavity optomechanical system to the probe in the presence of the coupling field ε_c. Thus, we find the component of the output field oscillating at the probe frequency ω_p. The result of such a calculation is that ε_T is now given by

$$\varepsilon_T = \frac{2\kappa}{d(\delta)}\{(\delta^2 - \omega_m^2 + i\gamma_m\delta)[\kappa - i(\Delta + \delta)] - 2i\omega_m\beta\}, \tag{7.5}$$

where

$$\begin{aligned} d(\delta) &= (\delta^2 - \omega_m^2 + i\gamma_m\delta)[(\kappa - i\delta)^2 + \Delta^2)] + 4\Delta\omega_m\beta, \\ \delta &= \omega_p - \omega_c, \\ \Delta &= \omega_0 - \omega_c - \frac{2\beta\chi_0}{\omega_m}, \\ \beta &= \frac{\chi_0^2|\tilde{c}_0|^2}{2m\hbar\omega_m}, \\ \tilde{c}_0 &= \frac{\varepsilon_c}{\kappa + i\Delta}. \end{aligned} \tag{7.6}$$

The coupling field has modified the output field at the probe frequency. Note that ε_T is nonperturbative in terms of the strength of the coupling field ω_c. We concentrate on the output field. However, all the results for ε_T also apply to the cavity field at ω_p as the two quantities are proportional to each other.

In order to understand the coupling-field-induced modification of the probe response ε_T, we make reasonable approximations. We work in the sideband resolved limit $\omega_m \gg \kappa$. This is the limit in which normal mode splitting [47, 48, 50] has been discovered. Because it is known that the coupling between the nano-oscillator and the cavity is strongest whenever $\delta = \pm\omega_m$ or $\delta = \pm\Delta$, the case $\Delta \sim \omega_m$ is considered here. After some simplifications, we can write the output field in an instructive form,

$$\varepsilon_T = v_p + i\tilde{v}_p = \frac{2\kappa}{\kappa - ix + \frac{\beta}{\frac{\gamma_m}{2} - ix}} = \frac{A_+}{x - x_+} + \frac{A_-}{x - x_-}, \tag{7.7}$$

where $x = \delta - \omega_m$, which is the detuning from the line center. Further, it is seen that the denominator has two roots, which are

$$x_{\pm} = \frac{-i(\kappa + \frac{\gamma_m}{2}) \pm \sqrt{-(\kappa - \frac{\gamma_m}{2})^2 + 4\beta}}{2}, \tag{7.8}$$

whose nature depends on the power of the coupling laser. For coupling powers less than the critical power

$$\tilde{\wp}_c = \frac{\hbar\omega_c|\tilde{c}_0|^2(\kappa^2 + \omega_m^2)(\kappa - \frac{\gamma_m}{2})^2}{8\kappa\beta}, \tag{7.9}$$

the two roots are purely imaginary. For $\wp_c > \tilde{\wp}_c$, the roots are complex conjugates of each other. The region $\wp_c > \tilde{\wp}_c$ corresponds to the region where normal-mode splitting [47, 48, 50] occurs and has been studied recently using a very different technique. In the context of optical physics, this is the region where Autler-Townes splitting [184] occurs, although sometimes the distinction between different kinds of splittings is marred. However, for EIT, it is important to have $\gamma_m \ll \kappa$.

7.3 EIT in the Out Field

In order to bring out prominently features like EIT [76, 172, 173], we specifically examine the case when the coupling power is less than the critical power. Note that $x_+ \to -i\frac{\gamma_m}{2}$, $x_- \to -i\kappa$ as $\beta \to 0$. Thus, the quadratures of the output field have two distinct contributions in the limit of low values of the coupling laser strength. One contribution is extremely narrow as $\gamma_m \ll \kappa$. This characteristic property leads to the EIT dip. For numerical work, we use parameters from a recent experiment on the observation of the normal-mode splitting [50]: the wavelength of the laser $\lambda = 2\pi c/\omega_c = 1064$ nm, $L = 25$ mm, $m = 145$ ng, $\kappa = 2\pi \times 215$ kHz, $\omega_m = 2\pi \times 947$ kHz, $\gamma_m = 2\pi \times 141$ Hz, the mechanical quality factor $Q = \omega_m/\gamma_m = 6700$. We calculate the critical power $\tilde{\wp}_c$ to be 3.8 mW. In Figs. 7.2 and 7.3, we show each contribution in Eq. (7.7) separately and also the total contribution. We observe that

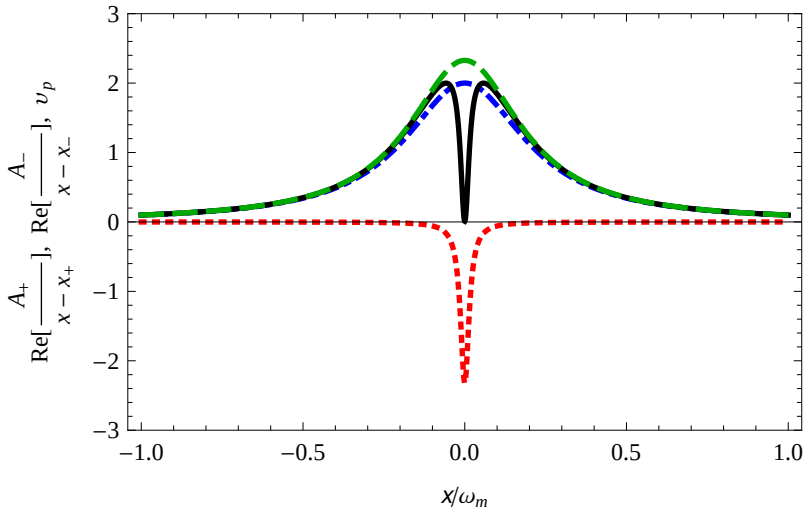

Figure 7.2: Quadrature of the output field υ_p (solid black curve) and the different contributions to it: the real parts of $\frac{A_+}{x-x_+}$ (dotted red curve) and $\frac{A_-}{x-x_-}$ (dashed green curve) as a function of the normalized frequency x/ω_m for input coupling laser power $\wp_c = 1$ mW. The dot-dashed blue curve is υ_p in the absence of the coupling laser.

the narrow contribution is inverted relative to the broad contribution, and this leads to the typical EIT-like line shape for the quadrature υ_p of the output field. The value at the dip is not exactly zero as $\gamma_m \neq 0$, though the value is very small as $\gamma_m \ll \kappa$. This is similar to what one has in the context of EIT in atomic systems where a strict zero is obtained if the ground-state atomic coherence has an infinite lifetime. In the absence of the coupling field, the narrow feature disappears (blue curve in Fig. 7.2). The narrow feature's width has a contribution which depends on the coupling laser power. In leading order, the width is $\frac{\gamma_m}{2} + \frac{\beta}{\kappa}$. For the plot of Fig. 7.3, the power-dependent contribution to the width in dimensionless units is $\beta/\kappa^2 \sim 0.065$. The quadrature $\tilde{\upsilon}_p$ exhibits dispersive behavior, and the coupling field changes the nature of dispersion from anomalous to normal in the region where quantum interferences are prominent. This behavior of dispersion is similar to the one found by Harris and collaborators in predictions of slow light [79, 80, 212] in atomic systems.

We next present the nature of interferences in the region when $\wp_c > \tilde{\wp}_c$ in Figs.

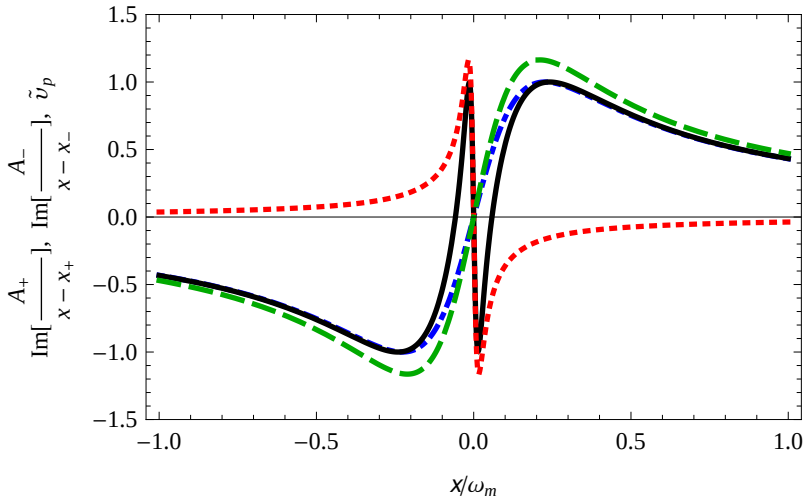

Figure 7.3: Quadrature of the output field $\tilde{v}_p$ (solid black curve) and the different contributions to it: the imaginary parts of $\frac{A_+}{x-x_+}$ (dotted red curve) and $\frac{A_-}{x-x_-}$ (dashed green curve) as a function of the normalized frequency x/ω_m for input coupling laser power $\wp_c = 1$ mW. The dot-dashed blue curve is $\tilde{v}_p$ in the absence of the coupling laser.

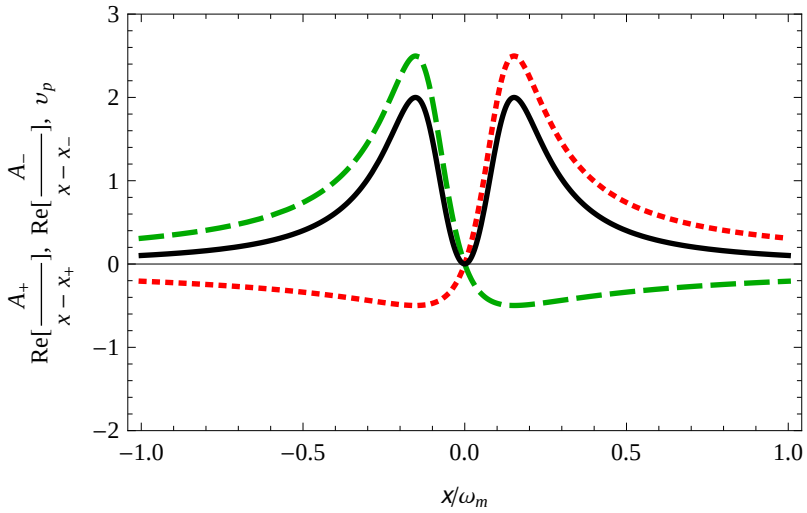

Figure 7.4: Same as in Fig. 7.2 except the input coupling laser power $\wp_c = 6.9$ mW and $\wp_c = 0$ case is not shown.

7.4 and 7.5. A typical behavior is shown in Fig. 7.4 which clearly shows how the interference of the two contributions in Eq. (7.7) leads to the formation of the dip.

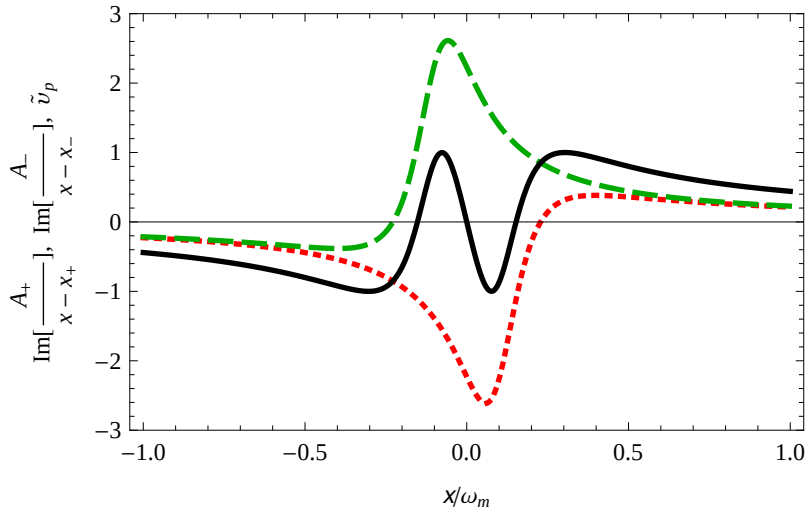

Figure 7.5: Same as in Fig. 7.3 except the input coupling laser power $\wp_c = 6.9$ mW and $\wp_c = 0$ case is not shown.

The two contributions in Eq. (7.7) lead to asymmetric profiles. In the region of EIT, the tails from these contributions interfere. Unlike the case given by Fig. 7.2, the two contributions have identical line widths. From Fig. 7.5, we also see how the dispersive behavior is changed by the coupling field from anomalous to normal in the region where quantum interferences are dominated. The inverted nature of the contribution A_+ should be noted, and it is this which changes the nature of dispersion.

We now explain the origin of the structure (7.7) for the probe response. Let us re-examine the Hamiltonian (7.1). Note that we drive the cavity with arbitrary pump field ε_p. This effectively prepares the cavity in a coherent state with a value $\tilde{c}_0$ if all the other interactions were zero. The trilinear interaction due to radiation pressure $\chi_0 c^\dagger c q$ can now be written as $\chi_0 q|\tilde{c}_0|^2 + \chi_0 q(\tilde{c}_0^* \delta c + \tilde{c}_0 \delta c^\dagger)+$ higher order terms if we write the cavity operator c as $\tilde{c}_0 + \delta c$. The pump thus has resulted in a bilinear interaction between the cavity oscillator and the mirror oscillator. The cavity oscillator is driven by the probe field, whereas the matter oscillator has no external drive. The cavity oscillator is damped at the rate κ, whereas the mirror is damped at the rate $\gamma_m \ll \kappa$. This situation typically results [177, 178, 179, 180, 181] in line shapes such as (7.7).

7.4 Conclusions

In conclusion, we have shown how an exact analog of EIT can occur in cavity optomechanics when such a system is driven by a weak probe in the presence of a strong coupling field. We find that the response function for the cavity field at the probe frequency as well as the output field has exactly the same features as the response of a Λ system provided the damping of the nanomechanical mirror is much smaller than the dissipation in the cavity. We further highlighted the interference effects in two distinct regions of the coupling power.

The content of this chapter has been published in *Phys. Rev. A* **81**, 041803(R) (2010).

CHAPTER 8

REACTIVE-COUPLING-INDUCED NORMAL MODE SPLITTINGS IN MICRODISK RESONATORS COUPLED TO WAVEGUIDES

8.1 Overview

In a recent paper Li *et al.* [67] presented a new design for an optomechanical system that consists of a microdisk resonator coupled to a waveguide. This design has several attractive features. Besides its universality, it enables one to study the reactive effects [67, 185] in optomechanical coupling. The origin of the reactive coupling is well explained in Ref. [69]. Its origin lies in the mechanical motion dependence of the extrinsic losses of the disk resonator. Further phase-dependent gradient forces lead to reactive coupling. Li *et al.* have also argued that this design is more effective in achieving cooling of the system to its ground state. While cooling is desirable for studying quantum effects at the macroscopic scale [35, 36, 38, 39, 117, 186], we examine other possibilities, which do not depend on the cooling of the system, to investigate the effects arising from strong reactive coupling. Since optomechanical coupling effects are intrinsically nonlinear, we examine the nonlinear response of the microdisk resonator to pump probe fields. We report reactive-coupling-induced normal mode splitting. Note that in previous works [47, 48, 50, 187] on normal mode splitting in optomechanical devices, only dispersive coupling was used. In this chapter, we report on normal mode splitting due to reactive effects.

The chapter is organized as follows. In Sec. II, the physical system is introduced and the time evolutions of the expectation values of the system operators are given and solved. In Sec. III, the expectation value of the output fields is calculated, and

the nonlinear susceptibilities for Stokes and anti-Stokes processes are obtained. In Sec. IV, we discuss normal mode splitting in output fields with or without reactive coupling. We find that there is no normal mode splitting in output fields in the absence of reactive coupling. However, normal mode splitting occurs in output fields in the presence of reactive coupling.

8.2 Model

We consider the system shown in Fig. 8.1, in which a microdisk cavity is coupled to a freestanding waveguide. A strong pump field with frequency ω_l and a weak Stokes field with frequency ω_s enter the system through the waveguide. The waveguide will move along the y direction under the action of the optical force exerted by the photons from the cavity. Further, considering the dispersive coupling and reactive coupling between the waveguide and the cavity, displacement q of the waveguide from its equilibrium position will change the resonant frequency of the cavity field and the cavity decay rate, represented by $\omega_c(q)$ and $\kappa_e(q)$, respectively.

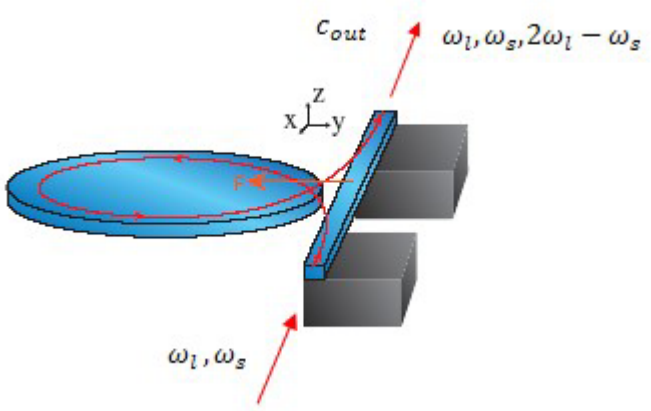

Figure 8.1: Sketch of the studied system (from Ref.[67]). The microdisk cavity is driven by a pump field and a Stokes field. The nonlinearity of the interaction also generates anti-Stokes field.

In a rotating frame at pump frequency ω_l, the Hamiltonian of the system is given by [67]

$$\begin{aligned} H = \hbar[\omega_c(q) - \omega_l]c^\dagger c + \frac{p^2}{2m} + \frac{1}{2}m\omega_m^2 q^2 + \hbar\frac{L}{c}\tilde{n}_g(\omega_l\varepsilon_l^2 + \omega_s|\varepsilon_s|^2) \\ +i\hbar\sqrt{2\kappa_e(q)}\varepsilon_l(c^\dagger - c) + i\hbar\sqrt{2\kappa_e(q)}(\varepsilon_s e^{-i\delta t}c^\dagger - \varepsilon_s^* e^{i\delta t}c). \end{aligned} \tag{8.1}$$

The first term is the energy of the cavity field, whose annihilation (creation) operators are denoted $c(c^\dagger)$. The second and third terms are the energy of the waveguide with mass m, frequency ω_m, and momentum operator p. The fourth term gives the interactions between the waveguide and the incident fields (the pump field and the Stokes field), L is the length of the waveguide, c is the speed of light in vacuum, $\tilde{n}_g$ is the group index of the waveguide optical mode [188], ε_l and $|\varepsilon_s|$ are the amplitudes of the pump field and the Stokes field, respectively, and they are related to their corresponding power $\wp_l$ and $\wp_s$ by $\varepsilon_l = \sqrt{\frac{\wp_l}{\hbar\omega_l}}$ and $|\varepsilon_s| = \sqrt{\frac{\wp_s}{\hbar\omega_s}}$. The latter two terms describe the coupling of the cavity field to the pump field and the Stokes field, respectively. And $\delta = \omega_s - \omega_l$ is the detuning between the Stokes field and the pump field. We would study the physical effects by scanning the Stokes laser.

For a small displacement q, $\omega_c(q)$ and $\kappa_e(q)$ can be expanded to the first order of q,

$$\begin{aligned} \omega_c(q) &\approx \omega_c + q\chi, \\ \kappa_e(q) &\approx \kappa_e + q\kappa_{om}, \end{aligned} \tag{8.2}$$

thus the quantities χ and κ_{om} describe the cavity-waveguide dispersive and reactive coupling strength, respectively. Further, note that the photons in the cavity can leak out of the cavity by an intrinsic damping rate κ_i of the cavity and by a rate of $\kappa_e(q)$ due to the reactive coupling between the waveguide and the cavity. In addition, the velocity of the waveguide is damped at a rate of γ_m. Applying the Heisenberg equation of motion and adding the damping terms, the time evolutions of the expectation values ($\langle q\rangle$, $\langle p\rangle$, and $\langle c\rangle$) for the system can be expressed as

$$\langle \dot{q} \rangle = \frac{\langle p \rangle}{m},$$

$$\langle \dot{p} \rangle = -m\omega_m^2 \langle q \rangle - \hbar\chi \langle c^\dagger \rangle \langle c \rangle - 2\hbar \frac{\kappa_{om}}{\sqrt{\kappa}} \mathrm{Im}[(\varepsilon_l + \varepsilon_s^* e^{i\delta t}) \langle c \rangle] - \gamma_m \langle p \rangle, \tag{8.3}$$

$$\langle \dot{c} \rangle = -[\kappa + \langle q \rangle \kappa_{om} + i(\omega_c - \omega_l + \langle q \rangle \chi)] \langle c \rangle + \sqrt{\kappa}[1 + \langle q \rangle \frac{\kappa_{om}}{\kappa}](\varepsilon_l + \varepsilon_s e^{-i\delta t}),$$

where we have used the mean field assumption $\langle qc \rangle = \langle q \rangle \langle c \rangle$, expanded $\kappa_e(q)$ to the first order of q, and assumed $\kappa_e \approx \kappa_i \approx \kappa/2$, where κ is the half-linewidth of the cavity field. It should be noted that the steady-state solution of Eq. (8.3) contains an infinite number of frequencies. Since the Stokes field ε_s is much weaker than the pump field ε_l, the steady-state solution of Eq. (8.3) can be simplified to first order in ε_s only. We find that in the limit $t \to \infty$, each $\langle q \rangle$,$\langle p \rangle$, and $\langle c \rangle$ has the form

$$\langle s \rangle = s_0 + s_+ \varepsilon_s e^{-i\delta t} + s_- \varepsilon_s^* e^{i\delta t}, \tag{8.4}$$

where s stands for any of the three quantities q, p, and c. Thus the expectation values ($\langle q \rangle, \langle p \rangle$, and $\langle c \rangle$) oscillate at three frequencies (ω_l, ω_s, and $2\omega_l - \omega_s$). Substituting Eq. (8.4) into Eq. (8.3), ignoring those terms containing the small quantities ε_s^2, ε_s^{*2}, $|\varepsilon_s|^2$, and equating coefficients of terms with the same frequency, respectively, we obtain the following results

$$\begin{aligned}
c_0 &= \frac{A\varepsilon_l}{\kappa + q_0\kappa_{om} + i\Delta}, \\
q_0 &= -\frac{\hbar}{m\omega_m^2}[\chi |c_0|^2 + i\frac{\kappa_{om}}{\sqrt{\kappa}} \varepsilon_l (c_0^* - c_0)], \\
c_+ &= \frac{1}{d(\delta)}[A(BE + FJ) - i\hbar \frac{\kappa_{om}}{\sqrt{\kappa}} c_0^* B F^*], \\
c_- &= \frac{F^*}{d^*(\delta)}(-AJ + i\hbar \frac{\kappa_{om}}{\sqrt{\kappa}} c_0 V), \\
q_+ &= \frac{B}{d(\delta)}(-AJ^* - i\hbar \frac{\kappa_{om}}{\sqrt{\kappa}} c_0^* V^*), \\
q_- &= (q_+)^*,
\end{aligned} \tag{8.5}$$

where

$$\Delta = \omega_c - \omega_l + \chi q_0, \tag{8.6}$$

$$d(\delta) = V^*(BE + FJ) + BF^*J^*, \tag{8.7}$$

and $A = \sqrt{\kappa}(1 + \frac{\kappa_{om}}{\kappa}q_0)$, $B = \kappa + q_0\kappa_{om} - i(\Delta + \delta)$, $E = m(\omega_m^2 - \delta^2 - i\gamma_m\delta)$, $F = -c_0^*(\kappa_{om} - i\chi) + \frac{\kappa_{om}}{\sqrt{\kappa}}\varepsilon_l$, $J = \chi\hbar c_0 + i\hbar\frac{\kappa_{om}}{\sqrt{\kappa}}\varepsilon_l$, $V = \kappa + q_0\kappa_{om} - i(\Delta - \delta)$. The approach used in this paper is similar to our earlier work [49] which dealt with optomechanical systems with dispersive coupling only.

8.3 Output Fields

To investigate the normal mode splitting of the output fields, we need to calculate their expectation value. It can be obtained by using the input-output relation [110] $\langle c_{out}\rangle = \sqrt{2\kappa_e(q)}\langle c\rangle$. If we write $\langle c_{out}\rangle$ as

$$\langle c_{out}\rangle = c_l + \varepsilon_s e^{-i\delta t}c_s + \varepsilon_s^* e^{i\delta t}c_{as}, \tag{8.8}$$

where c_l is the response at the pump frequency ω_l, c_s is the response at the Stokes frequency ω_s, and c_{as} is the field generated at the new anti-Stokes frequency $2\omega_l - \omega_s$. Then we have

$$\begin{aligned} c_l &= \sqrt{\kappa}(1 + \frac{\kappa_{om}}{\kappa}q_0)c_0, \\ c_s &= \frac{\kappa_{om}}{\sqrt{\kappa}}q_+c_0 + \sqrt{\kappa}(1 + \frac{\kappa_{om}}{\kappa}q_0)c_+, \\ c_{as} &= \frac{\kappa_{om}}{\sqrt{\kappa}}q_-c_0 + \sqrt{\kappa}(1 + \frac{\kappa_{om}}{\kappa}q_0)c_-. \end{aligned} \tag{8.9}$$

Furthermore, whether there is normal mode splitting in the output fields is determined by the roots of the denominator $d(\delta)$ of c_s. Here we examine the roots of $d(\delta)$ given by Eq. (8.7) numerically.

The response of the system is expected to be especially significant if we choose ω_s corresponding to a sideband $\omega_s = \omega_l \pm \omega_m$ or $\omega_s = \omega_l \pm \Delta$, so we consider the case $\Delta = \omega_m$. The other parameters are chosen from a recent experiment focusing

on the effect of the reactive force on the waveguide [67]: the wavelength of the laser $\lambda = 2\pi c/\omega_l = 1564.25$ nm, $\chi = 2\pi \times 2$ MHz/nm, $m = 2$ pg (density of the silicon waveguide, 2.33 g/cm^3; length, 10 μm; width, 300 nm; height, 300 nm), $\kappa = 0.2\omega_m$, $\omega_m = 2\pi \times 25.45$ MHz, and the mechanical quality factor $Q = \omega_m/\gamma_m = 5000$. In the following, we work in the stable regime of the system.

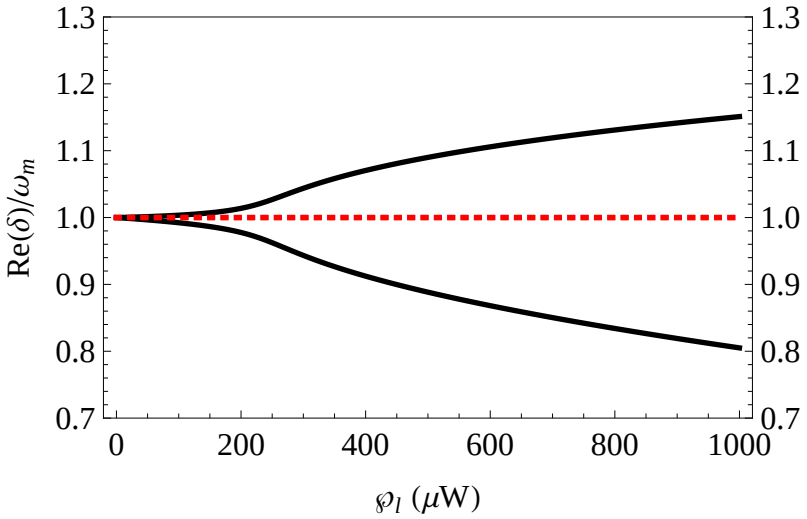

Figure 8.2: The real roots of $d(\delta)$ in the domain $\mathrm{Re}(\delta) > 0$ as a function of the pump power $\wp_l$ for $\kappa_{om} = 0$ (dotted curve) and $\kappa_{om} = -2\pi \times 26.6$ MHz/nm (solid curve).

Figure 8.2 shows the variation of the real parts of the roots of $d(\delta)$ in the domain $\mathrm{Re}(\delta) > 0$ with increasing pump power for no reactive coupling, $\kappa_{om} = 0$, and for $\kappa_{om} = -2\pi \times 26.6$ MHz/nm. For $\kappa_{om} = 0$, the interaction of the waveguide with the cavity is purely dispersive; the cavity decay rate does not depend on the displacement of the waveguide. In this case, the real parts of the roots of $d(\delta)$ always have two equal values with increasing pump power. Thus there is no splitting because the dispersive coupling is not strong enough. However, for $\kappa_{om} = -2\pi \times 26.6$ MHz/nm, the system has both dispersive and reactive couplings, the cavity decay rate depends on the displacement of the waveguide, and the real parts of the roots of $d(\delta)$ will change from two equal values to two different values with increasing pump power. And the

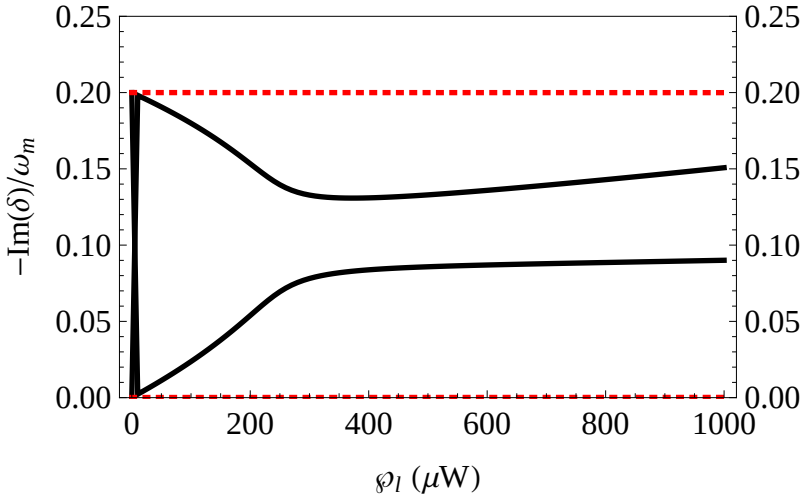

Figure 8.3: Imaginary parts of the roots of $d(\delta)$ as a function of the pump power $\wp_l$ for $\kappa_{om} = 0$ (dotted curve) and $\kappa_{om} = -2\pi \times 26.6$ MHz/nm (solid curve).

difference between two real parts of the roots of $d(\delta)$ in the domain $\mathrm{Re}(\delta) > 0$ is increased with increasing pump power. Therefore, the reactive coupling between the waveguide and the cavity can result in normal mode splitting of the output fields, and the peak separation becomes larger with increasing pump power. Figure 8.3 shows the variation of the imaginary parts of the roots of $d(\delta)$ with increasing pump power for zero reactive coupling $\kappa_{om} = 0$ and nonzero reactive coupling $\kappa_{om} = -2\pi \times 26.6$ MHz/nm. For $\kappa_{om} = 0$, the imaginary parts of the roots of $d(\delta)$ do not change with increasing pump power. However, for $\kappa_{om} = -2\pi \times 26.6$ MHz, the imaginary parts of the roots of $d(\delta)$ change with increasing pump power. We thus conclude that for the present microdisk resonator coupled to a waveguide the normal mode splitting is solely due to the reactive coupling.

8.4 Normal Mode Splitting In Output Fields

We now discuss how the output fields depend on the behavior of the roots of $d(\delta)$. For convenience, we normalize all quantities to the input Stokes power $\wp_s$. Assuming

that ε_s is real, we express the output power at the Stokes frequency ω_s in terms of the input Stokes power

$$G_s = \frac{\hbar\omega_s|\varepsilon_s c_s|^2}{\wp_s} = |c_s|^2. \tag{8.10}$$

Further, we introduce the two quadratures of the Stokes component of the output fields by $\upsilon_s = \dfrac{c_s + c_s^*}{2}$ and $\tilde{\upsilon}_s = \dfrac{c_s - c_s^*}{2i}$. One can measure either the quadratures of the output by homodyne techniques or the intensity of the output. For brevity, we only show υ_s and G_s as a function of the normalized detuning between the Stokes field and the pump field δ/ω_m for this model, without reactive coupling (κ_{om}=0) and with it ($\kappa_{om} = -2\pi \times 26.6$ MHz/nm), for different pump powers in Figs. 8.4–8.5.

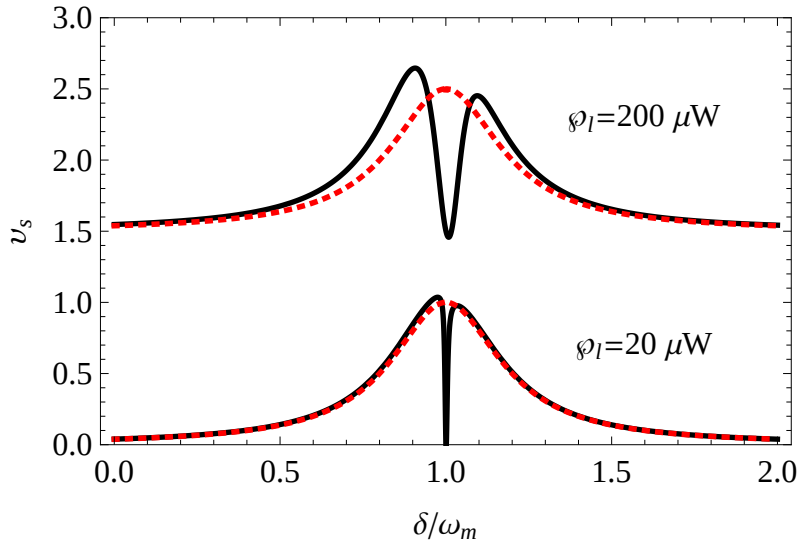

Figure 8.4: The lower two curves show the normalized quadrature v_s as a function of the normalized detuning between the Stokes field and the pump field, δ/ω_m for $\kappa_{om} = 0$ (dotted curve) and $\kappa_{om} = -2\pi \times 26.6$ MHz/nm (solid curve) for pump power $\wp_l = 20$ μW. The upper two curves give the normalized quadrature v_s+1.5 for pump power $\wp_l = 200$ μW.

For κ_{om}=0, it is found that υ_s has a Lorentzian lineshape corresponding to the absorptive behavior. Note that υ_s and G_s exhibit no splitting when κ_{om}=0. However, for $\kappa_{om} = -2\pi \times 26.6$ MHz/nm, it is clearly seen that normal mode splitting appears

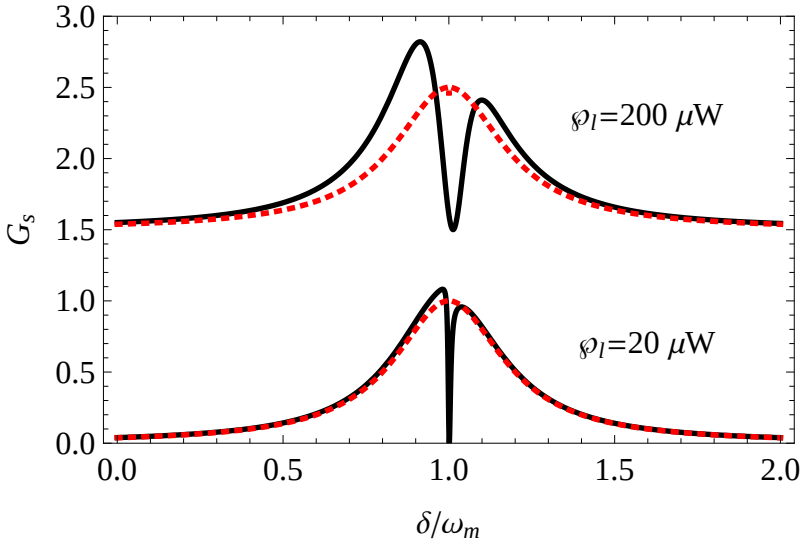

Figure 8.5: The lower two curves show the normalized output power G_s as a function of the normalized detuning between the Stokes field and the pump field, δ/ω_m for $\kappa_{om} = 0$ (dotted curve) and $\kappa_{om} = -2\pi \times 26.6$ MHz/nm (solid curve) for pump power $\wp_l = 20$ μW. The upper two curves give the normalized output power G_s+1.5 for pump power $\wp_l = 200$ μW.

in υ_s and G_s. Therefore reactive coupling can lead to the appearance of normal mode splitting in the output Stokes field. And the peak separation increases with increasing pump power [189]. The dip at the line center exhibits power broadening. We also find that the Stokes field can be amplified by the stimulated process. Obviously the maximum gain G_s for the Stokes field depends on the system parameters. For a pump power $\wp_l = 200$ μW, the maximum gain for the Stokes field is about 1.3.

Note that the nonlinear nature of the reactive coupling generates anti-Stokes radiation. In a similar way, we define a normalized output power at the anti-Stokes frequency $2\omega_l - \omega_s$ as

$$G_{as} = \frac{\hbar(2\omega_l - \omega_s)|\varepsilon_s c_{as}|^2}{\wp_s} = |c_{as}|^2. \tag{8.11}$$

The plots of G_{as} versus the normalized detuning between the Stokes field and the pump field δ/ω_m for this model, without reactive coupling (κ_{om}=0) and with it (κ_{om} =

$-2\pi \times 26.6$ MHz/nm), for different pump powers are presented in Fig. 8.6. We can

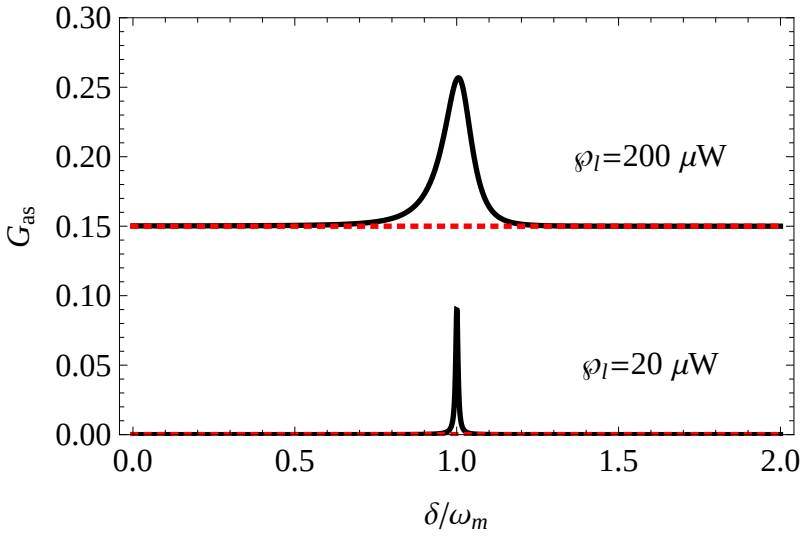

Figure 8.6: The lower two curves show the normalized output power G_{as} as a function of the normalized detuning between the Stokes field and the pump field, δ/ω_m for $\kappa_{om} = 0$ (dotted curve) and $\kappa_{om} = -2\pi \times 26.6$ MHz/nm (solid curve) for pump power $\wp_l = 20$ μW. The upper two curves give the normalized output power G_{as}+0.15 for pump power $\wp_l = 200$ μW.

see that $G_{as} \approx 0$ for κ_{om}=0. The reason is that the dispersive coupling constant χ is too small. However, for $\kappa_{om} = -2\pi \times 26.6$ MHz/nm, G_{as} is not equal to zero. This shows that the optomechanical system can generate an anti-Stokes field with frequency $(2\omega_l - \omega_s)$ due to the reactive coupling. For pump power $\wp_l = 200$ μW, the maximum gain defined with reference to the input Stokes power for the anti-Stokes field is about 0.1.

8.5 Conclusions

In conclusion, we have observed normal mode splitting of output fields due to reactive coupling between the waveguide and the cavity. Meanwhile, the separation of the peaks increases for larger pump powers. Further, the reactive coupling can also

cause four-wave mixing, which creates an anti-Stokes component generated by the optomechanical system.

The content of this chapter has been published in *Phys. Rev. A* **81**, 053810 (2010).

CHAPTER 9

CAN REACTIVE COUPLING BEAT MOTIONAL QUANTUM LIMIT OF NANO WAVEGUIDES COUPLED TO MICRODISK RESONATOR

9.1 Overview

Methods for beating the standard quantum limit of radiation fields have become fairly standard. Most methods are based on nonlinear interactions of the field in a highly nonlinear medium. The question of beating the quantum limit of the mechanical motion which could range from kHz to GHz range is attracting increasing attention [22, 26, 31, 117, 132, 215, 137, 138, 140, 182, 190, 191, 192]. Fortunately a nano mechanical mirror [NMO] placed in an optical cavity interacts with the field in the cavity in nonlinear fashion and this can be described by a nonlinear Hamiltonian. A scheme to beat the standard quantum limit for mechanical motion is to drive the system by a combination of a laser field and squeezed light such that the beat frequency matches the frequency of the NMO [32]. More recently other designs of NMO have been used [12, 67, 185, 193]. These have certain attractive features and appear quite versatile; for example, in the design of Li *et al.* [67], the nano waveguide interacts reactively with the microdisk resonator. In other words the fields leak from resonator to the waveguide. Even though the coupling is of dissipative nature such a system exhibits several novel features such as normal mode splitting which traditionally was a feature of two strongly coupled oscillators described by the Hamiltonian framework [47, 48, 50, 194].

In this chapter, we go one step further. We give first example of dissipative nonlinear coupling produced quantum fluctuations of the mechanical motion of the

waveguide which are below the standard quantum limit. This is rather counterintuitive, as dissipation is always thought to produce negative effects, i.e., is generally thought to suppress the quantum nature of the system.

The chapter is organized as follows. In Sec. II, we introduce the model, present the equation of motion for the system, and give the mean values of the system operators in steady state. In Sec. III, we calculate the quantum fluctuations in the mechanical motion of the waveguide and obtain the variance of momentum of the waveguide. In Sec. IV, we present the numerical result and show that the reactive coupling can reduce the momentum fluctuations of the waveguide below the standard quantum limit. The numbers are rather attractive; for example, at a temperature of 20 mK, achievable by a dilution refrigerator, the maximum momentum squeezing of the waveguide is about 60%.

9.2 Model

Let us consider a free-standing waveguide with length L interacting with a microdisk resonator [67]. Suppose a laser with amplitude ε_l at frequency ω_l drives the resonator mode c, and a quantum field c_{in} at frequency ω_s is sent into the resonator through the waveguide with mass m and frequency ω_m. For convenience, we adopt the notation $Q = \sqrt{\frac{2m\omega_m}{\hbar}}q$ and $P = \sqrt{\frac{2}{m\hbar\omega_m}}p$ for the dimensionless position and momentum quadratures of the waveguide with $[Q, P] = 2i$. The waveguide vibrates along the y direction due to the dispersive and reactive couplings with the resonator, which are characterized by the position dependence of the resonator resonance frequency $\omega_c(Q)$ and the photon decay rate $\kappa_e(Q)$, respectively. Moreover, the waveguide is damped at a rate of γ_m due to its interaction with its environment at a low temperature T.

In a frame rotating at the laser frequency ω_l, the Hamiltonian describing the whole

system takes the form [67]

$$H = \hbar[\omega_c(Q) - \omega_l]c^\dagger c + \frac{\hbar\omega_m}{4}(Q^2 + P^2) + \hbar\frac{L}{c}\tilde{n}_g\omega_l\varepsilon_l^2 \\ +i\hbar\sqrt{2\kappa_e(Q)}[\varepsilon_l(c^\dagger - c) + c^\dagger c_{in} - c_{in}^\dagger c]. \tag{9.1}$$

where the first two terms describe the free energies of the resonator and the waveguide, respectively. The third term is the interaction between the waveguide and the laser, c is the speed of light in vacuum, $\tilde{n}_g$ is the group index of the waveguide optical mode [188], and ε_l is related to the input power $\wp_l$ by $\varepsilon_l = \sqrt{\frac{\wp_l}{\hbar\omega_l}}$. The last term gives the interactions of the resonator with the laser and the quantum field. The characteristics of the quantum field would be specified later.

For a small displacement Q, we can assume that both $\omega_c(Q)$ and $\kappa_e(Q)$ are coupled linearly to the displacement Q,

$$\omega_c(Q) \approx \omega_c + gQ, \\ \kappa_e(Q) \approx \kappa_e + \kappa_{om}Q = \kappa_e(1 + \eta Q), \tag{9.2}$$

where ω_c is the resonator resonance frequency for $Q = 0$, κ_e is the photon decay rate for $Q = 0$, and g and κ_{om} are the dispersive and reactive coupling constants between the waveguide and the resonator, respectively. We set $\eta = \frac{\kappa_{om}}{\kappa_e}$. Since in the scheme of Li *et al.* [67] the effects of reactive coupling are dominant, we will take $g \sim 0$.

For simplicity, we assume that there is no intrinsic photon losses. Employing the Heisenberg equation of motion and adding the damping and noise terms, the equations of motion for Q, P, and c can be expressed as

$$\begin{aligned} \dot{Q} &= \omega_m P, \\ \dot{P} &= -i\eta[\tilde{\varepsilon}_l(c^\dagger - c) + \sqrt{2\kappa_e}(c^\dagger c_{in} - c_{in}^\dagger c)] - \omega_m Q - \gamma_m P + \xi, \\ \dot{c} &= -[\kappa_e + \kappa_{om}Q + i(\omega_c - \omega_l)]c + (1 + \frac{\eta}{2}Q)(\tilde{\varepsilon}_l + \sqrt{2\kappa_e}c_{in}), \end{aligned} \tag{9.3}$$

where $\tilde{\varepsilon}_l = \sqrt{2\kappa_e}\varepsilon_l$, and we have introduced ξ as the thermal noise force acting on the waveguide with standard correlation [108]. We first examine the mean values of the

physical variables in steady state. These can be obtained by using the factorization ansatz i.e. mean value of the product of two operators is the same as the product of the mean values. We find that these are given by

$$\begin{aligned} P_s &= 0, \\ Q_s &= -\frac{2\eta}{\omega_m}\tilde{\varepsilon}_l \mathrm{Im}[c_s], \\ c_s &= \frac{(1+\frac{\eta}{2}Q_s)\tilde{\varepsilon}_l}{\kappa_e + \kappa_{om}Q_s + i\Delta}, \end{aligned} \tag{9.4}$$

where the resonator detuning Δ is defined by

$$\Delta = \omega_c - \omega_l. \tag{9.5}$$

Note that the steady-state position Q_s of the waveguide and the steady-state complex amplitude c_s of the resonator depend on η. In obtaining results (9.4) we assumed that the quantum field c_{in} had zero mean value. This would be the case generally unless the quantum field is a coherent field. We already examined the case of a coherent field in a previous publication [166].

9.3 Beating the Motional Quantum Limit for the Waveguide

In this section, we investigate whether the motional quantum limit for the waveguide can be beaten even when the basic coupling is reactive. This would be quite counterintuitive as the dissipation generally leads to the loss of decoherence and fluctuations above the quantum limit. The fluctuations in q and p are subject to the Heisenberg uncertainty relation. For the mechanical oscillator in ground state one has $\langle \delta q^2 \rangle = \frac{\hbar}{2m\omega_m}\langle \delta Q^2 \rangle$ and $\langle \delta p^2 \rangle = \frac{m\hbar\omega_m}{2}\langle \delta P^2 \rangle$, in which $\langle \delta Q^2 \rangle = \langle \delta P^2 \rangle = 1$. Thus the reduction of fluctuations below unity is an indication that the standard quantum limit is broken. The question is if the fluctuations in either Q or P can go below the value unity.

Since we are interested in the squeezing of the waveguide, it is instructive to calculate the fluctuations of the system's operators around their steady state values. Provided that the steady-state amplitude of the resonator satisfies $|c_s| \gg 1$, we linearize Eq. (9.3) around its steady-state value by substituting $Q = Q_s + \delta Q$, $P = P_s + \delta P$, and $c = c_s + \delta c$ into Eq. (9.3), where δQ, δP, and δc are the small fluctuations with zero mean value. After linearization, the quantum Langevin equations can be written in the form

$$\dot{f}(t) = Zf(t) + F(t), \tag{9.6}$$

where

$$f(t) = \begin{pmatrix} \delta Q \\ \delta P \\ \delta c \\ \delta c^\dagger \end{pmatrix}, \tag{9.7}$$

and Z is a 4×4 matrix, and the quantum noise $F(t)$ is given by

$$F(t) = \begin{pmatrix} 0 \\ \xi - i\eta\sqrt{2\kappa_e}(c_s^* c_{in} - c_{in}^\dagger c_s) \\ Jc_{in} \\ Jc_{in}^\dagger \end{pmatrix}, \tag{9.8}$$

in which $J = \sqrt{2\kappa_e}(1 + \frac{\eta}{2}Q_s)$.

With the aid of the Fourier transform i.e., $f(t) = \frac{1}{2\pi}\int_{-\infty}^{+\infty} f(\omega)e^{-i\omega t}d\omega$ and $f^\dagger(t) = \frac{1}{2\pi}\int_{-\infty}^{+\infty} f^\dagger(-\omega)e^{-i\omega t}d\omega$, where $f^\dagger(-\omega) = [f(-\omega)]^\dagger$, we solve Eq. (9.6) in the frequency domain, and obtain the solution of Eq. (9.6)

$$f(\omega) = VF(\omega), \tag{9.9}$$

where $V = (-i\omega - Z)^{-1}$. From Eq. (9.9), we can obtain the fluctuations in the momentum variable

$$\delta P(\omega) \;=\; P_T(\omega)\xi(\omega) + P_S(\omega)c_{in}(\omega) + P_S^*(-\omega)c_{in}^\dagger(-\omega), \tag{9.10}$$

in which

$$\begin{aligned} P_T(\omega) &= \frac{-i\omega}{d(\omega)} A(\omega)A^*(-\omega), \\ P_S(\omega) &= \eta[\frac{\omega\tilde{\varepsilon}_l}{d(\omega)} A(\omega)J - i\sqrt{2\kappa_e}c_s^* P_T(\omega)], \end{aligned} \tag{9.11}$$

where

$$d(\omega) = A(\omega)A^*(-\omega)R - i\eta\tilde{\varepsilon}_l\omega_m[A(\omega)U - A^*(-\omega)U^*], \tag{9.12}$$

and

$$\begin{aligned} A(\omega) &= \kappa_e + \kappa_{om}Q_s - i(\Delta + \omega), \\ R &= \omega_m^2 - \omega^2 - i\gamma_m\omega, \\ U &= -\kappa_{om}c_s + \frac{\eta}{2}\tilde{\varepsilon}_l. \end{aligned} \tag{9.13}$$

In Eq. (9.10), the first term results from the thermal environment of the waveguide, the last two terms arise from the input quantum field. Thus the fluctuations in the momentum variable in the time domain would be $\delta P(t) = \frac{1}{2\pi}\int_{-\infty}^{+\infty}\delta P(\omega)e^{-i\omega t}d\omega$. Further the variance of momentum $\langle\delta\tilde{P}^2\rangle$ can be expressed as

$$\langle\delta P(t)^2\rangle = \frac{1}{4\pi^2}\int\int_{-\infty}^{+\infty} d\omega d\Omega e^{-i(\omega+\Omega)t}\langle\delta P(\omega)\delta P(\Omega)\rangle. \tag{9.14}$$

Inserting Eq. (9.10) into Eq. (9.14), $\langle\delta P(t)^2\rangle$ can be written as

$$\begin{aligned} \langle\delta P(t)^2\rangle &= \frac{1}{4\pi^2}\int\int_{-\infty}^{+\infty} d\omega\, d\Omega\, e^{-i(\omega+\Omega)t} \\ &\{P_T(\omega)P_T(\Omega)\langle\xi(\omega)\xi(\Omega)\rangle + 2\mathrm{Re}[P_S(\omega)P_S(\Omega)\langle c_{in}(\omega)c_{in}(\Omega)\rangle] \\ &+P_S(\omega)P_S^*(-\Omega)\langle c_{in}(\omega)c_{in}^\dagger(-\Omega)\rangle + P_S^*(-\omega)P_S(\Omega)\langle c_{in}^\dagger(-\omega)c_{in}(\Omega)\rangle\}. \end{aligned} \tag{9.15}$$

We assume that the quantum field is a squeezed field centered around the frequency ω_s with a finite width,

$$\begin{aligned} \langle c_{in}(\omega)c_{in}(\Omega)\rangle &= 2\pi\frac{M\Gamma^2}{\Gamma^2 + (\omega-\omega_m)^2}\delta(\omega+\Omega-2\omega_m), \\ \langle c_{in}(\omega)c_{in}^\dagger(-\Omega)\rangle &= 2\pi\left[\frac{N\Gamma^2}{\Gamma^2+(\omega-\omega_m)^2}+1\right]\delta(\omega+\Omega), \end{aligned} \tag{9.16}$$

where $N = \sinh^2(r)$ and $M = \sinh(r)\cosh(r)e^{i\varphi}$ characterize the squeezed vacuum, r is the squeezing parameter of the squeezed vacuum, φ is the phase of the squeezed vacuum, and we set $\varphi = 0$. We work in the sideband resolved limit i.e. we assume that $\omega_s - \omega_l = \omega_m$. The squeezed vacuum has a finite bandwidth Γ around ω_m, which is smaller than ω_m but larger than the resonator width. The antinormally ordered term has a broad band contribution coming from vacuum noise. Moreover, the thermal noise ξ owns the correlation function [108]:

$$\langle \xi(\omega)\xi(\Omega)\rangle = 4\pi\gamma_m \frac{\omega}{\omega_m}\left[1 + \coth\left(\frac{\hbar\omega}{2K_BT}\right)\right]\delta(\omega+\Omega), \tag{9.17}$$

where K_B is the Boltzmann constant.

Substituting Eqs. (9.16) and (9.17) into Eq. (9.15), the time independent variance $\langle \delta P^2\rangle$ will be

$$\begin{aligned}\langle \delta P^2\rangle &= \frac{1}{2\pi}\int_{-\infty}^{+\infty} d\omega P_T(\omega)P_T(-\omega)2\gamma_m\frac{\omega}{\omega_m}\left[1+\coth\left(\frac{\hbar\omega}{2K_BT}\right)\right] \\ &\quad +2\mathrm{Re}\left[\frac{1}{2\pi}\int_{-\infty}^{+\infty} d\nu P_S(\omega_m+\nu)P_S(\omega_m-\nu)\frac{M\Gamma^2}{\Gamma^2+\nu^2}\right] \\ &\quad +2\left[\frac{1}{2\pi}\int_{-\infty}^{+\infty} d\nu |P_S(\omega_m+\nu)|^2\frac{N\Gamma^2}{\Gamma^2+\nu^2}\right] + \frac{1}{2\pi}\int_{-\infty}^{+\infty} d\omega |P_S(\omega)|^2.\end{aligned} \tag{9.18}$$

The details of the calculations are given in Appendix A.

9.4 Numerical Results for Nano Waveguide Fluctuations below Standard Quantum Limit

We use available experimental parameters [67]: the wavelength of the laser $\lambda = 2\pi c/\omega_l = 1564.25$ nm, the mass of the waveguide $m = 2$ pg (the density of the silicon waveguide 2.33 g/cm^3, length 10 μm, width 300 nm, height 300 nm), the frequency of the waveguide $\omega_m = 2\pi \times 25.45$ MHz, the extrinsic photon decay rate $\kappa_e = 0.05\omega_m$, the reactive coupling constant $\kappa_{om} = -2\pi \times 26.6$ MHz/nm $\times\sqrt{\frac{\hbar}{2m\omega_m}}$, the mechanical

quality factor $Q = \omega_m/\gamma_m = 5000$, and the bandwidth of the squeezed vacuum $\Gamma = 5\kappa_e$.

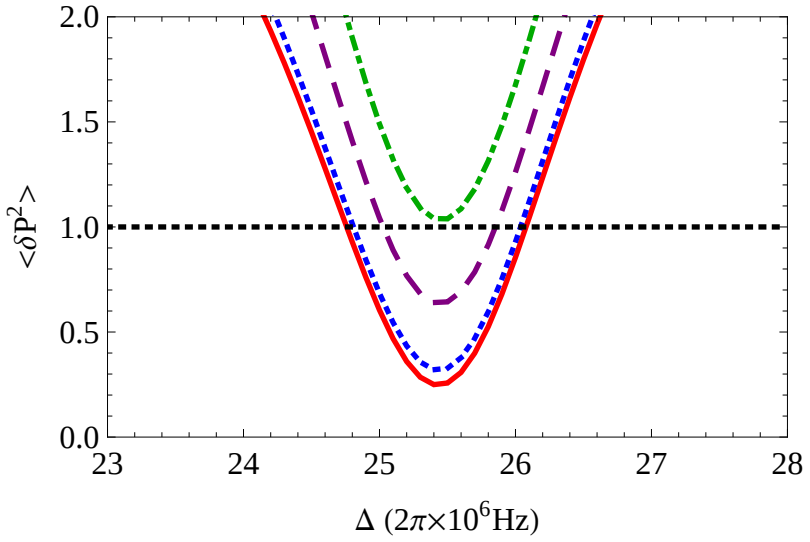

Figure 9.1: The variance of momentum $\langle \delta P^2 \rangle$ as a function of the detuning Δ ($2\pi \times 10^6$Hz) for different temperatures of the environment: $T = 1$ mK (red solid), $T = 10$ mK (blue dotted), $T = 50$ mK (purple dashed), and $T = 100$ mK (green dotdashed). The horizontal dotted line represents the standard quantum limit ($\langle \delta P^2 \rangle$=1). The parameters: the pump power $\wp_l = 20$ μW, $r = 1$.

We start the investigation with the influence of the reactive coupling on the squeezing of the waveguide. If the quantum field is the ordinary vacuum ($r = 0$), we calculate the variances of position and momentum, and find that $\langle \delta Q^2 \rangle$ and $\langle \delta P^2 \rangle$ are always larger than unity, there is no squeezing appearance. If the quantum field is the squeezed vacuum, and $r = 1$, it has been found that there is no squeezing in the variance of position $\langle \delta Q^2 \rangle$, but the variance of momentum $\langle \delta P^2 \rangle$ may be squeezed. For pump power $\wp_l = 20$ μW, the variances of momentum $\langle \delta P^2 \rangle$ versus the detuning Δ ($2\pi \times 10^6$ Hz) for different temperatures of the environment are shown in Fig. 9.1. For $T = 1$, 10, or 50 mK, we can see the variance of momentum $\langle \delta P^2 \rangle$ falls below the standard quantum limit, so the momentum squeezing takes place. The minimum

value of $\langle \delta P^2 \rangle$ is about 0.250 at $T = 1$ mK, this shows the maximum momentum squeezing of the waveguide is about 75 %. Note that the maximum momentum squeezing of the waveguide decreases with increasing the temperature due to large thermal noise. Even at $T = 50$ mK, the momentum squeezing is about 40%.

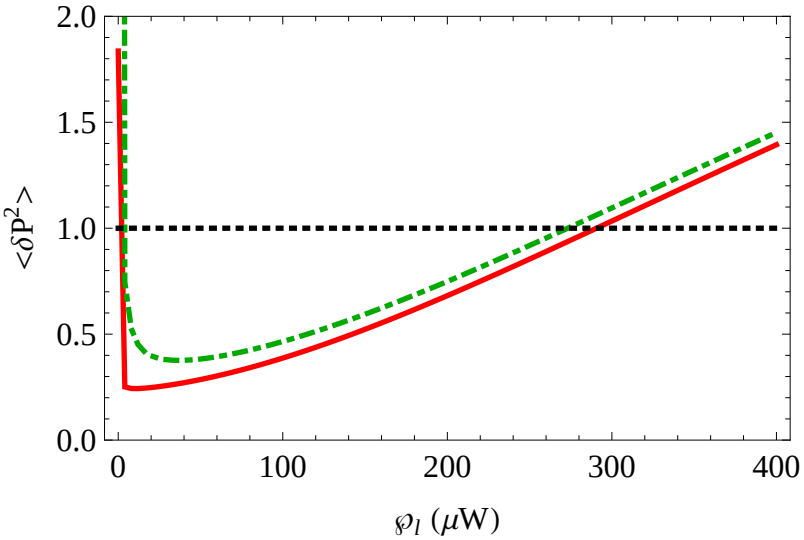

Figure 9.2: The variance of momentum $\langle \delta P^2 \rangle$ as a function of the pump power (μW) for different temperatures of the environment: $T = 1$ mK (red solid) and $T = 20$ mK (green dotdashed). The horizontal dotted line represents the standard quantum limit ($\langle \delta P^2 \rangle$=1). The parameters: $\Delta = \omega_m$, $r = 1$.

Next we consider the resonance case $\Delta = \omega_m$ in the presence of the reactive coupling, and fix $r = 1$, the dependence of the variance of momentum $\langle \delta P^2 \rangle$ on the pump power $\wp_l$ (μW) for $T = 1$ and 20 mK is shown in Fig. 9.2. It is seen that the variance of momentum $\langle \delta P^2 \rangle$ clearly exhibits the squeezing effect over a large range of pump power ($\wp_l = 0 \sim 290$ μW). The minimum value of $\langle \delta P^2 \rangle$ is 0.243 at a very low pump power ($\wp_l = 12$ μW) for $T = 1$ mK, so the maximum momentum squeezing of the waveguide is about 75 %. For $T = 20$ mK, the maximum momentum squeezing is about 60%. Note that temperatures like 20 mK are realizable by standard dilution refrigerators [195].

9.5 Conclusions

We have shown that quantum squeezing effects in the motion of the waveguide can be generated solely due to the reactive coupling between the waveguide and the resonator by use of a squeezed vacuum. The maximum momentum squeezing is about 75%, which can be achieved at a very low pump power ($\wp_l = 12\mu$W). We show in the Appendix B the relation between the quantum fluctuations of the waveguide and the output field. Thus the squeezing of nano waveguide can be studied by examining the fluctuations of the output field of the waveguide.

The content of this chapter has been published in *Phys. Rev. A* **82**, 033811 (2010).

CHAPTER 10

ELECTROMAGNETICALLY INDUCED TRANSPARENCY FROM TWO PHOTON PROCESSES IN QUADRATICALLY COUPLED MEMBRANES

10.1 Overview

The radiation pressure coupling between the nano-mirror and the radiation field is known to depend on the displacement of the mirror via the cavity frequency [196]. This coupling can depend linearly or quadratically on the displacement depending on the location of the mirror with respect to nodes and antinodes of the cavity modes. The case most extensively discussed in the literature corresponds to placing the mirror at a node so that the coupling is linear in displacement [35, 38, 47, 50, 59, 193, 197, 198, 199]. Nanomechanical systems with linear reactive coupling have also been studied [67, 185, 194]. The case of quadratic coupling has not been studied that extensively as the coupling is generally small. However, recent works [10, 11, 12] have shown a way to get much larger quadratic couplings, and therefore, one should study the unique consequences of quadratic coupling in detail. The quadratic coupling in a phonon picture implies two-phonon processes, as explained in detail in Sec. II, and such couplings in analogy to well-known quantum optical Hamiltonians [110] naturally lead to the possibility of squeezing the mechanical oscillator [66, 191, 200]. The question that we examine in this chapter is how to probe the effects of such two-phonon processes by using pump and probe fields of respective frequencies ω_c and ω_p. We expect that the two-phonon processes should show up when the frequency difference $\omega_p - \omega_c$ is about $2\omega_m$, where ω_m is the frequency of the mechanical oscillator

and when ω_p is close to the cavity frequency. At the outset, we want to mention the following: in case of single-phonon processes (linear coupling), the mean displacement of the oscillator is nonzero, and it leads to the modulation of the output fields, whereas for two-phonon processes the mean response of the oscillator is zero [41], and thus, any modulation of the output fields has to come from mean values of the square of the displacement, which is a temperature-dependent quantity. We further reveal the possibility of an analog of electromagnetically induced transparency (EIT) arising from a temperature-dependent oscillator's mean potential energy. This is different from the linear coupling case where the mean displacement of the oscillator determines the EIT behavior [51, 53, 54]. For our case of two-phonon processes the role of atomic coherence in traditional EIT is played by the mean of the square of the displacement, which, in addition to temperature, also depends on the strength of the coupling field.

The chapter is organized as follows. In Sec. II, we describe the model under study. We explain some key differences from the case of linearly coupled nanomechanical mirrors, and we give the equation of motion for the system operators and obtain the output field at the probe frequency. In Sec. III, we discuss the effect of the quadratic optomechanical coupling on the output field at the probe frequency. We find that the EIT-like dip appears in the output field at the probe frequency.

10.2 Model

Let us start with a sketch of the system as shown in Fig. 10.1 [10, 11]. A membrane with finite reflectivity R is placed inside the cavity formed by two fixed mirrors separated from each other by a distance L. A strong coupling field of amplitude ε_c and a weak probe field of amplitude ε_p are sent into the cavity through the partially transmitting left mirror, the right mirror is perfectly reflecting. To ensure that the membrane locates at an antinode of the cavity modes, the cavity frequency must be $\omega(q) = \omega_n + \frac{\pi}{\tau} - \frac{1}{\tau}[\sin^{-1}(\sqrt{R}\cos 2k_n q) + \sin^{-1}(\sqrt{R})]$ so that there is an odd number of

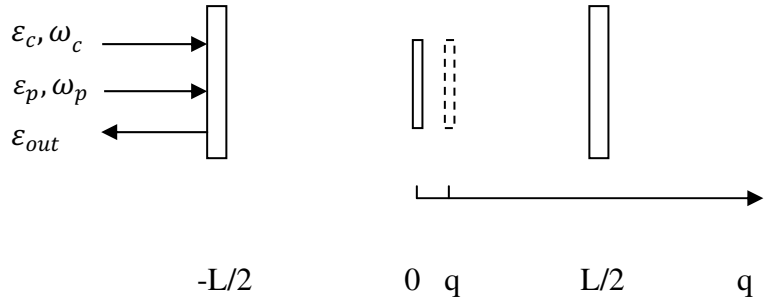

Figure 10.1: Sketch of the studied system. A strong coupling field at frequency ω_c and a weak probe field at frequency ω_p are injected into the cavity through the left mirror. A membrane with finite reflectivity is located at the middle position of the cavity. After the interaction between the cavity field and the membrane, the output field will contain three frequencies (ω_c, ω_p, and $2\omega_c - \omega_p$).

half wavelengths in the whole cavity, where $\omega_n = \frac{2n\pi c}{L}$ is the resonant frequencies of the two subcavities as $R = 1$, $q = 0$, and $k_n = \omega_n/c$, $\tau = L/c$ [41]. If the membrane with mass m is located at an antinode of the frequency $\omega(q)$ of the cavity field, the cavity frequency can be approximated to the second order of q, $\omega(q) = \omega_0 + \frac{1}{2}\frac{d^2\omega}{dq^2}|_{q=0}q^2$. Thus the cavity is quadratically coupled to the displacement of the membrane. We denote the quadratic coupling constant by g, and $g = \frac{1}{2}\frac{d^2\omega}{dq^2}|_{q=0} = \frac{8\pi^2 c}{\lambda^2 L}\sqrt{\frac{R}{1-R}}$ [201], where c is the speed of light in a vacuum and λ is the wavelength of the coupling field. Moreover, the membrane is in contact with the environment in thermal equilibrium at temperature T. Hence the system's Hamiltonian takes the form

$$\begin{aligned} H &= \hbar\omega_0 c^\dagger c + \hbar g c^\dagger c q^2 + \frac{p^2}{2m} + \frac{1}{2}m\omega_m^2 q^2 \\ &\quad + i\hbar\varepsilon_c(c^\dagger e^{-i\omega_c t} - c e^{i\omega_c t}) + i\hbar(\varepsilon_p c^\dagger e^{-i\omega_p t} - \varepsilon_p^* c e^{i\omega_p t}), \end{aligned} \tag{10.1}$$

in which c and $c^\dagger$ denote the annihilation and creation operators of the cavity, while q and p are the position and momentum operators of the membrane. ε_c and ε_p are

defined by $\varepsilon_c = \sqrt{2\kappa\wp_c/(\hbar\omega_c)}$ and $\varepsilon_p = \sqrt{2\kappa\wp_p/(\hbar\omega_p)}$, where $\wp_c$ is the power of the coupling field, $\wp_p$ is the power of the probe field, and κ is the cavity decay rate.

Before proceeding further we examine the interaction term in Eq. (10.1). The cavity field c is expected to have the form

$$c \to c_p e^{-i\omega_p t} + c_c e^{-i\omega_c t} + \cdots, \tag{10.2}$$

and the displacement of the membrane would have the form

$$q \to q_+ e^{-i\omega_m t} + q_- e^{i\omega_m t} + \cdots. \tag{10.3}$$

Here $\cdots$ denotes terms generated at other frequencies due to the nonlinear interaction term in Eq. (10.1). Clearly, $c^\dagger c q^2$ would give rise to a contribution of the form

$$q_+^2 e^{-2i\omega_m t + i\omega_p t - i\omega_c t} c_p^\dagger c_c, \tag{10.4}$$

which physically corresponds to the conversion of the ω_c field into the ω_p field via absorption of two phonons, as shown in Fig. 10.2. The conversion process would be

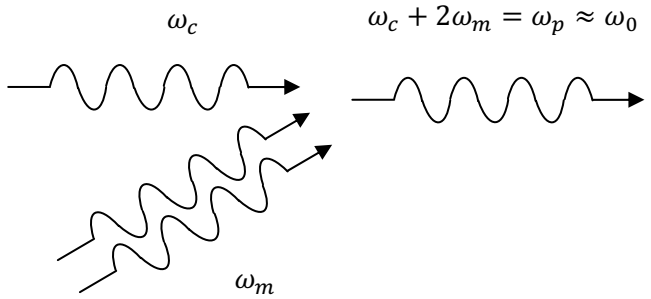

Figure 10.2: Sketch of two-phonon process. For a one-phonon case the corresponding condition on frequencies will be $\omega_c + \omega_m = \omega_p \approx \omega_0$.

quite efficient if ω_p is near the cavity resonance frequency. This is to be contrasted to

the linear coupling case $c^\dagger cq$, where a single phonon is involved in the up-conversion process.

In the rotating frame at the frequency ω_c of the coupling field, $c(t) = \tilde{c}(t)e^{-i\omega_c t}$; using the Heisenberg equation of motion and adding the corresponding noise and damping terms, we can obtain the equation of motion for the mirror and the cavity variables.

$$\begin{aligned}
\frac{dq}{dt} &= \frac{p}{m}, \\
\frac{dp}{dt} &= -m\omega_m^2 q - 2\hbar g\tilde{c}^\dagger\tilde{c}q - \gamma_m p + \xi, \\
\frac{d\tilde{c}}{dt} &= -[\kappa + i(\omega_0 - \omega_c + gq^2)]\tilde{c} + \varepsilon_c + \varepsilon_p e^{-i(\omega_p-\omega_c)t} + \sqrt{2\kappa}\tilde{c}_{in}, \\
\frac{d\tilde{c}^\dagger}{dt} &= -[\kappa - i(\omega_0 - \omega_c + gq^2)]\tilde{c}^\dagger + \varepsilon_c + \varepsilon_p^* e^{i(\omega_p-\omega_c)t} + \sqrt{2\kappa}\tilde{c}_{in}^\dagger,
\end{aligned} \tag{10.5}$$

in which γ_m is the damping rate of the membrane, ξ is the Langevin force arising from the interaction with environment, and $\tilde{c}_{in}$ is the input vacuum noise with zero mean value.

We next examine if we can get an analog of EIT for the case of a quadratically coupled membrane. We sketch the relation between the EIT in atomic systems and the analog of the EIT in mechanical effects of light in Fig. 10.3. The EIT occurs in atomic systems when (i) decay of the optical coherence described by the density matrix element ρ_{13} is much faster than the decay of atomic coherence ρ_{23}, (ii) $\omega_p = \omega_c + \omega_m$, (iii) atomic coherence $\rho_{13} \neq 0$. In mechanical effects of light, (a) $(\gamma_m)^{-1}$ is like the life-time of atomic coherence, (b) κ^{-1} is like the life time of optical coherence, (c) the condition that atomic coherence decays much slower compared to optical coherence is then $\gamma_m \ll \kappa$, (d) generally, ω_p and ω_c are well separated, and thus, we need $\omega_m \gg \kappa$, which corresponds to the side-band-resolved limit, and (e) the nonvanishing of atomic coherence would correspond to the nonvanishing of the displacement $\langle q \rangle$ of the oscillator. All these conditions are well met, which leads us to predict EIT [51] in mechanical effects of light, which has been clearly seen in a recent experiment

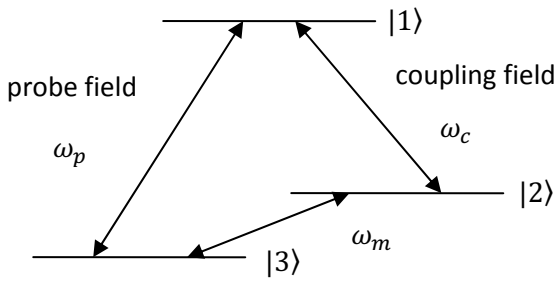

Figure 10.3: Level diagram for the atomic EIT. For optocavity mechanics, $|1\rangle \leftrightarrow |3\rangle$ would be the excitation at cavity frequency; $|2\rangle \leftrightarrow |3\rangle$ would be the excitation of the mechanical oscillator. For the quadratically coupled membrane, $|2\rangle \rightarrow |3\rangle$ would be the two-phonon excitation which makes $\langle q\rangle = 0$.

[53]. All the conditions listed above except one are met for quadratically coupled membranes. Here $\langle q\rangle$, i.e., the coherence term, is zero, as seen from Eq. (10.5). We can find the expectation values of the system operators at the steady state. These are

$$q_0 = 0, p_0 = 0, c_0 = \frac{\varepsilon_c}{\kappa + i(\omega_0 - \omega_c)}, \tag{10.6}$$

where from here on we drop the tilde from $\tilde{c}_0$. It is seen that at steady state, the membrane's displacement is zero, and the amplitude c_0 of the cavity field is unrelated to the position of the membrane so that the output field is not modified by the mean displacement of the membrane, which is different from that in the linear coupling case. A further analysis shows that the value of $\langle q\rangle$ to first order in the field ε_p is also zero. This is because the nonlinear term $\tilde{c}^\dagger \tilde{c} q$ in the equation for the momentum leads to no driving term in first order in the probe field. This situation is different from the case of one-phonon EIT, where $\langle q\rangle$ to first order in the field ε_p is nonzero. Hence, a key element for the occurrence of EIT for a quadratically coupled membrane is zero. We propose here a way out of this difficulty. Since the mean value of q is zero,

its variance, which is proportional to potential energy $\frac{1}{2}m\omega_m^2\langle q^2\rangle$ of the membrane, is expected to be nonzero. This is so even if the membrane is not interacting with any fields. The thermal and zero-point fluctuations make $\langle q^2\rangle \neq 0$. Thus, in our proposal for EIT with quadratically coupled optomechanical systems the quantity $\langle q^2\rangle$ will be central. This peculiarity is related to the fact that the underlying physical process is a two-phonon process. Thus, in the following, we turn to calculate the evolutions of the expectation values of q^2, p^2, and $qp+pq$, which can be obtained with the help of Eq. (10.5) and the factorization assumption $\langle abc\rangle = \langle a\rangle\langle b\rangle\langle c\rangle$. Using the same method, we also can obtain the evolution of the expectation values of c and $c^\dagger$. Hence, the complete set of underlying equations for our system would be

$$\begin{aligned}
\frac{d}{dt}\langle c\rangle &= -[\kappa + i(\omega_0 - \omega_c + g\langle q^2\rangle)]\langle c\rangle + \varepsilon_c \\
&\quad +\varepsilon_p e^{-i(\omega_p-\omega_c)t}, \\
\frac{d}{dt}\langle c^\dagger\rangle &= -[\kappa - i(\omega_0 - \omega_c + g\langle q^2\rangle)]\langle c^\dagger\rangle + \varepsilon_c + \varepsilon_p^* e^{i(\omega_p-\omega_c)t}, \\
\frac{d}{dt}\langle q^2\rangle &= \frac{1}{m}\langle pq+qp\rangle, \\
\frac{d}{dt}\langle p^2\rangle &= -(m\omega_m^2 + 2\hbar g\langle c^\dagger\rangle\langle c\rangle)\langle qp+pq\rangle - 2\gamma_m\langle p^2\rangle + 2\gamma_m(1+2n)\frac{m\hbar\omega_m}{2}, \\
\frac{d}{dt}\langle qp+pq\rangle &= \frac{2}{m}\langle p^2\rangle - 2(m\omega_m^2 + 2\hbar g\langle c^\dagger\rangle\langle c\rangle)\langle q^2\rangle - \gamma_m\langle qp+pq\rangle,
\end{aligned} \tag{10.7}$$

in which the constant $2\gamma_m(1+2n)\frac{m\hbar\omega_m}{2}$ is due to the coupling of the membrane to the thermal environment and $n = [e^{\frac{\hbar\omega_m}{k_BT}} - 1]^{-1}$ is the mean phonon occupation number of energy $\hbar\omega_m$ at temperature T, where k_B is Boltzmann's constant. Note that the constant $(1+2n)\frac{m\hbar\omega_m}{2}$ is the mean value of the square of the momentum of the membrane.

We would solve Eq. (10.7) under the assumption that the coupling field is much stronger than the probe field. The steady state solution of Eq. (10.7) then can be

written as

$$\begin{pmatrix} \langle c \rangle \\ \langle c^\dagger \rangle \\ \langle q^2 \rangle \\ \langle p^2 \rangle \\ \langle qp + pq \rangle \end{pmatrix} = \begin{pmatrix} c_0 \\ c_0^* \\ X_0 \\ Y_0 \\ Z_0 \end{pmatrix} + \varepsilon_p e^{-i(\omega_p - \omega_c)t} \begin{pmatrix} c_+ \\ c_-^* \\ X_+ \\ Y_+ \\ Z_+ \end{pmatrix} + \varepsilon_p^* e^{i(\omega_p - \omega_c)t} \begin{pmatrix} c_- \\ c_+^* \\ X_- \\ Y_- \\ Z_- \end{pmatrix}. \quad (10.8)$$

The solution contains three components, which in the original frame oscillate at ω_c, ω_p, and $2\omega_c - \omega_p$, respectively. Substituting Eq. (10.8) into Eq. (10.7), dropping those terms that contain the product of more than one small quantity, and then equating coefficients of terms with the same frequency, we obtain

$$\begin{aligned} X_0 &= \frac{Y_0}{m^2\omega_m^2(1+2\alpha)}, \\ Y_0 &= (1+2n)\frac{m\hbar\omega_m}{2}, \\ c_0 &= \frac{\varepsilon_c}{\kappa + i\Delta}, \\ c_+ &= \frac{1}{d(\delta)}\{[\kappa - i(\Delta+\delta)](\gamma_m - i\delta)(\delta^2 - 4\omega_m^2 + 2i\gamma_m\delta \\ &\quad -8\alpha\omega_m^2) - 4i\alpha\beta\omega_m^3(2\gamma_m - i\delta)\}, \\ c_- &= \frac{1}{d^*(\delta)}[-4i\alpha\beta\omega_m^3\frac{c_0^2}{|c_0|^2}(2\gamma_m + i\delta)], \end{aligned} \quad (10.9)$$

where

$$\begin{aligned} \alpha &= \hbar g|c_0|^2/(m\omega_m^2), \\ \beta &= gX_0/\omega_m, \\ \Delta &= \omega_0 - \omega_c + \beta\omega_m, \\ \delta &= \omega_p - \omega_c, \\ d(\delta) &= [\kappa + i(\Delta - \delta)][\kappa - i(\Delta + \delta)](\gamma_m - i\delta) \\ &\quad \times(\delta^2 - 4\omega_m^2 + 2i\gamma_m\delta - 8\alpha\omega_m^2) + 8\Delta\alpha\beta\omega_m^3(2\gamma_m - i\delta). \end{aligned} \quad (10.10)$$

From Eqs. (10.9) and (10.10), we find that the cavity field at the probe frequency ω_p is related to the component X_0 of the mean-square displacement of the membrane,

which depends on the pump power and the temperature of the environment. Also, the coupling strength between the cavity field at the frequency ω_p and the membrane is affected by the quadratic coupling constant g and the photon number $|c_0|^2$ in the cavity. Note that the parameter β is a measure of the frequency shift of the cavity due to quadratic coupling. The parameter α is the ratio of the radiation pressure energy to the potential energy of the membrane.

Further, the output field can be derived by using the input-output relation

$$\varepsilon_{out}(t) + \varepsilon_p e^{-i\delta t} + \varepsilon_c = 2\kappa\langle\tilde{c}\rangle. \tag{10.11}$$

If we write $\varepsilon_{out}(t)$ as

$$\varepsilon_{out}(t) = \varepsilon_{out0} + \varepsilon_{out+}\varepsilon_p e^{-i\delta t} + \varepsilon_{out-}\varepsilon_p^* e^{i\delta t}, \tag{10.12}$$

where ε_{out0} is the response at the frequency ω_c of the coupling field, ε_{out+} is the response at the frequency ω_p of the probe field, and ε_{out-} is the response at the new frequency $2\omega_c - \omega_p$. Combining Eqs. (10.11) and (10.12), we obtain

$$\begin{aligned} \varepsilon_{out0} &= 2\kappa c_0 - \varepsilon_c, \\ \varepsilon_{out+} &= 2\kappa c_+ - 1, \\ \varepsilon_{out-} &= 2\kappa c_-. \end{aligned} \tag{10.13}$$

We examine the total output field at the frequency ω_p defined as $\varepsilon_T = \varepsilon_{out+}+1 = 2\kappa c_+$, so ε_T is also affected by the pump power and the temperature of the environment. In the absence of the quadratic optomechanical coupling ($g = 0$), ε_T is given by

$$\varepsilon_T = \frac{2\kappa}{\kappa + i(\Delta - \delta)}. \tag{10.14}$$

10.3 EIT in the Output Field

In this section, we calculate numerically the output field at the frequency ω_p to bring out the EIT-like phenomenon due to the interaction between the cavity field and the

membrane, which is quadratically dependent on the position of the membrane. For convenience, we write ε_T as

$$\varepsilon_T = \upsilon_p + i\tilde{\upsilon}_p, \tag{10.15}$$

where υ_p and $\tilde{\upsilon}_p$ give the in-phase and out-of-phase quadratures of the output field. The quadratures can be measured via homodyne technique [110].

In order to explicitly demonstrate the possibility of EIT in quadratically coupled optomechanical systems we use parameters that are similar to those in Ref. [10], which discusses many different possible scenarios for quadratic couplings. A later paper [12] gives an experimental demonstration of how to achieve much larger quadratic couplings. We list the parameters used in numerical results. The wavelength of the coupling field $\lambda = \frac{2\pi c}{\omega_c} = 532$ nm, the total cavity length $L = 6.7$ cm, the frequency of the membrane $\omega_m = 2\pi \times 10^5$ Hz, the cavity decay rate $\kappa = 2\pi \times 10^4$ Hz, the decay rate of the membrane $\gamma_m = 20\ \mathrm{s}^{-1}$, the mechanical quality factor $Q = \frac{\omega_m}{\gamma_m} = 3.14 \times 10^4$, the membrane's reflectivity $R = 0.45$, the coupling constant $g = 2\pi \times 1.8 \times 10^{23}$ Hz/m^2, the pump power $\wp_c = 90\ \mu$W, and the temperature of the environment $T = 90$ K. The mass of the membrane we use is $m = 10^{-9}$g, which is less than that in Ref. [10]. In addition, we consider the two-phonon resonance case $\Delta = 2\omega_m$. It is good to compare the magnitude of the optomechanical coupling to the potential energy of the membrane. The parameter $\hbar g|c_0|^2$ at $\Delta = 2\omega_m$ is 0.002 J/m^2, whereas the parameter $m\omega_m^2$ is 0.4 J/m^2.

Figure 10.4 shows the phase quadrature υ_p as a function of the normalized frequency δ/ω_m in the absence (red dotted line) and presence (blue solid line) of the optomechanical coupling. In the absence of the optomechanical coupling, it is seen that υ_p has the standard Lorentzian absorption shape. However, in the presence of the optomechanical coupling (blue solid line in Fig. 10.4), one can clearly see an EIT-like dip in the quadrature υ_p when the two-phonon process dominates ($\delta \approx 2\omega_m$). The position of the EIT-like dip is not exactly at $\delta = 2\omega_m$ due to the term $8\alpha\omega_m^2$ in c_+

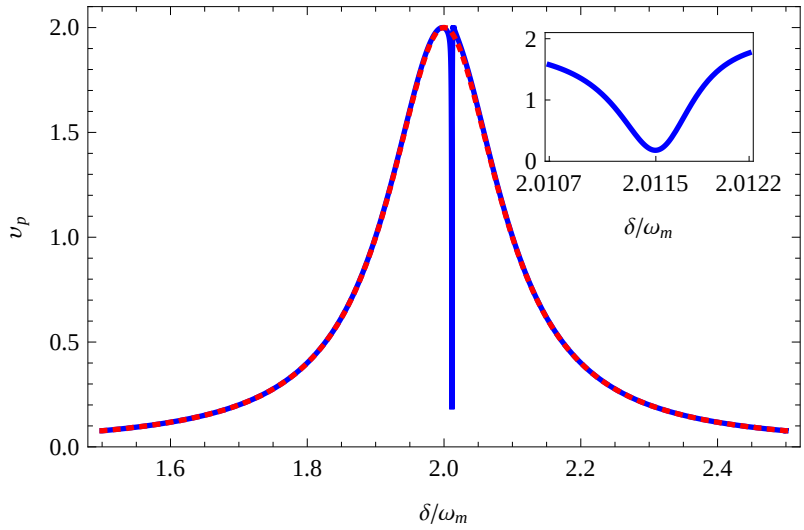

Figure 10.4: Quadrature of the output field υ_p as a function of the normalized frequency δ/ω_m in the absence (red dotted line) and presence (blue solid line) of the quadratic coupling. Parameters are as follows: $R = 0.45$, $\wp_c = 90$ μW, $T = 90$ K. The inset zooms the EIT-like dip.

and $d(\delta)$, in which $\alpha \approx 0.005$. Note that the linewidth of the dip is extremely narrow due to $\gamma_m \ll \kappa$. The linewidth is about 408 s^{-1}, which is mostly due to the power of the coupling field and the temperature.

However, for other set of parameters, the EIT window can become wider. For membrane reflectivity $R = 0.81$, coupling constant $g = 2\pi \times 4.1 \times 10^{23}$ Hz/m^2, pump power $\wp_c = 20$ μW, and temperature of the environment $T = 90$ K, the phase quadratures υ_p and $\tilde{\upsilon}_p$ as a function of the normalized frequency δ/ω_m in the absence (red dotted line) and presence (blue solid line) of the optomechanical coupling are given in Figs. 10.5 and 10.6. From the blue solid line in Fig. 10.5, we can see the linewidth of the EIT-like dip is about 471 s^{-1}. We also find the position of the EIT-like dip is at $\delta \approx 2.0058\omega_m$, close to $\delta = 2\omega_m$, which is due to the small value of the parameter $8\alpha\omega_m^2$, where $\alpha \approx 0.003$. Moreover, in the case without the optomechanical coupling, from the red dotted line in Fig. 10.6, it is seen that $\tilde{\upsilon}_p$

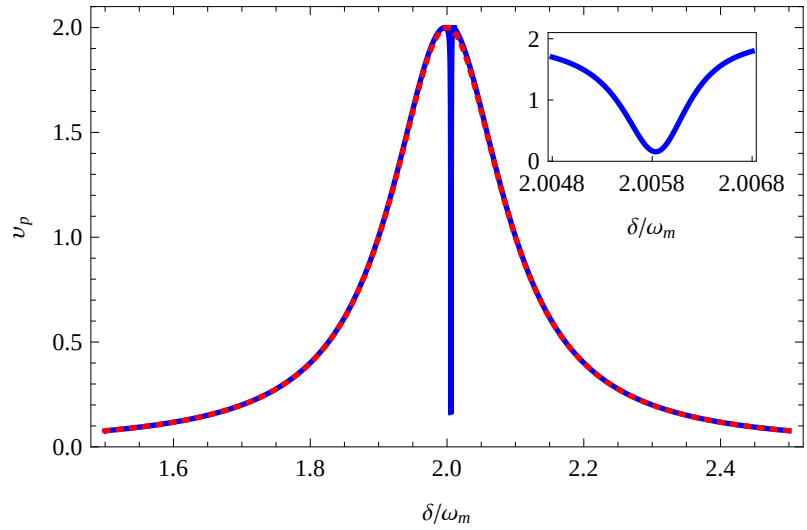

Figure 10.5: Quadrature of the output field υ_p as a function of the normalized frequency δ/ω_m in the absence (red dotted line) and presence (blue solid line) of the quadratic coupling. Parameters are as follows: $R = 0.81$, $\wp_c = 20$ μW, $T = 90$ K. The inset zooms the EIT-like dip.

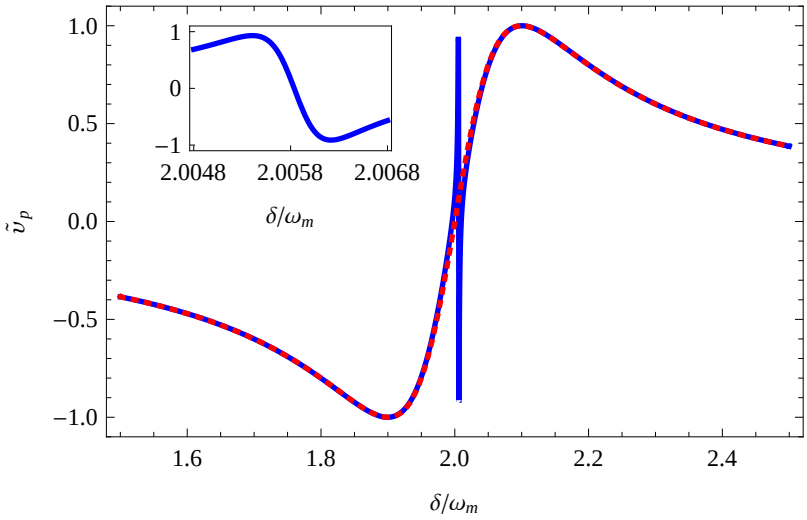

Figure 10.6: Quadrature of the output field $\tilde{\upsilon}_p$ as a function of the normalized frequency δ/ω_m in the absence (red dotted line) and presence (blue solid line) of the quadratic coupling. Parameters are as follows: $R = 0.81$, $\wp_c = 20$ μW, $T = 90$ K. The inset zooms the change in the dispersion produced by the coupling field.

has a standard dispersion shape. But in the case with the optomechanical coupling, from the blue solid line in Fig. 10.6, we can see the phase quadrature $\tilde{v}_p$ exhibits abnormal dispersion. We have further carried out a detailed numerical study of the temperature dependence of EIT. We find that, for example, for $R = 0.81$, $\wp_c = 50$ μW, the width of the EIT dip increases linearly with temperature - the values being 628, 1256, and 2513 s^{-1} for $T = 50$, 100, and 200 K, respectively [202].

10.4 Conclusions

In conclusion we have shown how EIT-like effects can arise in two-phonon processes in optomechanical systems. The EIT in quadratically coupled membranes is a different from the usual paradigm because what plays the role of atomic coherence is zero for quadratically coupled systems. The basic quantity leading to EIT in our system is the fluctuation in the displacement of the membrane. Interestingly enough the EIT-like behavior can occur at low-coupling powers, such as tens of microwatts, even though the underlying process is a two-phonon process.

The content of this chapter has been published in *Phys. Rev. A* **83**, 023823 (2011).

CHAPTER 11

ELECTROMAGNETICALLY INDUCED TRANSPARENCY WITH QUANTIZED FIELDS IN OPTOCAVITY MECHANICS

11.1 Overview

The interaction of a nano-mechanical system via radiation pressure [41, 163] is like a three-wave interaction in nonlinear optics [161]. This interaction can lead to processes like upconversion; for example, a photon of frequency ω_c can be converted into a photon of frequency $\omega_p = \omega_c + \omega_m$, where ω_m is the frequency of the mechanical oscillator. Such upconversion processes have been useful in cooling nano-mechanical systems [8, 9, 58, 120]. In a previous article [51], we showed how such upconversion processes can lead to electromagnetically induced transparency (EIT) in optomechanical systems. The EIT in such systems turned out to share many of the features of EIT in atomic vapors. The EIT in optomechanical systems has been seen experimentally [53, 54, 55]. Traditionally, almost of all the EIT experiments in atomic systems and other systems have been done with coherent pump and probe fields [172, 173, 203]. Akamatsu et al. [204] did the very first experiment on EIT using squeezed light in atomic vapors. They essentially reported that squeezing of the probe is not degraded much by the quantum noise of the medium under EIT conditions. Subsequently, a number of other experiments [205, 206] on EIT using quantized fields were reported. The EIT with quantized fields is very significant in the storage of fields at the single-photon level [86, 219, 208, 209].

In this chapter, we examine EIT in optomechanical systems using quantized fields. In optomechanical systems, noise is added by both the resonator and the mechanical

system. We find the conditions when the perfect EIT of the quantized field results. We study how the temperature of the mechanical system can degrade EIT. We present detailed results for the designs of nano-mechanical systems as used in Refs. [50, 53]. We find that certain designs of nano-mechanical systems are good even at temperatures on the order of 100 mK. Thus, such systems would be quite useful as optical memories at the single-photon level. The results that we present can be extended to the reactive case [67, 194, 210].

The organization of the chapter is as follows. In Sec. II, we describe the model, derive the equations of motion for the system, and obtain the steady-state mean values. In Sec. III, we show how to detect the EIT with quantized fields, and we present a homodyne detection and obtain the relevant spectrum. In Sec. IV, we discuss the impact of the coupling field on the homodyne spectrum of the output field and show the existence of the EIT in the homodyne spectrum of the quantized field at the output.

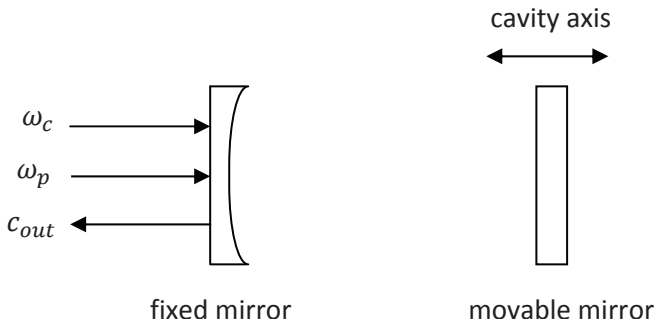

Figure 11.1: Sketch of the studied system. A coherent coupling field at frequency ω_c and a squeezed vacuum at frequency ω_p enter the cavity through the partially transmitting mirror.

11.2 Model

The model that we are going to consider has been discussed in detail previously [32, 33] and is sketched in Fig. 11.1. The cavity consists of a fixed mirror and a movable mirror separated by a distance L. The fixed mirror is partially transmitting, while the movable mirror is 100% reflecting. The cavity is driven by a strong coupling field at frequency ω_c. A quantized weak probe field in a squeezed vacuum state at frequency ω_p is injected into the cavity through the fixed mirror. The movable mirror interacts with the cavity field through radiation pressure. The movable mirror is modeled as a harmonic oscillator with mass m, frequency ω_m, and decay rate γ_m. Moreover, the movable mirror and its environment are in thermal equilibrium at a low temperature T.

In such a system, the coupling between the movable mirror and the cavity field is dispersive, so the frequency $\omega_0(q)$ of the cavity field depends on the displacement q of the movable mirror: $\omega_0(q) = n\pi c/(L+q)$, where c is the light speed in vacuum and n is the mode number in the cavity. For $q \ll L$, we can expand $\omega_0(q)$ to the first order of q; thus, we have $\omega_0(q) \approx \omega_0(0) + \frac{\partial\omega_0(q)}{\partial q}q \approx \omega_0 - \frac{\omega_0}{L}q$, where we write $\omega_0(0)$ as ω_0.

Let c ($c^\dagger$) be the annihilation (creation) operators for the cavity field and Q and P be the dimensionless operators for the position and momentum of the movable mirror with $Q = \sqrt{\frac{2m\omega_m}{\hbar}}q$ and $P = \sqrt{\frac{2}{m\hbar\omega_m}}p$. Note that the commutation relation for Q and P is $[Q, P] = 2i$. In a frame rotating at the frequency ω_c of the coupling field, the Hamiltonian for the system is

$$H = \hbar(\omega_0 - \omega_c)c^\dagger c - \hbar g c^\dagger c Q + \frac{\hbar\omega_m}{4}(Q^2 + P^2) + i\hbar\varepsilon(c^\dagger - c), \qquad (11.1)$$

In the above equation, the parameter $g = (\omega_c/L)\sqrt{\hbar/(2m\omega_m)}$ is the coupling strength between the cavity field and the movable mirror, where we assume $\omega_0 \simeq \omega_c$. The parameter ε is the real amplitude of the coupling field, depending on its power $\wp$ by

$\varepsilon = \sqrt{\frac{2\kappa\wp}{\hbar\omega_c}}$, where κ is the photon loss rate due to the transmission of the fixed mirror.

The time evolution of the total system is obtained from the Hamiltonian Eq. (11.1) by deriving the Heisenberg equations of motion and adding the damping and noise terms. The basic equations are given by

$$\begin{aligned}
\dot{Q} &= \omega_m P, \\
\dot{P} &= 2gn_c - \omega_m Q - \gamma_m P + \xi, \\
\dot{c} &= i(\omega_c - \omega_0 + gQ)c + \varepsilon - \kappa c + \sqrt{2\kappa}c_{in}, \\
\dot{c}^\dagger &= -i(\omega_c - \omega_0 + gQ)c^\dagger + \varepsilon - \kappa c^\dagger + \sqrt{2\kappa}c_{in}^\dagger.
\end{aligned} \tag{11.2}$$

Here, we have introduced the thermal Langevin force ξ with a vanishing mean value, resulting from the coupling of the movable mirror to the environment. The Langevin force ξ has the correlation function in the frequency domain

$$\langle \xi(\omega)\xi(\Omega)\rangle = 4\pi\gamma_m \frac{\omega}{\omega_m}\left[1 + \coth\left(\frac{\hbar\omega}{2k_BT}\right)\right]\delta(\omega+\Omega), \tag{11.3}$$

where k_B is the Boltzmann constant. Throughout this paper, the following Fourier relations are used:

$$\begin{aligned}
f(t) &= \frac{1}{2\pi}\int_{-\infty}^{+\infty} f(\omega)e^{-i\omega t}d\omega, \\
f^\dagger(t) &= \frac{1}{2\pi}\int_{-\infty}^{+\infty} f^\dagger(-\omega)e^{-i\omega t}d\omega,
\end{aligned} \tag{11.4}$$

where $f^\dagger(-\omega) = [f(-\omega)]^\dagger$. c_{in} represents the input quantum field, which is centered around the frequency $\omega_p = \omega_c + \omega_m$ with a finite bandwidth Γ. The quantized field has the following nonvanishing correlation functions:

$$\begin{aligned}
\langle c_{in}(\omega)c_{in}(\Omega)\rangle &= 2\pi\frac{M\Gamma^2}{\Gamma^2 + (\omega-\omega_m)^2}\delta(\omega+\Omega-2\omega_m), \\
\langle c_{in}(\omega)c_{in}^\dagger(-\Omega)\rangle &= 2\pi\left[\frac{N\Gamma^2}{\Gamma^2 + (\omega-\omega_m)^2} + 1\right]\delta(\omega+\Omega),
\end{aligned} \tag{11.5}$$

where N is the photon number in the squeezed vacuum and $M = \sqrt{N(N+1)}$. The antinormally ordered term has a broadband contribution coming from vacuum noise.

Note that by setting $M = 0$ we would obtain a standard phase-independent quantum field with a mean number of photons $\frac{N\Gamma^2}{\Gamma^2+(\omega-\omega_m)^2}$ around the frequency $\omega = \omega_m$.

The mean values at steady state can be obtained from Eq. (11.2) by setting all of the time derivatives to zero. These are found to be

$$P_s = 0,\, Q_s = \frac{2g|c_s|^2}{\omega_m},\, c_s = \frac{\varepsilon}{\kappa + i\Delta}, \tag{11.6}$$

where

$$\Delta = \omega_0 - \omega_c - gQ_s \tag{11.7}$$

is the effective cavity detuning.

11.3 The Output Field and its Measurement

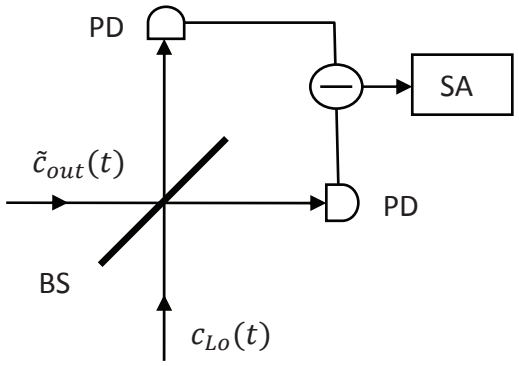

Figure 11.2: Sketch of the measurement of the output field. The output field $\tilde{c}_{out}(t)$ is mixed with a strong local field $c_{lo}(t)$ centered around the probe frequency ω_p at a beam splitter, where $\tilde{c}_{out}(t)$ is defined as the sum of the output field $c_{out}(t)$ from the cavity and the input quantized field $c_{in}(t)$. BS, 50:50 beam splitter; PD, photodetector; SA, spectrum analyzer.

The output field is a quantum field; it contains many Fourier components. Since the quantized input field is centered around $\omega_p = \omega_c + \omega_m$, the interesting component of the output field is near the probe frequency ω_p, so we mix the output field $\tilde{c}_{out}(t)$

with a strong local field $c_{lo}(t)$ centered around the probe frequency ω_p at a 50:50 beam splitter, as shown in Fig. 11.2. In a frame rotating at the frequency ω_c, $c_{lo}(t) = c_{lo}e^{-i\delta_0 t}$, where $\delta_0 = \omega_p - \omega_c$. The difference between the output signals from the two photodetectors is sent to the spectrum analyzer, and the output signal from the spectrum analyzer depends on the phase of c_{lo}. If c_{lo} is real, then the homodyne spectrum $X(\omega)$ of the output field measured by the spectrum analyzer is given by

$$\begin{aligned} & \langle [c_{lo}^*(t)\tilde{c}_{out}(t) + c.c.][c_{lo}^*(t')\tilde{c}_{out}(t') + c.c.]\rangle \\ = \; & \frac{c_{lo}^2}{2\pi}\int d\omega e^{-i\omega(t-t')}X(\omega). \end{aligned} \tag{11.8}$$

Thus, in our investigations of EIT with quantized fields, $X(\omega)$ is the quantity of interest.

In order to study the EIT effect in the homodyne spectrum $X(\omega)$ of the output field, we will calculate the fluctuations of the output field. The steady-state part would not contribute as it is at the frequency of the coupling field. We assume that the photon number in the cavity is large enough so that each operator can be written as a linear sum of the steady-state mean value and a small fluctuation, which yields

$$Q = Q_s + \delta Q, \quad P = P_s + \delta P, \quad c = c_s + \delta c, \tag{11.9}$$

where δQ, δP, and δc are the small fluctuations around the steady state. By substituting Eq. (11.9) into Eq. (11.2), one can arrive at the linearized equations for the fluctuation operators. Further, we transform the linearized equations into the frequency domain by Eq. (11.4) and solve it; we can obtain the fluctuations $\delta c(\omega)$ of the cavity field. Then, using the input-output relation $c_{out}(\omega) = \sqrt{2\kappa}c(\omega) - c_{in}(\omega)$, we can find the fluctuations $\delta c_{out}(\omega)$ of the output field. For the purpose of Fig. 11.2, we define the output field as $\tilde{c}_{out}(\omega) = c_{out}(\omega) + c_{in}(\omega)$; then we find the result

$$\delta\tilde{c}_{out}(\omega) = V(\omega)\xi(\omega) + E(\omega)c_{in}(\omega) + F(\omega)c_{in}^{\dagger}(-\omega), \tag{11.10}$$

in which

$$\begin{aligned} V(\omega) &= \frac{\sqrt{2\kappa}gc_s\omega_m i}{d(\omega)}[\kappa - i(\omega+\Delta)], \\ E(\omega) &= \frac{2\kappa}{d(\omega)}\{2ig^2|c_s|^2\omega_m + (\omega_m^2 - \omega^2 - i\gamma_m\omega) \\ &\quad \times[\kappa - i(\omega+\Delta)]\}, \\ F(\omega) &= \frac{4\kappa}{d(\omega)}\omega_m g^2 c_s^2 i, \end{aligned} \tag{11.11}$$

where

$$d(\omega) = -4\omega_m\Delta g^2|c_s|^2 + (\omega_m^2 - \omega^2 - i\gamma_m\omega)[(\kappa - i\omega)^2 + \Delta^2]. \tag{11.12}$$

The first term on the right-hand side of Eq. (11.10) refers to the contribution of the thermal noise of the movable mirror, and the other two terms represent the contribution of the squeezed vacuum. To illustrate the meaning of the last two terms, let the squeezed vacuum be a single mode, i.e., $c_{in}(t) = Ce^{-i(\omega_p-\omega_c)t}$; then $c_{in}(\omega) = 2\pi C\delta(\omega - \omega_p + \omega_c)$ and $c_{in}^\dagger(-\omega) = 2\pi C^\dagger\delta(\omega + \omega_p - \omega_c)$. Thus, the fluctuations of the output field $\delta\tilde{c}_{out}(t) = \frac{1}{2\pi}\int_{-\infty}^{+\infty} V(\omega)\xi(\omega)e^{-i\omega t}d\omega + CE(\omega_p - \omega_c)e^{-i(\omega_p-\omega_c)t} + C^\dagger F(\omega_c - \omega_p)e^{-i(\omega_c-\omega_p)t}$. Therefore, $E(\omega_p - \omega_c)$ is the component at the probe frequency ω_p, which in the rotating frame is $\omega_p - \omega_c$, and $F(\omega_c - \omega_p)$ is the component at the new frequency $2\omega_c - \omega_p$, which in the rotating frame is $\omega_c - \omega_p$, due to the nonlinear interaction between the movable mirror and the cavity field.

By the aid of the correlation functions of the noise operators $c_{in}(\omega)$ and $\xi(\omega)$ and neglecting fast oscillating terms at frequency $\pm 2\omega_m$, we obtain the homodyne spectrum $X(\omega)$ of the output field as measured by the setup of Fig. 11.2,

$$\begin{aligned} X(\omega) &= E(\omega+\omega_m)E(-\omega+\omega_m)\frac{M\Gamma^2}{\Gamma^2+\omega^2} + |E(\omega+\omega_m)|^2\frac{N\Gamma^2}{\Gamma^2+\omega^2} \\ &\quad + E^*(-\omega+\omega_m)E^*(\omega+\omega_m)\frac{M\Gamma^2}{\Gamma^2+\omega^2} + |E(-\omega+\omega_m)|^2\frac{N\Gamma^2}{\Gamma^2+\omega^2} \\ &\quad + |E(\omega+\omega_m)|^2 + |F(-\omega+\omega_m)|^2 \\ &\quad + |V(\omega+\omega_m)|^2 2\gamma_m\frac{\omega+\omega_m}{\omega_m}\left\{1 + \coth\left[\frac{\hbar(\omega+\omega_m)}{2k_BT}\right]\right\} \end{aligned}$$

$$+|V(-\omega+\omega_m)|^2 2\gamma_m \frac{\omega-\omega_m}{\omega_m}\left\{1+\coth\left[\frac{\hbar(\omega-\omega_m)}{2k_BT}\right]\right\}, \qquad (11.13)$$

where the first four terms in Eq. (11.13) originate from the squeezed vacuum, the next two terms not involving N and M are the contributions of the spontaneous emission of the input vacuum noise, and the last two terms result from the thermal noise of the movable mirror.

11.4 EIT in the Homodyne Spectrum of the Output Quantized Field

After having derived the homodyne spectrum of the output field, we next examine it numerically to explore the EIT phenomenon in the homodyne spectrum of the output field. Since the original Eqs. (11.2) are nonlinear, these can have instabilities. Thus, in the following, we work in the stable regime of the system. We first examine the frequency at which we expect transparency. This is $\omega = 0$. For $N \approx M$,

$$X(0) \;=\; N[E(\omega_m)+E^*(\omega_m)]^2+|E(\omega_m)|^2+|F(\omega_m)|^2+4|V(\omega_m)|^2\gamma_m \coth\left[\frac{\hbar\omega_m}{2k_BT}\right]. \qquad (11.14)$$

We use the parameters from the experimental paper [53] focusing on the EIT in the optomechanical system: the wavelength of the coupling field $\lambda = 2\pi c/\omega_c = 775$ nm, the coupling constant $g = 2\pi \times 12$ GHz/nm$\sqrt{\hbar/(2m\omega_m)}$, the mass of the movable mirror $m = 20$ ng, the frequency of the movable mirror $\omega_m = 2\pi \times 51.8$ MHz, the cavity decay rate $\kappa = 2\pi \times 15$ MHz, $\kappa/\omega_m = 0.289$, the mechanical damping rate $\gamma_m = 2\pi \times 41$ kHz, and the mechanical quality factor $Q' = \omega_m/\gamma_m = 1263$. In addition, we choose the linewidth of the squeezed vacuum $\Gamma = 2\kappa$ and consider the resonant case $\Delta = \omega_m$.

For $N = 10$ and $M = \sqrt{N(N+1)} \approx 10$, $\wp = 20$ mW, and $T = 20$ mK, the first term in Eq. (11.14), which is the contribution of the squeezed vacuum, is about 6.5×10^{-4}, the sum of the second and third terms in Eq. (11.14), which are the

contributions of the input vacuum noise is about 0.16, and the last term arising from the thermal noise of the movable mirror is about 0.14. The contribution of the input quantum field in principle can be obtained by doing the experiment with and without the quantized field and by subtracting the data, i.e., by studying $X(0) - X(0)|_{N=0}$. The squeezed field part in a sense exhibits perfect EIT. If $M = 0$, i.e., the input quantized field is phase insensitive, then such a field leads to a term $2N|E(\omega_m)|^2$, which is equal to 1.6 for the above-mentioned parameters, and hence there is no perfect EIT. The squeezed field changes $2N|E(\omega_m)|^2$ to $N[E(\omega_m) + E^*(\omega_m)]^2$, and for the above parameters, the number changes from 1.6 to 6.5×10^{-4}.

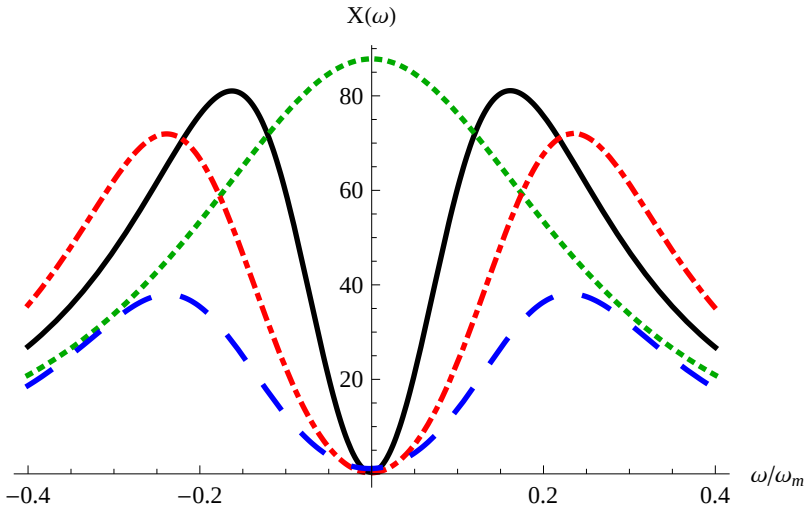

Figure 11.3: Homodyne spectrum $X(\omega)$ as a function of ω/ω_m for $N = 5$ in the absence (dotted curve) and the presence (solid, dot-dashed, and dashed curves) of the coupling field for the temperature of the environment $T = 20$ mK. The solid curve is for $\wp = 10$ mW and $M = \sqrt{N(N+1)}$, the dotdashed curve is for $\wp = 20$ mW and $M = \sqrt{N(N+1)}$, and the dashed curve is for $\wp = 20$ mW and $M = 0$.

For $N = 5$, $M = \sqrt{N(N+1)}$ and 0, and $T = 20$ mK, we plot the homodyne spectrum $X(\omega)$ of the output field as a function of the normalized frequency ω/ω_m in the absence (dotted curve) and presence (solid, dot-dashed, and dashed curves) of

the coupling field in Fig. 11.3. First, let us look at the case that the input quantum field is phase dependent [$M = \sqrt{N(N+1)}$]. In the absence of the coupling field, one can note that the homodyne spectrum of the output field has a Lorentzian line shape. However, in the presence of the coupling field at different power levels, the solid curve [$\wp = 10$ mW and $M = \sqrt{N(N+1)}$] and the dot-dashed curve [$\wp = 20$ mW and $M = \sqrt{N(N+1)}$] exhibit the EIT dip, which is the result of the destructive interference between the squeezed vacuum and the scattering quantum field at the probe frequency ω_p generated by the interaction of the coupling field with the movable mirror. For $\wp = 20$ mW and $M = \sqrt{N(N+1)}$, the minimum value of $X(\omega)$ is about 0.22. Moreover, the linewidth of the dip for $\wp = 20$ mW is larger than that for $\wp = 10$ mW due to power broadening. Generally, the EIT dip has a contribution to its width that is proportional to the power of the coupling field. We indeed find that the width for $\wp = 20$ mW is $0.26\omega_m$, which is about twice the width for $\wp = 10$ mW. If the input quantum field is phase independent ($M = 0$) (the dashed curve), then we can see that the maximum value of $X(\omega)$ for $\wp = 20$ mW and $M = 0$ is about half that for $\wp = 20$ mW and $M = \sqrt{N(N+1)}$.

Next, we increase the temperature to 100 mK. Figure 11.4 displays the homodyne spectrum $X(\omega)$ of the output field against the normalized frequency ω/ω_m in the absence (dotted curves) and presence (solid curves) of the coupling field for $N = 1$ and 5 and $M = \sqrt{N(N+1)}$. In the presence of the coupling field ($\wp = 10$ mW), it is seen that the EIT dip still appears in the homodyne spectrum of the output field for $N = 1$ and 5. Note that the two dips almost have the same minimum values (about 1.43) and the same linewidth (about $0.15\omega_m$). Hence the temperature of the environment is not detrimental to the EIT behavior.

The effects discussed above occur under a wide range of parameters. We demonstrate this by using the experimental parameters [50] $\lambda = 2\pi c/\omega_c = 1064$ nm, $L = 25$ mm, $g \approx 2\pi \times 11.28$ MHz/nm$\sqrt{\hbar/(2m\omega_m)}$, $m = 145$ ng, $\omega_m = 2\pi \times 947$ kHz,

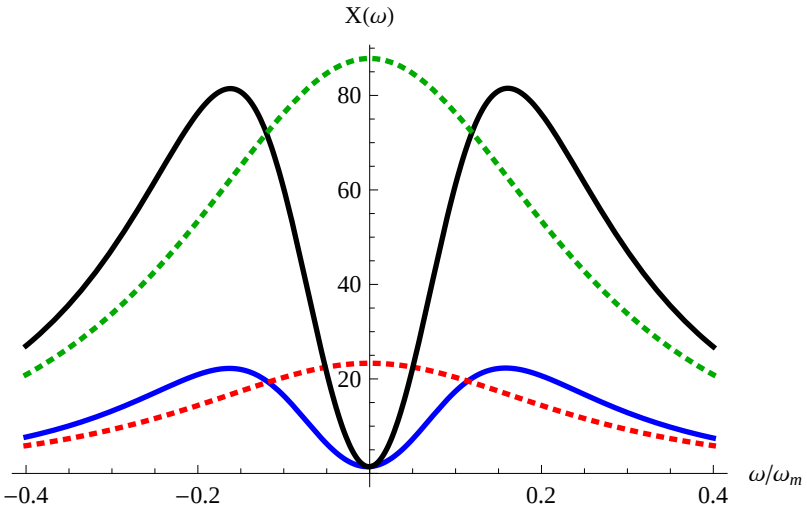

Figure 11.4: Homodyne spectrum $X(\omega)$ as a function of ω/ω_m for different values of the parameter N and $M = \sqrt{N(N+1)}$ in the absence (dotted curves) and the presence (solid curves) of a coupling field with power $\wp = 10$ mW and temperature of the environment $T = 100$ mK. The upper two curves are for $N = 5$, and the lower two curves are for $N = 1$.

$\kappa = 2\pi \times 215$ kHz, $\kappa/\omega_m = 0.227$, $\gamma_m = 2\pi \times 141$ Hz, and $Q' = \omega_m/\gamma_m = 6700$. The values for the parameters T, $\wp$, N, M, Γ, and Δ are the same as those in Fig. 11.4. Shown in Fig. 11.5 is the homodyne spectrum $X(\omega)$ of the output field as the normalized frequency ω/ω_m is varied for $T = 100$ mK and $\wp = 0$ and 10 mW. Note that the EIT exists for $N = 1$ and 5 in the presence of the coupling field. The linewidth of the dip for $N = 5$ is about $0.2\omega_m$ and as expected gets broadened due to power. We have further studied the effect of temperature, and we find that there is a rather weak dependence of the EIT curves on temperature. Therefore, current optomechanical designs can be used to realize quantum optical memory at the single-photon level. This can be demonstrated using the numerical simulations and following the standard procedure as in Refs. [86, 208, 209]. One has to modulate the squeezed vacuum field c_{in} so that it is a pulse field and uses, say, a super-Gaussian for the coupling field. The super-Gaussian enables one to conveniently switch on and off the coupling field

[211].

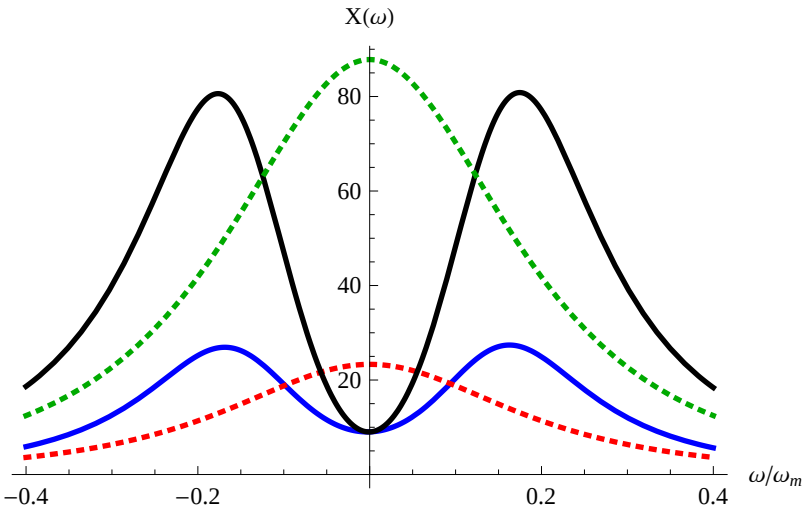

Figure 11.5: As in Fig. 11.4 but now the parameters used are from Ref. [50].

11.5 Conclusions

In conclusion, we have demonstrated EIT using quantum fields in optomechanical systems under a wide range of conditions. For squeezed quantum fields, we obtained the perfect EIT. The EIT gets degraded in phase-insensitive quantum fields. We have shown that even temperature is not critical for observations of EIT. The results can be generalized to optomechanical systems working on the reactive coupling [69, 194, 210]. Our work suggests that optomechanical systems could be used as elements for quantum memory, but explicit demonstration will be given elsewhere.

The content of this chapter has been published in *Phys. Rev. A* **83**, 043826 (2011).

CHAPTER 12

OPTOMECHANICAL SYSTEMS AS SINGLE PHOTON ROUTERS

12.1 Overview

It is well known that building up of all optical devices requires strong interactions between radiation and matter as photons by themselves do not interact. One of enabling technologies in the context of quantum control is the design of an optical switch or a photon router operating at a single photon level. Several proposals have been made for the realization of an optical switch—In an early work Harris and Yamamoto [212] had suggested how quantum interference can be used to operate a switch. More recently atomic EIT with cavity fields has been suggested to realize optical switch. Single atom EIT in a cavity has been realized by using very strong atom cavity interactions [213]. Further even the vacuum induced transparency has been observed [214]. Other proposals on photon switch are based on using single atom in a strongly coupled waveguide array [215, 216, 217, 218]; use of strongly coupled atom via surface plasmons on a nanowire [219]. There are also reports of single photon switch at telecom wavelengths using strong cross phase modulation [220], and in microwave domain using a superconducting transmon qubit [221]. It was known earlier that the optomechanical systems exhibit analog of electromagnetically induced transparency [51, 222] which has been observed in several experiments [24, 53, 54, 55]. Here we show how nanomechanical mirrors in optical cavities can be used to build single photon routers i.e. single photon switches. For this purpose we propose a different configuration in which the nanomechanical mirror is in the middle of a cavity which is bounded by two high quality mirrors [10]. A single photon would

be transmitted; on the other hand if we appropriately drive the system by a strong field then we show that the single photon is reflected. Thus the driving field switches the route of the single photon. Even low driving fields like few microwatt are good. We present exact conditions for this to happen. We further investigate the effects of vacuum and thermal noise on the performance of this system as a single photon router. We show that the effect of these noise sources is only few percent at temperatures of the order of 20 mK.

12.2 Model

Consider first a Fabry-Perot cavity with both mirrors with equal reflectivity. It is known that the transmission of a Fabry-Perot cavity goes to unity when the incident field is on resonance with the cavity. This result also applies if a single photon is incident on the cavity. In order to see this let us consider the input-output relations [110] for the cavity as shown in Fig. 12.1.

Figure 12.1: A double-ended cavity.

Here c_{in} and d_{in} are the quantum fields incident on the cavity. If there are no photons incident from the right, then d_{in} would be the vacuum field. Let 2κ be the rate at which photons leak out from each of the cavity mirrors. Let $c(\omega)$ be the cavity field operator, then

$$c_{out}(\omega) = \sqrt{2\kappa}c(\omega) - c_{in}(\omega),$$

$$d_{out}(\omega) = \sqrt{2\kappa}c(\omega) - d_{in}(\omega), \tag{12.1}$$

and the equation of motion for the cavity field is

$$\dot{c} = -2\kappa c - i\omega_0 c + \sqrt{2\kappa}(c_{in} + d_{in}). \tag{12.2}$$

From (12.1) and (12.2) we find in steady state

$$c_{out}(\omega) = \frac{i(\omega - \omega_0)c_{in}(\omega) + 2\kappa d_{in}(\omega)}{2\kappa - i(\omega - \omega_0)}, \tag{12.3}$$

$$d_{out}(\omega) = \frac{2\kappa c_{in}(\omega) + i(\omega - \omega_0)d_{in}(\omega)}{2\kappa - i(\omega - \omega_0)}. \tag{12.4}$$

Here $d_{in}(\omega)$ is the vacuum field and hence its normally ordered correlation is zero. Defining the spectrum of the field via

$$\langle c^\dagger(-\Omega)c(\omega)\rangle = 2\pi S_c(\omega)\delta(\omega + \Omega). \tag{12.5}$$

Using (12.3)-(12.5), we obtain

$$S_{cout}(\omega) = \frac{(\omega - \omega_0)^2}{4\kappa^2 + (\omega - \omega_0)^2} S_{cin}(\omega), \tag{12.6}$$

$$S_{dout}(\omega) = \frac{4\kappa^2}{4\kappa^2 + (\omega - \omega_0)^2} S_{cin}(\omega). \tag{12.7}$$

For $\omega = \omega_0$, $S_{cout}(\omega_0) \to 0$, $S_{dout}(\omega_0) = S_{cin}(\omega_0)$. Therefore we have established that a single photon at the cavity frequency is completely transmitted. We next establish how a nanomechanical oscillator in the cavity acts as a single photon router i.e., it would reflect the single photon i.e.,

$$S_{cout}(\omega_0) = S_{cin}(\omega_0),\ S_{dout}(\omega_0) = 0. \tag{12.8}$$

Consider now the configuration shown in Fig. 12.2 where a partially transparent nanomechanical mirror placed at the middle position of the Fabry-Perot cavity formed by two fixed mirrors, which have finite identical transmission [10]. The whole cavity length is L. The cavity field is driven by a strong coupling field at frequency ω_c from the left-hand mirror. Further, a field in a single photon Fock state at frequency ω_p,

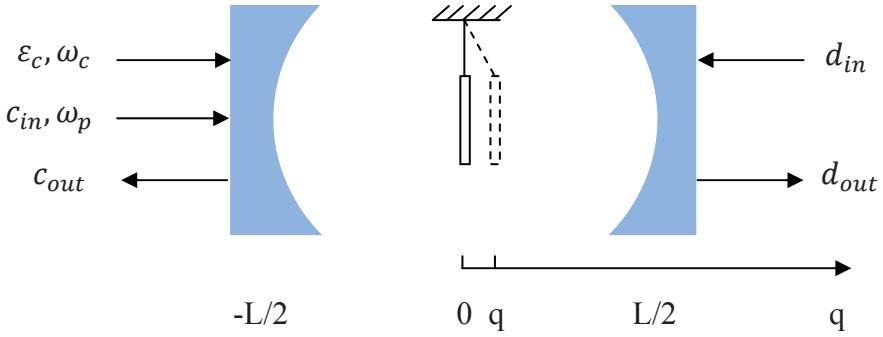

Figure 12.2: A double-ended cavity with a moving nanomechanical mirror as a single photon router.

is incident into the cavity through the left-hand mirror. The input field is centered near the cavity frequency i.e. its spectrum is given by

$$S_{cin}(\omega) = \frac{\Gamma/\pi}{(\omega-\omega_0)^2+\Gamma^2}, \int S_{cin}(\omega)d\omega = 1. \tag{12.9}$$

The correlation functions for the input field are therefore given by

$$\begin{aligned} \langle c_{in}^\dagger(-\Omega)c_{in}(\omega)\rangle &= 2\pi\delta(\omega+\Omega)S_{cin}(\omega), \\ \langle c_{in}(\omega)c_{in}^\dagger(-\Omega)\rangle &= 2\pi\delta(\omega+\Omega)(1+S_{cin}(\omega)). \end{aligned} \tag{12.10}$$

The photons in the cavity will exert a radiation pressure force on the movable mirror, causing it to move. In turn, the displacement q of the movable mirror shifts the cavity resonance frequency. We assume that the movable mirror is located at the node of the cavity mode, thus the cavity resonance frequency depends linearly on the displacement q of the movable mirror. Here, the movable mirror is treated as a quantum harmonic oscillator with effective mass m, frequency ω_m, and momentum operator p. Let c and $c^\dagger$ be the annihilation and creation operators for the cavity field. The Hamiltonian of the system in the rotating frame at the frequency ω_c of the coupling field is given by

$$H = \hbar(\omega_0-\omega_c)c^\dagger c + \hbar g c^\dagger c q + \frac{p^2}{2m} + \frac{1}{2}m\omega_m^2 q^2 + i\hbar\varepsilon_c(c^\dagger - c), \tag{12.11}$$

in which g is the optomechanical coupling strength between the movable mirror and the cavity field, which also depends on the transmission of the movable mirror [10]. By choosing the transmission of the movable mirror $T = 0.7$, the optomechanical coupling strength can be half of that for a perfectly reflecting movable mirror so that $g = -\frac{\omega_c}{L}$ [118]. The ε_c is the driving strength, depends on the power $\wp$ of the coupling field by $\varepsilon_c = \sqrt{\frac{2\kappa\wp}{\hbar\omega_c}}$. Note that the movable mirror is coupled to the thermal surrounding at the temperature T, which results in the mechanical damping rate γ_m and thermal noise force ξ with frequency-domain correlation function:

$$\langle \xi(\omega)\xi(\Omega)\rangle = 2\pi\hbar\gamma_m m\omega \left[1 + \coth\left(\frac{\hbar\omega}{2k_B T}\right)\right]\delta(\omega+\Omega), \tag{12.12}$$

where k_B is the Boltzmann constant. In addition the cavity field c would be coupled to the input quantum fields c_{in} and d_{in}. These couplings are included in the standard way by writing quantum Langevin equations for the cavity field operators. The incoming vacuum field d_{in} is characterized by $\langle d_{in}(\omega)d_{in}^{\dagger}(-\Omega)\rangle = 2\pi\delta(\omega+\Omega)$ with $S_{din}(\omega) = 0$. Putting together all the quantum fields, thermal fluctuations and the Heisenberg equations that follow from the Hamiltonian (12.11), we obtain the working quantum Langevin equations

$$\begin{aligned}
\dot{q} &= \frac{p}{m}, \quad \dot{p} = -\hbar g c^{\dagger}c - m\omega_m^2 q - \gamma_m p + \xi, \\
\dot{c} &= -[2\kappa + i(\omega_0 - \omega_c + gq)]c + \varepsilon_c + \sqrt{2\kappa}c_{in} + \sqrt{2\kappa}d_{in}, \\
\dot{c}^{\dagger} &= -[2\kappa - i(\omega_0 - \omega_c + gq)]c^{\dagger} + \varepsilon_c + \sqrt{2\kappa}c_{in}^{\dagger} + \sqrt{2\kappa}d_{in}^{\dagger},
\end{aligned} \tag{12.13}$$

where mean values of noise terms ξ, c_{in}, and d_{in} are zero.

Using the Langevin equations (12.13) we want to calculate the spectrum of the output fields c_{out} and d_{out}. We adopt the standard quantum optical procedure [26]. We first find the steady state for the mean values of the observable and then linearize the Langevin equations around the mean values to calculate quantum fluctuations. We quote the result of such a calculation, we find that the spectrum of the output

fields has the form

$$\begin{aligned} S_{cout}(\omega) &= S_{cin}(\omega)\cdot R(\omega) + S^{(v)}(\omega) + S^{(T)}(\omega), \\ S_{dout}(\omega) &= S_{cin}(\omega)\cdot T(\omega) + S^{(v)}(\omega) + S^{(T)}(\omega), \end{aligned} \tag{12.14}$$

where

$$R(\omega) = |E(\omega) - 1|^2, \quad T(\omega) = |E(\omega)|^2, \tag{12.15}$$

and

$$\begin{aligned} S^{(v)}(\omega) &= 2|X(\omega)|^2, \\ S^{(T)}(\omega) &= |V(\omega)|^2 \hbar\gamma_m m(-\omega)\left[1 + \coth\left(-\frac{\hbar\omega}{2k_BT}\right)\right], \end{aligned}$$

$$\begin{aligned} E(\omega) &= \frac{2\kappa}{d(\omega)}\{m(\omega_m^2 - \omega^2 - i\gamma_m\omega)[2\kappa - i(\Delta+\omega)] + i\hbar g^2|c_s|^2\}, \\ X(\omega) &= \frac{2\kappa}{d(\omega)} i\hbar g^2 c_s^2, \\ V(\omega) &= \frac{\sqrt{2\kappa}}{d(\omega)}\{-igc_s[2\kappa - i(\Delta+\omega)]\}, \\ d(\omega) &= m(\omega_m^2 - \omega^2 - i\gamma_m\omega)[(2\kappa - i\omega)^2 + \Delta^2] - 2\hbar g^2|c_s|^2\Delta, \\ q_s &= -\frac{\hbar g|c_s|^2}{m\omega_m^2}, \quad c_s = \frac{\varepsilon_c}{2\kappa + i\Delta}, \end{aligned} \tag{12.16}$$

where $\Delta = \omega_0 - \omega_c + gq_s$ is the effective detuning, including the frequency shift due to radiation pressure, $|c_s|^2$ is the number of intracavity photons, and q_s is the steady state position of the movable mirror. The roots of $d(\omega)$ determine essentially the behavior of the output fields. These are complex and depend on the power of the coupling field.

In Eq. (12.14), $R(\omega)$ and $T(\omega)$ are the contributions arising from the presence of the single photon in the input field. The $S^{(v)}(\omega)$ is the contribution from the incoming vacuum field. The nonlinear coupling of the cavity field with the mirror converts the vacuum photon at frequency $\omega_c - \Omega$ to $\omega_c + \Omega$ via the mixing process $\omega_c + \omega_c - (\omega_c - \Omega) \to \omega_c + \Omega$. Note that $X(\omega)$ is at least of order two in the amplitude

of the coupling field and this determines the nature of the vacuum contribution. The $S^{(T)}(\omega)$ is the contribution from the fluctuations of the mirror. The equation (12.14) shows that even if there were no incoming photon, the output signal is generated via quantum and thermal noises. For the purpose of achieving single photon router, the key quantities are $R(\omega)$ and $T(\omega)$. Further the performance of the single photon router should not be deteriorated by the quantum and thermal noise terms $S^{(v)}(\omega)$ and $S^{(T)}(\omega)$. We also note in passing that in a treatment where the probe field is treated classically, then the output semiclassical fields would be $(E(\omega)-1)$ and $E(\omega)$ on the left and right ports, respectively.

12.3 EIT in the Reflection Spectrum of the Single Photon

Now we present numerical results using our analytical results (12.14). We would work in the sideband resolved limit i.e. $\omega_m \gg \kappa$, further we will take $\Delta = \omega_m$. We use the parameters from an experimental paper [10]. The wavelength of the coupling field $\lambda = 1054$ nm, $L = 6.7$ cm, $m = 40$ ng, $\omega_m = 2\pi \times 134$ kHz, $Q = 1.1 \times 10^6$, $\gamma_m = \omega_m/Q = 0.76$ sec^{-1}, and $\kappa = \omega_m/10$. In the following, we work in the stable regime of the system i.e. we use control power such that there are no instabilities.

We present the behavior of the reflection and transmission spectra $R(\omega)$ and $T(\omega)$ of the single photon as a function of the normalized frequency ω/ω_m in the absence and the presence of the coupling field in Figs. 12.3 and 12.4. In the absence of the coupling field, one observes an inverted Lorentzian and a standard Lorentzian in the reflection and transmission spectra of the single photon. Note that $R(\omega_m) \approx 0$ and $T(\omega_m) \approx 1$. So the single photon is completely transmitted through the cavity to the right output port. However, in the presence of the coupling field, the situation is completely different. The reflection and transmission spectra of the single photon exhibit an inverted dip and a dip at $\omega = \omega_m$, and $R(\omega_m) \approx 1$ and $T(\omega_m) \approx 0$. The single photon is totally reflected to the left output port. In the presence of the coupling field, the

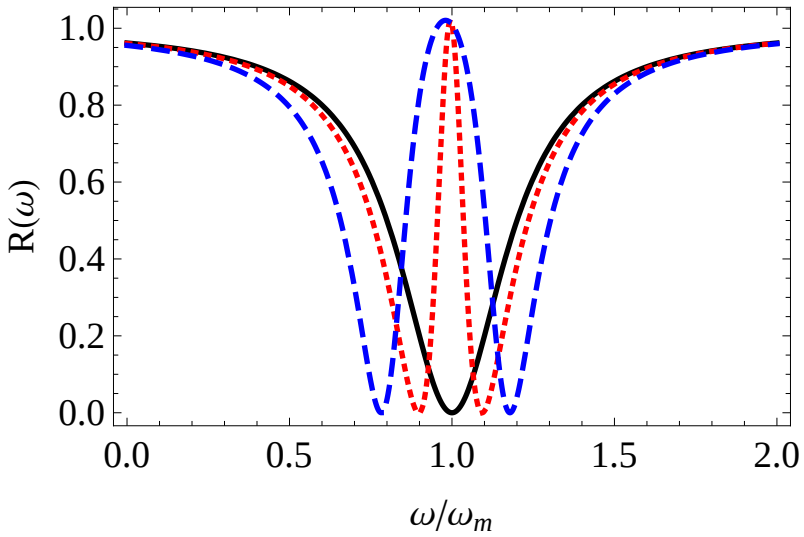

Figure 12.3: The reflection spectrum $R(\omega)$ of the single photon as a function of the normalized frequency ω/ω_m without and with the coupling field. $\wp = 0$ (solid), 5 μW (dotted), 20 μW (dashed).

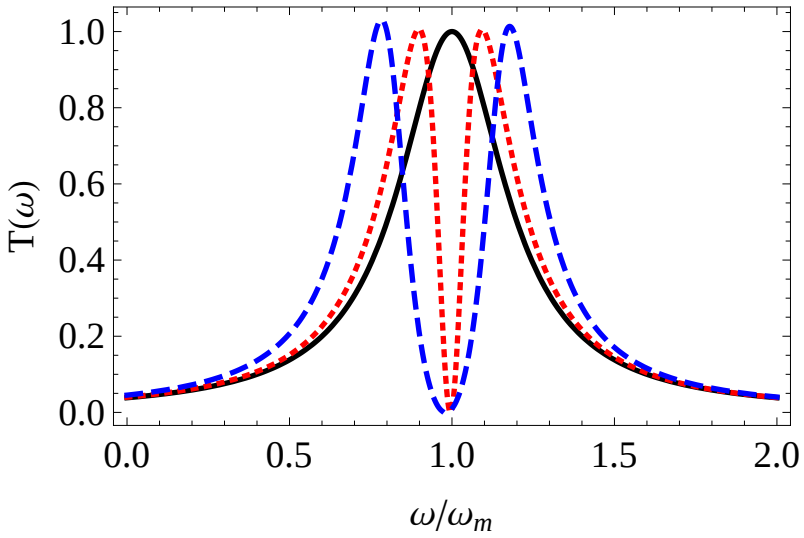

Figure 12.4: The transmission spectrum $T(\omega)$ of the single photon as a function of the normalized frequency ω/ω_m without and with the coupling field. $\wp = 0$ (solid), 5 μW (dotted), 20 μW (dashed).

nano mirror participates in the transmission or reflection of the photon and we have all the conditions for occurrence of EIT fulfilled ($\gamma_m \ll \kappa \ll \omega_m,\ \omega_p = \omega_c + \omega_m$). Therefore the incident single photon is totally reflected. In an earlier work dealing with coherent light it was shown that the reflected outgoing field would even have a well defined phase. However for router action phase does not play a role. The width of the reflection peak (transmission dip) depends on the power of the coupling field—the width increases with increase in the coupling power, and thus we can also treat the switching of a narrow width single photon pulse.

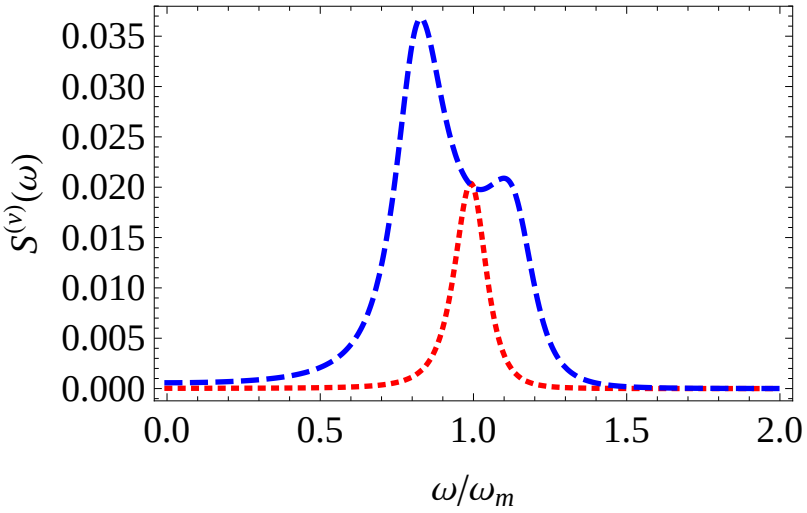

Figure 12.5: The vacuum noise spectrum $S^{(v)}(\omega)$ as a function of the normalized frequency ω/ω_m with the coupling field. $\wp = 5\ \mu$W (dotted), 20 μW (dashed).

Next we discuss the effects of the quantum and thermal noises on the reflection and transmission spectra of the single photon. We exhibit the behavior of the vacuum noise $S^{(v)}(\omega)$ for two different values of the coupling power in Fig. 12.5. The contribution of the vacuum noise is about 2 % at $\omega = \omega_m$ and is thus insignificant. Note that for larger coupling powers, $S^{(v)}(\omega)$ splits into two peaks—this is connected with the normal mode splitting [50], arising from the two roots of $d(\omega)$. The thermal noise could be more critical in deteriorating the performance of the single photon router. However if we work with mirror temperatures like 20 mK, then the thermal noise

term is insignificant as shown in Fig. 12.6. Even at a relatively large temperature like 50 mK, the maximum thermal noise is 15 %. In the light of rather small sources of noise, we conclude that the nanomechanical mirror in an optical cavity as a single photon router is an excellent device.

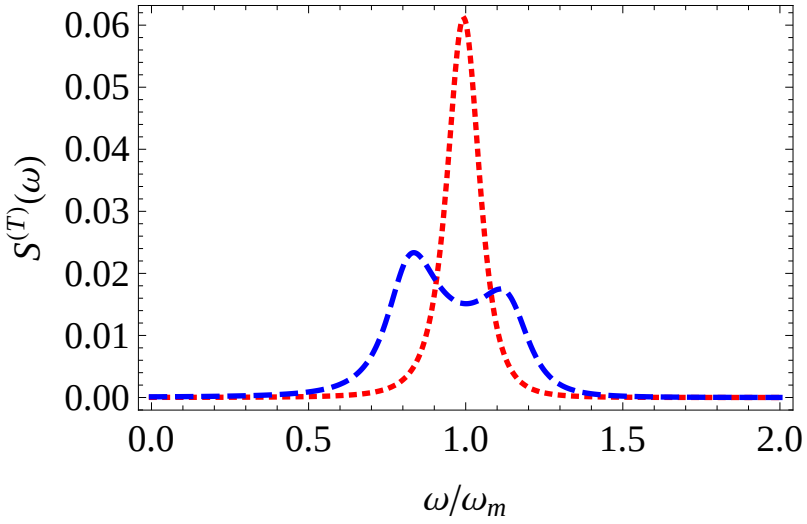

Figure 12.6: The thermal noise spectrum $S^{(T)}(\omega)$ as a function of the normalized frequency ω/ω_m with the coupling field for $T = 20$ mK. $\wp = 5$ μW (dotted), 20 μW (dashed).

12.4 Conclusions

In conclusion, we have shown how a cavity optomechanical system can be used as a single photon router. The physical mechanism that enables this application is the EIT behavior that such systems exhibit. We further showed that the effects of quantum noise sources on such a single photon router are very minimal.

The content of this chapter has been accepted for publication.

CHAPTER 13

SUMMARY AND FUTURE DIRECTIONS

13.1 Summary

In this thesis, several effects in the dispersive or dissipative optomechanical system on a macroscopic scale were explored. These effects included cooling of the mechanical resonator, normal mode splitting, the squeezed mechanical state, entangling two mechanical oscillators, electromagnetically induced transparency, and so on.

First we have investigated an optical parametric amplifier inside a cavity could be used to enhance the optical cooling of the micromechanical mirror. Our calculations indicate that the temperature of the micromechanical mirror can be reduced to sub-Kelvin temperature, which is much lower than what is achievable in the absence of the parametric amplifier. Further, We show that the mirror can be cooled to millikelvin temperatures if it is precooled to 1 K by cryogenic cooling method. The reason is that the OPA inside the cavity increases the photon number in the cavity, enhances the radiation pressure effects on the mirror, and leads to lower cooling of the mirror.

We have also demonstrated that an optical parametric amplifier inside the cavity can affect the normal-mode splitting behavior of the coupled movable mirror and the cavity field. We work in the resolved sideband regime. The spectra are found to exhibit a double-peak structure as the parametric gain is increased. Moreover, for a fixed parametric gain, increasing the input laser power can make the double-peak structure of the spectrum more pronounced.

Then we have developed a scheme to generate the squeezing of a nanomechanical mirror by injecting a broad band squeezed vacuum light and laser light into a Fabry-

Perot cavity. We work in the resolved sideband regime. We find that the momentum squeezing of the movable mirror reaches a maximal value when the squeezing parameter of the input light is about 1. We can obtain more than 70% squeezing. Besides, for a fixed squeezing parameter, the momentum squeezing increases with decreasing the temperature of the environment or increasing the laser power. We find very large squeezing with respect to thermal fluctuations, for instance at 1 mK, the momentum fluctuations go down by a factor more than one hundred.

We have also proposed a method to entangle two separated nanomechanical oscillators in a ring cavity by injecting broad band squeezed vacuum light and laser light. We work in the resolved sideband regime. The maximum entanglement of the two oscillators can be reached when the squeezing parameter of the input light is about 1. We find that entanglement can survive over a very wide range of power levels of the pump and temperatures of the environment.

Next we have studied the stimulated Stokes and anti-Stokes processes in cavity optomechanics. We observe that the dispersive optomechanical coupling between the cavity field and the movable mirror via radiation pressure force can induce normal-mode splitting in both the output Stokes and anti-Stokes fields. We discover lifetime splitting for pump power less than a critical power. We find that the Stokes field is amplified. We also discuss the correlation between the Stokes and anti-Stokes photons produced spontaneously by the optomechanical system. We find that the correlation between these photons shows photon nonclassical antibunching feature, and the nonclassical correlation becomes weaker with increasing pump power.

Then we have presented the theoretical results describing an exact analog of electromagnetically induced transparency in the linearly optomechanical system, in which the cavity field is linearly coupled to the displacement of the mechanical oscillator. Our calculations show explicitly the origin of EIT-like dips as well as the characteristic changes in dispersion from anomalous to normal at the line center. We find that

the linewidth of the EIT-like dip depends on the coupling laser power.

Further we have shown that the reactive optomechanical coupling between the optical resonator and the waveguide via the optical gradient force also can induce the normal mode splitting in the output fields. We find that the peak separation increases with increasing pump power. We also find that the reactive coupling leads to the generation of an anti-Stokes field.

In addition, we have demonstrated that the reactive coupling between the waveguide and the microdisk resonator can generate the squeezing of the waveguide by injecting a quantum field and laser into the resonator through the waveguide. The results show that the maximal momentum squeezing of the waveguide is about 7075% for temperature about 110 mK.

Moreover, we have presented a theoretical analysis of EIT-like effects in quadratically coupled optomechanical systems, in which the cavity field is coupled to the square of the displacement of the mechanical oscillator. In such systems, the mean displacement of the mechanical oscillator, which plays the role of atomic coherence in traditional EIT, is zero. The quantity leading to EIT in such systems is mean values of the square of the displacement of the mechanical oscillator.

Then we have demonstrated EIT using quantum fields in optomechanical systems. We show how the EIT effect can be detected by probing the outgoing light. We find that the EIT dip exists even though the photon number in the squeezed vacuum is at the single-photon level. The EIT gets degraded if the quantum field is phase-insensitive. We find that the temperature of the environment is not detrimental to the EIT behavior. Our work suggests that optomechanical systems could be useful in optical memory.

Finally we have presented a single-photon router by using the double-ended cavity with a moving mirror. We find that the probe field can be sent to the right output port or the left output port by switching the coupling field off or on, which is based

on the effect of EIT. We further showed that the effects of quantum noise sources on such a single photon router are very minimal.

13.2 Future Directions

The attractive and repulsive (bipolar) optical forces allow one to manipulate mechanical components on the silicon chip in both directions. Thus they can be applied in all-optical switching, tunable microphotonics devices and nanomechanical systems. Presently, tunable bipolar optical force in neighboring waveguides has been demonstrated theoretically [223] and experimentally [69, 224]. They showed the sign of the force depends on the relative phase of the coupled lightwaves. Here, we suggest the optomechanical system (Fig. 1.2) can generate a bipolar force by applying a weak probe field and a strong coupling field. The optical force exerted by the photons from the probe field on the waveguide is bipolar in the presence of the coupling field. And the sign of the force is tunable by changing the detuning between the probe field and the coupling field.

BIBLIOGRAPHY

[1] P. Lebedev, "Untersuchungen über die Druckkräfte des Lichtes", Annalen der Physik, (1901).

[2] E. F Nichols and G. F. Hull, The Astrophysical Journal **17**, 315 (1903).

[3] S. Chu, Science **253**, 861 (1991).

[4] S. Stenholm, Rev. Mod. Phys. **58**, 699 (1986).

[5] D. Leibfried, R. Blatt, C. Monroe, and D. Wineland, Rev. Mod. Phys. **75**, 281 (2003).

[6] C. H. Metzger and K. Karrai, Nature (London) **432**, 1002 (2004).

[7] D. Kleckner and D. Bouwmeester, Nature (London) **444**, 75 (2006).

[8] S. Gigan, H. R. Böhm, M. Paternostro, F. Blaser, G. Langer, J. B. Hertzberg, K. C. Schwab, D. Bäuerle, M. Aspelmeyer, and A. Zeilinger, Nature (London) **444**, 67 (2006).

[9] O. Arcizet, P. F. Cohadon, T. Briant, M. Pinard, and A. Heidmann, Nature (London) **444**, 71 (2006).

[10] J. D. Thompson, B. M. Zwickl, A. M. Jayich, F. Marquardt, S. M. Girvin, and J. G. E. Harris, Nature (London) **452**, 72 (2008).

[11] A. M. Jayich, J. C. Sankey, B. M. Zwickl, C. Yang, J. D. Thompson, S. M. Girvin, A. A. Clerk, F. Marquardt, and J. G. E. Harris, New J. Phys. **10**, 095008 (2008).

[12] J. C. Sankey, C. Yang, B. M. Zwickl, A. M. Jayich, and J. G. E. Harris, Nature Physics **6**, 707 (2010).

[13] D. J. Wilson, C. A. Regal, S. B. Papp, and H. J. Kimble, Phys. Rev. Lett. **103**, 207204 (2009).

[14] F. Brennecke, S. Ritter, T. Donner, and T. Esslinger, Science **322**, 235 (2008).

[15] K. W. Murch, K. L. Moore, S. Gupta and D. M. Stamper-Kurn, Nature Physics **4**, 561 (2008).

[16] R. Ma, A. Schliesser, P. DelHaye, A. Dabirian, G. Anetsberger, and T. J. Kippenberg, Optics Letters **32**, 2200 (2007).

[17] T. J. Kippenberg, H. Rokhsari, T. Carmon, A. Scherer, and K. J. Vahala, Phys. Rev. Lett. **95**, 033901 (2005).

[18] A. Schliesser, P. DelHaye, N. Nooshi, K. J. Vahala, and T. J. Kippenberg, Phys. Rev. Lett. **97**, 243905 (2006).

[19] L. Ding, C. Baker, P. Senellart, A. Lemaitre, S. Ducci, G. Leo, and I. Favero, Phys. Rev. Lett. **105**, 263903 (2010).

[20] M. Eichenfield, J. Chan, R. M. Camacho, K. J. Vahala, and O. Painter, Nature(London) **462**, 78 (2009).

[21] C. A. Regal, J. D. Teufel, K. W. Lehnert, Nature Physics **4**, 555 (2008).

[22] J. D. Teufel, T. Donner, M. A. Castellanos-Beltran, J. W. Harlow, and K. W. Lehnert, Nat. Nanotech. **4**, 820 (2009).

[23] T. Rocheleau, T. Ndukum, C. Macklin, J. B. Hertzberg, A. A. Clerk, and K. C. Schwab, Nature (London) **463**, 72 (2010).

[24] J. D. Teufel, D. Li, M. S. Allman, K. Cicak, A. J. Sirois, J. D. Whittaker, and R. W. Simmonds, Nature (London) **471**, 204 (2011).

[25] C. Fabre, M. Pinard, S. Bourzeix, A. Heidmann, E. Giacobino, and S. Reynaud, Phys. Rev. A **49**, 1337 (1994).

[26] S. Mancini and P. Tombesi, Phys. Rev. A **49**, 4055 (1994).

[27] S. Bose, K. Jacobs, and P. L. Knight, Phys. Rev. A **59**, 3204 (1999).

[28] W. Marshall, C. Simon, R. Penrose, and D. Bouwmeester, Phys. Rev. Lett. **91**, 130401 (2003).

[29] K. Jacobs, P. Tombesi, M. J. Collett, and D. F. Walls, Phys. Rev. A **49**, 1961 (1994).

[30] M. Pinard, C. Fabre, and A. Heidmann, Phys. Rev. A **51**, 2443 (1995).

[31] A. Mari and J. Eisert, Phys. Rev. Lett. **103**, 213603 (2009).

[32] K. Jähne, C. Genes, K. Hammerer, M. Wallquist, E. S. Polzik, and P. Zoller, Phys. Rev. A **79**, 063819 (2009).

[33] S. Huang and G. S. Agarwal, arXiv:0905.4234.

[34] V. Giovannetti, S. Mancini, and P. Tombesi, Europhys. Lett. **54**, 559 (2001).

[35] M. Paternostro, D. Vitali, S. Gigan, M. S. Kim, C. Brukner, J. Eisert, and M. Aspelmeyer, Phys. Rev. Lett. **99**, 250401 (2007).

[36] D. Vitali, S. Gigan, A. Ferreira, H. R. Böhm, P. Tombesi, A. Guerreiro, V. Vedral, A. Zeilinger, and M. Aspelmeyer, Phys. Rev. Lett. **98**, 030405 (2007).

[37] M. Pinard, A. Dantan, D. Vitali, O. Arcizet, T. Briant and A. Heidmann, Europhys. Lett. **72**, 747 (2005).

[38] M. J. Hartmann and M. B. Plenio, Phys. Rev. Lett. **101**, 200503 (2008).

[39] S. Huang and G. S. Agarwal, New J. Phys. **11**, 103044 (2009).

[40] B. S. Sheard, M. B. Gray, C. M. Mow-Lowry, and D. E. McClelland, Phys. Rev. A **69**, 051801(R)(2004).

[41] P. Meystre, E. M. Wright, J. D. McCullen, and E. Vignes, J. Opt. Soc. Am. B **2**, 1830 (1985).

[42] A. Dorsel, J. D. McCullen, P. Meystre, E. Vignes, and H. Walther, Phys. Rev. Lett. **51**, 1550 (1983).

[43] F. Marquardt, J. G. E. Harris, and S. M. Girvin, Phys. Rev. Lett. **96**, 103901 (2006).

[44] T. Carmon, H. Rokhsari, L. Yang, T. J. Kippenberg, and K. J. Vahala, Phys. Rev. Lett. **94**, 223902 (2005).

[45] C. Höhberger and K. Karrai, Nanotechnology 2004, Proceedings of the 4th IEEE Conference on Nanotechnology (2004), p. 419.

[46] C. Metzger, M. Ludwig, C. Neuenhahn, A. Ortlieb, I. Favero, K. Karrai, and F. Marquardt, Phys. Rev. Lett. **101**, 133903 (2008).

[47] F. Marquardt, J. P. Chen, A. A. Clerk, and S. M. Girvin, Phys. Rev. Lett. **99**, 093902 (2007).

[48] J. M. Dobrindt, I. Wilson-Rae, and T. J. Kippenberg, Phys. Rev. Lett. **101**, 263602 (2008).

[49] S. Huang and G. S. Agarwal, Phys. Rev. A **81**, 033830 (2010).

[50] S. Gröblacher, K. Hammerer, M. Vanner, and M. Aspelmeyer, Nature (London) **460**, 724 (2009).

[51] G. S. Agarwal and S. Huang, Phys. Rev. A **81** 041803(R) (2010).

[52] A. Schliesser and T. J. Kippenberg, arXiv:1003.5922.

[53] S. Weis, R. Riviere, S. Deleglise, E. Gavartin, O. Arcizet, A. Schliesser, and T. J. Kippenberg, Science **330** 1520 (2010).

[54] Q. Lin, J. Rosenberg, D. Chang, R. Camacho, M. Eichenfield, K. J. Vahala, O. Painter, Nat. Photon. **4**, 236 (2010).

[55] A. H. Safavi-Naeini, T. P. Mayer Alegre, J. Chan, M. Eichenfield, M.Winger, Q. Lin, J. T. Hill, D. E. Chang, and O. Painter, Nature (London) **472**, 69 (2011).

[56] A. Naik, O. Buu, M. D. LaHaye, A. D. Armour, A. A. Clerk, M. P. Blencowe, and K. C. Schwab, Nature (London) **443**, 193 (2006).

[57] A. Schliesser, O. Arcizet, R. Rivière, G. Anetsberger, and T. J. Kippenberg, Nat. Phys. **5**, 509 (2009).

[58] Y. Park and H. Wang, Nat. Phys. **5**, 489 (2009).

[59] S. Gröblacher, J. B. Hertzberg, M. R. Vanner, G. D. Cole, S. Gigan, K. C. Schwab and M. Aspelmeyer, Nat. Phys. **5**, 485 (2009).

[60] R. Rivière, S. Deläeglise, S. Weis, E. Gavartin, O. Arcizet, A. Schliesser, and T. J. Kippenberg, Phys. Rev. A **83**, 063835 (2011).

[61] A. D. O'Connell, M. Hofheinz, M. Ansmann, R. C. Bialczak, M. Neeley, D. Sank, H. Wang, M. Weides, J. Wenner, J. M. Martinis, and A. N. Cleland, Nature (London) **464**, 697 (2010).

[62] J. D. Teufel, T. Donner, D. Li, J. W. Harlow, M. S. Allman, Whittaker, K. W. Lehnert, and R. W. Simmonds, Nature (London) **475**, 359 (2011).

[63] J. Chan, T. P. Mayer Alegre, A. H. Safavi-Naeini, J. T. Hill, M. Aspelmeyer, and O. Painter, arXiv:1106.3614v1 (2011)

[64] C. K. Law, Phys. Rev. A **51**, 2537 (1995).

[65] M. L. Gorodetksy, A. Schliesser, G. Anetsberger, S. Deleglise, and T. J. Kippenberg, Optics Express **18**, 23236 (2010).

[66] I. Wilson-Rae, N. Nooshi, W. Zwerger, and T. J. Kippenberg, Phys. Rev. Lett. **99**, 093901 (2007).

[67] M. Li, W. H. P. Pernice, and H. X. Tang, Phys. Rev. Lett. **103**, 223901 (2009).

[68] M. Li, W. H. Pernice, C. Xiong, T. Baehr-Jones, M. Hochberg, and H. X. Tang, Nature (London) **456**, 480 (2008).

[69] M. Li, W. H. P. Pernice, and H. X. Tang, Nat. Photonics **3**, 464 (2009).

[70] G. Anetsberger, O. Arcizet, Q. P. Unterreithmeier, R. Rivière, A. Schliesser, E. M. Weig, J. P. Kotthaus, and T. J. Kippenberg, Nat. Phys. **5**, 909 (2009).

[71] M. Eichenfield, R. Camacho, J. Chan, K. J. Vahala, and O. Painter, Nature (London) **459**, 550 (2009).

[72] M. O. Scully and M. S. Zubairy, *Quantum Optics* (Cambridge University Press, Cambridge, 1997).

[73] C. C. Gerry and P. L. Knight, *Introductory Quantum Optics* (Cambridge University Press, Cambridge, 2005).

[74] A. Imamoglu and S. E. Harris, Opt. Lett. **14**, 1344 (1989).

[75] K.-J. Boller, A. Imamoglu, and S. E. Harris, Phys. Rev. Lett. **66**, 2593 (1991).

[76] S. E. Harris, Phys. Today **50** (7), 36 (1997).

[77] A. M. Akulshin, S. Barreiro, and A. Lezama, Phys. Rev. A **57**, 2996 (1998);

[78] A. Lezama, A. M. Akulshin, and S. Barreiro, Phys. Rev. A **59**, 4732 (1999).

[79] L. V. Hau, S. E. Harris, Z. Dutton, and C. H. Behroozi, Nature (London) **397**, 594 (1999).

[80] M. M. Kash, V. A. Sautenkov, A. S. Zibrov, L. Hollberg, G. R. Welch, M. D. Lukin, Y. Rostovtsev, E. S. Fry, and M. O. Scully, Phys. Rev. Lett. **82**, 5229 (1999).

[81] D. D. Budker, D. F. Kimball, S. M. Rochester, and V. V. Yashchuk, Phys. Rev. Lett. **83**, 1767 (1999).

[82] Y. -Q. Li and M. Xiao, Optics Letters **20**, 1489 (1995).

[83] D. Philips, A. Fleischhauer, A. Mair, R. Walsworth, and M. D. Lukin, Phys. Rev. Lett. **86**, 783 (2001).

[84] T. Chanelière, D. N. Matsukevich, S. D. Jenkins, S.-Y. Lan, T. A. B. Kennedy, and A. Kuzmich, Nature (London) **438**, 833 (2005).

[85] K. Akiba, K. Kashiwagi, T. Yonehara, and M. Kozuma, Phys. Rev. A **76**, 023812 (2007).

[86] J. Appel, E. Figueroa, D. Korystov, M. Lobino, and A. I. Lvovsky, Phys. Rev. Lett. **100**, 093602 (2008).

[87] K. C. Schwab and M. L. Roukes, Phys. Today, **58**, 36 (2005).

[88] M. D. LaHaye, O. Buu, B. Camarota, and K. C. Schwab, Science **304**, 74 (2004).

[89] R. Loudon, Phys. Rev. Lett. **47**, 815 (1981).

[90] V. B. Braginsky and F. Ya. Khalili, *Quantum Measurement* (Cambridge University Press, Cambridge, 1992).

[91] A. Abramovici, W. E. Althouse, R. W. P. Drever, Y. Gürsel, S. Kawamura, F. J. Raab, D. Shoemaker, L. Sievers, R. E. Spero, K. S. Thorne, R. E. Vogt, R. Weiss, S. E. Whitcomb, and M. E. Zucker, Science **256**, 325 (1992).

[92] S. Mancini, D. Vitali, and P. Tombesi, Phys. Rev. Lett. **80**, 688 (1998).

[93] P. F. Cohadon, A. Heidmann, and M. Pinard, Phys. Rev. Lett. **83**, 3174 (1999).

[94] M. Poggio, C. L. Degen, H. J. Mamin, and D. Rugar, Phys. Rev. Lett. **99**, 017201 (2007).

[95] M. Paternostro, S. Gigan, M. S. Kim, F. Blaser, H. R. Böhm, and M. Aspelmeyer, New J. Phys. **8**, 107 (2006).

[96] S.Gröblacher, S. Gigan, H. R. Böhm, A. Zeilinger, and M. Aspelmeyer, Europhys. Lett. **81**, 54003 (2008).

[97] L. A. Wu, M. Xiao, and H. J. Kimble, J. Opt. Soc. Am. B **4**, 1465 (1987).

[98] L. A. Wu, H. J. Kimble, J. L. Hall, and H. Wu, Phys. Rev. Lett. **57**, 2520 (1986).

[99] B. Yurke, Phys. Rev. A **29**, 408 (1984).

[100] Y. J. Lu and Z. Y. Ou, Phys. Rev. Lett. **88**, 023601 (2001).

[101] M. Wolinsky and H. J. Carmichael, Phys. Rev. Lett. **60**, 1836 (1988).

[102] H. Deng, D. Erenso, R. Vyas, and S. Singh, Phys. Rev. Lett. **86**, 2770 (2001).

[103] G. S. Agarwal and G. Adam, Phys. Rev. A **39**, 6259 (1989).

[104] G. S. Agarwal, Phys. Rev. Lett. **97**, 023601 (2006).

[105] H. L. Ma, C. G. Ye, D. Wei, and J. Zhang, Phys. Rev. Lett. **95**, 233601 (2005).

[106] C. K. Law, Phys. Rev. A **49**, 433 (1994).

[107] H. B. G. Casimir, Proc. Kon. Ned. Akad. Wet. **51**, 793 (1948).

[108] V. Giovannetti and D. Vitali, Phys. Rev. A **63**, 023812 (2001).

[109] C. W. Gardiner and P. Zoller, *Quantum Noise* (Springer-Verlag, Berlin, 1991).

[110] D. F. Walls and G. J. Milburn, *Quantum Optics* (Springer-Verlag, Berlin, 1994).

[111] L. A. Lugiato, Progress in Optics **21**, 70 (1984).

[112] A. Hurwitz, *Selected Papers on Mathematical Trends in Control Theory*, edited by R. Bellman and R. Kalaba (Dover, New York,1964).

[113] E. X. DeJesus and C. Kaufman, Phys. Rev. A **35**, 5288 (1987).

[114] S. Bose, K. Jacobs, and P. L. Knight, Phys. Rev. A **56**, 4175 (1997).

[115] M. Bhattacharya, P.-L. Giscard, and P. Meystre, Phys. Rev. A **77**, 030303(R) (2008).

[116] M. Poggio, C. L. Degen, H. J. Mamin, and D. Rugar, Phys. Rev. Lett. **99**, 017201 (2007).

[117] M. Bhattacharya and P. Meystre, Phys. Rev. Lett. **99**, 073601 (2007).

[118] M. Bhattacharya, H. Uys, and P. Meystre, Phys. Rev. A **77**, 033819 (2008).

[119] M. Bhattacharya and P. Meystre, Phys. Rev. A **78**, 041801(R) (2008).

[120] A. Schliesser, R. Rivière, G. Anetsberger, O. Arcizet, and T. J. Kippenberg, Nature Physics **4**, 415 (2008).

[121] J. J. Sanchez-Mondragon, N. B. Narozhny, and J. H. Eberly, Phys. Rev. Lett. **51**, 550 (1983).

[122] G. S. Agarwal, Phys. Rev. Lett. **53**, 1732 (1984).

[123] M. G. Raizen, R. J. Thompson, R. J. Brecha, H. J. Kimble, and H. J. Carmichael, Phys. Rev. Lett. **63**, 240 (1989).

[124] A. Boca, R. Miller, K. M. Birnbaum, A. D. Boozer, J. McKeever, and H. J. Kimble, Phys. Rev. Lett. **93**, 233603 (2004).

[125] P. Maunz, T. Puppe, I. Schuster, N. Syassen, P. W. H. Pinkse, and G. Rempe, Phys. Rev. Lett. **94**, 033002 (2005).

[126] S. Huang and G. S. Agarwal, Phys. Rev. A **79**, 013821 (2009).

[127] This is derived by setting κ and γ_m in $d(\omega)$ zero. A better estimate can be obtained by dropping $i\gamma_m\omega$ and κ^2, but keeping the term $-2i\kappa\omega$. This is because $\kappa/\omega_m(\simeq 0.22)$ is not much smaller than 1.

[128] See Ref. [110], p124, Eq. (7.18).

[129] J. M. Courty, A. Heidmann, and M. Pinard, Phys. Rev. Lett. **90**, 083601 (2003).

[130] O. Arcizet, T. Briant, A. Heidmann, and M. Pinard, Phys. Rev. A **73**, 033819 (2006).

[131] C. M. Caves, Phys. Rev. Lett. **45**, 75 (1980).

[132] H. Ian, Z. R. Gong, Y. X. Liu, C. P. Sun, and F. Nori, Phys. Rev. A **78**, 013824 (2008).

[133] P. Rabl, A. Shnirman, and P. Zoller, Phys. Rev. B **70**, 205304 (2004).

[134] X. Zhou and A. Mizel, Phys. Rev. Lett. **97**, 267201 (2006).

[135] W. Huo and G. Long, Appl. Phys. Lett. **92**, 133102 (2008).

[136] K. Moon and S. M. Girvin, Phys. Rev. Lett. **95**, 140504 (2005).

[137] A. A. Clerk, F. Marquardt, and K. Jacobs, New J. Phys. **10**, 095010 (2008).

[138] M. J. Woolley, A. C. Doherty, G. J. Milburn, and K. C. Schwab, Phys. Rev. A **78**, 062303 (2008).

[139] R. Ruskov, K. Schwab, and A. N. Korotkov, Phys. Rev. B **71**, 235407 (2005).

[140] D. Vitali, S. Mancini, L. Ribichini, and P. Tombesi, Phys. Rev. A **65**, 063803 (2002).

[141] C. W. Gardiner, Phys. Rev. Lett. **56**, 1917 (1986).

[142] M. A. Nielsen and I. L. Chuang, *Quantum Computation and Quantum Information*, (Cambridge University 2000).

[143] V. Vedral, New J. Phys. **6**, 102 (2004).

[144] B. Deb and G. S. Agarwal, Phys. Rev. A **78**, 013639 (2008).

[145] A. Sørensen, L-M Duan, J. I. Ciracand, and P. Zoller, Nature(London) **409**, 63 (2001).

[146] C. W. Chou, H. de Riedmatten, D. Felinto, S. V. Polyakov, S. J. van Enk, and H. J. Kimble, Nature (London) **438**, 828 (2005).

[147] S. Mancini, V. Giovannetti, D. Vitali, and P. Tombesi, Phys. Rev. Lett. **88**, 120401 (2002).

[148] J. Zhang, K. Peng, and S. L. Braunstein, Phys. Rev. A **68**, 013808 (2003).

[149] D. Vitali, S. Mancini, and P. Tombesi, J. Phys. A: Math. Theor. **40**, 8055 (2007).

[150] D. Vitali, S. Mancini, L. Ribichini, and P. Tombesi, J. Opt. Soc. Am. B **20**, 1054 (2003).

[151] S. Pirandola, D. Vitali, P. Tombesi, and S. Lloyd, Phys. Rev. Lett. **97**, 150403 (2006).

[152] G. Vacanti, M. Paternostro, G. M. Palma, and V. Vedral, New J. Phys. **10**, 095014 (2008).

[153] S. Bose and G. S. Agarwal, New J. Phys. **8**, 34 (2006).

[154] L. -M. Duan, G. Giedke, J. I. Cirac, and P. Zoller, Phys. Rev. Lett. **84**, 2722 (2000).

[155] J. M. Aguirregabiria and L. Bel, Phys. Rev. A **36**, 3768 (1987).

[156] G. Calucci, J. Phys. A **25**, 3873 (1992).

[157] K. Karrai, I. Favero, and C. Metzger, Phys. Rev. Lett. **100**, 240801 (2008).

[158] T. Corbitt, C. Wipf, T. Bodiya, D. Ottaway, D. Sigg, N. Smith, S. Whitcomb, and N. Mavalvala, Phys. Rev. Lett. **99**, 160801 (2007).

[159] S. Gröblacher, S. Gigan, H. R. Böhm, A. Zeilinger, and M. Aspelmeyer, Europhys. Lett. **81**, 54003 (2008).

[160] J. Klinner, M. Lindholdt, B. Nagorny, and A. Hemmerich, Phys. Rev. Lett. **96**, 023002 (2006).

[161] R. W. Boyd, *Nonlinear Optics*, 2nd ed. (Academic, San Diego, 2003).

[162] M. Hossein-Zadeh, H. Rokhsari, A. Hajimiri, and K. J. Vahala, Phys. Rev. A **74**, 023813 (2006).

[163] S. Mancini, V. I. Man'ko, and P. Tombesi, Phys. Rev. A **55**, 3042 (1997).

[164] V. B. Braginsky, S. E. Strigin, and S. P. Vyatchanin, Phys. Lett. A **287**, 331 (2001).

[165] V. B. Braginsky, S. E. Strigin, and S. P. Vyatchanin, Phys. Lett. A **305**, 111 (2002).

[166] S. Huang and G. S. Agarwal, Phys. Rev. A **80**, 033807 (2009).

[167] P. Kolchin, S. Du, C. Belthangady, G. Y. Yin, and S. E. Harris, Phys. Rev. Lett. **97**, 113602 (2006).

[168] S. D. Gupta and G. S. Agarwal, Opt. Commun. **115**, 597 (1995).

[169] A. K. Patnaik, G. S. Agarwal, C. H. Raymond Ooi, and M. O. Scully, Phys. Rev. A **72**, 043811 (2005).

[170] C. W. Chou, S. V. Polyakov, A. Kuzmich, and H. J. Kimble, Phys. Rev. Lett. **92**, 213601 (2004).

[171] V. A. Sautenkov, Y. V. Rostovtsev, and M. O. Scully, Phys. Rev. A **72**, 065801 (2005).

[172] S. E. Harris, J. E. Field, and A. Imamoglu, Phys. Rev. Lett. **64**, 1107 (1990).

[173] K.-J. Boller, A. Imamoglu, and S. E. Harris, Phys. Rev. Lett. **66**, 2593 (1991).

[174] M. Fleischhauer, A. Imamoglu, and J. P. Marangos, Rev. Mod. Phys. **77**, 633 (2005).

[175] S. E. Harris, J. E. Field, and A. Kasapi, Phys. Rev. A **46**, R29 (1992).

[176] B. S. Ham, M. S. Shahriar, M. K. Kim, and P. R. Hemmer, Opt. Lett. **22**, 1849 (1997).

[177] S. Zhang, D. A. Genov, Y. Wang, M. Liu, and X. Zhang, Phys. Rev. Lett. **101**, 047401 (2008).

[178] N. Papasimakis, V. A. Fedotov, N. I. Zheludev, and S. L. Prosvirnin, Phys. Rev. Lett. **101**, 253903 (2008).

[179] P. Tassin, L. Zhang, T. Koschny, E. N. Economou, and C. M. Soukoulis, Phys. Rev. Lett. **102**, 053901 (2009).

[180] S. Y. Chiam, R. Singh, C. Rockstuhl, F. Lederer, W. Zhang, and A. A. Bettiol, Phys. Rev. B **80**, 153103 (2009).

[181] D. D. Smith, H. Chang, K. A. Fuller, A. T. Rosenberger, and R. W. Boyd, Phys. Rev. A **69**, 063804 (2004).

[182] C. Genes, A. Mari, P. Tombesi, and D. Vitali, Phys. Rev. A **78**, 032316 (2008).

[183] I. Favero and K. Karrai, Nature Photonics **3**, 201 (2009).

[184] S. H. Autler and C. H. Townes, Phys. Rev. **100**, 703 (1955).

[185] F. Elste, S. M. Girvin, and A. A. Clerk, Phys. Rev. Lett. **102**, 207209 (2009).

[186] S. Bose, K. Jacobs, and P. L. Knight, Phys. Rev. A **56**, 4175 (1997).

[187] S. Huang and G. S. Agarwal, Phys. Rev. A **81**, 033830 (2010). [this paper deals exclusively with designs where only dispersive optomechanical coupling occurs.]

[188] W. H. P. Pernice, M. Li, and H. X. Tang, Opt. Express **17**, 1806 (2009).

[189] G. S. Agarwal and S. Huang, Phys. Rev. A **81**, 041803(R) (2010); P. Anisimov and O. Kocharovskaya, J. Mod. Opt. **55**, 3159 (2008).

[190] M. Bhattacharya and P. Meystre, Phys. Rev. Lett. **99**, 153603 (2007).

[191] A. Nunnenkamp, K. Borkje, J. G. E. Harris, and S. M. Girvin, Phys. Rev. A **82**, 021806(R) (2010)

[192] J. B. Hertzberg, T. Rocheleau, T. Ndukum, M. Savva, A. A. Clerk, and K. C. Schwab, Nature Physics **6**, 213 (2010).

[193] G. Anetsberger, E. Gavartin, O. Arcizet, Q. P. Unterreithmeier, E. M. Weig, M. L. Gorodetsky, J. P. Kotthaus, and T. J. Kippenberg, arXiv:1003.3752v1.

[194] S. Huang and G. S. Agarwal, Phys. Rev. A **81**, 053810 (2010).

[195] Press release, 28th of January 2010, Oxford instruments, www.oxford-instruments.com; M. J. Martínez-Pérez, J. Sesé, F. Luis, D. Drung, and T. Schurig, Rev. Sci. Instrum. **81**, 016108 (2010).

[196] M. Bhattacharya, H. Uys, and P. Meystre, Phys. Rev. A **77**, 033819 (2008).

[197] J. M. Dobrindt and T. J. Kippenberg, Phys. Rev. Lett. **104**, 033901 (2010).

[198] M. Bhattacharya, P. -L. Giscard, and P. Meystre, Phys. Rev. A **77**, 013827 (2008).

[199] For a recent review of the subject see A. Schliesser and T. J. Kippenberg, *Advances in Atomic, Molecular, and Optical Physics*, **58**, (2010), pages 207-323.

[200] A. Rai and G. S. Agarwal, Phys. Rev. A **78**, 013831 (2008).

[201] In order to check the validity of the approximation of the cavity frequency, we compare the exact cavity frequency and the approximate cavity frequency. The exact cavity frequency is $\omega(q) = \omega_n + \frac{\pi}{\tau} - \frac{1}{\tau}[\sin^{-1}(\sqrt{R}\cos 2k_n q) + \sin^{-1}(\sqrt{R})]$, whereas the approximate cavity frequency is $\omega(q) = \omega_0 + gq^2$. The difference between these in units of the membrane's frequency ω_m are -2.89×10^{-8} and -2.63×10^{-7} for $R = 0.45$ and 0.81 at $q = 10^{-10}$m and $\omega_m = 2\pi \times 10^5$ Hz.

[202] We note that, although we discuss different physical phenomenon, Ref. [19] discusses in detail the effect of the temperature of the membrane when driven only by the coupling field ($\varepsilon_p = 0$). In the regime where we work, $\gamma n_{th} > \kappa$, they report significant changes in the phonon number distribution of the membrane. Furthermore, it is interesting to note their nonlinear damping equation [just before their Eq. (5)] would imply that β=0, which is consistent with our finding that $q_0 = 0$.

[203] O. Kocharovskaya, Y. Rostovtsev, and M. O. Scully, Phys. Rev. Lett. **86**, 628 (2001).

[204] D. Akamatsu, K. Akiba, and M. Kozuma, Phys. Rev. Lett. **92**, 203602 (2004).

[205] D. Akamatsu, Y. Yokoi, M. Arikawa, S. Nagatsuka, T. Tanimura, A. Furusawa, and M. Kozuma, Phys. Rev. Lett. **99**, 153602 (2007).

[206] M. Arikawa, K. Honda, D. Akamatsu, Y. Yokoil, K. Akiba, S. Nagatsuka, A. Furusawa, and M. Kozuma, Optics Express, **15**, 11849 (2007).

[207] M. D. Eisaman, A. Andre, F. Massou, M. Fleischhauer, A. S. Zibrov, and M. D. Lukin, Nature (London) **438**, 837 (2005).

[208] M. Lobino, C. Kupchak, E. Figueroa, and A. I. Lvovsky, Phys. Rev. Lett. **102**, 203601 (2009).

[209] K. Honda, D. Akamatsu, M. Arikawa, Y. Yokoi, K. Akiba, S. Nagatsuka, T. Tanimura, A. Furusawa, and M. Kozuma, Phys. Rev. Lett. **100**, 093601 (2008).

[210] S. Huang and G. S. Agarwal, Phys. Rev. A **82**, 033811 (2010).

[211] T. N. Dey and G. S. Agarwal, Phys. Rev. A **67**, 033813 (2003).

[212] S. E. Harris and Y. Yamamoto, Phys. Rev. Lett. **81**, 3611 (1998).

[213] M. Mücke, E. Figueroa, J. Bochmann, C. Hahn, K. Murr, S. Ritter, C. J. Villas-Boas, and G. Rempe, Nature (London) **465**, 755 (2010).

[214] H. Tanji-Suzuki, W. Chen, R. Landig, J. Simon, and V. Vuletić, Science **333**, 1266 (2011).

[215] L. Zhou, Z. R. Gong, Y. X. Liu, C. P. Sun, and F. Nori, Phys. Rev. Lett. **101**, 100501 (2008).

[216] P. Bermel, A. Rodriguez, S. G. Johnson, J. D. Joannopoulos, and M. Soljačić, Phys. Rev. A **74**, 043818 (2006).

[217] P. Longo, P. Schmitteckert, and K. Busch, Phys. Rev. Lett. **104**, 023602 (2010).

[218] S. Sandlu, M. L. Povinelli, and S. Fan, Appl. Phys. Lett. **96**, 231108 (2010).

[219] D. E. Chang, A. S. Sørensen, E. A. Demler, and M. D. Lukin, Nature Physics **3**, 807 (2007).

[220] M. A. Hall, J. B. Altepeter, and P. Kumar, Phys. Rev. Lett. **106**, 053901 (2011).

[221] I. C. Hoi, C. M. Wilson, G. Johansson, T. Palomaki, B. Peropadre, and P. Delsing, Phys. Rev. Lett. **107**, 073601 (2011).

[222] S. Huang and G. S. Agarwal, Phys. Rev. A **83**, 043826 (2011).

[223] M. L. Povinelli, M. Loncar, M. Ibanescu, E. J. Smythe, S. G. Johnson, F. Capasso, and J. D. Joannopoulos, Opt. Lett. **30**, 3042 (2005).

[224] J. Roels, I. D. Vlaminck, L. Lagae, B. Maes, D. V. Thourhout, and R. Baets, Nature Nanotechnology **4**, 510 (2009).

APPENDIX A

THE VARIANCE OF MOMENTUM-DERIVATION OF EQUATION EQ. (9.18)

With the aid of Eq. (9.17), the first term of Eq. (9.15) is

$$\begin{aligned} & \frac{1}{4\pi^2}\int\int_{-\infty}^{+\infty} d\omega\, d\Omega\, e^{-i(\omega+\Omega)t} P_T(\omega)P_T(\Omega)\langle\xi(\omega)\xi(\Omega)\rangle \\ = \; & \frac{1}{2\pi}\int_{-\infty}^{+\infty} d\omega P_T(\omega)P_T(-\omega)2\gamma_m\frac{\omega}{\omega_m}\left[1+\coth\left(\frac{\hbar\omega}{2K_BT}\right)\right]. \end{aligned} \tag{A.1}$$

Then with the help of Eq. (9.16), the second term of Eq. (9.15) will be

$$\begin{aligned} & \frac{1}{4\pi^2}\int\int_{-\infty}^{+\infty} d\omega\, d\Omega e^{-i(\omega+\Omega)t} P_S(\omega)P_S(\Omega)\langle c_{in}(\omega)c_{in}(\Omega)\rangle \\ = \; & \frac{1}{2\pi}\int_{-\infty}^{+\infty} d\nu\, e^{-2i\omega_m t} P_S(\omega_m+\nu)P_S(\omega_m-\nu)\frac{M\Gamma^2}{\Gamma^2+\nu^2}, \end{aligned} \tag{A.2}$$

and the third term of Eq. (9.15) becomes

$$\begin{aligned} & \frac{1}{4\pi^2}\int\int_{-\infty}^{+\infty} d\omega\, d\Omega e^{-i(\omega+\Omega)t} P_S(\omega)P_S^*(-\Omega)\langle c_{in}(\omega)c_{in}^\dagger(-\Omega)\rangle \\ = \; & \frac{1}{2\pi}\int_{-\infty}^{+\infty} d\nu |P_S(\omega_m+\nu)|^2\frac{N\Gamma^2}{\Gamma^2+\nu^2} + \frac{1}{2\pi}\int_{-\infty}^{+\infty} d\omega |P_S(\omega)|^2. \end{aligned} \tag{A.3}$$

Therefore, the variance $\langle\delta P(t)^2\rangle$ can be calculated by

$$\begin{aligned} \langle\delta P(t)^2\rangle \; = \; & \frac{1}{2\pi}\int_{-\infty}^{+\infty} d\omega P_T(\omega)P_T(-\omega)2\gamma_m\frac{\omega}{\omega_m}\left[1+\coth\left(\frac{\hbar\omega}{2K_BT}\right)\right] \\ & +2\mathrm{Re}\left[\frac{1}{2\pi}\int_{-\infty}^{+\infty} d\nu e^{-2i\omega_m t} P_S(\omega_m+\nu)P_S(\omega_m-\nu)\frac{M\Gamma^2}{\Gamma^2+\nu^2}\right] \\ & +2\left[\frac{1}{2\pi}\int_{-\infty}^{+\infty} d\nu |P_S(\omega_m+\nu)|^2\frac{N\Gamma^2}{\Gamma^2+\nu^2}\right] + \frac{1}{2\pi}\int_{-\infty}^{+\infty} d\omega |P_S(\omega)|^2. \end{aligned} \tag{A.4}$$

The variance has terms oscillating at twice the frequency of the nanomechanical oscillator. These terms can be removed in the standard way by working in an interaction

picture defined with respect to the frequency ω_m. This is equivalent to setting $e^{\pm 2i\omega_m t}$ as unity, hence (A4) leads to Eq. (9.18).

APPENDIX B

RELATION BETWEEN THE QUANTUM FLUCTUATIONS OF NANO WAVEGUIDE AND THE OUTPUT FIELD

In the following, we show the squeezing of the waveguide can be measured through the y component of the output field. Using the input-output relation [110] $c_{out}(t) = \sqrt{2\kappa_e(Q)}c(t)$, the fluctuations of the output field can be written as

$$\begin{aligned} \delta c_{out}(\omega) &= J\delta c(\omega) + \frac{\eta}{2}\sqrt{2\kappa_e}c_s\delta Q(\omega) \\ &= J\delta c(\omega) + \frac{\eta}{2}\sqrt{2\kappa_e}c_s\frac{i\omega_m}{\omega}\delta P(\omega). \end{aligned} \tag{B.1}$$

From Eq. (9.9), we find the fluctuations of the resonator field

$$\delta c(\omega) = \frac{1}{A^*(-\omega)}[\frac{i\omega_m}{\omega}U\delta P(\omega) + Jc_{in}(\omega)]. \tag{B.2}$$

Combining Eqs. (B.1) and (B.2), and defining the y component of the output field as $\delta y_{out}(t) = i[\delta c^\dagger_{out}(t) - \delta c_{out}(t)]$ so that $\delta y_{out}(\omega) = i[\delta c^\dagger_{out}(-\omega) - \delta c_{out}(\omega)]$, one can write the fluctuations in the momentum variable of the waveguide in terms of the y component of the output field

$$\delta P(\omega) = -\frac{\omega}{\omega_m} \times \frac{A(\omega)A^*(-\omega)\delta y_{out}(\omega) - J^2 i[A^*(-\omega)c^\dagger_{in}(-\omega) - A(\omega)c_{in}(\omega)]}{\frac{\eta}{2}\sqrt{2\kappa_e}(c_s^* - c_s)A(\omega)A^*(-\omega) + J[A^*(-\omega)U^* - A(\omega)U]}. \tag{B.3}$$

It is seen that the fluctuations in the momentum variable of the waveguide is related to the y component of the output field.

VITA

Sumei Huang

Candidate for the Degree of

Doctor of Philosophy

Dissertation: ELECTROMAGNETICALLY INDUCED TRANSPARENCY AND QUANTUM EFFECTS IN OPTOMECHANICAL SYSTEMS

Major Field: Physics

Biographical:

Personal Data: Born in Putian, Fujian, China on Oct. 20, 1974.

Education:

Received Bachelor of Science degree in Physics Education from Fujian Normal University, Fuzhou, Fujian, China, in July 2001;
Received Master of Science degree in Theoretical Physics from Fujian Normal University, Fuzhou, Fujian, China, in July 2004;
Completed the requirements for the degree of Doctor of Philosophy with a major in Physics at Oklahoma State University in December 2011.

Experience:

Assistant Lecturer in College Physics and General Physics Experiment, Department of Mathematics and Physics, Fujian University of Technology, Fujian, China, from Aug. 2004 to July 2006.
Teaching Assistant in General Physics, Department of Physics, Oklahoma State University, from Aug. 2006 to Dec. 2008.
Graduate Research Assistant, Department of Physics, Oklahoma State University, from Jan. 2009 to present.

Professional membership :

American Physical Society,
Optical Society of America.

Name: Sumei Huang Date of Degree: December, 2011

Institution: Oklahoma State University Location: Stillwater, Oklahoma

Title of Study: ELECTROMAGNETICALLY INDUCED TRANSPARENCY AND QUANTUM EFFECTS IN OPTOMECHANICAL SYSTEMS

Pages in Study: 193 Candidate for the Degree of Doctor of Philosophy

Major Field: Physics

In this thesis, we study cooling, normal mode splitting, squeezing, entanglement, and electromagnetically induced transparency in the macroscopic optomechancial system. We show that a type I optical parametric amplifier in a Fabry-Perot cavity can considerably improve cooling of a mechanical oscillator, and it also can affect the normal-mode splitting behavior of the movable mirror and the output field. Next, we discover that squeezing of a mechanical oscillator in a Fabry-Perot cavity and the entanglement between two mechanical oscillators in a ring cavity can be generated by injecting a broadband squeezed vacuum along with laser light. Then, we study that the strong dispersive optomechanical coupling between the optical and mechanical oscillators can induce the normal mode splitting in the two quadratures of the output fields by the injection of coherent coupling and probe fields. Further, we study that electromagnetically induced transparency can occur in the output field at the probe frequency in the linear optomechanical coupling system which is driven by a weak probe field in the presence of a strong-coupling field. Next we present that the strong reactive optomechanical coupling between the optical resonator and the waveguide can also induce the normal mode splitting in the two quadratures of the output fields by the injection of coherent coupling and probe fields. In addition, We discuss that the standard quantum limit of the waveguide can be beaten by inputting a narrowband squeezed vacuum and laser light into a reactive optomechanical coupling system. Further, we study that electromagnetically induced transparency also can occur in the output field at the probe frequency in the quadratic optomechanical coupling system. We also investigate that electromagnetically induced transparency can arise in the homodyne spectrum of the output field by use of a weak probe field in a squeezed vacuum state in the presence of a strong coupling field. Finally, we show that the optomechanical systems can serve as single photon routers.

ADVISOR'S APPROVAL: _____